frontiers | Research Topics

Frontiers in the midlands society of physiological sciences (2023-2024)

Edited by
Surabhi Chandra, William C. W. Chen, Hong Zheng, Harold D. Schultz and Yifan Li

Published in
Frontiers in Physiology

ISSN 1664-8714
ISBN 978-2-8325-6635-0
DOI 10.3389/978-2-8325-6635-0

Generative AI statement
Any alternative text (Alt text) provided alongside figures in the articles in this ebook has been generated by Frontiers with the support of artificial intelligence and reasonable efforts have been made to ensure accuracy, including review by the authors wherever possible. If you identify any issues, please contact us.

About Frontiers

Frontiers is more than just an open access publisher of scholarly articles: it is a pioneering approach to the world of academia, radically improving the way scholarly research is managed. The grand vision of Frontiers is a world where all people have an equal opportunity to seek, share and generate knowledge. Frontiers provides immediate and permanent online open access to all its publications, but this alone is not enough to realize our grand goals.

Frontiers journal series

The Frontiers journal series is a multi-tier and interdisciplinary set of open-access, online journals, promising a paradigm shift from the current review, selection and dissemination processes in academic publishing. All Frontiers journals are driven by researchers for researchers; therefore, they constitute a service to the scholarly community. At the same time, the *Frontiers journal series* operates on a revolutionary invention, the tiered publishing system, initially addressing specific communities of scholars, and gradually climbing up to broader public understanding, thus serving the interests of the lay society, too.

Dedication to quality

Each Frontiers article is a landmark of the highest quality, thanks to genuinely collaborative interactions between authors and review editors, who include some of the world's best academicians. Research must be certified by peers before entering a stream of knowledge that may eventually reach the public - and shape society; therefore, Frontiers only applies the most rigorous and unbiased reviews. Frontiers revolutionizes research publishing by freely delivering the most outstanding research, evaluated with no bias from both the academic and social point of view. By applying the most advanced information technologies, Frontiers is catapulting scholarly publishing into a new generation.

What are Frontiers Research Topics?

Frontiers Research Topics are very popular trademarks of the *Frontiers journals series*: they are collections of at least ten articles, all centered on a particular subject. With their unique mix of varied contributions from Original Research to Review Articles, Frontiers Research Topics unify the most influential researchers, the latest key findings and historical advances in a hot research area.

Find out more on how to host your own Frontiers Research Topic or contribute to one as an author by contacting the Frontiers editorial office: frontiersin.org/about/contact

Frontiers in the midlands society of physiological sciences (2023-2024)

Topic editors

Surabhi Chandra — University of Nebraska at Kearney, United States
William C. W. Chen — University of South Dakota, United States
Hong Zheng — University of South Dakota, United States
Harold D. Schultz — University of Nebraska Medical Center, United States
Yifan Li — University of South Dakota, United States

Citation

Chandra, S., Chen, W. C. W., Zheng, H., Schultz, H. D., Li, Y., eds. (2025). *Frontiers in the midlands society of physiological sciences (2023-2024)*.
Lausanne: Frontiers Media SA. doi: 10.3389/978-2-8325-6635-0

Table of contents

frontiers | Frontiers in Physiology

TYPE Editorial
PUBLISHED 09 July 2025
DOI 10.3389/fphys.2025.1654264

OPEN ACCESS

EDITED AND REVIEWED BY
Geoffrey A. Head,
Baker Heart and Diabetes Institute, Australia

*CORRESPONDENCE
William C. W. Chen,
william.chen@usd.edu

RECEIVED 26 June 2025
ACCEPTED 27 June 2025
PUBLISHED 09 July 2025

CITATION
Natarajan SK, Zheng H, Chandra S, Schultz HD and Chen WCW (2025) Editorial: Frontiers in the midlands society of physiological sciences (2023-2024).
Front. Physiol. 16:1654264.
doi: 10.3389/fphys.2025.1654264

Editorial: Frontiers in the midlands society of physiological sciences (2023-2024)

Sathish Kumar Natarajan[1], Hong Zheng[2], Surabhi Chandra[3], Harold D. Schultz[4] and William C. W. Chen[2]*

[1]Department of Nutrition and Health Sciences, University of Nebraska–Lincoln, Lincoln, NE, United States, [2]Division of Biomedical and Translational Sciences, Sanford School of Medicine, University of South Dakota, Vermillion, SD, United States, [3]Department of Biology, University of Nebraska at Kearney, Kearney, NE, United States, [4]Department of Cellular and Integrative Physiology, College of Medicine, University of Nebraska Medical Center, Omaha, NE, United States

KEYWORDS

cardiovascular system, heart failure, artificial intelligence, machine learning, neuroscience, metabolism, endocrine, corpus luteum

Editorial on the Research Topic
Frontiers in the midlands society of physiological sciences (2023-2024)

This Research Topic covers original studies and reviews submitted by participating members of the Midlands Society of Physiological Sciences (MSPS) from 2023 to 2024. MSPS is a regional nonprofit organization affiliated with the American Physiological Society (APS). MSPS members primarily represent academic and healthcare institutions in Nebraska and South Dakota, advocating for the importance of physiology in education, research, career development, and public awareness. Research within MSPS encompasses a wide range of disciplines and fields, spanning from molecular to whole-organism interrogation in both physiological and disease conditions Figure 1.

Basic and translational cardiovascular sciences have been major research focuses within MSPS for decades. Herein, Lira et al. established a "double-hit" protocol that induces heart failure (HF) with preserved ejection fraction (HFpEF) in FVB/N mice with dysfunction of the myocardial ubiquitin-proteasome system, suggesting its pathogenic role in HFpEF development and/or progression. This protocol simultaneously induces metabolic syndrome and hypertension, producing key features of HFpEF mimicking the clinical syndrome in patients, such as glucose intolerance, elevated blood pressure, and concentric left ventricular hypertrophy with preserved systolic function.

Besides, Zhang et al. interrogated the dose-dependent effects of single interleukin-10 treatment (IL-10) on macrophage phenotype regulation and cardiac remodeling after myocardial infarction (MI). This study demonstrated that an intermediate dose range of IL-10, but not high doses, effectively shifts macrophages toward an anti-inflammatory, reparative phenotype and facilitate cardiac recovery post-MI. Particularly, 250 ng IL-10 exhibited the best overall outcome, whereas ≥1,000 ng IL-10 triggered mixed responses transiently perturbing inflammatory responses and impairing cardiac function, underscoring the importance of IL-10 dosage to maximize its benefits while minimizing potential adverse effects.

Kitzerow et al. used a rat model of MI to map and quantify plasma extravasation (PEx) in multiple organs over time, revealing that PEx occurs in a stage- and

FIGURE 1
Representative Photos from the 6th MSPS Annual Meeting (2024). This event took place in the Lee Medicine and Science building at the University of South Dakota in Vermillion, South Dakota, United States on 19 October 2024. **(A)** A photo showing one of the talks delivered by a local speaker (photo courtesy of Dr. Jee-Yeon Hwang). **(B)** A photo showing the scientific discussions during the poster session.

organ-specific manner during the progression of chronic HF. Cardiac PEx was highest in the early phase but persisted in scar regions, whereas lung PEx remained significantly elevated,. Abdominal organs such as the liver, pancreas, and spleen showed delayed and increasing PEx correlating with advancing HF. This study suggests that the differential timing and severity of vascular permeability in various organs may contribute to the multi-organ dysfunction observed in chronic HF.

Further, MSPS members leverage recent advances in artificial intelligence (AI) and machine learning (ML) that are revolutionizing medical practice to accelerate translational and clinical research development. Chowdhury et al. reviewed the clinical progress and challenges of stem cell therapy for HF, noting that while numerous clinical trials within the past decade have shown encouraging results in cardiac repair, significant limitations remain due to discrepancies between preclinical models and human outcomes. The authors highlight that advances in multiomics, precision medicine, and AI/ML can help overcome these hurdles by optimizing cell quality, targeting, and personalized treatment strategies, outlining a roadmap for next-generation stem cell-based therapies that integrate cutting-edge technologies to improve both the structural and functional recovery in HF patients.

In addition, many MSPS members work on basic and translational neurosciences, brain-organ axes, sex differences, and neuropsychiatry. For example, Boomer et al. reported a novel role of the regulators of G-protein signaling 2 (RGS2) in the hypothalamic paraventricular nucleus (PVN) that critically regulates sympathetic activities in a rat model of hypertension. With central adenoviral RGS2 transfection, the authors found that the action of RGS2 on angiotensin-II-induced Gq-protein activation modulated blood pressure, sympathetic activities, and kidney function, providing new insights into the central regulation of blood pressure and potential targets to treat hypertension. Kamra et al. investigated sex-based differences in chemoreflex activation under acute lung injury (ALI), utilizing a bleomycin-induced ALI animal model. The authors highlighted male vs. female chemoreflex changes during the recovery from ALI and emphasized the importance of sex as a determinant in respiratory responses. These findings point to a need for a broader understanding of sex-based variations in lung disorders and underscore the significance of sex as a crucial factor in respiratory research.

Ma et al. described a key role of a genetic polymorphism of brain-derived neurotrophic factor (BDNF) that possibly mediates the sexual difference in idiopathic autism spectrum disorder (ASD) and human autism. Using humanized mice with genetic knock-in of the target human BDNF methionine (Met) allele, the authors showed that diminished activity-dependent BDNF signaling resulted in an increased excitability of prefrontal cortex pyramidal neurons in male, but not female, $BDNF^{+/Met}$ mice. This study revealed the necessity of examining sex as a biological variable in neuropsychiatric disorders and provides avenues for exploring targeted therapies for genetic variations in neural development.

Moreover, MSPS members have worked on metabolic and endocrine physiology for many years. Here, Evans et al. examined the correlation between leptin resistance and cardiac vagal postganglionic (CVP) neuronal dysfunction in type 2 diabetes mellitus (T2DM). Leptin acts on pro-opiomelanocortin (POMC) neurons to regulate satiety. However, in T2DM, leptin resistance develops along with complications such as CVP neuronal dysfunction. In a rodent model using a high-fat diet and low-dose streptozotocin, the authors observed reductions in leptin receptor expression and uncoupling protein 2 in CVP neurons as T2DM progressed and reduced cardiac parasympathetic activity, possibly due to neuronal remodeling and insulin resistance.

Monaco and Davis reviewed the angioregression of corpus luteum and factors associated with luteolysis on luteal vasculature. This review article is an excellent summary of the work in Dr. John S. Davis's laboratory at the University of Nebraska Medical Center (UNMC) and other research groups focusing on corpus luteum in the last 3 decades. This article extensively summarizes the essential roles of pro-angiogenic, anti-angiogenic, and pro-inflammatory factors involved in luteal angioregression, such as vascular endothelial growth factor, thrombospondin 1, and tumor necrosis factor alpha. Besides, this review outlines

the underlying mechanisms in luteal angioregression, including vascular physiology and endothelial cell apoptosis.

Overall, the articles contained in this Research Topic fully reflect the width and depth of the research among MSPS members. MSPS will continue to promote the creation, application, and translation of novel theories, innovative methodologies, and advanced therapeutics to support the development of modern physiology and to improve human health and welfare in America's Heartland.

Author contributions

SN: Writing – original draft, Writing – review and editing. HZ: Writing – original draft, Writing – review and editing. SC: Writing – original draft, Writing – review and editing. HS: Conceptualization, Writing – review and editing, Writing – original draft. WC: Writing – original draft, Funding acquisition, Resources, Writing – review and editing, Conceptualization, Project administration, Supervision, Visualization.

Funding

The author(s) declare that financial support was received for the research and/or publication of this article. This work was supported in part by the US Department of Defense (W81XWH2110089 to WC; FA9550-23-1-0495 to the University of South Dakota), the American Heart Association Career Development Award (855260 to WC), the US Department of Education (P116Z240151 to the University of South Dakota, supervised by WC and others), and the South Dakota Board of Regents (Governor's Research Fund to WC).

Acknowledgments

We thank the many reviewers who reviewed the manuscripts submitted to this Research Topic and the independent editors who handled and reviewed specific manuscripts in this Research Topic.

Conflict of interest

The authors declare that the research was conducted in the absence of any commercial or financial relationships that could be construed as a potential conflict of interest.

The author(s) declared that they were an editorial board member of Frontiers, at the time of submission. This had no impact on the peer review process and the final decision.

Generative AI statement

The author(s) declare that no Generative AI was used in the creation of this manuscript.

Publisher's note

frontiers | Frontiers in Physiology

TYPE Original Research
PUBLISHED 08 June 2023
DOI 10.3389/fphys.2023.1208153

OPEN ACCESS

EDITED BY
Harold D. Schultz,
University of Nebraska Medical Center,
United States

REVIEWED BY
Lai-Hua Xie,
Rutgers, The State University of New Jersey, United States
Sathish Kumar Natarajan,
University of Nebraska-Lincoln,
United States
Paras Kumar Mishra,
University of Nebraska Medical Center,
United States

*CORRESPONDENCE
Xuejun Wang,
xuejun.wang@usd.edu

†These authors have contributed equally to this work

RECEIVED 18 April 2023
ACCEPTED 26 May 2023
PUBLISHED 08 June 2023

CITATION
Lira JR, Guymon AL, Yang L, Sternburg JO, Giri S and Wang X (2023), The double-hit protocol induces HFpEF and impairs myocardial ubiquitin-proteasome system performance in FVB/N mice.
Front. Physiol. 14:1208153.
doi: 10.3389/fphys.2023.1208153

The double-hit protocol induces HFpEF and impairs myocardial ubiquitin-proteasome system performance in FVB/N mice

Jose R. Lira†, Andrew L. Guymon†, Liuqing Yang, Jack O. Sternburg, Samiksha Giri and Xuejun Wang*

Division of Basic Biomedical Sciences, University of South Dakota Sanford School of Medicine, Vermillion, SD, United States

Heart failure with preserved ejection fraction (HFpEF) is a leading cause of death and disability, with its prevalence surpassing that of heart failure with reduced ejection fraction. Obesity and hypertension are often associated with HFpEF. HFpEF can be modeled through simultaneous metabolic and hypertensive stresses in male C57BL/6N mice provoked by a combination treatment of a high-fat diet (HFD) and constitutive nitric oxide synthase inhibition by Nω-nitro-L-arginine methyl-ester (L-NAME). Ubiquitin-proteasome system (UPS) dysfunction was detected in many forms of cardiomyopathy, but whether it occurs in HFpEF remains unknown. We report successful modeling of HFpEF in male FVB/N mice and, by taking advantage of a transgenic UPS reporter mouse, we have detected myocardial UPS functioning impairment during HFpEF, suggesting a pathogenic role for impaired protein degradation in the development and progression of HFpEF.

KEYWORDS

heart failure with preserved ejection fraction (HFpEF), high fat diet (HFD), Nω-nitro-L-arginine methyl-ester (L-NAME), ubiquitin-proteasome system (UPS), FVB/N mice

Introduction

Heart failure with preserved ejection fraction (HFpEF) is a lethal clinical syndrome associated with poor quality of life and substantial healthcare resource utilization comprising over half of all heart failure but with very limited pharmaceutical interventions (Dunlay et al., 2017). From clinical understanding of HFpEF in humans, HFpEF is strongly associated with numerous comorbidities including hypertension, obesity, diabetes, exercise intolerance, atrial fibrillation, chronic kidney disease, and coronary artery disease (Shah et al., 2013a). Notably, HFpEF is not strongly associated with acute coronary syndrome; instead, it is accompanied by a plethora of comparatively more chronic diseases. Such accompaniment substantially increases the difficulty of engineering a HFpEF mouse model that accurately recapitulates the disease in an efficient amount of time. In lieu of this, the "two-hit" HFpEF mouse model utilizes the two most dominant avenues of HFpEF pathology: hypertension and obesity/metabolic syndrome. The "two-hit" hypothesis subjected C57BL/6N wild-type mice to a treatment of high fat diet (HFD) and Nω-nitro-L-arginine methyl-ester (L-NAME) to produce a HFpEF mouse model that recapitulates numerous hallmarks of HFpEF including hypertension, obesity, left ventricular myocardial remodeling, exercise intolerance in the absence of significant histopathological, molecular, or strength

abnormalities in skeletal muscle, increased LV filling pressure, increase in lung weight, cardiomyocyte hypertrophy, cardiac fibrosis, myocardial capillary rarefaction but maintained left ventricular (LV) ejection fraction (EF) (Schiattarella et al., 2019). The "two-hit" HFpEF mouse model has quickly become one of the leading HFpEF animal models.

The pathophysiology of HFpEF is complex and is not well understood. However, some hallmark characteristics remain. End-diastolic pressure elevation occurs due to an intricate interplay between diastolic malfunction, elusive systolic malfunction, and reduced atrial, LV, and arterial compliance (Gevaert et al., 2019). Most HFpEF patients demonstrate multiple pathological derailments, including cardiac and noncardiac dysfunction. Cardiac elements include diastolic dysfunction, reduced cardiac output reserve, atrial fibrillation, and coronary artery disease. In contrast, noncardiac elements include reduced vasodilation, increased arterial stiffness, ventilatory dysfunction, skeletal myopathy, activation of the autonomic nervous system, and renal dysfunction (Gevaert et al., 2019). Underlying pathologies may also be classified according to their contribution to endothelial damage (increased inflammation and decreased repair), exercise intolerance due to cardiac and noncardiac mechanisms, and comorbidities such as aging, metabolic syndrome, and iron deficiency (Gevaert et al., 2019). Clearly, numerous interactions account for the HFpEF phenotype, albeit some underlying pathologies may dominate in individual patients (Borlaug, 2014). Markedly important is the ambitious attempt to deepen our understanding of HFpEF by developing animal models that recapitulate not only the presenting symptoms of HFpEF but also the diverse array of molecular abnormalities.

The molecular pathophysiology of HFpEF is aberrantly complex and fluid, citing endothelial dysfunction in the setting of metabolic inflammation, abnormalities in nitric oxide (NO) synthesis and bioavailability (Chistiakov et al., 2015; Schiattarella et al., 2019), impeded endothelial repair (Gevaert et al., 2019), cardiomyocyte maladaptation impairing diastolic function (Leucker and Jones, 2014), fibroblast dysfunction, and recent discoveries of misfolded protein accumulation (Gonzalez-Lopez et al., 2015; Wang and Wang, 2020). Targeted degradation of misfolded proteins by the ubiquitin-proteasome system (UPS) is pivotal to protein quality control (Wang and Wang, 2020), a vital part of the mechanisms maintaining proteostasis in the cell (Frankowska et al., 2022). Approximately 13% of HFpEF patients suffer from wild-type transthyretin (TTR) amyloidosis stemming from increased cardiac protein deposition (Gonzalez-Lopez et al., 2015). Myocardial UPS functional insufficiency was observed in a widely used mouse model of cardiac proteinopathy where pre-amyloid oligomers are increased in cardiomyocytes (Chen et al., 2005; Liu et al., 2006). Animal model and cell culture studies have established both the sufficiency and, in some cases, the necessity of proteasome functional insufficiency as a significant pathogenic factor in the heart (Wang and Robbins, 2014). Clinically, the proteasome inhibiting drugs bortezomib and carfilzomib have been shown to cause cardiotoxicity, including heart failure (Enrico et al., 2007; Das et al., 2022; Makris et al., 2022; Georgiopoulos et al., 2023).

Potential treatments addressing cardiac proteotoxicity seem within reach, further emphasizing the urgency of exploring impaired proteostasis as a pathological basis of HFpEF. Overexpression of proteasome activator 28α (PA28α) is cardioprotective against numerous challenges without altering normal protein turnover or cardiac function (Li et al., 2011; Wang and Wang, 2020). Potentially meeting HFpEF at the intersection of diabetes and HF, overexpression of PA28α attenuates diabetes-induced proteotoxic stress and cardiomyopathy (Li et al., 2017). An upregulated unfolded protein response (UPR) ameliorated the diastolic dysfunction essential to HFpEF, suggesting that impaired proteostasis plays a key role in HFpEF pathogenesis (Schiattarella et al., 2019). By activating the cGMP-dependent protein kinase (PKG), phosphodiesterase 5 (PDE5) inhibition by sildenafil slows down cardiac disease progression in a mouse model of $CryAB^{R120G}$-based cardiac proteinopathy (Ranek et al., 2013); and inhibition of PDE1 induces cAMP-dependent protein kinase (PKA) and PKG-mediated promotion of proteasomal degradation of misfolded proteins and thereby effectively treats diastolic malfunction and delays premature death in $CryAB^{R120G}$-based cardiac proteinopathy mice (Zhang et al., 2019).

Impaired myocardial UPS performance has been observed in both pressure overload induced HF and diabetic cardiomyopathy (Ranek et al., 2015; Li et al., 2017). Plus, both myocardial UPS impairment and diastolic malfunction are co-existed in mouse models of cardiac proteinopathy (Zhang et al., 2019). Since metabolic syndrome/diabetes and hypertension are common co-morbidities of HFpEF, it is very likely that myocardial UPS functioning is impaired during HFpEF but no reported studies have examined that. Perhaps the most powerful tool to probe *in vivo* UPS performance is the transgenic mouse model with ubiquitous expression of a green fluorescence protein (GFP) that has been modified with carboxyl fusion of degron CL-1 (Bence et al., 2001), known as GFPdgn that has been validated as an inverse UPS functioning reporter (Kumarapeli et al., 2005). Employing the GFPdgn mice has allowed researchers to unveil *in vivo* UPS dysfunction in various cardiac disorders (Chen et al., 2005; Liu et al., 2006; Li et al., 2011; Li et al., 2017). Applying the "two-hit" hypothesis to FVB/N GFPdgn transgenic mice may provide an animal model of HFpEF that accurately recapitulates the disease's diverse etiologies and pathologies while probing into the disease's proteotoxic nature and UPS dysfunction.

Here we report that the HFD+L-NAME treatment can induce HFpEF in FVB/N male mice; myocardial UPS functioning is impaired during HFpEF and warrants further comprehensive investigation.

Methods

Experimental animals and treatments

All experiments followed ethical and legal standards according to The Guide for the Care and Use of Laboratory Animals published by the US National Institutes of Health (NIH Publication 8th edition, update 2011) and the Institutional Animal Care and Use Committee of the University of South Dakota. The creation and validation of the GFPdgn transgenic mice for monitoring the dynamic changes in UPS performance *in vivo* was previously described (Kumarapeli

TABLE 1 qPCR Primer Sequences.

mRNA target	Sense/Antisense	Primer sequence (5′-3′)
Gapdh	Sense	ATGACATCAAGAAGGTGGTG
	Antisense	CATACCAGGAAATGAGCTTG
Nppa	Sense	GGAGGAGAAGATGCCGGTAGA
	Antisense	GCTTCCTCAGTCTGCTCACTC
Nppb	Sense	CTGCTGGAGCTGATAAGAGA
	Antisense	TGCCCAAAGCAGCTTGAGAT
GFPdgn	Sense	TCTATATCATGGCCGACAAGCAGA
	Antisense	ACTGGGTGCTCAGGTAGTGGTTGT
Pln	Sense	CAATACCTCACTCGCTCGGC
	Antisense	GCGGTGCGTTGCTTCCC

et al., 2005). Littermate male GFPdgn transgenic and non-transgenic mice in the FVB/N inbred background at 6–7 months of age were randomly assigned to the CHOW group or the HFD+L-NAME group throughout the study. The CHOW (control diet) group had unrestricted access to a standard murine chow diet of 19.1% protein, 6.5% fat, and 47% carbohydrates (2020X from Teklad) and water. The HFD+L-NAME group had unrestricted access to an HFD where 60% of the calories were from fat (lard and soybean oil), 20% from proteins, and 20% from carbohydrates (D12492, Research Diets, Inc) and water spiked with L-NAME (0.5 g/L; Sigma Aldrich, Catalog #: N5751-10G). Body weight of each mouse was measured weekly for 18 weeks at the same time of day. The age of mice at the initiation time of this study (6–7 months of age), an age that should be more clinically relevant to HFpEF that naturally occurs in humans compared to the much younger age (8–10 weeks of age) used in the prior report of this double-hit method (Schiattarella et al., 2019).

Glucose tolerance test

A bolus intraperitoneal injection of 20% glucose solution (1 g/kg in water) was conducted after 6-h fasting. Blood from the tail was collected and measured immediately before (0 min) and 15, 30, 60, 90, and 120 min after the injection using Bayer Contour® Next EZ Glucose Meter Kit and Contour® Next Blood Glucose Test Strips.

Exercise tolerance test

Mice ran on an Exer-3/6 treadmill with Stimulus Detection (Columbus Instruments, Columbus, OH) on a 10-degree incline. The day before the test, animals were subjected to an acclimation at 5 m/min for 4 min, then increased to 10 m/min for 10 min. For the final test, mice were randomly grouped in a lane and perform at 5 m/min for 4 min then at 14 m/min for 2 min. Speed was increased by 2 m/min every 2 min until exhaustion. Exhaustion is defined as the animal getting shocked continuously for 5 s. The Treadmill Software (Columbus Instruments, Columbus, OH) measured running distance, time ran, and exhaustion.

Non-invasive blood pressure measurement

The tail-cuff method was used to measure systolic blood pressure. Animals were trained in the instrument for at least 2 months before the final test. The mice were acclimated in the temperature-controlled chamber for 15 min, and results were measured, then another 15 min were allowed for resting data. Blood pressure was then recorded for 4 days, and readings averaged.

Echocardiography

Echocardiography was performed as previously reported in a double-blinded manner (Zhang et al., 2019). In brief, mice were kept in light anesthesia with inhalation of Isoflurane (4% for induction and 1.5% for maintenance) via a face mask. Transthoracic echocardiography was performed using the Visual Sonics Vevo 3100 system and a 40-MHz probe (FUJIFILM Visual Sonics, Toronto, ON, Canada). A two-dimensional guided M-mode episode was acquired through the left ventricular (LV) anterior and posterior walls at short axis view. Parameters of LV were derived from primary measurements using Vevo LAB software.

Western blot analysis

Ventricular myocardial tissues were homogenized in 1x loading buffer (41 mM tris-HCI, 1.2% SDS, 8% glycerol). The homogenates were boiled for 5 min, then centrifuged for 20 min at 4°C at 14,000 rpm, and the supernatant was collected. Protein concentration of the samples were measured using Pierce BCA Protein Assay Reagent (Thermofisher, Rockford, Illinois). Equal amounts of proteins were loaded to each lane of a 10% SDS-PAGE

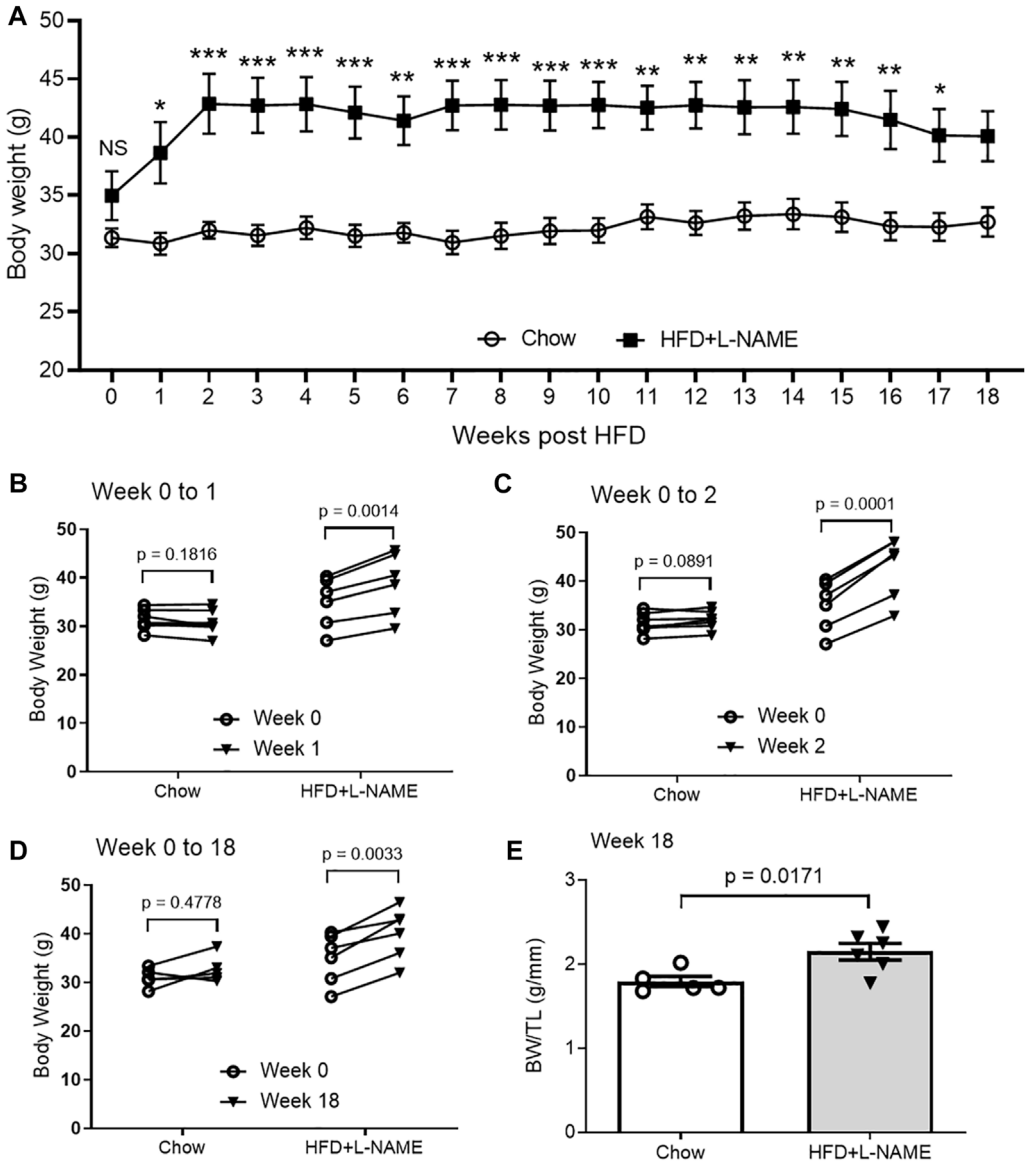

FIGURE 1
Changes in body weight (BW) of HFD+L-NAME or chow treated mice. **(A)**, Comparison of the time courses of changes in BW measured immediately before (Week 0) and weekly after the initiation of the HFD or control diet (Chow) treatment. Shown are line graphs superimposed by mean ± SEM of each time point. The *p* values shown are adjusted *p* values derived from multiple two-sided unpaired *t*-tests with correction for multiple comparisons using the Bonferroni-Dunn method; NS, not significant; $*p < 0.05$, $**p < 0.01$, $***p < 0.001$. The Chow group started with 7 mice but a mouse dropped out at Week 8 and another at Week 14. The HFD+L-NAME group had 6 mice throughout. **(B–D)**, Longitudinal comparison of BW from Week 0 to Week 1 **(B)**, to Week 2 **(C)**, or to Week 18 **(D)**. Each circle represents a mouse. *P* values are derived from two-sided paired *t*-tests. **(E)**, BW/TL ratio measured at terminal experiment (Week 18). TL, tibial length. Shown are scatter plots superimposed by mean ± SEM; each circle or dot represents a mouse. The *p*-value is derived from two-sided unpaired *t*-test.

gel and fractionated by electrophoresis, then electrically transferred to a PVDF membrane overnight in 4°C. The PVDF membrane was washed and incubated in blocking buffer for 60 min before being probed with the primary antibody overnight followed by incubation with HRP-conjugated secondary antibodies. The bound secondary antibodies on the PVDF were then detected with the SuperSignal West Pico PLUS Chemiluminescent Substrates (ThermoScientific) and imaged with a ChemiDoc MP imaging system (Bio-Rad). Densitometry quantification was performed using the ImageLab software (Bio-Rad).

RNA isolation, reverse transcription, and real time PCR (qPCR)

Total RNA was extracted from left ventricular myocardium using TRI Reagent® (Molecular Research Center Inc., Cincinnati, OH). Thermo Scientific™ NanoDrop 2000 UV Spectrophotometer was used to determine the concentration and purity of the RNA. Reverse transcription utilized the High Capacity cDNA Reverse Transcription Kit (Applied Biosystems™) and a total of 900 ng of extracted RNA as template. qPCR reactions used 2 µL of 1:

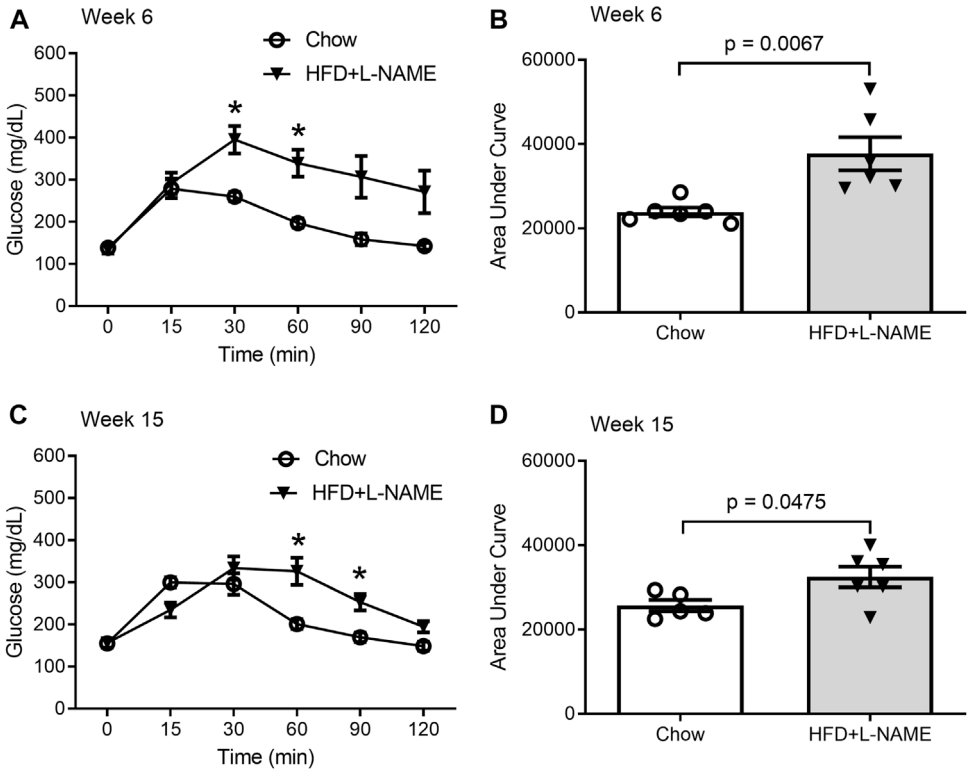

FIGURE 2
Glucose tolerance tests (GTTs) performed at week 6 and 15. A peritoneal injection of 20% glucose solution (1 g/kg) was administered after 6-h fasting. Blood from the tail was collected immediately before (0 min) and 15, 30, 60, 90, and 120 min after the injection for glucose concentration measurement. **(A,B)**, GTTs at week 6. Shown are the time course of blood glucose levels during GTTs **(A)** and the area under curve (AUC) comparison **(B)** between the Chow and the HFD+L-NAME groups. Multiple t-tests reveal the P values for comparisons at 0, 15, 30, 60, 90, and 120 min are respectively 0.791, 0.711, 0.003, 0.002, 0.016, and 0.031; * denotes that the difference at 30- and 60-min is statistically significant after correction for multiple comparisons using the Holm-Sidak method. **(C,D)**, GTTs at week 15 weeks. Shown are the time course of blood glucose levels during GTTs **(C)** and the area under curve (AUC) comparison **(D)** between the Chow and the HFD+L-NAME groups. Multiple t-tests reveal the P values for comparisons at 0, 15, 30, 60, 90, and 120 min are respectively 0.955, 0.017, 0.35, 0.008, 0.006, and 0.026; * denotes that the difference at 60 and 90 min is statistically significant after correction for multiple comparisons using the Holm-Sidak method. Each circle or dot in B and D represents a mouse and *p* values are derived from two-sided unpaired *t*-tests, the same for all subsequent Figures.

10 nuclease-free water diluted cDNA solution and PowerUp SYBR Green master mix (Applied Biosystems) for the following gene products: Atrial Natriuretic Factor (*Nppa*), Brain Natriuretic Peptide (*Nppb*), *GFPdgn*, Phospholamban (*Pln*), and Glyceraldehyde-3-phosphate dehydrogenase (*GAPDH*). All reactions for target genes (*Nppa*, *Nppb*, *GFPdgn*, and *Pln*) were performed in duplicate. The $2^{-\Delta\Delta CT}$ relative quantification method using *GAPDH* as the normalization gene was used to compute the relative expression of the target genes. The primer sequences for the qPCR reactions are shown in Table 1.

Statistical methods

GraphPad Prism software 9.2.0 (GraphPad Software, Inc., La Jolla, CA) was used for all statistical analysis. Results are presented as the mean ± SEM. Datum was deemed an outlier according to the Grubbs test ($p < 0.05$). Two-tailed unpaired Student's t-test was used unless indicated otherwise. In addition, the Welches correction for unequal variance was used when analyzing gene expression results. Researchers were blinded to the individual genotypes during the data collection and data analysis. A *p*-value or adjusted *p*-value of <0.05 was considered statistically significant.

Results

The "double-hit" method induced metabolic syndrome in FVB/N mice

HFD can induce obesity and the latter inevitably increases body weight (BW). Thus, we measured mouse BW immediately before (week 0) and weekly after initiation of the HFD+L-NAME treatment. No significant changes in BW were observed in the Chow group throughout the 18 weeks of study (Figure 1). The difference in BW between the Chow and the HFD+L-NAME groups was not statistically significant at week 0 ($p > 0.9999$) but became significant from week 1 to week 17 (Figure 1A). Self-comparisons show significant BW increases in the HFD+L-NAME group as early as week 1 ($p = 0.0014$; Figure 1B) and the increases peaked at week 2 ($p = 0.0001$; Figures 1A,C) and plateaued thereafter (Figures 1A–D). Longitudinal BW comparisons between week 0 and week 1

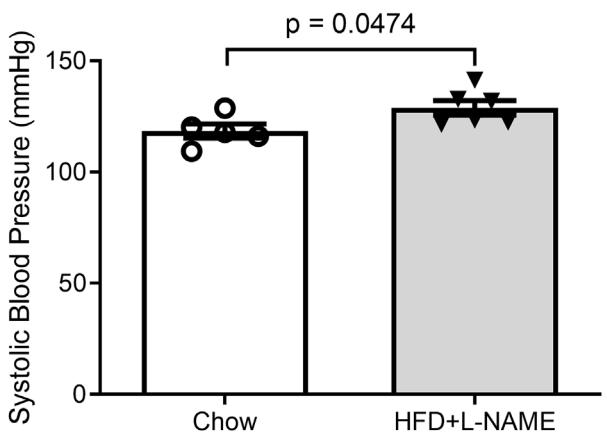

FIGURE 3
Systolic blood pressure measured at week 17 with the tail-cuff method.

(Figure 1B, p = 0.182 and 0.001 for the Chow and the HFD+L-NAME groups, respectively), between week 0 and week 2 (Figure 1C, p = 0.0891 and 0.0001), or between week 0 and week 18 (Figure 1D, p = 0.4778 and 0.0033) are also summarized in Figure 1. The BW to tibial length (TL) ratio (BW/TL) of the HFD+L-NAME group was greater than that of the Chow group (p = 0.0171, Figure 1E) at week 18 when the terminal experiments were performed.

Obesity can cause glucose intolerance; hence, we performed glucose tolerance tests on these animals at weeks 6 and 15. A bolus intraperitoneal injection of glucose induced increases in blood glucose levels in both groups, but the peak increase was significantly greater (week 6) and the increases lasted longer (weeks 6 and 15) in the HFD+L-NAME group compared with the Chow group (Figure 2), indicating that glucose intolerance was induced as early as week 6 by HFD+L-NAME. Administration of L-NAME is known to induce hypertension (Schiattarella et al., 2019); hence, we measured blood pressure using the tail-cuff method at week 17 and found that systolic blood pressure was significantly higher in the HFD+L-NAME group than in the Chow group (p = 0.0474, Figure 3). All three components of metabolic syndrome: hypertension, obesity, and glucose intolerance, are at least common comorbidities of HFpEF (Dunlay et al., 2017), and even can be an aspect of the multifactorial comorbidity driven pathology of the HFpEF syndrome (Tourki and Halade, 2021). The increased body weight, glucose intolerance, and hypertension observed in the HFD+L-NAME group are in alignment with recapitulating the metabolic syndrome central to HFpEF. and provide a catalyst for afterload induced cardiac remodeling of the left ventricle. Together, these pathologies formed the foundation for more advanced HFpEF manifestations.

The "double-hit" method induced cardiac hypertrophy in FVB/N mice

Serial echocardiography was performed to evaluate the dynamic changes in cardiac morphometry and function in live mice. Consistent with an increase in systolic blood pressure observed in the HFD+L-NAME group, left ventricular (LV) concentric hypertrophy was detected at both week 7 and week 15. This is evidenced by significantly greater LV end-diastolic posterior wall thickness (LVPW; d, Figure 4) and a tendency of deceased LV end-diastolic chamber diameter (Figure 5) in the HFD+L-NAME mice, compared with the Chow group disclosing diastolic dysfunction.

At the terminal experiment, we detected that LV myocardial mRNA levels of fetal genes *Nppb* (p = 0.1092) and *Nppa* (p = 0.1327) tended to be higher and *Pln* mRNA levels (p = 0.1154) lower in the HFD+L-NAME group than in the Chow group (Figure 6) although the differences did not reach a statistical significance due to a large variation within each group.

HFD+L-NAME impaired exercise tolerance in FVB/N mice

Exercise tolerance tests performed at both weeks 7 and 16 revealed that the maximum distance and time of running to exhaustion by the HFD+L-NAME mice were markedly shorter than that by the Chow control group (Figure 7). At week 7 the Chow group ran an average of 269 m (18:07 min) while the HFD+L-NAME group ran an average of 168 m (13:30 min) prior to exhaustion. Similarly, at week 16 the Chow group ran 303 m (19: 51 min) while the HFD+L-NAME group ran 167 m (13:21 min). These data indicate that exercise intolerance occurred as early as 7 weeks after HFD+L-NAME treatment. Reduced exercise tolerance including dyspnea and fatigue on mild exertion are common complaints seen in HFpEF patients clinically. The exercise intolerance in the HFD+L-NAME group indicate that the mouse model began to recapitulate the clinical aspects of HFpEF as early as week 7.

Preserved ejection fraction

Despite the numerous characteristics of heart failure in the HFD+L-NAME treated mice, their LV ejection fraction (EF) and fractional shortening (FS) were not decreased throughout the study compared with those of the Chow control group (Figure 8), indicating that the systolic function was preserved in the HFD+L-NAME treatment group, one of the essential criteria for the diagnosis of HFpEF.

Evidence of UPS impairment

The GFPdgn transgenic mice, which were created and have been maintained in the FVB/N inbred background, have been extensively used to probe changes in UPS functioning in mice (Chen et al., 2005; Liu et al., 2006; Li et al., 2011); in absence of GFPdgn protein synthesis, the steady state level of GFPdgn protein inversely reflect UPS performance in the tissue or cell examined (Bence et al., 2001; Kumarapeli et al., 2005). We observed equivalent myocardial mRNA expression (p = 0.241) but significantly elevated GFPdgn protein levels (p = 0.0497) and

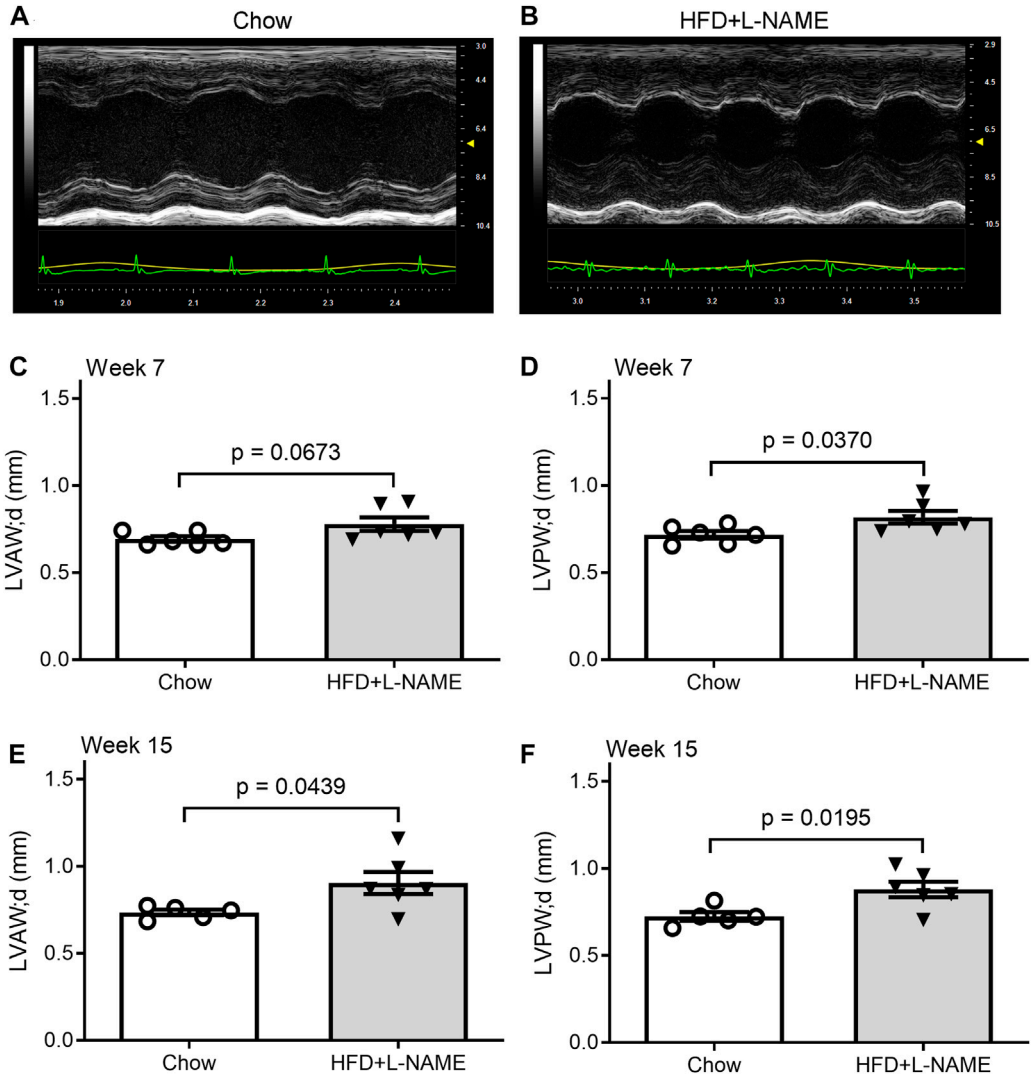

FIGURE 4
HFD+L-NAME induced cardiac hypertrophy as revealed by serial echocardiography. **(A,B)**, Representative echographs of the Chow and the HFD+L-NAME groups recorded at week 15. **(C)**, Left ventricular anterior wall thickness at the end of diastole (LVAW; d) at week 7. **(D)**, Left ventricular posterior wall thickness at the end of diastole (LVPW; d) at week 7. **(E)**, LVAW; d at week 15. **(F)**, LVPW; d at week 15.

greater GFPdgn protein to mRNA ratios (p = 0.0379) in the HFD+L-NAME treatment group compared with the CHOW group (Figure 9), indicating that elevated GFPdgn protein is not due to increased transcription, which provides compelling evidence that myocardial UPS performance is impaired in the HFpEF mouse.

Discussion

HFpEF is one of the most debilitating, lethal, and prevalent healthcare challenges of the twenty-first century (Dunlay et al., 2017), with very limited proven treatments. The uncontrolled nature of HFpEF is largely due to the challenges in effectively recapitulating the disease in animal models and poorly understood of underlying pathogenic mechanisms (Horgan et al., 2014). The groundbreaking "two-hit" mouse model produced HFpEF in male C57BL/6N mice (Schiattarella et al., 2019), representing a milestone for HFpEF research. Here, we report successful emulation of HFpEF using the "two-hit" method in FVB/N mice, paving the way for use of mice with the FVB/N inbred background to further study HFpEF. This is important because many genetically engineered mouse models, especially those harboring a transgene driven by the murine Myh6 promoter, have been made in the FVB/N inbred background. The use of those mouse genetic models is expected to facilitate the experimental investigations into the pathogenesis and therapies of HFpEF. Moreover, taking advantage of the UPS performance reporter mouse, the present study also provides exciting evidence indicative of UPS malfunction in this HFpEF model, identifying a potentially new pathogenic pathway for HFpEF.

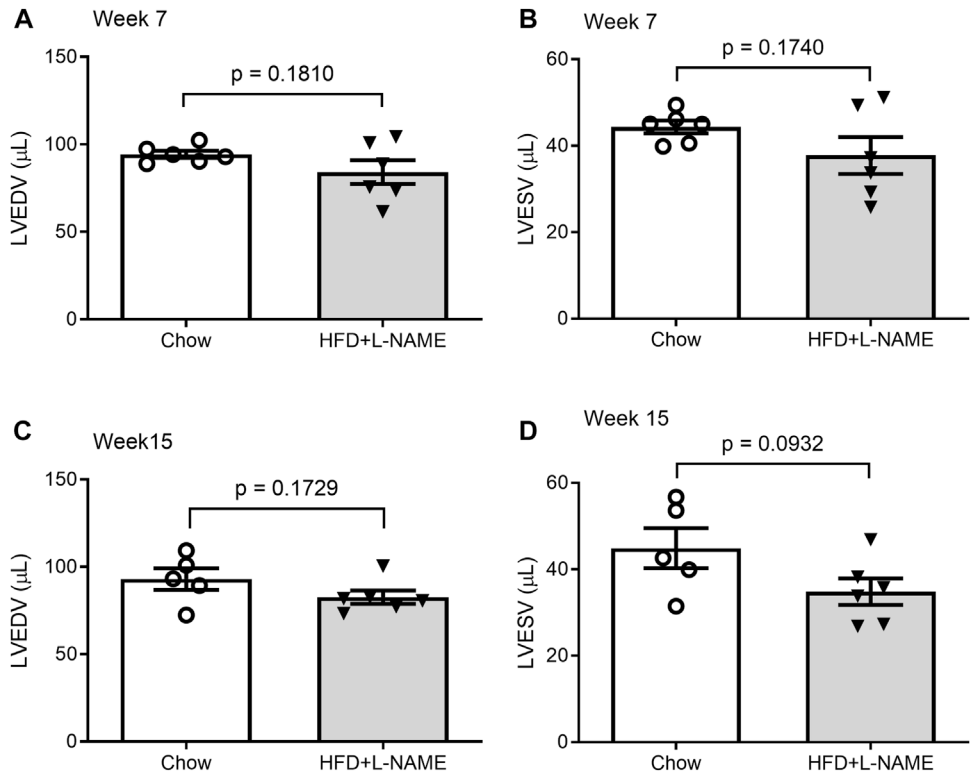

FIGURE 5
Comparisons of LV end-diastolic volume (LVEDV) and end-systolic volume (LVESV) between the Chow and the HFD+L-NMAE groups at week 7 **(A,B)** and week 15 **(C,D)**.

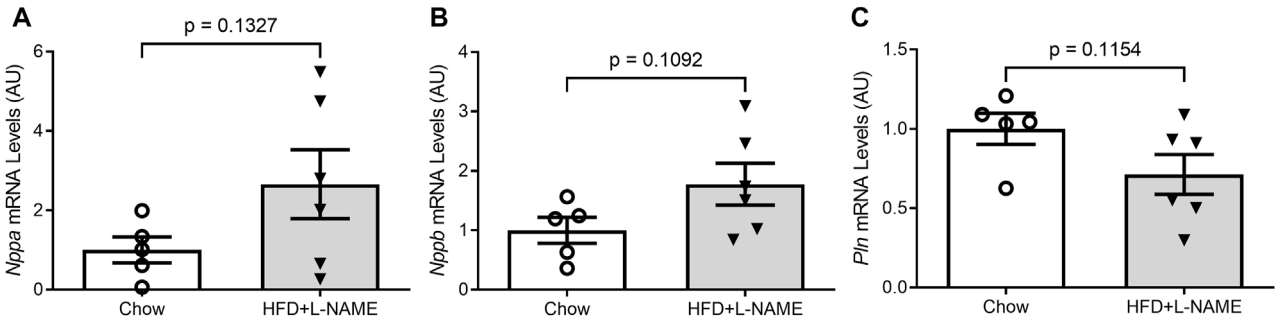

FIGURE 6
Reactivation of the fetal gene program in the ventricles. At the terminal experiment (week 18), LV myocardium was sampled, preserved in the RNA-Later reagent, and stored in −80°C until total RNA extraction. Total RNA was used for reverse transcription to synthesize the first-strand cDNA that was subsequently used for real time PCR to measure the mRNA levels with gene-specific primer sets for *Nppa* **(A)**, *Nppb* **(B)**, and *Pln* **(C)**.

Induction of HFpEF by the two-hit protocol in FVB/N male mice

The reactivation of the fetal gene program and a downregulation of *PLN* are often associated with and indicative of pathological hypertrophy and heart failure (Loffredo et al., 2014) (Man et al., 2018). Hence, these changes in gene expression are consistent with the significantly increased wall thickness revealed by echocardiography in the HFD+L-NAME group and the conclusion of induced cardiac remodeling in the HFD+L-NAME group. Clinically, diastolic dysfunction in HFpEF results in reduced cardiac output with maintained EF due to limited cardiac filling but at higher left ventricular end diastolic pressures. The increased systolic and diastolic wall thickness, while not essential, are characteristic of HFpEF as traditionally defined (Shah, 2013), while the reduction in *PLN* mRNA is indicative of the signature diastolic dysfunction of

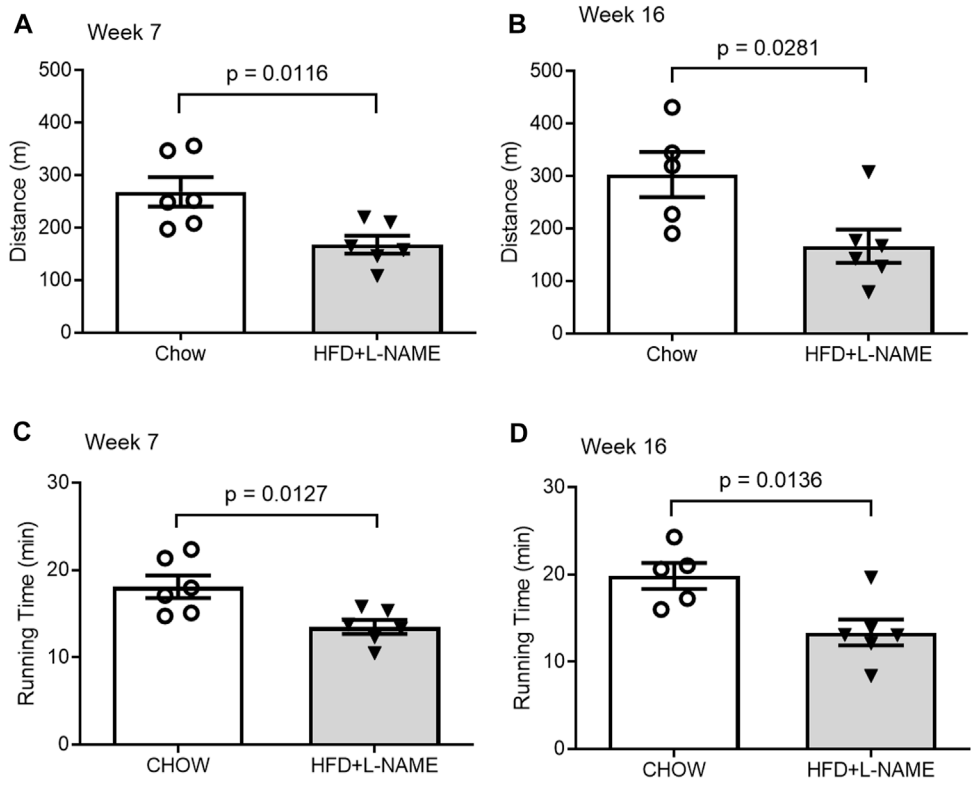

FIGURE 7
Comparisons of exercise tolerance between the Chow and the HFD+L-NAME groups at week 7 **(A,C)** and week 16 **(B,D)**.

HFpEF (Grote Beverborg et al., 2021). Further, under the same "two-hit" hypothesis, diastolic dysfunction has been well described by invasively and non-invasively measured elevated LV filling pressures, histologically reported cardiac fibrosis and capillary rarefaction, pulmonary congestion, and reduction in coronary flow reserve. Although clear exercise intolerance was observed, the "two-hit" hypothesis is known to produce exercise intolerance without histopathological, molecular, or strength abnormalities in skeletal muscle indicating that decrement in exercise intolerance is not due to a skeletal muscle deficiency (Schiattarella et al., 2019). Taken together, the hypertensive afterload stress and metabolic syndrome pathologies, likely created an environment for pathologic hypertrophic cardiac remodeling and diastolic dysfunction to occur, a hallmark of HFpEF. Despite these changes, serial echocardiographic analyses displayed preserved ejection fraction across both groups through at least week 15 (Figure 8). Therefore, the present study demonstrates compellingly that HFpEF can be produced with the "two-hit" protocol in male FVB/N mice.

HFpEF is traditionally considered a disease of the elderly resulting in challenges studying the disease *in vivo* in a time and cost-efficient manner. To construct a model that most quickly emulates the complete severity and mortality of HFpEF, male mice were used exclusively (Patten, 2007) (Tromp et al., 2018). In an aim of striking a balance between time efficiency and model validity, mice six to 7 months of age were used. While the maiden voyage of the two-hit hypothesis successfully recapitulated the disease using mice 8–12 weeks of age (Schiattarella et al., 2019), mice 3 months senior likely accounted for the age-related etiology of HFpEF to a greater degree.

Conventionally, the "two-hit" HFpEF mouse model uses C57BL/6N wild-type mice (Schiattarella et al., 2019), a lineage traditionally renowned as the gold standard for producing diet induced obesity and metabolic syndrome. However, recent studies comparing FVB/N and C57BL/6J have begun to question this notion. FVB/N ob/ob and C57BL/6J ob/ob mice are used to study obesity and its comorbidities as both murine lineages are leptin deficient thus maximizing hunger and the effects of the HFD. Compared to the C57BL/6N ob/ob lineage, FVB/N ob/ob mice demonstrate increased hyperglycemia, whole body and muscle insulin resistance, and reduced clearance of circulating triglycerides (Haluzik et al., 2004), suggesting that the FVB/N murine lineage exhibits significant benefits over the C57BL/6J strain in modeling metabolic dysfunction, a quintessential comorbidity of HFpEF. Likewise, Nascimento-Sales et al. (2017), found that while C57BL/6N mice develop obesity more quickly than FVB/N mice, FVB/N mice actually show a significantly greater degree of metabolic intolerance after treatment with a HFD as evidenced by higher insulin resistance, greater liver steatosis, and a large degree of epididymal white adipose tissue induced inflammation. Notably, they conclude by recommending the FVB/N lineage as a new tool to uncover the complex multifactorial symptoms of obesity and metabolic syndrome of which HFpEF is inevitably intertwined.

Between 40%–50% of HFpEF patients are obese (Shah et al., 2013a). Similarly, 45% of HFpEF patients have diabetes (McHugh et al., 2019).

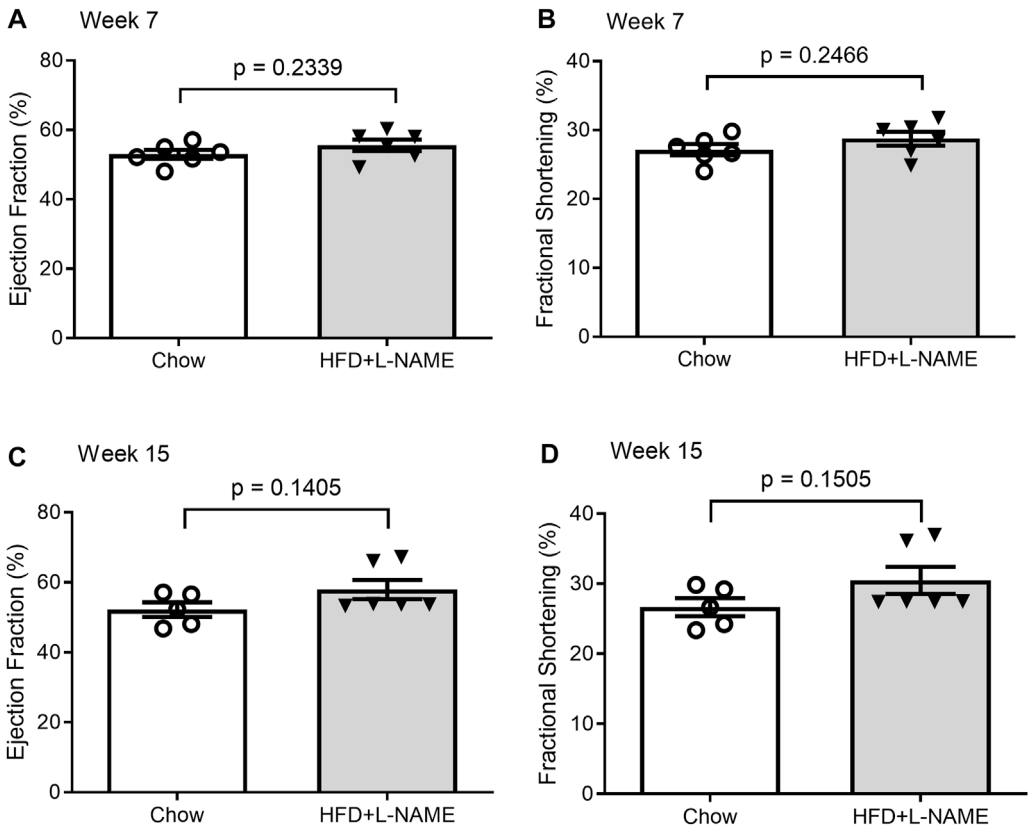

FIGURE 8
Comparisons of LV ejection fraction (EF) and fractional shortening (FS) between the Chow and the HFD+L-NMAE groups at week 7 **(A,B)** and week 15 **(C, D)**.

However, due to the decreased prevalence of diabetes relative to obesity, HFpEF is more specific towards the diabetic population. This is perhaps because HF and metabolic syndrome share numerous underlying derangements that result in increased HF risk including insulin resistance, metabolic derangements, endothelial dysfunction, oxidative stress, mitochondrial dysfunction, and autonomic neuropathy (Dhingra and Vasan, 2012; Oktay et al., 2013). Type 2 diabetes mellitus (T2DM) shares the pathologies of sodium retention, impaired skeletal muscle function, and metabolic derangements with HFpEF, implying an integrated pathogenesis of both diseases, (Shah et al., 2013b). As more insight into comorbid HFpEF and T2DM is acquired, it is anticipated physicians will be better equipped to provide effective unique treatments for commonly comorbid HFpEF and T2DM.

Further, Reduced exercise tolerance and increased myocardial remodeling are critical features of HFpEF (Paulus and Tschope, 2013; Gevaert et al., 2019). FVB/N mice demonstrate higher capabilities and cooperativity of daytime exercise tolerance testing (Gibb et al., 2016). In response to exercise tolerance training, FVB/N mice display increased cardiac remodeling compared to C57BL/6J mice (Massett and Berk, 2005; Gibb et al., 2016). A higher level of myocardium hypertrophy in response to increased exercise stress is suggestive that FVB/N mice may also develop a greater degree of cardiac remodeling due to increased afterload stress elicited by HFpEF hypertension.

Mouse models emulating HFpEF generally originate from three different avenues of the most prominent risk factors of HFpEF: hypertensive models, diabetic (obesity) models, and aging models (Horgan et al., 2014). The novel "two-hit" hypothesis developed a HFpEF mouse model from both the hypertensive and diabetic avenues. The FVB/NJ mice strain has been used to illuminate the pathologies of HFpEF through the aging model avenue (Koch et al., 2013). We report a HFpEF mouse model that potentially utilizes all three avenues of the most significant HFpEF murine models (hypertensive, metabolic dysfunction, and aging) to emulate HFpEF. Finally, applying the "two-hit" protocol to the FVB/NJ mice may not only emulate the clinical symptoms of HFpEF but could also optimize the exercise tolerance measurements, essential cardiac remodeling, and circadian misalignments of the disease (Massett and Berk, 2005; Gibb et al., 2016). A deeper understanding of the "two-hit" hypothesis and HFpEF pathophysiology may be explored by expanding the protocol across murine lineages, namely, the FVB/NJ lineage.

Impairment of UPS performance in HFpEF mice

The UPS is the primary pathway responsible for the targeted degradation of abnormal, misfolded, damaged, or oxidized proteins,

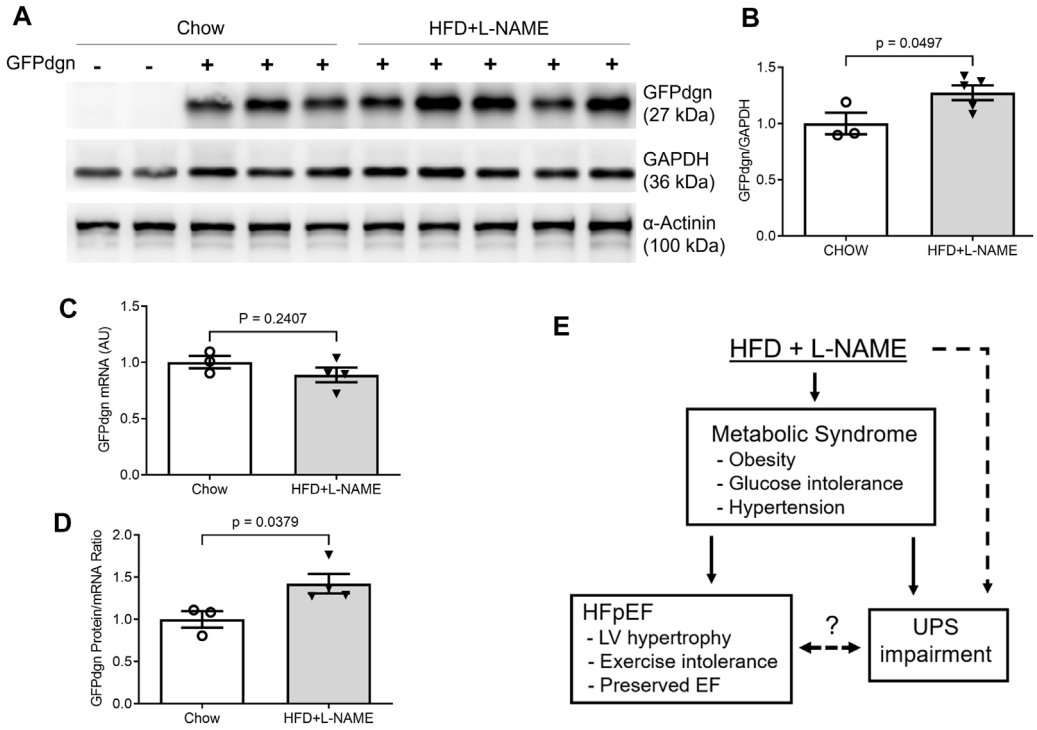

FIGURE 9
Myocardial mRNA and protein expression of GFPdgn in HFpEF and control mice. At the terminal experiment (week 18), a segment of left ventricular myocardium of each mouse was collected, snap-frozen in liquid nitrogen, and stored in a −80°C freezer until total protein extraction. The tissue preservation for total RNA extraction was the same as described in Figure 6. **(A,B)**, Representative images **(A)** and pooled densitometry data **(B)** of western blot analysis for myocardial GFPdgn. **(C)**, Comparison of GFPdgn mRNA levels as measured with qPCR. **(D)**, Comparison of GFPdgn protein/mRNA level ratios. **(E)**, A summary of overall findings. Dot line denotes a potential causative relationship. The question mark denotes the relationship remains to be determined. EF, ejection fraction; UPS, ubiquitin-proteasome system.

in addition to for the degradation of normal but no longer needed proteins (Wang et al., 2013). In response to the recent reports of accumulated misfolded proteins (Gonzalez-Lopez et al., 2015) and altered unfolded protein response (UPR) playing a pivotal role in the pathogenesis of HFpEF (Schiattarella et al., 2019), we hypothesized that myocardial UPS performance could be impaired during HFpEF. Beginning to examine this hypothesis, the present study applied the "two-hit" protocol to the transgenic mice with ubiquitous expression of GFPdgn, a surrogate substrate of the UPS (Kumarapeli et al., 2005). In absence of changes in GFPdgn protein synthesis, changes in its steady-state protein levels reflect inversely UPS performance (Kumarapeli et al., 2005). Notably, the GFPdgn mRNA expression between CHOW and HFD+L-NAME groups was not significantly different, but GFPdgn protein levels were elevated in the HFD+L-NAME group (Figure 9), indicating diminished UPS function in HFpEF. Such impairment is consistent with the other preliminary studies suggesting that the accumulation and mismanagement of misfolded, damaged, and abnormal proteins play a vital role in the development of HFpEF (Wang et al., 2014; Gonzalez-Lopez et al., 2015; Schiattarella et al., 2019).

Evidence of impaired UPS functioning in HFpEF beckons for further investigation to provide a deeper understanding of the pathogenesis and devise new treatment strategies for HFpEF. For example, it will be important to elucidate the main factors that impair UPS performance during HFpEF. To this end, both diabetes and hypertension have been shown to impair myocardial UPS performance and proteasome functional insufficiency (Ranek et al., 2015; Li et al., 2017), but more detailed molecular mechanisms remain to be delineated. It is also conceivable that UPS impairment could affect myocardial proteostasis and thereby cardiac function through both slowing down the turnover of normal proteins and accumulating abnormal proteins, and both are quite detrimental to the heart in many ways. Ultimately, we report successful modeling of HFpEF in male FVB/N mice and, by taking advantage of a transgenic UPS reporter mouse, we have detected myocardial UPS functioning impairment during HFpEF, suggesting a pathogenic role for impaired protein degradation in the development and progression of HFpEF but insist on further exploration (Figure 9E).

Limitations and future directions

This study has potential limitations. While the power of the study was sufficient for the primary readouts, the number of mice per group is not enough to decipher whether the GFPdgn transgenic expression has an impact on the occurrence of HFpEF. No female mice were included, leaving it untested whether the "double hit" method could cause HFpEF in

female FVB/N mice or not. Additionally, mice were treated with HFD+L-NAME for up to 18 weeks. Despite both Schiattarella et al. and our results providing convincing evidence of HFpEF within this time frame, the pathogenesis of HFpEF is known to develop over the course of decades in humans (Lam et al., 2011). It begs the question, was HFpEF established in its completeness within the 18-week treatment course? Would longer treatment periods elicit models with grander disease severity, more confluent outcomes, and ultimately a clearer window into HFpEF etiologies? In response, the degree of HFpEF could be graded through measurement of the E/A ratio during echocardiology. Murine blood pressures were measured using tail-cuff methodology instead of telemetry. While tail-cuff methods have been validated against telemetry for measuring more course changes in blood pressure, telemetry allows for a longer period of measurement, giving greater power to the study so that fewer animals are needed (Fraser et al., 2001). Likewise, echocardiology was used to measure ventricular wall thickness as a surrogate for cardiomyocyte hypertrophy, fibrosis, and increasing filling pressures when histological data using wheat germ agglutinin, hematoxylin and eosin staining, and pressure volume loop data would have measured these more directly. Analysis of *Nppa, Nppb, Pln,* and *GFPdgn* may have been more suited for normalization with *36B4* rather than *GAPDH* as *GAPDH* has been shown to change during obesity and metabolic syndrome (Fan et al., 2020). Despite preliminary affirmation of the role of UPS malfunction in the pathogenesis of HFpEF, more in-depth deciphering the specific defect in UPS-mediated protein degradation pathway will provide concise guidance for therapeutic interventions should the UPS impairment play an important pathogenic role. It will be extremely important to address questions such as "does HFpEF drive UPS dysfunction or does UPS dysfunction drive HFpEF?"

In summary, the present study demonstrates for the first time that impaired UPS performance can occur in an animal model of HFpEF; thus, further investigation into a potential cause-effect relationship between UPS impairment and HFpEF is warranted.

Data availability statement

The original contributions presented in the study are included in the article/supplementary materials, further inquiries can be directed to the corresponding author.

Ethics statement

The animal study was reviewed and approved by the Institutional Animal Care and Use Committee of the University of South Dakota.

Author contributions

Conception and experimental design (XW, JL), data collection and interpretation (JL, AG, LY, JS, SG), and manuscript preparation (AG, JL, XW). All authors contributed to the article and approved the submitted version.

Funding

This study is supported in part by NIH grants (R01HL072166, R01HL153614, P20GM103443-21S2), the American Heart Association grant (20TPA35490091), and the Medical Student Research Program of University of South Dakota Sanford School of Medicine.

Conflict of interest

The authors declare that the research was conducted in the absence of any commercial or financial relationships that could be construed as a potential conflict of interest.

Publisher's note

Supplementary material

The Supplementary Material for this article can be found online at: https://www.frontiersin.org/articles/10.3389/fphys.2023.1208153/full#supplementary-material

References

Bence, N. F., Sampat, R. M., and Kopito, R. R. (2001). Impairment of the ubiquitin-proteasome system by protein aggregation. *Science* 292 (5521), 1552–1555. doi:10.1126/science.292.5521.1552

Borlaug, B. A. (2014). The pathophysiology of heart failure with preserved ejection fraction. *Nat. Rev. Cardiol.* 11 (9), 507–515. doi:10.1038/nrcardio.2014.83

Chen, Q., Liu, J. B., Horak, K. M., Zheng, H., Kumarapeli, A. R., Li, J., et al. (2005). Intrasarcoplasmic amyloidosis impairs proteolytic function of proteasomes in cardiomyocytes by compromising substrate uptake. *Circ. Res.* 97 (10), 1018–1026. doi:10.1161/01.RES.0000189262.92896.0b

Chistiakov, D. A., Orekhov, A. N., and Bobryshev, Y. V. (2015). Endothelial barrier and its abnormalities in cardiovascular disease. *Front. Physiol.* 6, 365. doi:10.3389/fphys.2015.00365

Das, A., Dasgupta, S., Gong, Y., Shah, U. A., Fradley, M. G., Cheng, R. K., et al. (2022). Cardiotoxicity as an adverse effect of immunomodulatory drugs and proteasome inhibitors in multiple myeloma: A network meta-analysis of randomized clinical trials. *Hematol. Oncol.* 40 (2), 233–242. doi:10.1002/hon.2959

Dhingra, R., and Vasan, R. S. (2012). Diabetes and the risk of heart failure. *Heart Fail Clin.* 8 (1), 125–133. doi:10.1016/j.hfc.2011.08.008

Dunlay, S. M., Roger, V. L., and Redfield, M. M. (2017). Epidemiology of heart failure with preserved ejection fraction. *Nat. Rev. Cardiol.* 14 (10), 591–602. doi:10.1038/nrcardio.2017.65

Enrico, O., Gabriele, B., Nadia, C., Sara, G., Daniele, V., Giulia, C., et al. (2007). Unexpected cardiotoxicity in haematological bortezomib treated patients. *Br. J. Haematol.* 138 (3), 396–397. doi:10.1111/j.1365-2141.2007.06659.x

Fan, X., Yao, H., Liu, X., Shi, Q., Lv, L., Li, P., et al. (2020). High-fat diet alters the expression of reference genes in male mice. *Front. Nutr.* 7, 589771. doi:10.3389/fnut.2020.589771

Frankowska, N., Lisowska, K., and Witkowski, J. M. (2022). Proteolysis dysfunction in the process of aging and age-related diseases. *Front. Aging* 3, 927630. doi:10.3389/fragi.2022.927630

Fraser, T. B., Turner, S. W., Mangos, G. J., Ludbrook, J., and Whitworth, J. A. (2001). Comparison of telemetric and tail-cuff blood pressure monitoring in adrenocorticotrophic hormone-treated rats. *Clin. Exp. Pharmacol. Physiol.* 28 (10), 831–835. doi:10.1046/j.1440-1681.2001.03531.x

Georgiopoulos, G., Makris, N., Laina, A., Theodorakakou, F., Briasoulis, A., Trougakos, I. P., et al. (2023). Cardiovascular toxicity of proteasome inhibitors: Underlying mechanisms and management strategies: Jacc: CardioOncology state-of-the-art review. *JACC CardioOncol* 5 (1), 1–21. doi:10.1016/j.jaccao.2022.12.005

Gevaert, A. B., Boen, J. R. A., Segers, V. F., and Van Craenenbroeck, E. M. (2019). Heart failure with preserved ejection fraction: A review of cardiac and noncardiac pathophysiology. *Front. Physiol.* 10, 638. doi:10.3389/fphys.2019.00638

Gibb, A. A., McNally, L. A., Riggs, D. W., Conklin, D. J., Bhatnagar, A., and Hill, B. G. (2016). FVB/NJ mice are a useful model for examining cardiac adaptations to treadmill exercise. *Front. Physiol.* 7, 636. doi:10.3389/fphys.2016.00636

Gonzalez-Lopez, E., Gallego-Delgado, M., Guzzo-Merello, G., de Haro-Del Moral, F. J., Cobo-Marcos, M., Robles, C., et al. (2015). Wild-type transthyretin amyloidosis as a cause of heart failure with preserved ejection fraction. *Eur. Heart J.* 36 (38), 2585–2594. doi:10.1093/eurheartj/ehv338

Grote Beverborg, N., Spater, D., Knoll, R., Hidalgo, A., Yeh, S. T., Elbeck, Z., et al. (2021). Phospholamban antisense oligonucleotides improve cardiac function in murine cardiomyopathy. *Nat. Commun.* 12 (1), 5180. doi:10.1038/s41467-021-25439-0

Haluzik, M., Colombo, C., Gavrilova, O., Chua, S., Wolf, N., Chen, M., et al. (2004). Genetic background (C57BL/6J versus FVB/N) strongly influences the severity of diabetes and insulin resistance in ob/ob mice. *Endocrinology* 145 (7), 3258–3264. doi:10.1210/en.2004-0219

Horgan, S., Watson, C., Glezeva, N., and Baugh, J. (2014). Murine models of diastolic dysfunction and heart failure with preserved ejection fraction. *J. Card. Fail* 20 (12), 984–995. doi:10.1016/j.cardfail.2014.09.001

Koch, S. E., Haworth, K. J., Robbins, N., Smith, M. A., Lather, N., Anjak, A., et al. (2013). Age- and gender-related changes in ventricular performance in wild-type FVB/N mice as evaluated by conventional and vector velocity echocardiography imaging: A retrospective study. *Ultrasound Med. Biol.* 39 (11), 2034–2043. doi:10.1016/j.ultrasmedbio.2013.04.002

Kumarapeli, A. R., Horak, K. M., Glasford, J. W., Li, J., Chen, Q., Liu, J., et al. (2005). A novel transgenic mouse model reveals deregulation of the ubiquitin-proteasome system in the heart by doxorubicin. *FASEB J.* 19 (14), 2051–2053. doi:10.1096/fj.05-3973fje

Lam, C. S., Donal, E., Kraigher-Krainer, E., and Vasan, R. S. (2011). Epidemiology and clinical course of heart failure with preserved ejection fraction. *Eur. J. Heart Fail* 13 (1), 18–28. doi:10.1093/eurjhf/hfq121

Leucker, T. M., and Jones, S. P. (2014). Endothelial dysfunction as a nexus for endothelial cell-cardiomyocyte miscommunication. *Front. Physiol.* 5, 328. doi:10.3389/fphys.2014.00328

Li, J., Horak, K. M., Su, H., Sanbe, A., Robbins, J., and Wang, X. (2011). Enhancement of proteasomal function protects against cardiac proteinopathy and ischemia/reperfusion injury in mice. *J. Clin. Investig.* 121 (9), 3689–3700. doi:10.1172/JCI45709

Li, J., Ma, W., Yue, G., Tang, Y., Kim, I. M., Weintraub, N. L., et al. (2017). Cardiac proteasome functional insufficiency plays a pathogenic role in diabetic cardiomyopathy. *J. Mol. Cell. Cardiol.* 102, 53–60. doi:10.1016/j.yjmcc.2016.11.013

Liu, J., Chen, Q., Huang, W., Horak, K. M., Zheng, H., Mestril, R., et al. (2006). Impairment of the ubiquitin-proteasome system in desminopathy mouse hearts. *FASEB J.* 20 (2), 362–364. doi:10.1096/fj.05-4869fje

Loffredo, F. S., Nikolova, A. P., Pancoast, J. R., and Lee, R. T. (2014). Heart failure with preserved ejection fraction: Molecular pathways of the aging myocardium. *Circ. Res.* 115 (1), 97–107. doi:10.1161/CIRCRESAHA.115.302929

Makris, N., Georgiopoulos, G., Laina, A., Tselegkidi, M. E., Fotiou, D., Kanellias, N., et al. (2022). Cardiac mechanics in response to proteasome inhibition: A prospective study. *Eur. Heart J. Cardiovasc Imaging* 24, 643–652. doi:10.1093/ehjci/jeac168

Man, J., Barnett, P., and Christoffels, V. M. (2018). Structure and function of the Nppa-Nppb cluster locus during heart development and disease. *Cell. Mol. Life Sci.* 75 (8), 1435–1444. doi:10.1007/s00018-017-2737-0

Massett, M. P., and Berk, B. C. (2005). Strain-dependent differences in responses to exercise training in inbred and hybrid mice. *Am. J. Physiol. Regul. Integr. Comp. Physiol.* 288 (4), R1006–R1013. doi:10.1152/ajpregu.00476.2004

McHugh, K., DeVore, A. D., Wu, J., Matsouaka, R. A., Fonarow, G. C., Heidenreich, P. A., et al. (2019). Heart failure with preserved ejection fraction and diabetes: JACC state-of-the-art review. *J. Am. Coll. Cardiol.* 73 (5), 602–611. doi:10.1016/j.jacc.2018.11.033

Nascimento-Sales, M., Fredo-da-Costa, I., Borges Mendes, A. C. B., Melo, S., Ravache, T. T., Gomez, T. G. B., et al. (2017). Is the FVB/N mouse strain truly resistant to diet-induced obesity? *Physiol. Rep.* 5 (9), e13271. doi:10.14814/phy2.13271

Oktay, A. A., Rich, J. D., and Shah, S. J. (2013). The emerging epidemic of heart failure with preserved ejection fraction. *Curr. Heart Fail Rep.* 10 (4), 401–410. doi:10.1007/s11897-013-0155-7

Patten, R. D. (2007). Models of gender differences in cardiovascular disease. *Drug Discov. Today Dis. Models* 4 (4), 227–232. doi:10.1016/j.ddmod.2007.11.002

Paulus, W. J., and Tschope, C. (2013). A novel paradigm for heart failure with preserved ejection fraction: Comorbidities drive myocardial dysfunction and remodeling through coronary microvascular endothelial inflammation. *J. Am. Coll. Cardiol.* 62 (4), 263–271. doi:10.1016/j.jacc.2013.02.092

Ranek, M. J., Terpstra, E. J., Li, J., Kass, D. A., and Wang, X. (2013). Protein kinase g positively regulates proteasome-mediated degradation of misfolded proteins. *Circulation* 128 (4), 365–376. doi:10.1161/CIRCULATIONAHA.113.001971

Ranek, M. J., Zheng, H., Huang, W., Kumarapeli, A. R., Li, J., Liu, J., et al. (2015). Genetically induced moderate inhibition of 20S proteasomes in cardiomyocytes facilitates heart failure in mice during systolic overload. *J. Mol. Cell. Cardiol.* 85, 273–281. doi:10.1016/j.yjmcc.2015.06.014

Schiattarella, G. G., Altamirano, F., Tong, D., French, K. M., Villalobos, E., Kim, S. Y., et al. (2019). Nitrosative stress drives heart failure with preserved ejection fraction. *Nature* 568 (7752), 351–356. doi:10.1038/s41586-019-1100-z

Shah, A. M. (2013). Ventricular remodeling in heart failure with preserved ejection fraction. *Curr. Heart Fail Rep.* 10 (4), 341–349. doi:10.1007/s11897-013-0166-4

Shah, R. V., Abbasi, S. A., Heydari, B., Rickers, C., Jacobs, D. R., Jr., Wang, L., et al. (2013). Insulin resistance, subclinical left ventricular remodeling, and the obesity paradox: MESA (Multi-Ethnic study of atherosclerosis). *J. Am. Coll. Cardiol.* 61 (16), 1698–1706. doi:10.1016/j.jacc.2013.01.053

Shah, S. J., Heitner, J. F., Sweitzer, N. K., Anand, I. S., Kim, H. Y., Harty, B., et al. (2013). Baseline characteristics of patients in the treatment of preserved cardiac function heart failure with an aldosterone antagonist trial. *Circ. Heart Fail* 6 (2), 184–192. doi:10.1161/CIRCHEARTFAILURE.112.972794

Tourki, B., and Halade, G. V. (2021). Heart failure syndrome with preserved ejection fraction is a metabolic cluster of non-resolving inflammation in obesity. *Front. Cardiovasc Med.* 8, 695952. doi:10.3389/fcvm.2021.695952

Tromp, J., MacDonald, M. R., Tay, W. T., Teng, T. K., Hung, C. L., Narasimhan, C., et al. (2018). Heart failure with preserved ejection fraction in the young. *Circulation* 138 (24), 2763–2773. doi:10.1161/CIRCULATIONAHA.118.034720

Wang, X., Pattison, J. S., and Su, H. (2013). Posttranslational modification and quality control. *Circ. Res.* 112 (2), 367–381. doi:10.1161/CIRCRESAHA.112.268706

Wang, X., and Robbins, J. (2014). Proteasomal and lysosomal protein degradation and heart disease. *J. Mol. Cell. Cardiol.* 71, 16–24. doi:10.1016/j.yjmcc.2013.11.006

Wang, X., and Wang, H. (2020). Priming the proteasome to protect against proteotoxicity. *Trends Mol. Med.* 26 (7), 639–648. doi:10.1016/j.molmed.2020.02.007

Wang, Z. V., Deng, Y., Gao, N., Pedrozo, Z., Li, D. L., Morales, C. R., et al. (2014). Spliced X-box binding protein 1 couples the unfolded protein response to hexosamine biosynthetic pathway. *Cell.* 156 (6), 1179–1192. doi:10.1016/j.cell.2014.01.014

Zhang, H., Pan, B., Wu, P., Parajuli, N., Rekhter, M. D., Goldberg, A. L., et al. (2019). PDE1 inhibition facilitates proteasomal degradation of misfolded proteins and protects against cardiac proteinopathy. *Sci. Adv.* 5 (5), eaaw5870. doi:10.1126/sciadv.aaw5870

frontiers | Frontiers in Physiology

TYPE Review
PUBLISHED 28 September 2023
DOI 10.3389/fphys.2023.1254943

OPEN ACCESS

EDITED BY
William C. W. Chen,
University of South Dakota, United States

REVIEWED BY
Marta Tesone,
University of Buenos Aires, Argentina
Mahita Kadmiel,
Allegheny College, United States

*CORRESPONDENCE
John S. Davis,
jsdavis@unmc.edu

RECEIVED 17 July 2023
ACCEPTED 18 September 2023
PUBLISHED 28 September 2023

CITATION
Monaco CF and Davis JS (2023), Mechanisms of angioregression of the corpus luteum.
Front. Physiol. 14:1254943.
doi: 10.3389/fphys.2023.1254943

Mechanisms of angioregression of the corpus luteum

Corrine F. Monaco[1,2] and John S. Davis[2,3]*

[1]Department of Cellular and Integrative Physiology, University of Nebraska Medical Center, Omaha, NE, United States, [2]Department of Obstetrics and Gynecology, University of Nebraska Medical Center, Omaha, NE, United States, [3]US Department of Veterans Affairs Nebraska-Western Iowa Healthcare System, Omaha, NE, United States

The corpus luteum is a transient ovarian endocrine gland that produces the progesterone necessary for the establishment and maintenance of pregnancy. The formation and function of this gland involves angiogenesis, establishing the tissue with a robust blood flow and vast microvasculature required to support production of progesterone. Every steroidogenic cell within the corpus luteum is in direct contact with a capillary, and disruption of angiogenesis impairs luteal development and function. At the end of a reproductive cycle, the corpus luteum ceases progesterone production and undergoes rapid structural regression into a nonfunctional corpus albicans in a process initiated and exacerbated by the luteolysin prostaglandin F2α (PGF2α). Structural regression is accompanied by complete regression of the luteal microvasculature in which endothelial cells die and are sloughed off into capillaries and lymphatic vessels. During luteal regression, changes in nitric oxide transiently increase blood flow, followed by a reduction in blood flow and progesterone secretion. Early luteal regression is marked by an increased production of cytokines and chemokines and influx of immune cells. Microvascular endothelial cells are sensitive to released factors during luteolysis, including thrombospondin, endothelin, and cytokines like tumor necrosis factor alpha (TNF) and transforming growth factor β 1 (TGFB1). Although PGF2α is known to be a vasoconstrictor, endothelial cells do not express receptors for PGF2α, therefore it is believed that the angioregression occurring during luteolysis is mediated by factors downstream of PGF2α signaling. Yet, the exact mechanisms responsible for angioregression in the corpus luteum remain unknown. This review describes the current knowledge on angioregression of the corpus luteum and the roles of vasoactive factors released during luteolysis on luteal vasculature and endothelial cells of the microvasculature.

KEYWORDS

corpus luteum, angioregression, endothelial cells, PGF2α, luteolysis, ovary

1 Introduction

Vascular remodeling occurs in various disease states such as myocardial infarction, traumatic spinal cord injury (Olive et al., 2003; Benton et al., 2008), neurovascular disease (Planas, 2020), and various hypertensive disorders (Intengan and Schiffrin, 2001). Degradation of blood vessels, or angioregression, also occurs in disease states such as chronic graft nephropathy (Ishii et al., 2005) and muscle degeneration (Dedkov et al., 2002; Malek et al., 2010; Olenich et al., 2014). Vast non-pathological angioregression occurs during normal development (Yin and Pacifici, 2001; McKeller et al., 2002; Nayak et al., 2018); however, it is not prevalent in most adult tissues. There are some instances where physiological angioregression occurs, such as in uterine remodeling during pregnancy

(Henry et al., 2006), mammary gland involution (Djonov et al., 2001), and during luteolysis of the ovarian corpus luteum during the female reproductive cycle (Augustin, 2000).

The corpus luteum is a temporary, dynamic endocrine gland formed from the remnants of the ovulated follicle (Stocco et al., 2007). It produces the progesterone that is necessary for successful establishment and maintenance of pregnancy. Following ovulation, the remaining granulosa and theca cells of the ovulated follicle undergo rapid, but limited, division and then differentiation as the ovary shifts from making estradiol to making progesterone in a process known as luteinization (Smith et al., 1994; Fraser and Duncan, 2009). Notably, endothelial cells from the theca layer of the follicle undergo rapid division, comparable to that of tumor angiogenesis, forming the vast microvasculature of the corpus luteum, with around 50% of cells in the mature corpus luteum comprised of endothelial cells (Rodgers et al., 1984; O'shea et al., 1989). In addition to the steroidogenic and endothelial cells, the corpus luteum contains small populations of fibroblasts, mesenchymal-like cells that produce and regulate extracellular matrix, and immune cells (O'shea et al., 1989; Van Linthout et al., 2014). The luteal vasculature contains mostly capillaries, and nearly every steroidogenic cell is in contact with a microvascular endothelial cell (Zheng et al., 1993; Fraser and Duncan, 2009). As a result, the corpus luteum has one of the highest blood supplies, per unit of any organ system (Smith et al., 1994), as well as high blood flow and low vascular resistance compared to the surrounding ovarian stroma (Wiltbank et al., 1990). The microvasculature is crucial for luteal function, as blockage of angiogenesis during luteal formation results in dysfunctional corpora lutea (Yamashita et al., 2008). The luteal vasculature is important for both transport of progesterone from steroidogenic cells to the rest of the body and for nourishment of the corpus luteum (Woad and Robinson, 2016). Early studies in rabbits demonstrated the importance of the corpus luteum for the production of progesterone and pregnancy (Mesiano, 2022). In women, luteal function is crucial for pregnancy, as removal of the corpus luteum within the first 7 weeks of pregnancy results in termination of said pregnancy (Csapo et al., 1974). Progesterone secreted from the corpus luteum is crucial for creating optimal conditions for embryo implantation, a crucial point in pregnancy (Kolatorova et al., 2022).

In a reproductive cycle that does not result in pregnancy, the corpus luteum must cease progesterone production so the next reproductive cycle can begin. In many species including bovines (Knickerbocker et al., 1988), ovines (Goding, 1974), guinea pigs (Evans, 1987), and rats (Wang et al., 1993), luteal regression (luteolysis) is initiated by pulses of prostaglandin F2α (PGF2α) produced by the uterus. In primates, it is believed to be initiated by the lack of gonadotropin support and a concomitant rise in intra-ovarian PGF2α production (Stouffer et al., 2013). Luteolysis occurs in two steps: (1) functional regression, in which progesterone production declines, and (2) structural regression, in which the corpus luteum dissipates into a fibrotic corpus albicans within the ovarian stroma. Structural regression involves various pathways of tissue remodeling, including immune cell infiltration, breakdown and buildup of extracellular matrix, and regression of the microvasculature. Although it is known that blood flow is impaired and the vascular endothelial cells are sensitive to various factors released during luteolysis, the exact mechanism of angioregression in the corpus luteum remains unknown. This review will highlight current knowledge on angioregression of the corpus luteum: from macrovascular changes, dilation and constriction of luteal vasculature and subsequent impedance of blood flow, to microvascular changes, such as the effects of growth factors, cytokines, and thrombospondins on microvascular endothelial cells.

2 Blood flow

Electron microscopy of regressing guinea pig and bovine corpora lutea revealed that endothelial cells detach from the basement membrane, slough off the capillaries, and clog the vessels; yet the capillary walls remain intact (Azmi and O'Shea, 1984; Modlich et al., 1996). However, luteal capillaries eventually disappear throughout regression. Twelve hours after PGF2α-induced regression, there were noticeably fewer capillaries in ovine corpora lutea (Nett et al., 1976), but more arterial vessels were present (Bauer et al., 2003). These vessels contain thicker walls of smooth muscle (Bauer et al., 2003), which is further evidenced by increased smooth muscle actin positive cells surrounding arterioles in regressing bovine corpora lutea (Hojo et al., 2009). The diameter of these vessels was demonstrated to be smaller compared to fully functional mid-cycle corpora lutea (Lei et al., 1991; Nio-Kobayashi et al., 2016), indicating that vasoconstriction may be occurring in luteal regression. Similarly, arterial wall thickening is associated with various cardiovascular diseases including atherosclerosis, thrombosis, and hypertension (Burke et al., 1995; Corinaldesi and Corinaldesi, 2008). Changes in blood flow during luteal regression as a result of vasoactive factors are illustrated in Figure 1.

Early studies in the rabbit indicate that luteal blood flow is highly correlated to progesterone levels in pseudopregnant rabbit corpora lutea (Janson et al., 1981). Due to their size and prominent vascular blood supply, corpora lutea from larger species such as ruminants and humans can be identified via ultrasonography. Doppler ultrasound has been utilized to study corpora lutea during natural and PGF2α-induced regression. Doppler readings in human corpora lutea have identified that blood flow drops in the days nearing menstruation, which correlates to the reduction in progesterone production in the late luteal phase (Miyazaki et al., 1998), and pregnant cattle exhibited a much higher luteal blood flow than non-pregnant cattle (Kanazawa et al., 2022). Additionally, *in vivo* studies of cows injected with PGF2α to induce luteolysis have identified that there is an early increase in blood flow after 2 h of treatment that ultimately decreases below baseline levels after 8 h of treatment (Acosta et al., 2002; Miyamoto et al., 2005; Jonczyk et al., 2021). A study in the ovine suggested that ovarian blood flow to the luteal ovary decreased 4 h post-PGF2α treatment, followed by a decline in progesterone 6 h post-PGF2α treatment (Nett et al., 1976). Similar findings were reported in the equine and the donkey (Ginther et al., 2007; Miró et al., 2015). Also, luteal blood flow and plasma progesterone followed a more similar trend in the cycling bovine corpus luteum than did luteal size, which is commonly used to identify luteal stage (Herzog et al., 2010), thus implicating blood flow as an accurate measure of luteal function. However, the opposite has been determined for the midcycle in lactating dairy cows (Lüttgenau et al., 2011). The reason for the

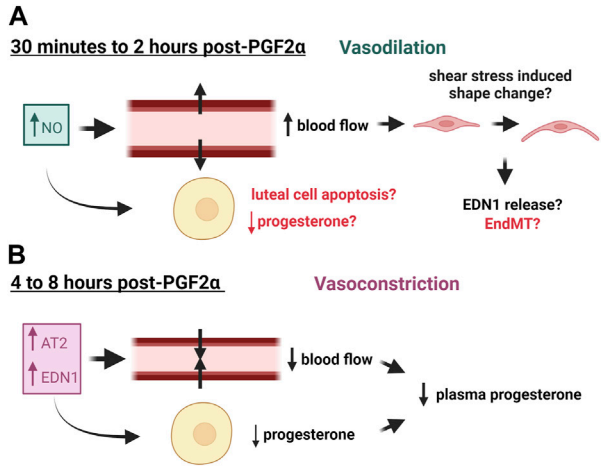

FIGURE 1
Effects of Vasoactive Factors released in response to PGF2α on blood flow of the corpus luteum. **(A)** Nitric Oxide (NO) is released early in luteal regression and causes vasodilation and subsequent increased blood flow, which may consequently alter endothelial cell phenotype. **(B)** Later in luteal regression, vasoconstrictors such as Angiotensin II (AT2) and endothelin 1 (EDN1) are released, causing decreased blood flow and decreased plasma progesterone. These factors may also impair progesterone production of luteal steroidogenic cells. This figure was made with Biorender.com.

discrepancy is likely due to the enhanced hepatic metabolism of progesterone in lactating dairy cows (Wiltbank et al., 2006).

The transient increase in blood flow seen early in luteal regression is believed to be a result of the increased synthesis of the vasodilator, nitric oxide (NO) (Miyamoto et al., 2005; Shirasuna et al., 2008). Evidence across various species has shown that shear stress from increased blood flow changes the shape of vascular endothelial cells from their signature cobblestone shape to one that is more spindle-like and oriented towards the direction of flow (reviewed in (Masuda et al., 2003; Campinho et al., 2020)). This has been observed in endothelial cells derived from the carotid arteries of rabbits (Masuda et al., 1999) and mouse cardiac and pulmonary endothelial cells (Merna et al., 2018). High stretch of cultured endothelial cells induces a similar phenotype in which the cells acquire a spindle-like shape via phalloidin remodeling and produce increased reactive oxygen species (Girão-Silva et al., 2021). This change in endothelial cell phenotype is suggested to be mediated by calcium signaling and tyrosine kinase phosphorylation in cultured bovine aortic endothelial cells (Malek and Izumo, 1996). More recent studies show that increased shear stress causes retinal endothelial cells cultured in 3D (Luu et al., 2023) and human aortic endothelial cells (Kidder et al., 2023) to adopt a more mesenchymal phenotype. There are no reports to our knowledge of this phenomenon occurring in luteal endothelial cells; however, shear stress from a compensatory blood flow increase early in luteal regression may contribute to the changes in capillary basement membrane that are seen during regression, which could result in the release of endothelial cells from the capillary. Another hypothesis is that the shear stress could cause the endothelial cells to transition to a mesenchymal phenotype, as increased matrix stiffness is associated with fibrosis and endothelial cell destabilization (Yu et al., 2023). It is also important to note that endothelial cells are sensitive to many factors released during luteal regression as discussed later; therefore, changes in blood flow are likely not the sole contributor to luteal angioregression.

3 Effect of vasoactive factors on luteal vasculature and endothelial cells

Outside of the corpus luteum, PGF2α is more commonly known as a vasoconstrictor, in which it does so by activating calcium signaling and inducing contraction of smooth muscle cells (Watts, 2007). In addition to PGF2α, various other vasoactive agents are increased in luteal regression, such as NO, angiotensin II (AT2), and endothelin 1 (EDN1) (Davis et al., 2003; Skarzynski et al., 2008; Shirasuna et al., 2012b). The known changes in vasoactive factors contributing to blood flow in luteal regression are summarized in Table 1.

3.1 Nitric oxide (NO)

Nitric oxide (NO) is commonly known as a vasodilator that is produced by nitric oxide synthase (NOS) enzymes. There are three identified NOS enzymes (NOS1-3), two of the three being uniquely expressed in specific cell types, neuronal NOS (nNOS or NOS1) and endothelial NOS (eNOS or NOS3). The third NOS enzyme is inducible NOS (iNOS or NOS2) (Förstermann and Sessa, 2012). Both eNOS and iNOS have been identified in luteal tissue, with eNOS primarily being localized to the endothelial cells and iNOS exhibiting weak localization to the steroidogenic cells (Fridén et al., 2000; Tao et al., 2004). One study identified increased eNOS in naturally regressing bovine corpora and in corpora lutea induced to regress following treatment with PGF2α (Shirasuna et al., 2008). Studies in the human report increased iNOS at mid and late luteal phase (Vega et al., 2000). However, others reported decreased eNOS immunolocalization and transcription during the bovine late luteal phase and luteal regression (Rosiansky-Sultan et al., 2006). Such differences can be attributed to differences in staging of the corpus luteum as opposite effects of PGF2α treatment were seen in early corpora lutea compared to midcycle corpora lutea, as well as whether the tissue sample was in the middle or periphery of the corpus luteum, as eNOS was elevated only in the periphery of midcycle corpora lutea in the bovine (Shirasuna et al., 2008). Direct intra-luteal delivery of an NO donor temporarily increased blood flow but then caused both blood flow and progesterone to fall to levels below baseline (Shirasuna et al., 2008). Similar results have been reported in other species. For instance, NO donor treatment decreased serum progesterone but increased ovarian PGF2α production in pseudopregnant rats, and the same has been reported in cultured human luteal cells (Motta et al., 1999; Fridén et al., 2000). Such differences may be due to pharmacologic administration of NO donors *in vivo* and species-to-species variations.

In addition to its ability to stimulate PGF2α, it has been suggested that NO may have a direct effect on luteal cells. L-arginine, an NOS substrate, increased apoptosis of cultured human luteal tissue, which was suppressed by treatment with an

TABLE 1 Summary of Vasoactive, Pro-angiogenic, and Anti-angiogenic factors that are regulated during luteal angioregression.

	Factor	Expression during luteal regression	Source	Effect on endothelial cells	Proposed role in angioregression	References
Vasoactive factors						
NO	Nitric Oxide	↑ (early)	Endothelial cells (eNOS) Steroidogenic cells (iNOS)	Inhibits apoptosis	Vasodilation, increased blood flow, stimulation of PGF2α	(Dimmeler and Zeiher, 1999; Motta et al., 1999; Fridén et al., 2000; Tao et al., 2004; Shirasuna et al., 2008; Förstermann and Sessa, 2012)
AT2	Angiotensin II	↑	Circulating, ovary	Proliferation	Vasoconstriction, increase PGF2α	(Hayashi and Miyamoto, 1999; Benigni et al., 2010)
EDN 1	Endothelin 1	↑	Endothelial cells	Proliferation, prostaglandin release	Vasoconstriction	(Girsh et al., 1996b; Hinckley and Milvae, 2001; Tanfin et al., 2011)
Pro-angiogenic factors						
VEGF	Vascular Endothelial Growth Factor	↓	Perivascular cells, steroidogenic cells	Proliferation	Decrease during luteal regression causes vessel dysfunction	(Gospodarowicz et al., 1989; Hazzard et al., 2000; Neuvians et al., 2004a)
FGF2	Fibroblast Growth Factor 2	↑	Steroidogenic cells and endothelial cells	Proliferation	Fibroblast division, sensitization of endothelial cells (via increased type 1 collagen)	(Gospodarowicz, 1974; Asakai et al., 1993; Robinson et al., 2007; Maroni and Davis, 2011; Zalman et al., 2012; Alan and Kulak, 2021; Monaco et al., 2023)
ANGPT1	Angiopoietin 1	—	Perivascular cells, steroidogenic cells	Proliferation	Decrease in relation to ANGPT2 inhibits angiogenesis	(Maisonpierre et al., 1997; Wulff et al., 2000; Sugino et al., 2005; Fiedler et al., 2006; Eklund and Saharinen, 2013)
Anti-angiogenic factors						
ANGPT2	Angiopoietin 2	↑	Endothelial cells, potentially steroidogenic cells	Inhibits ANGPT1-induced effects (Tie2 antagonist)	Inhibits new angiogenesis, sensitization of endothelial cells	(Maisonpierre et al., 1997; Wulff et al., 2000; Tanaka et al., 2004; Sugino et al., 2005; Eklund and Saharinen, 2013)
THBS1	Thrombospondin 1	↑	Endothelial cells, steroidogenic cells	Apoptosis (via TGFB1)	Endothelial cell death, vessel fibrosis (synergy with TGFB1)	(Mondal et al., 2011; Zalman et al., 2012; Berisha et al., 2016b; Farberov and Meidan, 2016)
TNF	Tumor Necrosis Factor α	↑	Immune cells, endothelial cells, possibly steroidogenic cells	Apoptosis	Endothelial cell death, PGF2α production	(Sakumoto et al., 2000; Pru et al., 2003; Cherry et al., 2008; Henkes et al., 2008; Sakumoto et al., 2011; Talbott et al., 2017)
IL1B	Interleukin 1β	↑	Immune cells ($CD11b^+$), potentially fibroblasts and steroidogenic cells	Chemokine release	Immune cell recruitment, PGF2α production, potentially vessel fibrosis via EndMT	(Kobayashi and Terao, 1997; Estevez et al., 2003; Lopez-Castejon and Brough, 2011; Bourdiec et al., 2013; Bishop et al., 2017; Talbott et al., 2017; Baddela et al., 2018)
TGFB1	Transforming Growth Factor β1	↑	Ubiquitous	Apoptosis, dysregulation of capillary structures	Endothelial cell death, vessel fibrosis	(Branton and Kopp, 1999; Maroni and Davis, 2011; Maroni and Davis, 2012; Talbott et al., 2017)

NO inhibitor (Vega et al., 2000). Similarly, treatment of bovine luteal cells with the NO donor, NONOate, increased levels of cleaved caspase 3, a marker of apoptosis (Korzekwa et al., 2006; Kowalczyk-Zieba et al., 2014). Conversely, treatment of luteinized goat granulosa cells with NO donor increased progesterone production, whereas treatment with an NOS inhibitor decreased progesterone and increased apoptosis (Guo et al., 2019). Such differences may be due to differences in culture conditions and the presence of multiple cell types (endothelial cells and immune cells) in the cultures. Collectively, these data indicate that NO may contribute to luteolysis beyond the vasculature and may have a direct effect on steroidogenesis. Although there is some evidence

that NO may be an inhibitor of apoptosis in endothelial cells (Dimmeler and Zeiher, 1999, this phenomenon has yet to be studied in luteal endothelial cells.

3.2 Angiotensin II (AT2)

Angiotensin II (AT2) is a potent vasoconstrictor that is derived from angiotensinogen produced by the liver. Angiotensinogen is converted to angiotensin I by the enzyme renin, and angiotensin I is converted to angiotensin II by angiotensin converting enzyme (ACE) (Ng and Vane, 1967). AT2 has pleiotropic effects that include production of aldosterone, which increases blood pressure, or it can act as an independent vasoactive factor or act on other systems such as the kidney to raise blood pressure (Fyhrquist et al., 1995; Santos, 2014). Such effects, along with pro-inflammatory and pro-fibrotic effects are mediated by the angiotensin receptor 1 (AGTR1) (Benigni et al., 2010). Angiotensin II is also capable of binding to the AGTR2, which induces vasodilation and anti-inflammatory and anti-fibrotic effects (Benigni et al., 2010). Interestingly, AGTR1 levels remain consistent throughout the luteal phase, but AGTR2 levels are decreased at midcycle (days 8–12) but are increased during the late luteal phase (days 13–17) and regression (> day 18) in bovine corpora lutea, but were also found to be elevated to the same level in the corpus luteum of pregnancy (Hayashi et al., 2000; Kobayashi et al., 2001; Schams et al., 2003). Although this seems contradictory to the increased inflammation and fibrosis seen during luteal regression, it is possible that (1) these studies only accounted for AGTR2 mRNA and not for desensitization or endocytosis of the AGTR2, or (2) AGTR2 actions ensure that the regression is tightly controlled.

The ovary is capable of producing renin and AT2 (Yoshimura, 1997; Palumbo et al., 2016). Additionally, ACE has been identified in endothelial cells of the bovine corpus luteum during early luteal phase (Hayashi et al., 2000). The luteal renin-angiotensin-aldosterone system (RAAS) may serve an important role in pregnancy in women, as increased corpus luteum number was associated with differential levels of RAAS components, but there were no differences in birth outcomes (Wiegel et al., 2021).

PGF2α has been shown to increase AT2 levels in microdialyzed bovine corpora lutea *in vitro* (Hayashi and Miyamoto, 1999), and AT2 has been demonstrated to increase PGF2α levels but also progesterone levels alone and in conjunction with PGF2α treatment *in vitro* (Kobayashi et al., 2001). In that study, AT2 increased secretion of oxytocin, another luteolytic factor. In rat luteal cells, AT2 had no effect on basal progesterone, but inhibition of AGTR2 slightly decreased progesterone secretion (Pepperell et al., 2006). However, in another study, AT2 decreased progesterone after 14 h alone and after 4 h in conjunction with PGF2α in microdialyzed bovine corpora lutea (Hayashi and Miyamoto, 1999). It is possible that such effects are mediated by angiotensin reactive proteins in the luteal endothelial cells, as ACE is present in bovine luteal endothelial cells, and treatment with an ACE inhibitor, captopril, decreased AT2 secretion from luteal endothelial cells (Hayashi et al., 2000). Therefore, it is possible that endothelial-derived AT2 may aid in decreasing progesterone either alone or through the release of luteolytic factors.

3.3 Endothelin-1 (EDN1)

Endothelin 1 (EDN1) is a 21 amino acid protein derived from endothelial cells that is known to be a potent vasoconstrictor (Yanagisawa et al., 1988). It is produced in endothelial cells as a larger pro-endothelin which is then cleaved to active endothelin by endothelin converting enzyme (ECE) (Sawamura et al., 1989; Tanfin et al., 2011). Studies in the cow and the ewe have identified that luteal endothelin 1 levels increase during natural and PGF2α-induced luteal regression (Girsh et al., 1996b; Ohtani et al., 1998; Hinckley and Milvae, 2001), and PGF2α induces secretion of EDN1 from microdialysed bovine corpora lutea (Miyamoto et al., 1997). Furthermore, tumor necrosis factor α (TNF), an inflammatory cytokine that is elevated in luteal regression, increased EDN1 production by bovine aorta endothelial cells (Marsden and Brenner, 1992) therefore EDN1 secretion may be regulated by PGF2α, inflammatory cytokines, and other secondary responses to PGF2α.

Although EDN1 is well known for its role as a vasoconstrictor, it may have some direct effects on steroidogenic cells in the corpus luteum. *In vitro,* EDN1 decreased progesterone secretion of ovine luteal minces and decreased basal and LH-induced progesterone production by large, but not small bovine luteal cells (Girsh et al., 1996a; Doerr et al., 2008). *In vivo*, EDN1 decreased progesterone in a synergistic manner with PGF2α in the bovine (Shirasuna et al., 2006). Given this information, the luteolytic role of EDN1 may involve both vasoconstriction and direct action on luteal steroidogenic cells.

4 Pro- and anti-angiogenic factors in luteolysis

In addition to the presence of factors affecting vessel dilation or contraction during luteal regression, luteolysis is associated with decreased expression of pro-angiogenic factors such as vascular endothelial growth factor (VEGF) and increased expression of anti-angiogenic factors, such as thrombospondin 1 (THBS1), EDN1, transforming growth factor β 1 (TGFB1) and pro-inflammatory cytokines (Skarzynski et al., 2008; Shirasuna et al., 2012b; Berisha et al., 2016a; Talbott et al., 2017). The proposed effects of these factors on luteal vasculature are illustrated in Figure 2. These events are triggered by a luteolytic dose of PGF2α *in vivo*; however, multiple studies have demonstrated that endothelial cells do not express the receptor for PGF2α (Liptak et al., 2005; Maroni and Davis, 2011). Therefore, the effects of the luteolytic cascade on microvascular endothelial cells must be from release of factors following the initial PGF2α pulses. Furthermore, luteal endothelial cells are known to be sensitive to such factors, and thus are believed to be the first to die during luteal regression (Azmi and O'Shea, 1984). Additionally, the luteal rescue signal, interferon tau, increases endothelial cell survival and decreases transcription of luteolytic factors like *THBS1*, *EDN1*, and *TGFB1* in bovine luteal slices (Basavaraja et al., 2017). Therefore, the presence or absence of secreted factors relating to angiogenesis may contribute to luteal angioregression.

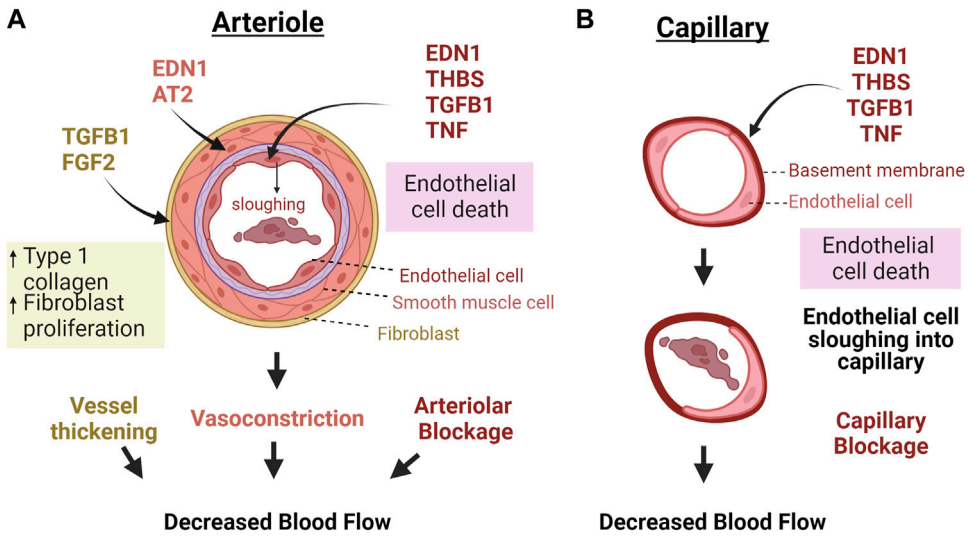

FIGURE 2
Macro vs. microvascular changes in response to factors secreted during luteal regression. **(A)** Because the luteal microvasculature also contains smooth muscle and pericytes, vasoactive factors cause contraction of vascular smooth muscle cells and consequent vasoconstriction, in addition to TGFB1 and FGF2 activating fibroblasts to produce more collagen, thereby thickening and stiffening the vessels. Capillaries do not have these bordering cells **(B)**. Therefore, these vessels would mostly be impacted by factors that directly impact endothelial cells. In both cases, death of endothelial cells causes sloughing into the capillaries which can clog vessels and impair blood flow. Abbreviations: Endothelin 1 = EDN1, Angiotensin II = AT2, Fibroblast growth factor 2 = FGF2, Transforming growth factor β-1 = TGFB1, Thrombospondin 1 = THBS1, Tumor necrosis factor α = TNF. The figure was made using Biorender.com.

4.1 Pro-angiogenic factors

4.1.1 Vascular endothelial growth factor (VEGF)

Vascular endothelial growth factor (VEGF) is growth factor that acts as a potent mitogen on endothelial cells (Gospodarowicz et al., 1989). There are five VEGF isoforms which can bind to three receptors, VEGFR1 (Flt1), VEGFR2 (KDR or Flk1) and VEGFR3 (Flk4) (Geva and Jaffe, 2000). Because rapid angiogenesis is necessary to build the luteal microvasculature, VEGF is highly prominent in the developing corpus luteum (Redmer et al., 1996; Woad and Robinson, 2016). Interruption of VEGF during ovulation results in decreased luteal formation (Duncan et al., 2008). In the late luteal phase, and in PGF2α-induced regression across multiple species, luteal *VEGF* mRNA decreases (Otani et al., 1999; Hazzard et al., 2000; Neuvians et al., 2004a; Vonnahme et al., 2006). The rapid reduction in VEGF expression indicates that no active angiogenesis is occurring during luteal regression, a finding confirmed by studies across various species, including the rat (Tamura and Greenwald, 1987), sheep (Reynolds and Redmer, 1999) and pig (Ricke et al., 1999), indicating that little endothelial cell proliferation occurs during luteal regression. The reduction in VEGF may reduce support for the luteal vasculature, leading to vascular regression. Such a phenomenon has been witnessed in tumors where withdrawal of VEGF will cause regression of the vessels that had built up in that tumor (Benjamin and Keshet, 1997; Baffert et al., 2006), and this phenomenon is a current target for anti-cancer therapeutics (Meadows and Hurwitz, 2012; Frezzetti et al., 2017). However, this has yet to be confirmed in the regressing corpus luteum.

4.1.2 Fibroblast growth factor 2 (FGF2)

Fibroblast growth factor 2, or basic fibroblast growth factor (FGF2) is a heparin binding protein, discovered for its ability to induce proliferation of NIH 3T3 fibroblast cell lines (Gospodarowicz, 1974). FGF2 is a prominent angiogenic factor, potentially even more so than VEGF, and it is necessary for luteal formation, as blockade of FGF2 at the time of ovulation results in corpora lutea that have malformed blood vessels and lower progesterone (Robinson et al., 2007; Yamashita et al., 2008). Immunohistochemical studies reveal FGF2 localization in endothelial cells and steroidogenic cells of the corpus luteum (Asakai et al., 1993; Alan and Kulak, 2021).

Unlike VEGF, FGF2 expression is increased during luteal regression (Neuvians et al., 2004a; Neuvians et al., 2004b; Zalman et al., 2012; Monaco et al., 2023). These findings indicate that an elevation in luteal FGF2 is not sufficient to prevent the loss of endothelial cells and capillaries that occurs during early luteal regression, nor does FGF2 cotreatment affect progesterone levels of cows treated with PGF2α *in vivo* (Piotrowska-Tomala et al., 2021). An explanation for this phenomenon could be that the increased FGF2 transcription is a compensatory effect and slows down the luteolytic process (Neuvians et al., 2004b). Another explanation is that FGF2 acts on stromal or fibrotic components of the corpus luteum. In support of this idea, using smooth muscle actin as a marker, Reynolds and Redmer observed that fibroblast number was elevated in the corpus luteum during the late luteal phase of sheep, and collagen production was also elevated following PGF2α treatment (Reynolds and Redmer, 1999; Vonnahme et al., 2006). A recent study showed that FGF2 induced both proliferation and collagen production of bovine luteal fibroblasts (Monaco et al.,

2023). Furthermore, *in vitro* studies reveal that the presence of type 1 collagen causes endothelial cells to become more sensitive to TGFB1 (Maroni and Davis, 2011). Therefore, FGF2 in the regressing corpus luteum may be acting as a luteal pro-fibrotic factor that contributes to sensitizing endothelial cells to luteolytic ligands.

4.1.3 Angiopoietins 1 & 2 (ANGPT1/2)

Angiopoietins (ANGPTs) are growth factors that regulate angiogenesis through binding to tyrosine kinase receptors Tie1 and Tie2. ANGPT1 is known to be secreted by pericytes and smooth muscle cells adjacent to endothelial cells, and ANGPT2 is believed to be exclusive to endothelial cells (Eklund and Saharinen, 2013). However, *in situ* hybridization and immunohistochemistry of the human corpus luteum revealed ANGPT 1 and 2 distribution in both steroidogenic and endothelial cells (Wulff et al., 2000; Sugino et al., 2005), and a similar result was revealed in the buffalo corpus luteum (Mishra et al., 2016). ANGPT1 binds to Tie2 on endothelial cells to promote angiogenesis by inducing proliferation and migration. In contrast, ANGPT2 acts as a Tie2 receptor antagonist to ANGPT1 and plays a role in vessel stabilization rather than new vessel formation (Maisonpierre et al., 1997). The ANGPT2/ANGPT1 ratio was reported to be elevated in regressing corpora lutea, suggesting that angiogenesis does not occur during luteal regression (Goede et al., 1998). Expression of *ANGPT1* transcripts in corpora lutea may be species-dependent, as it was highest at mid-luteal phase in bubaline (Mishra et al., 2016) and bovine (Tanaka et al., 2004) corpora lutea, and in corpora lutea of pregnancy in human (Sugino et al., 2005), but highest at late cycle in rhesus monkey corpora lutea (Hazzard et al., 2000). *ANGPT2* expression was lowest at midluteal phase in human corpora lutea and decreased in corpora lutea of pregnancy, when the corpus luteum was fully functional (Sugino et al., 2005), whereas it was highest in the late luteal phase in the rhesus monkey (Hazzard et al., 2000) and bubaline corpus luteum (Mishra et al., 2016). In the bovine corpus luteum, no changes in luteal *ANGPT2* mRNA were detected throughout the luteal phase but *ANGPT2* mRNA was transiently elevated 2 h post-PGF2α injection, and then decreased after 4 h of PGF2α treatment (Tanaka et al., 2004). Although there are no reports of the effects of ANGPT2 on luteal endothelial cells, ANGPT2 has been shown to sensitize endothelial cells to the pro-apoptotic effects of TNF (Fiedler et al., 2006). Tanaka et al. found that ANGPT2 decreased progesterone secretion of bovine corpora lutea at 4–8 h of treatment at higher concentrations (100 ng/mL) in an *in vitro* microdialysis system (Tanaka et al., 2004). This is inconsistent with what was reported in the buffalo, in which ANGPT1 and 2 increased progesterone production in cultured bubaline luteal cells after 24 h of treatment at 100 ng/mL (Mishra et al., 2016). Because ANGPTs are known to act primarily on endothelial cells (Eklund and Saharinen, 2013), more studies using primary luteal endothelial cells are needed to elucidate their role in angioregression.

4.2 Anti angiogenic factors

4.2.1 Thrombospondin 1 (THBS1)

Thrombospondins are a family of calcium-binding glycoproteins that influence a variety of functions, including angiogenesis, vessel biology, and wound healing. They are known to regulate several factors such as AT2, TGFB1, and even matrix metalloproteinases (Adams and Lawler, 2011), but the well-established function of thrombospondins 1 and 2 is dysregulation of angiogenesis (Armstrong and Bornstein, 2003). The role of thrombospondins in the corpus luteum has been reviewed in detail (Farberov et al., 2019). Localization of THBS1 was identified in endothelial cells and steroidogenic cells in the corpus luteum (Berisha et al., 2016b), and *THBS1* expression is increased in the regressing corpus luteum and is reduced in the corpus luteum of pregnancy (Mondal et al., 2011; Zalman et al., 2012; Romero et al., 2013; Farberov and Meidan, 2016). Treatment of luteal tissue slices with interferon tau, the maternal signal for luteal rescue in bovines, decreased *THBS1* mRNA and protein (Basavaraja et al., 2017). It is believed that THBS1 exerts anti-angiogenic effects on the regressing corpus luteum, as it has been demonstrated to decrease numbers of bovine and rabbit luteal endothelial cells in culture (Bagavandoss and Wilks, 1990; Farberov and Meidan, 2016). Thrombospondin 1 may act in part through TGFB1 signaling, as THBS1-treated luteal cells exhibited increased downstream TGFB1 signaling, which was decreased with THBS1 knockdown; however, inhibition of TGFB1 signaling did not ameliorate THBS1-induced endothelial cell death (Farberov and Meidan, 2016). Therefore, other signaling factors must come into play. For instance, a TGFB superfamily member, Nodal, which is increased in hypoxic conditions, elevated THBS1 and CD36 and downregulated CD31 (an endothelial cell marker) in equine luteal explants (Walewska et al., 2019). Furthermore, despite its elevation in luteolysis, THBS1 has been shown to be upregulated after ovulation and induced migration of monkey ovarian endothelial cells (Bender et al., 2019). Therefore, the action of THBS1 must depend on multiple signaling pathways and the presence of other factors in the corpus luteum, as the pro or anti-angiogenic effect of THBS1 is dependent on the target receptor. Thrombospondin 1 acts as an anti-angiogenic factor when bound to CD36 (Dawson et al., 1997), and as a pro-angiogenic factor when bound to the low density lipoprotein receptor-related protein-1 (LRP1) receptor (Orr et al., 2003). CD36 was elevated in PGF2α-induced luteolysis of the bovine corpus luteum (Berisha et al., 2016b). However, it has been shown in the ovary that THBS1 can inhibit VEGF through LRP1 binding (Greenaway et al., 2007). THBS1 has also been demonstrated to sequester FGF2 by binding to its heparin-binding site (Farberov et al., 2019). The ability of THBS1 to bind to many targets including angiogenic factors and cytokines such as TGFB1, makes it an ideal candidate for further investigation of factors that can influence cytokine levels and angioregression in the corpus luteum.

5 Effects of cytokines on endothelial cells

5.1 Tumor necrosis factor α (TNF)

In most cells, TNF binding to its receptor (TNFR1) results in inflammatory responses and/or programmed cell death. TNF protein is elevated in the pseudopregnant mouse corpus luteum following treatment with a luteolytic dose of PGF2α (Henkes et al., 2008). In the bovine, mRNA for TNF is upregulated early in PGF2α induced luteolysis (Talbott et al., 2017) and in the natural cycle (Friedman et al., 2000; Sakumoto et al., 2000). TNF has been shown to be localized to immune cells and faintly in steroidogenic cells in the bovine corpus luteum (Sakumoto et al., 2011); however, others

have found TNF to be localized in the vascular immune cells of the porcine corpus luteum (Hehnke-Vagnoni et al., 1995). TNF affects steroidogenesis directly by decreasing LH-stimulated progesterone production in luteinized murine granulosa cells (Adashi et al., 1990) and in porcine (Pitzel et al., 1993) and bovine (Benyo and Pate, 1992; Sakumoto et al., 2000) luteal cells. Furthermore, TNF can induce production of PGF2α, thus creating a positive feedback loop within the regressing corpus luteum (Sakumoto et al., 2000).

Luteal endothelial cells are sensitive to inflammatory cytokines, as TNF induces apoptosis of luteal endothelial cells (Friedman et al., 2000; Pru et al., 2003; Cherry et al., 2008; Henkes et al., 2008). Endothelial cells are a rich source of acid sphingomyelinase (ASMase), a common mediator of cytokine signaling. A report by Henkes et al. shows that TNF, but not PGF2α, activated ASMase and cell death in murine ovarian endothelial cells, a response that was not present in endothelial cells lacking ASMase (Henkes et al., 2008). *In vivo* studies revealed that mice treated with Etanercept, a TNF receptor inhibitor, were resistant to PGF2α-induced luteal regression. Additionally, mice lacking ASMase were protected from PGF2α-induced luteal regression. There was no gross evidence of PGF2α-induced disruption of the corpus luteum in the ASMase deficient mice, findings supported by the maintenance of progesterone levels (Henkes et al., 2008). These results suggest that TNF-mediated activation of ASMase serves a pivotal role in altering the luteal vasculature during PGF2α-induced luteal regression. The absence of direct cytotoxic effects of PGF2α on isolated luteal endothelial cells argues that luteal regression in response to PGF2α requires cytokines like TNF to disrupt vascular integrity. *In vitro* studies with bovine luteal endothelial cells show that TNF also induces apoptosis by inducing ASMase, production of ceramide, and activation of Jun-N-terminal Kinase (JNK) MAPK signaling (Pru et al., 2003). TNF-induced endothelial cell death may increase vascular permeability, allowing for increased infiltration of immune cells, which release more TNF, thereby exacerbating angioregression. However, further studies need to be performed to determine whether TNF affects luteal vascular permeability *in vivo*.

5.2 Interleukin 1 β (IL1B)

Interleukin 1 β (IL1B) is a pro-inflammatory cytokine that, like TNF, is upregulated early in luteal regression (Talbott et al., 2017). Also like TNF, IL1B is produced in immune cells, based on previous studies (Lopez-Castejon and Brough, 2011), although some studies indicate that fibroblasts may be able to secrete inflammatory cytokines like IL1B (Kobayashi and Terao, 1997; Bartok and Firestein, 2010), and a transcriptomic study identified the presence of *IL1B* mRNA in small steroidogenic cells of the bovine corpus luteum (Baddela et al., 2018). Although the exact localization of IL1B has not been determined in the corpus luteum, flow cytometry of the primate corpus luteum indicated that IL1B is produced by $CD11b^+$ cells in the late luteal phase (Bishop et al., 2017). Unlike TNF, the role of IL1B has not been investigated in luteal endothelial cells; however, in the corpus luteum, IL1B has been demonstrated to impair steroidogenesis and increase cyclooxygenase and subsequent PGF2α production in cultured rat ovarian tissue (Estevez et al., 2003), indicating cytokines like IL1B can potentially contribute to a positive-feedback loop to enhance PGF2α production and action.

In studies of human umbilical vein endothelial cells (HUVECs), IL1B induces matrix metalloprotease 9 and decreases levels of tissue inhibitor of matrix metalloprotease 1, suggesting that IL1B induces a net breakdown of matrix (Qin et al., 2012). In the same study, it was demonstrated that IL1B also increased endothelial cell permeability and altered expression of membrane cadherins and claudins, which could implicate increased immune cell recruitment (Qin et al., 2012). In agreement with this possibility, both TNF and IL1B increased neutrophil recruitment to HUVECs. Furthermore, the effect of IL1B was increased slightly in conditions of shear stress (Sheikh et al., 2005). A potential mechanism could be through the secretion of chemokines, which attract immune cells like neutrophils. For instance, IL1B increased secretion of IL8, a chemokine known to recruit neutrophils, in immortalized human microvascular endothelial cells (Bourdiec et al., 2013). Additionally, the receptor for IL1B, IL1R, has been implicated in shear-stressed induced EndMT, where endothelial cells transdifferentiate into myofibroblast-like cells (Kidder et al., 2023). Therefore, IL1B action in angioregression may be beyond generalized inflammation, and may even induce further inflammation through recruitment of immune cells and increased production of PGF2α.

5.3 Transforming growth factor β1 (TGFB1)

Similar to TNF and IL1B, TGFB1 is increased very early during luteal regression (Hou et al., 2008; Talbott et al., 2017). TGFB1 is a ubiquitously expressed cytokine that binds to tyrosine kinase TGFB receptors (TGFBRs) and activates a family of transcription factors called mothers against decapentaplegic, commonly known as SMADs, by phosphorylation (Branton and Kopp, 1999; Tzavlaki and Moustakas, 2020). One of the classic functions of TGFB1 is activating fibroblasts into myofibroblasts, in which they gain more actin fibers and produce more collagen (Vallée and Lecarpentier, 2019). Maroni and Davis demonstrated that TGFB1 induces collagen and laminin production by bovine luteal fibroblasts *in vitro* (Maroni and Davis, 2012). In luteal endothelial cells, TGFB1 decreased DNA incorporation, cell migration, and endothelial sprouting (Maroni and Davis, 2011). In that same study, TGFB1 increased caspase-3/7 activity of bovine luteal endothelial cells, disrupted the distribution of VE-cadherin, and increased endothelial cell permeability (Maroni and Davis, 2011). These findings demonstrate that TGFB1 has a direct effect on luteal angioregression by elimination of endothelial cells, increased vascular permeability, and fibrosis of the vasculature.

6 Summary and future directions

Although the exact mechanism of vascular regression of the corpus luteum remains unclear, it is known that blood flow transiently increases then is impaired. The early increase in blood flow may be from the release of vasodilators like NO during luteal regression. Based on observations in other tissues, shear stress may alter endothelial cell morphology and consequent function (Malek and Izumo, 1996; Watts, 2007). As mentioned in the review, endothelial cells themselves are also sensitive to growth factors and cytokines released during luteal regression. Increased production of cytokines in the luteal tissue microenvironment

during regression may contribute to such changes in morphology as well as death of endothelial cells. The cytokine-mediated events, in conjunction with the loss of growth factors that typically signal endothelial cell survival and proliferation, contribute to angioregression in the corpus luteum. Endothelial cell apoptosis may result in sloughing of cells into capillaries and increased permeability of the vessels.

In this review, we summarized the current knowledge on changes in blood flow, presence of vasoactive factors and inflammatory cytokines, which all may contribute to angioregression of the corpus luteum. However, endothelial cells themselves may also be acting as luteolytic agents. Luteal endothelial cells can produce cytokines such as TNF as well as chemokines like monocyte chemoattractant 1 protein, which attracts immune cells to the site of luteolysis (Liptak et al., 2005; Cherry et al., 2008). Furthermore, *in vivo* studies revealed that PGF2α rapidly induced P-selectin, a leukocyte adhesion molecule, in bovine endothelial cells and recruited polymorphonuclear neutrophils into the corpus luteum (Shirasuna et al., 2012a). Studies in the primate indicate infiltration of macrophages, neutrophils, and natural killer cells in the regressing corpus luteum (Bishop et al., 2017). Endothelial-immune cell interactions may exacerbate luteolysis, as *in vitro* studies revealed that contact co-culture of endothelial cells with peripheral blood mononuclear cells was required to synergistically increase monocyte chemoattractant protein 1 (Liptak et al., 2005). Endothelial cells also express class II major histocompatibility (MHC) proteins, which allow binding and subsequent activation of T lymphocytes (Cannon et al., 2007a). Luteal endothelial cells also express proteins that stabilize MHC II binding to T-cells as well as the costimulatory molecule CD80, which induces T-cell survival and proliferation (Cannon et al., 2006; Cannon et al., 2007b). However, most of the current research focuses on the influence of endothelial cells on immune cells rather than *vice versa*. Studies are needed to determine how immune cell binding to luteal endothelial cells affects vascular permeability, recruitment of other immune cells and viability.

This review has centered on the actions of a number of growth factors and cytokines, but newly developing research implicates additional factors like adipokines and neuropeptides in luteal regression. The potential role of many of these factors is the subject of a recent review (Mlyczyńska et al., 2022). Many of these factors impact metabolic pathways in cells that ultimately control cellular fate. How adipokines and neuropeptides contribute to luteal angioregression is a question requiring further investigation.

It is well established that structural regression of the corpus luteum involves programmed cell death of endothelial cells and steroidogenic cells. However, recent research indicates that apoptosis, autophagic cell death, and necroptosis may all contribute to regression of the bovine corpus luteum (Hojo et al., 2022). It is not known whether and how each of these processes contribute to the demise of endothelial cells. Additionally, non-apoptotic pathways of angioregression may also occur in the regressing corpus luteum, such as a change in endothelial cell phenotype. Senescence of vascular endothelial cells has been associated with vascular dysfunction in variety of disease states by impairing new angiogenesis and endothelial-mediated changes in vascular tone (Shosha et al., 2018; Kiss et al., 2020; Cohen et al., 2021; Bloom et al., 2023a; Bloom et al., 2023b; Han and Kim, 2023). Senescent cells exhibit a pro-inflammatory phenotype (Birch and Gil, 2020); thus, if endothelial cell senescence is present in the regressing corpus luteum, then these senescent endothelial cells may be producing the inflammatory mediators that contribute to angioregression and the viability of steroidogenic cells. Research is needed to determine the phenotypes of luteal endothelial cells before and during luteal regression.

Another possibility is that some endothelial cells are changing phenotype by transdifferentiation or EndMT. This phenomenon has been implicated in vascular dysfunction of various disease states such as cancer, vascular fibrosis, sclerosis, pulmonary hypertension, and atherosclerosis (Zeisberg et al., 2007; Manetti et al., 2017; Alvandi and Bischoff, 2021; Cai et al., 2021; Gorelova et al., 2021). EndMT is known to be initiated by TGFB1, and is exacerbated by TNF in cancer-associated fibroblasts (Yoshimatsu et al., 2020); therefore, it is possible that the increases in content of TNF and TGFB1 during luteal regression can contribute to EndMT. Because luteal endothelial cells exhibit a variety of phenotypes (Spanel-Borowski and van der Bosch, 1990; Spanel-Borowski, 1991; Fenyves et al., 1994; Davis et al., 2003), it is possible that different endothelial cells undergo different forms of regression, for instance cell death compared to senescence or EndMT. Lineage tracing models using a transgenic animal model can be used to study EndMT *in vivo* (Sánchez-Duffhues et al., 2018), but has yet to be done in the corpus luteum to track whether EndMT occurs or when it occurs in the regression process. It is possible that EndMT may appear later in regression, when fibrosis occurs, following inflammation.

Furthermore, many of these previous studies are done in cultured endothelial cells from whole digested luteal tissue. Thus, arteriolar, venular, and microvascular endothelial cells are all considered to be the same. However, studies in other tissues indicate that the type of vessel from which the endothelial cell belonged can have an effect of its responsiveness to certain environmental stressors. For instance, Polk et al. demonstrated that human dermal microvascular cells slightly oriented themselves in response to shear stress, and Reinitz et al. demonstrated that human brain microvascular endothelial cells did not change shape as HUVECs did in response to shear stress (Reinitz et al., 2015; Polk et al., 2022). It was also demonstrated that rat endothelial cells from different vessels respond differently to vasoactive factors, such as acetylcholine-induced relaxation (Abukabda et al., 2017). In that study, it was identified that titanium dioxide nanoparticles impaired acetylcholine-induced relaxation in endothelial cells from the aorta, third-, and fourth-order mesenteric arteries, whereas it had no effect in endothelial cells from the femoral artery (Abukabda et al., 2017). Additionally, human dermal microvascular endothelial cells exhibited less damage in response to *Candida albicans* compared to HUVECs but more damage in response to *Staphylococcus aureus* (Seidl et al., 2012). The human microvascular endothelial cells also released less IL-8 compared to HUVECs in response to either pathogen (Seidl

et al., 2012). Because of such differences between macro- and microvascular endothelial cell responses to pathogens and shear stress, it is important to decipher the macro- and microvascular responses separately when studying luteal angioregression. Various changes in the vasculature and causes of endothelial cell death have been identified in the corpus luteum (summarized in Table 1). However, a unifying mechanism of vascular regression has yet to be established. The current knowledge revolves around changes in blood flow and secreted factors that may affect endothelial cell viability; yet, neither the exact transcriptome or proteome of regressing vascular endothelial cells nor their varying phenotypes has yet to be studied. Single-cell proteomic or transcriptomic studies conducted during luteal regression could provide new insight on how changes in the luteal microenvironment in response to PGF2α lead to angioregression.

Furthermore, the fibrosis of various luteal vessels has yet to be explored. Studies show that while the microvasculature is disappearing the walls of larger vessels become thicker during luteal regression (Bauer et al., 2003). The presence of myofibroblast-like cells in the regressing corpus luteum (Nio-Kobayashi et al., 2016) may contribute to a fibrotic response. As reviewed above, many endothelial-reactive factors may contribute to fibrosis. Fibroblast activation by TGFB1 and FGF2 (Monaco et al., 2023) and deposition of matrix may be a major contributor to this process. EDN1 has been implicated in pulmonary fibrosis and TNF-induced EndMT in cardiac fibrosis (Swigris and Brown, 2010; Hu et al., 2023). Thrombospondins may also contribute to vascular fibrosis through TGFB1 (Sweetwyne and Murphy-Ullrich, 2012). Given that the end stage of luteal regression is a fibrotic corpus albicans, more studies are needed to elucidate the mechanism of luteal vascular regression beyond blood flow and apoptotic cell death of endothelial cells.

Author contributions

CM: Writing–original draft, Writing–review and editing. JD: Writing–original draft, Writing–review and editing.

Funding

The authors declare financial support was received for the research, authorship, and/or publication of this article. This research was supported by an American Heart Association Predoctoral Fellowship (https://doi.org/10.58275/AHA.23PRE1018741.pc.gr.161093) (CM), USDA NIFA Grants 2017-67015-26450 and 2023-67015-40795 (JD), NIH grants R03HD112585 and R01 HD092263 (JD), and Department of Veterans Affairs I01 BX004272 (JD). This work was also supported by The Olson Center for Women's Health. JD is the recipient of VA Senior Research Career Scientist Award (IK6BX005797).

Conflict of interest

The authors declare that the research was conducted in the absence of any commercial or financial relationships that could be construed as a potential conflict of interest.

Publisher's note

References

Abukabda, A. B., Stapleton, P. A., Mcbride, C. R., Yi, J., and Nurkiewicz, T. R. (2017). Heterogeneous vascular bed responses to pulmonary titanium dioxide nanoparticle exposure. *Front. Cardiovasc Med.* 4, 33. doi:10.3389/fcvm.2017.00033

Acosta, T. J., Yoshizawa, N., Ohtani, M., and Miyamoto, A. (2002). Local changes in blood flow within the early and midcycle corpus luteum after prostaglandin F(2 alpha) injection in the cow. *Biol. reproduction* 66, 651–658. doi:10.1095/biolreprod66.3.651

Adams, J. C., and Lawler, J. (2011). The thrombospondins. *Cold Spring Harb. Perspect. Biol.* 3, a009712. doi:10.1101/cshperspect.a009712

Adashi, E. Y., Resnick, C. E., Packman, J. N., Hurwitz, A., and Payne, D. W. (1990). Cytokine-mediated regulation of ovarian function: tumor necrosis factor alpha inhibits gonadotropin-supported progesterone accumulation by differentiating and luteinized murine granulosa cells. *Am. J. Obstet. Gynecol.* 162, 889–896. doi:10.1016/0002-9378(90)91289-o

Alan, E., and Kulak, Y. (2021). The immunoexpression patterns of fibroblast growth factors in the pregnant and postpartum rat ovary. *Reprod. Fertil. Dev.* 33, 817–830. doi:10.1071/RD21025

Alvandi, Z., and Bischoff, J. (2021). Endothelial-mesenchymal transition in cardiovascular disease. *Arterioscler. Thromb. Vasc. Biol.* 41, 2357–2369. doi:10.1161/ATVBAHA.121.313788

Armstrong, L. C., and Bornstein, P. (2003). Thrombospondins 1 and 2 function as inhibitors of angiogenesis. *Matrix Biol.* 22, 63–71. doi:10.1016/s0945-053x(03)00005-2

Asakai, R., Tamura, K., Eishi, Y., Iwamoto, M., Kato, Y., and Okamoto, R. (1993). Basic fibroblast growth factor (bFGF) receptors decrease with luteal age in rat ovarian luteal cells: colocalization of bFGF receptors and bFGF in luteal cells. *Endocrinology* 133, 1074–1084. doi:10.1210/endo.133.3.7689947

Augustin, H. G. (2000). Vascular morphogenesis in the ovary. *Baillieres Best. Pract. Res. Clin. Obstet. Gynaecol.* 14, 867–882. doi:10.1053/beog.2000.0132

Azmi, T. I., and O'Shea, J. D. (1984). Mechanism of deletion of endothelial cells during regression of the corpus luteum. *Lab. Invest.* 51, 206–217.

Baddela, V. S., Koczan, D., Viergutz, T., Vernunft, A., and Vanselow, J. (2018). Global gene expression analysis indicates that small luteal cells are involved in extracellular matrix modulation and immune cell recruitment in the bovine corpus luteum. *Mol. Cell. Endocrinol.* 474, 201–213. doi:10.1016/j.mce.2018.03.011

Baffert, F., Le, T., Sennino, B., Thurston, G., Kuo, C. J., Hu-Lowe, D., et al. (2006). Cellular changes in normal blood capillaries undergoing regression after inhibition of VEGF signaling. *Am. J. Physiology-Heart Circulatory Physiology* 290, H547–H559. doi:10.1152/ajpheart.00616.2005

Bagavandoss, P., and Wilks, J. (1990). Specific inhibition of endothelial cell proliferation by thrombospondin. *Biochem. biophysical Res. Commun.* 170, 867–872. doi:10.1016/0006-291x(90)92171-u

Bartok, B., and Firestein, G. S. (2010). Fibroblast-like synoviocytes: key effector cells in rheumatoid arthritis. *Immunol. Rev.* 233, 233–255. doi:10.1111/j.0105-2896.2009.00859.x

Basavaraja, R., Przygrodzka, E., Pawlinski, B., Gajewski, Z., Kaczmarek, M. M., and Meidan, R. (2017). Interferon-tau promotes luteal endothelial cell survival and inhibits specific luteolytic genes in bovine corpus luteum. *Reproduction* 154, 559–568. doi:10.1530/REP-17-0290

Bauer, M., Schilling, N., and Spanel-Borowski, K. (2003). Development and regression of non-capillary vessels in the bovine corpus luteum. *Cell tissue Res.* 311, 199–205. doi:10.1007/s00441-002-0640-x

Bender, H. R., Campbell, G. E., Aytoda, P., Mathiesen, A. H., and Duffy, D. M. (2019). Thrombospondin 1 (THBS1) promotes follicular angiogenesis, luteinization, and ovulation in primates. *Front. Endocrinol. (Lausanne)* 10, 727. doi:10.3389/fendo.2019.00727

Benigni, A., Cassis, P., and Remuzzi, G. (2010). Angiotensin II revisited: new roles in inflammation, immunology and aging. *EMBO Mol. Med.* 2, 247–257. doi:10.1002/emmm.201000080

Benjamin, L. E., and Keshet, E. (1997). Conditional switching of vascular endothelial growth factor (VEGF) expression in tumors: induction of endothelial cell shedding and regression of hemangioblastoma-like vessels by VEGF withdrawal. *Proc. Natl. Acad. Sci. U. S. A.* 94, 8761–8766. doi:10.1073/pnas.94.16.8761

Benton, R. L., Maddie, M. A., Worth, C. A., Mahoney, E. T., Hagg, T., and Whittemore, S. R. (2008). Transcriptomic screening of microvascular endothelial cells implicates novel molecular regulators of vascular dysfunction after spinal cord injury. *J. Cereb. Blood Flow. Metab.* 28, 1771–1785. doi:10.1038/jcbfm.2008.76

Benyo, D. F., and Pate, J. L. (1992). Tumor necrosis factor-alpha alters bovine luteal cell synthetic capacity and viability. *Endocrinology* 130, 854–860. doi:10.1210/endo.130.2.1733731

Berisha, B., Schams, D., Rodler, D., and Pfaffl, M. W. (2016a). Angiogenesis in the ovary - the most important regulatory event for follicle and corpus luteum development and function in cow - an overview. *Anat. Histol. Embryol.* 45, 124–130. doi:10.1111/ahe.12180

Berisha, B., Schams, D., Rodler, D., Sinowatz, F., and Pfaffl, M. W. (2016b). Expression and localization of members of the thrombospondin family during final follicle maturation and corpus luteum formation and function in the bovine ovary. *J. Reprod. Dev.* 62, 501–510. doi:10.1262/jrd.2016-056

Birch, J., and Gil, J. (2020). Senescence and the SASP: many therapeutic avenues. *Genes Dev.* 34, 1565–1576. doi:10.1101/gad.343129.120

Bishop, C. V., Xu, F., Steinbach, R., Ficco, E., Hyzer, J., Blue, S., et al. (2017). Changes in immune cell distribution and their cytokine/chemokine production during regression of the rhesus macaque corpus luteum. *Biol. Reprod.* 96, 1210–1220. doi:10.1093/biolre/iox052

Bloom, S. I., Islam, M. T., Lesniewski, L. A., and Donato, A. J. (2023a). Mechanisms and consequences of endothelial cell senescence. *Nat. Rev. Cardiol.* 20, 38–51. doi:10.1038/s41569-022-00739-0

Bloom, S. I., Liu, Y., Tucker, J. R., Islam, M. T., Machin, D. R., Abdeahad, H., et al. (2023b). Endothelial cell telomere dysfunction induces senescence and results in vascular and metabolic impairments. *Aging Cell* 22, e13875. doi:10.1111/acel.13875

Bourdiec, A., Bédard, D., Rao, C. V., and Akoum, A. (2013). Human chorionic gonadotropin regulates endothelial cell responsiveness to interleukin 1 and amplifies the cytokine-mediated effect on cell proliferation, migration and the release of angiogenic factors. *Am. J. Reprod. Immunol.* 70, 127–138. doi:10.1111/aji.12080

Branton, M. H., and Kopp, J. B. (1999). TGF-beta and fibrosis. *Microbes Infect.* 1, 1349–1365. doi:10.1016/s1286-4579(99)00250-6

Burke, G. L., Evans, G. W., Riley, W. A., Sharrett, A. R., Howard, G., Barnes, R. W., et al. (1995). Arterial wall thickness is associated with prevalent cardiovascular disease in middle-aged adults. The Atherosclerosis Risk in Communities (ARIC) Study. *Stroke* 26, 386–391. doi:10.1161/01.str.26.3.386

Cai, W., Sun, X., Jin, F., Xiao, D., Li, H., Sun, H., et al. (2021). PERK-eIF2α-ERK1/2 axis drives mesenchymal-endothelial transition of cancer-associated fibroblasts in pancreatic cancer. *Cancer Lett.* 515, 86–95. doi:10.1016/j.canlet.2021.05.021

Campinho, P., Vilfan, A., and Vermot, J. (2020). Blood flow forces in shaping the vascular system: A focus on endothelial cell behavior. *Front. Physiology* 11, 552. doi:10.3389/fphys.2020.00552

Cannon, M. J., Davis, J. S., and Pate, J. L. (2007b). Expression of costimulatory molecules in the bovine corpus luteum. *Reprod. Biol. Endocrinol.* 5, 5. doi:10.1186/1477-7827-5-5

Cannon, M. J., Davis, J. S., and Pate, J. L. (2006). Presence and regulation of messenger ribonucleic acids encoding components of the class II major histocompatibility complex-associated antigen processing pathway in the bovine corpus luteum. *Reproduction* 131, 689–698. doi:10.1530/rep.1.00906

Cannon, M. J., Davis, J. S., and Pate, J. L. (2007a). The class II major histocompatibility complex molecule BoLA-DR is expressed by endothelial cells of the bovine corpus luteum. *Reproduction* 133, 991–1003. doi:10.1530/REP-06-0362

Cherry, J. A., Hou, X., Rueda, B. R., Davis, J. S., and Townson, D. H. (2008). Microvascular endothelial cells of the bovine corpus luteum: A comparative examination of the estrous cycle and pregnancy. *J. Reproduction Dev.* 54, 183–191. doi:10.1262/jrd.19182

Cohen, C., Le Goff, O., Soysouvanh, F., Vasseur, F., Tanou, M., Nguyen, C., et al. (2021). Glomerular endothelial cell senescence drives age-related kidney disease through PAI-1. *EMBO Mol. Med.* 13, e14146. doi:10.15252/emmm.202114146

Corinaldesi, G., and Corinaldesi, C. (2008). Arterial wall thickness: marker of atherosclerosis or risk factor for thrombosis. *Blood* 112, 5470. doi:10.1182/blood.v112.11.5470.5470

Csapo, A. I., Pulkkinen, M. O., and Kaihola, H. L. (1974). The relationship between the timing of luteectomy and the incidence of complete abortions. *Am. J. Obstet. Gynecol.* 118, 985–989. doi:10.1016/0002-9378(74)90671-1

Davis, J. S., Rueda, B. R., and Spanel-Borowski, K. (2003). Microvascular endothelial cells of the corpus luteum. *Reprod. Biol. Endocrinol.* 1, 89. doi:10.1186/1477-7827-1-89

Dawson, D. W., Pearce, S. F. A., Zhong, R., Silverstein, R. L., Frazier, W. A., and Bouck, N. P. (1997). CD36 mediates the *in vitro* inhibitory effects of thrombospondin-1 on endothelial cells. *J. Cell Biol.* 138, 707–717. doi:10.1083/jcb.138.3.707

Dedkov, E., Kostrominova, T., Borisov, A., and Carlson, B. (2002). Resistance vessel remodeling and reparative angiogenesis in the microcirculatory bed of long-term denervated skeletal muscles. *Microvasc. Res.* 63, 96–114. doi:10.1006/mvre.2001.2372

Dimmeler, S., and Zeiher, A. M. (1999). Nitric oxide-an endothelial cell survival factor. *Cell Death Differ.* 6, 964–968. doi:10.1038/sj.cdd.4400581

Djonov, V., Andres, A. C., and Ziemiecki, A. (2001). Vascular remodelling during the normal and malignant life cycle of the mammary gland. *Microsc. Res. Tech.* 52, 182–189. doi:10.1002/1097-0029(20010115)52:2<182::AID-JEMT1004>3.0.CO;2-M

Doerr, M. D., Goravanahally, M. P., Rhinehart, J. D., Inskeep, E. K., and Flores, J. A. (2008). Effects of endothelin receptor type-A and type-B antagonists on prostaglandin F2alpha-induced luteolysis of the sheep corpus luteum. *Biol. reproduction* 78, 688–696. doi:10.1095/biolreprod.107.064105

Duncan, W. C., Van Den Driesche, S., and Fraser, H. M. (2008). Inhibition of vascular endothelial growth factor in the primate ovary up-regulates hypoxia-inducible factor-1alpha in the follicle and corpus luteum. *Endocrinology* 149, 3313–3320. doi:10.1210/en.2007-1649

Eklund, L., and Saharinen, P. (2013). Angiopoietin signaling in the vasculature. *Exp. Cell Res.* 319, 1271–1280. doi:10.1016/j.yexcr.2013.03.011

Estevez, A., Tognetti, T., Luchetti, C., Sander, V., and Motta, A. (2003). Sequence of interleukin 1beta actions on corpus luteum regression: relationship with inducible cyclooxygenase and nitric oxide synthase expression. *Reproduction* 126, 639–645. doi:10.1530/rep.0.1260639

Evans, J. J. (1987). The effect of prostaglandin F2 alpha administration on progesterone after hysterectomy of Guinea-pigs. *Prostaglandins* 33, 561–566. doi:10.1016/0090-6980(87)90279-6

Farberov, S., Basavaraja, R., and Meidan, R. (2019). Thrombospondin-1 at the crossroads of corpus luteum fate decisions. *Reproduction* 157, R73–R83. doi:10.1530/REP-18-0530

Farberov, S., and Meidan, R. (2016). Thrombospondin-1 affects bovine luteal function via transforming growth factor-beta1-dependent and independent actions. *Biol. Reproduction* 94, 25. doi:10.1095/biolreprod.115.135822

Fenyves, A. M., Saxer, M., and Spanel-Borowski, K. (1994). Bovine microvascular endothelial cells of separate morphology differ in growth and response to the action of interferon-gamma. *Experientia* 50, 99–104. doi:10.1007/BF01984942

Fiedler, U., Reiss, Y., Scharpfenecker, M., Grunow, V., Koidl, S., Thurston, G., et al. (2006). Angiopoietin-2 sensitizes endothelial cells to TNF-alpha and has a crucial role in the induction of inflammation. *Nat. Med.* 12, 235–239. doi:10.1038/nm1351

Förstermann, U., and Sessa, W. C. (2012). Nitric oxide synthases: regulation and function. *Eur. Heart J.* 33, 829–837. doi:10.1093/eurheartj/ehr304

Fraser, H. M., and Duncan, W. C. (2009). SRB reproduction, fertility and development award lecture 2008. Regulation and manipulation of angiogenesis in the ovary and endometrium. *Reprod. Fertil. Dev.* 21, 377–392. doi:10.1071/rd08272

Frezzetti, D., Gallo, M., Maiello, M. R., D'Alessio, A., Esposito, C., Chicchinelli, N., et al. (2017). VEGF as a potential target in lung cancer. *Expert Opin. Ther. Targets* 21, 959–966. doi:10.1080/14728222.2017.1371137

Fridén, B. E., Runesson, E., Hahlin, M., and Brannstrom, M. (2000). Evidence for nitric oxide acting as a luteolytic factor in the human corpus luteum. *Mol. Hum. Reprod.* 6, 397–403. doi:10.1093/molehr/6.5.397

Friedman, A., Weiss, S., Levy, N., and Meidan, R. (2000). Role of tumor necrosis factor alpha and its type I receptor in luteal regression: induction of programmed cell death in bovine corpus luteum-derived endothelial cells. *Biol. Reproduction* 63, 1905–1912. doi:10.1095/biolreprod63.6.1905

Fyhrquist, F., Metsärinne, K., and Tikkanen, I. (1995). Role of angiotensin II in blood pressure regulation and in the pathophysiology of cardiovascular disorders. *J. Hum. Hypertens.* 9 (5), S19–S24.

Geva, E., and Jaffe, R. B. (2000). Role of vascular endothelial growth factor in ovarian physiology and pathology. *Fertil. Steril.* 74, 429–438. doi:10.1016/s0015-0282(00)00670-1

Ginther, O., Gastal, E., Gastal, M., Utt, M., and Beg, M. (2007). Luteal blood flow and progesterone production in mares. *Animal Reproduction Sci.* 99, 213–220. doi:10.1016/j.anireprosci.2006.05.018

Girão-Silva, T., Fonseca-Alaniz, M. H., Ribeiro-Silva, J. C., Lee, J., Patil, N. P., Dallan, L. A., et al. (2021). High stretch induces endothelial dysfunction accompanied by oxidative stress and actin remodeling in human saphenous vein endothelial cells. *Sci. Rep.* 11, 13493. doi:10.1038/s41598-021-93081-3

Girsh, E., Milvae, R. A., Wang, W., and Meidan, R. (1996a). Effect of endothelin-1 on bovine luteal cell function: role in prostaglandin F2alpha-induced antisteroidogenic action. *Endocrinology* 137, 1306–1312. doi:10.1210/endo.137.4.8625904

Girsh, E., Wang, W., Mamluk, R., Arditi, F., Friedman, A., Milvae, R. A., et al. (1996b). Regulation of endothelin-1 expression in the bovine corpus luteum: elevation by

prostaglandin F 2 alpha. *Endocrinology* 137, 5191–5196. doi:10.1210/endo.137.12.8940334

Goding, J. R. (1974). The demonstration that PGF2alpha is the uterine luteolysin in the Ewe. *J. Reprod. Fertil.* 38, 261–271. doi:10.1530/jrf.0.0380261

Goede, V., Schmidt, T., Kimmina, S., Kozian, D., and Augustin, H. G. (1998). Analysis of blood vessel maturation processes during cyclic ovarian angiogenesis. *Lab. Invest.* 78, 1385–1394.

Gorelova, A., Berman, M., and Al Ghouleh, I. (2021). Endothelial-to-Mesenchymal transition in pulmonary arterial hypertension. *Antioxid. Redox Signal* 34, 891–914. doi:10.1089/ars.2020.8169

Gospodarowicz, D., Abraham, J. A., and Schilling, J. (1989). Isolation and characterization of a vascular endothelial cell mitogen produced by pituitary-derived folliculo stellate cells. *Proc. Natl. Acad. Sci. U. S. A.* 86, 7311–7315. doi:10.1073/pnas.86.19.7311

Gospodarowicz, D. (1974). Localisation of a fibroblast growth factor and its effect alone and with hydrocortisone on 3T3 cell growth. *Nature* 249, 123–127. doi:10.1038/249123a0

Greenaway, J., Lawler, J., Moorehead, R., Bornstein, P., Lamarre, J., and Petrik, J. (2007). Thrombospondin-1 inhibits VEGF levels in the ovary directly by binding and internalization via the low density lipoprotein receptor-related protein-1 (LRP-1). *J. Cell. physiology* 210, 807–818. doi:10.1002/jcp.20904

Guo, Y. X., Zhang, G. M., Yao, X. L., Tong, R., Cheng, C. Y., Zhang, T. T., et al. (2019). Effects of nitric oxide on steroidogenesis and apoptosis in goat luteinized granulosa cells. *Theriogenology* 126, 55–62. doi:10.1016/j.theriogenology.2018.12.007

Han, Y., and Kim, S. Y. (2023). Endothelial senescence in vascular diseases: current understanding and future opportunities in senotherapeutics. *Exp. Mol. Med.* 55, 1–12. doi:10.1038/s12276-022-00906-w

Hayashi, K., and Miyamoto, A. (1999). Angiotensin II interacts with prostaglandin F2alpha and endothelin-1 as a local luteolytic factor in the bovine corpus luteum *in vitro*. *Biol. Reproduction* 60, 1104–1109. doi:10.1095/biolreprod60.5.1104

Hayashi, K., Miyamoto, A., Berisha, B., Kosmann, M. R., Okuda, K., and Schams, D. (2000). Regulation of angiotensin II production and angiotensin receptors in microvascular endothelial cells from bovine corpus luteum. *Biol. Reproduction* 62, 162–167. doi:10.1095/biolreprod62.1.162

Hazzard, T., Christenson, L., and Stouffer, R. (2000). Changes in expression of vascular endothelial growth factor and angiopoietin-1 and-2 in the macaque corpus luteum during the menstrual cycle. *Mol. Hum. Reprod.* 6, 993–998. doi:10.1093/molehr/6.11.993

Hehnke-Vagnoni, K. E., Clark, C. L., Taylor, M. J., and Ford, S. P. (1995). Presence and localization of tumor necrosis factor alpha in the corpus luteum of nonpregnant and pregnant pigs. *Biol. Reproduction* 53, 1339–1344. doi:10.1095/biolreprod53.6.1339

Henkes, L. E., Sullivan, B. T., Lynch, M. P., Kolesnick, R., Arsenault, D., Puder, M., et al. (2008). Acid sphingomyelinase involvement in tumor necrosis factor alpha-regulated vascular and steroid disruption during luteolysis *in vivo*. *Proc. Natl. Acad. Sci. U. S. A.* 105, 7670–7675. doi:10.1073/pnas.0712260105

Henry, F., Quatresooz, P., Valverde-Lopez, J. C., and Piérard, G. E. (2006). Blood vessel changes during pregnancy: A review. *Am. J. Clin. Dermatol* 7, 65–69. doi:10.2165/00128071-200607010-00006

Herzog, K., Brockhan-Lüdemann, M., Kaske, M., Beindorff, N., Paul, V., Niemann, H., et al. (2010). Luteal blood flow is a more appropriate indicator for luteal function during the bovine estrous cycle than luteal size. *Theriogenology* 73, 691–697. doi:10.1016/j.theriogenology.2009.11.016

Hinckley, S., and Milvae, R. (2001). Endothelin-1 mediates prostaglandin F(2alpha)-induced luteal regression in the Ewe. *Biol. reproduction* 64, 1619–1623. doi:10.1095/biolreprod64.6.1619

Hojo, T., Al-Zi'Abi, M. O., Skarzynski, D. J., Acosta, T. J., and Okuda, K. (2009). Changes in the vasculature of bovine corpus luteum during the estrous cycle and prostaglandin F2alpha-induced luteolysis. *J. Reproduction Dev.* 55, 512–517. doi:10.1262/jrd.20257

Hojo, T., Skarzynski, D. J., and Okuda, K. (2022). Apoptosis, autophagic cell death, and necroptosis: different types of programmed cell death in bovine corpus luteum regression. *J. Reprod. Dev.* 68, 355–360. doi:10.1262/jrd.2022-097

Hou, X., Arvisais, E. W., Jiang, C., Chen, D.-B., Roy, S. K., Pate, J. L., et al. (2008). Prostaglandin F2alpha stimulates the expression and secretion of transforming growth factor B1 via induction of the early growth response 1 gene (EGR1) in the bovine corpus luteum. *Mol. Endocrinol.* 22, 403–414. doi:10.1210/me.2007-0272

Hu, H., Huang, J., Zhang, S., Zhang, B., Li, W., and Sun, K. (2023). Tumor necrosis factor-α stimulation endothelial-to-mesenchymal transition during cardiac fibrosis via endothelin-1 signaling. *J. Biochem. Mol. Toxicol.* 37, e23411. doi:10.1002/jbt.23411

Intengan, H. D., and Schiffrin, E. L. (2001). Vascular remodeling in hypertension: roles of apoptosis, inflammation, and fibrosis. *Hypertension* 38, 581–587. doi:10.1161/hy09t1.096249

Ishii, Y., Sawada, T., Kubota, K., Fuchinoue, S., Teraoka, S., and Shimizu, A. (2005). Injury and progressive loss of peritubular capillaries in the development of chronic allograft nephropathy. *Kidney Int.* 67, 321–332. doi:10.1111/j.1523-1755.2005.00085.x

Janson, P. O., Damber, J. E., and Axén, C. (1981). Luteal blood flow and progesterone secretion in pseudopregnant rabbits. *J. Reprod. Fertil.* 63, 491–497. doi:10.1530/jrf.0.0630491

Jonczyk, A. W., Piotrowska-Tomala, K. K., and Skarzynski, D. J. (2021). Comparison of intra-CL injection and peripheral application of prostaglandin F(2α) analog on luteal blood flow and secretory function of the bovine corpus luteum. *Front. Vet. Sci.* 8, 811809. doi:10.3389/fvets.2021.811809

Kanazawa, T., Seki, M., and Iga, K. (2022). Early pregnancy diagnosis based on luteal morphology and blood flow on Days 17-21 post-artificial insemination in Japanese Black cattle. *Theriogenology* 181, 69–78. doi:10.1016/j.theriogenology.2022.01.002

Kidder, E., Pea, M., Cheng, S., Koppada, S.-P., Visvanathan, S., Henderson, Q., et al. (2023). The interleukin-1 receptor type-1 in disturbed flow-induced endothelial mesenchymal activation. *Front. Cardiovasc. Med.* 10, 1190460. doi:10.3389/fcvm.2023.1190460

Kiss, T., Nyúl-Tóth, Á., Balasubramanian, P., Tarantini, S., Ahire, C., Delfavero, J., et al. (2020). Single-cell RNA sequencing identifies senescent cerebromicrovascular endothelial cells in the aged mouse brain. *Geroscience* 42, 429–444. doi:10.1007/s11357-020-00177-1

Knickerbocker, J. J., Wiltbank, M. C., and Niswender, G. D. (1988). Mechanisms of luteolysis in domestic livestock. *Domest. Anim. Endocrinol.* 5, 91–107. doi:10.1016/0739-7240(88)90011-2

Kobayashi, H., and Terao, T. (1997). Hyaluronic acid-specific regulation of cytokines by human uterine fibroblasts. *Am. J. Physiol.* 273, C1151–C1159. doi:10.1152/ajpcell.1997.273.4.C1151

Kobayashi, S., Berisha, B., Amselgruber, W., Schams, D., and Miyamoto, A. (2001). Production and localisation of angiotensin II in the bovine early corpus luteum: A possible interaction with luteal angiogenic factors and prostaglandin F2alpha. *J. Endocrinol.* 170, 369–380. doi:10.1677/joe.0.1700369

Kolatorova, L., Vitku, J., Suchopar, J., Hill, M., and Parizek, A. (2022). Progesterone: A steroid with wide range of effects in physiology as well as human medicine. *Int. J. Mol. Sci.* 23, 7989. doi:10.3390/ijms23147989

Korzekwa, A. J., Okuda, K., Woclawek-Potocka, I., Murakami, S., and Skarzynski, D. J. (2006). Nitric oxide induces apoptosis in bovine luteal cells. *J. Reprod. Dev.* 52, 353–361. doi:10.1262/jrd.17092

Kowalczyk-Zieba, I., Boruszewska, D., Sinderewicz, E., Skarzynski, D. J., and Woclawek-Potocka, I. (2014). Influence of lysophosphatidic acid on nitric oxide-induced luteolysis in steroidogenic luteal cells in cows. *Biol. Reprod.* 90, 17. doi:10.1095/biolreprod.113.113357

Lei, Z., Chegini, N., and Rao, C. V. (1991). Quantitative cell composition of human and bovine corpora lutea from various reproductive states. *Biol. reproduction* 44, 1148–1156. doi:10.1095/biolreprod44.6.1148

Liptak, A. R., Sullivan, B. T., Henkes, L. E., Wijayagunawardane, M. P. B., Miyamoto, A., Davis, J. S., et al. (2005). Cooperative expression of monocyte chemoattractant protein 1 within the bovine corpus luteum: evidence of immune cell-endothelial cell interactions in a coculture system. *Biol. Reproduction* 72, 1169–1176. doi:10.1095/biolreprod.104.032953

Lopez-Castejon, G., and Brough, D. (2011). Understanding the mechanism of IL-1β secretion. *Cytokine Growth Factor Rev.* 22, 189–195. doi:10.1016/j.cytogfr.2011.10.001

Lüttgenau, J., Ulbrich, S. E., Beindorff, N., Honnens, A., Herzog, K., and Bollwein, H. (2011). Plasma progesterone concentrations in the mid-luteal phase are dependent on luteal size, but independent of luteal blood flow and gene expression in lactating dairy cows. *Animal Reproduction Sci.* 125, 20–29. doi:10.1016/j.anireprosci.2011.02.002

Luu, R. J., Hoefler, B. C., Gard, A. L., Ritenour, C. R., Rogers, M. T., Kim, E. S., et al. (2023). Fibroblast activation in response to TGFβ1 is modulated by co-culture with endothelial cells in a vascular organ-on-chip platform. *Front. Mol. Biosci.* 10, 1160851. doi:10.3389/fmolb.2023.1160851

Maisonpierre, P. C., Suri, C., Jones, P. F., Bartunkova, S., Wiegand, S. J., Radziejewski, C., et al. (1997). Angiopoietin-2, a natural antagonist for Tie2 that disrupts *in vivo* angiogenesis. *Science* 277, 55–60. doi:10.1126/science.277.5322.55

Malek, A. M., and Izumo, S. (1996). Mechanism of endothelial cell shape change and cytoskeletal remodeling in response to fluid shear stress. *J. Cell Sci.* 109, 713–726. doi:10.1242/jcs.109.4.713

Malek, M. H., Olfert, I. M., and Esposito, F. (2010). Detraining losses of skeletal muscle capillarization are associated with vascular endothelial growth factor protein expression in rats. *Exp. Physiol.* 95, 359–368. doi:10.1113/expphysiol.2009.050369

Manetti, M., Romano, E., Rosa, I., Guiducci, S., Bellando-Randone, S., De Paulis, A., et al. (2017). Endothelial-to-mesenchymal transition contributes to endothelial dysfunction and dermal fibrosis in systemic sclerosis. *Ann. Rheum. Dis.* 76, 924–934. doi:10.1136/annrheumdis-2016-210229

Maroni, D., and Davis, J. S. (2011). TGFB1 disrupts the angiogenic potential of microvascular endothelial cells of the corpus luteum. *J. Cell Sci.* 124, 2501–2510. doi:10.1242/jcs.084558

Maroni, D., and Davis, J. S. (2012). Transforming growth factor Beta 1 stimulates profibrotic activities of luteal fibroblasts in cows. *Biol. Reprod.* 87, 127. doi:10.1095/biolreprod.112.100735

Marsden, P. A., and Brenner, B. M. (1992). Transcriptional regulation of the endothelin-1 gene by TNF-alpha. *Am. J. Physiol. Cell Physiol.* 262 (4), C854–C861. doi:10.1152/ajpcell.1992.262.4.C854

Masuda, H., Kawamura, K., Nanjo, H., Sho, E., Komatsu, M., Sugiyama, T., et al. (2003). Ultrastructure of endothelial cells under flow alteration. *Microsc. Res. Tech.* 60, 2–12. doi:10.1002/jemt.10237

Masuda, H., Zhuang, Y. J., Singh, T. M., Kawamura, K., Murakami, M., Zarins, C. K., et al. (1999). Adaptive remodeling of internal elastic lamina and endothelial lining during flow-induced arterial enlargement. *Arterioscler. Thromb. Vasc. Biol.* 19, 2298–2307. doi:10.1161/01.atv.19.10.2298

Mckeller, R. N., Fowler, J. L., Cunningham, J. J., Warner, N., Smeyne, R. J., Zindy, F., et al. (2002). The Arf tumor suppressor gene promotes hyaloid vascular regression during mouse eye development. *Proc. Natl. Acad. Sci.* 99, 3848–3853. doi:10.1073/pnas.052484199

Meadows, K. L., and Hurwitz, H. I. (2012). Anti-VEGF therapies in the clinic. *Cold Spring Harb. Perspect. Med.* 2, a006577. doi:10.1101/cshperspect.a006577

Merna, N., Wong, A. K., Barahona, V., Llanos, P., Kunar, B., Palikuqi, B., et al. (2018). Laminar shear stress modulates endothelial luminal surface stiffness in a tissue-specific manner. *Microcirculation* 25, e12455. doi:10.1111/micc.12455

Mesiano, S. (2022). Progesterone – historical perspective. *J. Steroid Biochem. Mol. Biol.* 223, 106157. doi:10.1016/j.jsbmb.2022.106157

Miró, J., Vilés, K., Anglada, O., Marín, H., Jordana, J., and Crisci, A. (2015). Color Doppler provides a reliable and rapid means of monitoring luteolysis in female donkeys. *Theriogenology* 83, 485–490. doi:10.1016/j.theriogenology.2014.10.007

Mishra, S., Parmar, M., Yadav, V., Reshma, R., Bharati, J., Bharti, M., et al. (2016). Expression and localization of angiopoietin family in corpus luteum during different stages of oestrous cycle and modulatory role of angiopoietins on steroidogenesis, angiogenesis and survivability of cultured buffalo luteal cells. *Reproduction Domest. Animals* 51, 855–869. doi:10.1111/rda.12739

Miyamoto, A., Kobayashi, S., Arata, S., Ohtani, M., Fukui, Y., and Schams, D. (1997). Prostaglandin F2 alpha promotes the inhibitory action of endothelin-1 on the bovine luteal function *in vitro*. *J. Endocrinol.* 152, R7–R11. doi:10.1677/joe.0.152r007

Miyamoto, A., Shirasuna, K., Wijayagunawardane, M. P., Watanabe, S., Hayashi, M., Yamamoto, D., et al. (2005). Blood flow: A key regulatory component of corpus luteum function in the cow. *Domest. Anim. Endocrinol.* 29, 329–339. doi:10.1016/j.domaniend.2005.03.011

Miyazaki, T., Tanaka, M., Miyakoshi, K., Minegishi, K., Kasai, K., and Yoshimura, Y. (1998). Power and colour Doppler ultrasonography for the evaluation of the vasculature of the human corpus luteum. *Hum. Reprod. Oxf. Engl.* 13, 2836–2841. doi:10.1093/humrep/13.10.2836

Mlyczyńska, E., Kieżun, M., Kurowska, P., Dawid, M., Pich, K., Respekta, N., et al. (2022). New aspects of corpus luteum regulation in physiological and pathological conditions: involvement of adipokines and neuropeptides. *Cells* 11, 957. doi:10.3390/cells11060957

Modlich, U., Kaup, F. J., and Augustin, H. G. (1996). Cyclic angiogenesis and blood vessel regression in the ovary: blood vessel regression during luteolysis involves endothelial cell detachment and vessel occlusion. *Lab. Invest.* 74, 771–780.

Monaco, C. F., Plewes, M. R., Przygrodzka, E., George, J. W., Qiu, F., Xiao, P., et al. (2023). Basic fibroblast growth factor induces proliferation and collagen production by fibroblasts derived from the bovine corpus luteum. *Biol. Reproduction* 109, 367–380. doi:10.1093/biolre/ioad065

Mondal, M., Schilling, B., Folger, J., Steibel, J. P., Buchnick, H., Zalman, Y., et al. (2011). Deciphering the luteal transcriptome: potential mechanisms mediating stage-specific luteolytic response of the corpus luteum to prostaglandin F2α. *Physiol. Genomics* 43, 447–456. doi:10.1152/physiolgenomics.00155.2010

Motta, A. B., Estevez, A., and De Gimeno, M. F. (1999). The involvement of nitric oxide in corpus luteum regression in the rat: feedback mechanism between prostaglandin F(2alpha) and nitric oxide. *Mol. Hum. Reprod.* 5, 1011–1016. doi:10.1093/molehr/5.11.1011

Nayak, G., Odaka, Y., Prasad, V., Solano, A. F., Yeo, E.-J., Vemaraju, S., et al. (2018). Developmental vascular regression is regulated by a Wnt/β-catenin, MYC and CDKN1A pathway that controls cell proliferation and cell death. *Development* 145, dev154898. doi:10.1242/dev.154898

Nett, T., Mcclellan, M., and Niswender, G. (1976). Effects of prostaglandins on the ovine corpus luteum: blood flow, secretion of progesterone and morphology. *Biol. reproduction* 15, 66–78. doi:10.1095/biolreprod15.1.66

Neuvians, T. P., Berisha, B., and Schams, D. (2004a). Vascular endothelial growth factor (VEGF) and fibroblast growth factor (FGF) expression during induced luteolysis in the bovine corpus luteum. *Mol. Reprod. Dev.* 67, 389–395. doi:10.1002/mrd.20032

Neuvians, T. P., Schams, D., Berisha, B., and Pfaffl, M. W. (2004b). Involvement of pro-inflammatory cytokines, mediators of inflammation, and basic fibroblast growth factor in prostaglandin F2alpha-induced luteolysis in bovine corpus luteum. *Biol. Reprod.* 70, 473–480. doi:10.1095/biolreprod.103.016154

Ng, K. K. F., and Vane, J. R. (1967). Conversion of angiotensin I to angiotensin II. *Nature* 216, 762–766. doi:10.1038/216762a0

Nio-Kobayashi, J., Miyazaki, K., Hashiba, K., Okuda, K., and Iwanaga, T. (2016). Histological analysis of arteriovenous anastomosis-like vessels established in the corpus luteum of cows during luteolysis. *J. Ovarian Res.* 9, 67. doi:10.1186/s13048-016-0277-0

O'Shea, J., Rodgers, R., and D'Occhio, M. (1989). Cellular composition of the cyclic corpus luteum of the cow. *Reproduction* 85, 483–487. doi:10.1530/jrf.0.0850483

Ohtani, M., Kobayashi, S., Miyamoto, A., Hayashi, K., and Fukui, Y. (1998). Real-time relationships between intraluteal and plasma concentrations of endothelin, oxytocin, and progesterone during prostaglandin F2alpha-induced luteolysis in the cow. *Biol. Reprod.* 58, 103–108. doi:10.1095/biolreprod58.1.103

Olenich, S. A., Audet, G. N., Roberts, K. A., and Olfert, I. M. (2014). Effects of detraining on the temporal expression of positive and negative angioregulatory proteins in skeletal muscle of mice. *J. Physiol.* 592, 3325–3338. doi:10.1113/jphysiol.2014.271213

Olive, J. L., Dudley, G. A., and Mccully, K. K. (2003). Vascular remodeling after spinal cord injury. *Med. Sci. Sports Exerc.* 35, 901–907. doi:10.1249/01.MSS.0000069755.40046.96

Orr, A. W., Elzie, C. A., Kucik, D. F., and Murphy-Ullrich, J. E. (2003). Thrombospondin signaling through the calreticulin/LDL receptor-related protein co-complex stimulates random and directed cell migration. *J. Cell Sci.* 116, 2917–2927. doi:10.1242/jcs.00600

Otani, N., Minami, S., Yamoto, M., Shikone, T., Otani, H., Nishiyama, R., et al. (1999). The vascular endothelial growth factor/fms-like tyrosine kinase system in human ovary during the menstrual cycle and early pregnancy. *J. Clin. Endocrinol. Metab.* 84, 3845–3851. doi:10.1210/jcem.84.10.6025

Palumbo, A., Ávila, J., and Naftolin, F. (2016). The ovarian renin-angiotensin system (ovras): A major factor in ovarian function and disease. *Reprod. Sci.* 23, 1644–1655. doi:10.1177/1933719116672588

Pepperell, J. R., Nemeth, G., Yamada, Y., Naftolin, F., and Merino, M. (2006). Localized accumulation of angiotensin II and production of angiotensin-(1-7) in rat luteal cells and effects on steroidogenesis. *Am. J. Physiol. Endocrinol. Metab.* 291, E221–E233. doi:10.1152/ajpendo.00205.2005

Piotrowska-Tomala, K. K., Jonczyk, A. W., Kordowitzki, P., Jalali, B. M., and Skarzynski, D. J. (2021). The effect of basic fibroblast growth factor 2 on the bovine corpus luteum depends on the stage of the estrous cycle and modulates prostaglandin F2α action. *Animal* 15, 100048. doi:10.1016/j.animal.2020.100048

Pitzel, L., Jarry, H., and Wuttke, W. (1993). Effects and interactions of prostaglandin F2 alpha, oxytocin, and cytokines on steroidogenesis of porcine luteal cells. *Endocrinology* 132, 751–756. doi:10.1210/endo.132.2.8425493

Planas, A. M. (2020). Top ten discoveries of the year: neurovascular disease. *Free Neuropathol.* 1, 1-5. doi:10.17879/freeneuropathology-2020-2615

Polk, T., Schmitt, S., Aldrich, J. L., and Long, D. S. (2022). Human dermal microvascular endothelial cell morphological response to fluid shear stress. *Microvasc. Res.* 143, 104377. doi:10.1016/j.mvr.2022.104377

Pru, J. K., Lynch, M. P., Davis, J. S., and Rueda, B. R. (2003). Signaling mechanisms in tumor necrosis factor alpha-induced death of microvascular endothelial cells of the corpus luteum. *Reprod. Biol. Endocrinol.* 1, 17. doi:10.1186/1477-7827-1-17

Qin, W., Lu, W., Li, H., Yuan, X., Li, B., Zhang, Q., et al. (2012). Melatonin inhibits IL1β-induced MMP9 expression and activity in human umbilical vein endothelial cells by suppressing NF-κB activation. *J. Endocrinol.* 214, 145–153. doi:10.1530/JOE-12-0147

Redmer, D., Dai, Y., Li, J., Charnock-Jones, D., Smith, S., Reynolds, L., et al. (1996). Characterization and expression of vascular endothelial growth factor (VEGF) in the ovine corpus luteum. *Reproduction* 108, 157–165. doi:10.1530/jrf.0.1080157

Reinitz, A., Destefano, J., Ye, M., Wong, A. D., and Searson, P. C. (2015). Human brain microvascular endothelial cells resist elongation due to shear stress. *Microvasc. Res.* 99, 8–18. doi:10.1016/j.mvr.2015.02.008

Reynolds, L., and Redmer, D. (1999). Growth and development of the corpus luteum. *J. Reprod. Fertil. Suppl.* 54, 181–191.

Ricke, W. A., Redmer, D. A., and Reynolds, L. P. (1999). Growth and cellular proliferation of pig corpora lutea throughout the oestrous cycle. *J. Reprod. Fertil.* 117, 369–377. doi:10.1530/jrf.0.1170369

Romero, J. J., Antoniazzi, A. Q., Smirnova, N. P., Webb, B. T., Yu, F., Davis, J. S., et al. (2013). Pregnancy-associated genes contribute to antiluteolytic mechanisms in ovine corpus luteum. *Physiol. Genomics* 45, 1095–1108. doi:10.1152/physiolgenomics.00082.2013

Robinson, R. S., Nicklin, L. T., Hammond, A. J., Schams, D., Hunter, M. G., and Mann, G. E. (2007). Fibroblast growth factor 2 is more dynamic than vascular endothelial growth factor A during the follicle-luteal transition in the cow. *Biol. Reproduction* 77, 28–36. doi:10.1095/biolreprod.106.055434

Rodgers, R. J., O'Shea, J. D., and Bruce, N. W. (1984). Morphometric analysis of the cellular composition of the ovine corpus luteum. *J. Anat.* 138, 757–770.

Rosiansky-Sultan, M., Klipper, E., Spanel-Borowski, K., and Meidan, R. (2006). Inverse relationship between nitric oxide synthases and endothelin-1 synthesis in bovine corpus luteum: interactions at the level of luteal endothelial cell. *Endocrinology* 147, 5228–5235. doi:10.1210/en.2006-0795

Sakumoto, R., Berisha, B., Kawate, N., Schams, D., and Okuda, K. (2000). Tumor necrosis factor-alpha and its receptor in bovine corpus luteum throughout the estrous cycle. *Biol. Reproduction* 62, 192–199. doi:10.1095/biolreprod62.1.192

Sakumoto, R., Vermehren, M., Kenngott, R. A., Okuda, K., and Sinowatz, F. (2011). Localization of gene and protein expressions of tumor necrosis factor-{alpha} and tumor necrosis factor receptor types I and II in the bovine corpus luteum during the estrous cycle. *J. Animal Sci.* 89, 3040–3047. doi:10.2527/jas.2010-3479

Sánchez-Duffhues, G., García De Vinuesa, A., and Ten Dijke, P. (2018). Endothelial-to-mesenchymal transition in cardiovascular diseases: developmental signaling pathways gone awry. *Dev. Dyn.* 247, 492–508. doi:10.1002/dvdy.24589

Santos, R. A. (2014). Angiotensin-(1–7). *Hypertension* 63, 1138–1147. doi:10.1161/HYPERTENSIONAHA.113.01274

Sawamura, T., Kimura, S., Shinmi, O., Sugita, Y., Yanagisawa, M., and Masaki, T. (1989). Analysis of endothelin related peptides in culture supernatant of porcine aortic endothelial cells: evidence for biosynthetic pathway of endothelin-1. *Biochem. Biophys. Res. Commun.* 162, 1287–1294. doi:10.1016/0006-291x(89)90813-9

Schams, D., Berisha, B., Neuvians, T., Amselgruber, W., and Kraetzl, W. D. (2003). Real-time changes of the local vasoactive peptide systems (angiotensin, endothelin) in the bovine corpus luteum after induced luteal regression. *Mol. Reprod. Dev.* 65, 57–66. doi:10.1002/mrd.10257

Seidl, K., Solis, N. V., Bayer, A. S., Hady, W. A., Ellison, S., Klashman, M. C., et al. (2012). Divergent responses of different endothelial cell types to infection with Candida albicans and *Staphylococcus aureus*. *PLoS One* 7, e39633. doi:10.1371/journal.pone.0039633

Sheikh, S., Rahman, M., Gale, Z., Luu, N. T., Stone, P. C., Matharu, N. M., et al. (2005). Differing mechanisms of leukocyte recruitment and sensitivity to conditioning by shear stress for endothelial cells treated with tumour necrosis factor-alpha or interleukin-1beta. *Br. J. Pharmacol.* 145, 1052–1061. doi:10.1038/sj.bjp.0706281

Shirasuna, K., Jiemtaweeboon, S., Raddatz, S., Nitta, A., and Schuberth, H. (2012a). *Rapid accumulation of polymorphonuclear neutrophils in the corpus.*

Shirasuna, K., Nitta, A., Sineenard, J., Shimizu, T., Bollwein, H., and Miyamoto, A. (2012b). Vascular and immune regulation of corpus luteum development, maintenance, and regression in the cow. *Domest. Anim. Endocrinol.* 43, 198–211. doi:10.1016/j.domaniend.2012.03.007

Shirasuna, K., Watanabe, S., Asahi, T., Wijayagunawardane, M. P., Sasahara, K., Jiang, C., et al. (2008). Prostaglandin F2alpha increases endothelial nitric oxide synthase in the periphery of the bovine corpus luteum: the possible regulation of blood flow at an early stage of luteolysis. *Reproduction* 135, 527–539. doi:10.1530/REP-07-0496

Shirasuna, K., Watanabe, S., Oki, N., Wijayagunawardane, M. P. B., Matsui, M., Ohtani, M., et al. (2006). A cooperative action of endothelin-1 with prostaglandin F(2alpha) on luteal function in the cow. *Domest. Anim. Endocrinol.* 31, 186–196. doi:10.1016/j.domaniend.2005.10.004

Shosha, E., Xu, Z., Narayanan, S. P., Lemtalsi, T., Fouda, A. Y., Rojas, M., et al. (2018). Mechanisms of diabetes-induced endothelial cell senescence: role of arginase 1. *Int. J. Mol. Sci.* 19, 1215. doi:10.3390/ijms19041215

Skarzynski, D. J., Ferreira-Dias, G., and Okuda, K. (2008). Regulation of luteal function and corpus luteum regression in cows: hormonal control, immune mechanisms and intercellular communication. *Reprod. Domest. Anim.* 43 (2), 57–65. doi:10.1111/j.1439-0531.2008.01143.x

Smith, M. F., Mcintush, E. W., and Smith, G. W. (1994). Mechanisms associated with corpus luteum development. *J. Anim. Sci.* 72, 1857–1872. doi:10.2527/1994.7271857x

Spanel-Borowski, K. (1991). Diversity of ultrastructure in different phenotypes of cultured microvessel endothelial cells isolated from bovine corpus luteum. *Cell Tissue Res.* 266, 37–49. doi:10.1007/BF00678709

Spanel-Borowski, K., and Van Der Bosch, J. (1990). Different phenotypes of cultured microvessel endothelial cells obtained from bovine corpus luteum. Study by light microscopy and by scanning electron microscopy (SEM). *Cell Tissue Res.* 261, 35–47. doi:10.1007/BF00329436

Stocco, C., Telleria, C., and Gibori, G. (2007). The molecular control of corpus luteum formation, function, and regression. *Endocr. Rev.* 28, 117–149. doi:10.1210/er.2006-0022

Stouffer, R. L., Bishop, C. V., Bogan, R. L., Xu, F., and Hennebold, J. D. (2013). Endocrine and local control of the primate corpus luteum. *Reprod. Biol.* 13, 259–271. doi:10.1016/j.repbio.2013.08.002

Sugino, N., Suzuki, T., Sakata, A., Miwa, I., Asada, H., Taketani, T., et al. (2005). Angiogenesis in the human corpus luteum: changes in expression of angiopoietins in the corpus luteum throughout the menstrual cycle and in early pregnancy. *J. Clin. Endocrinol. Metabolism* 90, 6141–6148. doi:10.1210/jc.2005-0643

Sweetwyne, M. T., and Murphy-Ullrich, J. E. (2012). Thrombospondin1 in tissue repair and fibrosis: TGF-β-dependent and independent mechanisms. *Matrix Biol.* 31, 178–186. doi:10.1016/j.matbio.2012.01.006

Swigris, J. J., and Brown, K. K. (2010). The role of endothelin-1 in the pathogenesis of idiopathic pulmonary fibrosis. *BioDrugs* 24, 49–54. doi:10.2165/11319550-000000000-00000

Talbott, H., Hou, X., Qiu, F., Zhang, P., Guda, C., Yu, F., et al. (2017). Early transcriptome responses of the bovine midcycle corpus luteum to prostaglandin F2α includes cytokine signaling. *Mol. Cell Endocrinol.* 452, 93–109. doi:10.1016/j.mce.2017.05.018

Tamura, H., and Greenwald, G. S. (1987). Angiogenesis and its hormonal control in the corpus luteum of the pregnant rat. *Biol. Reproduction* 36, 1149–1154. doi:10.1095/biolreprod36.5.1149

Tanaka, J., Acosta, T. J., Berisha, B., Tetsuka, M., Matsui, M., Kobayashi, S., et al. (2004). Relative changes in mRNA expression of angiopoietins and receptors tie in bovine corpus luteum during estrous cycle and prostaglandin F2alpha-induced luteolysis: A possible mechanism for the initiation of luteal regression. *J. Reprod. Dev.* 50, 619–626. doi:10.1262/jrd.50.619

Tanfin, Z., Leiber, D., Robin, P., Oyeniran, C., and Breuiller-Fouché, M. (2011). Endothelin-1: physiological and pathological roles in myometrium. *Int. J. Biochem. Cell Biol.* 43, 299–302. doi:10.1016/j.biocel.2010.10.009

Tao, Y., Fu, Z., Zhang, M., Xia, G., Yang, J., and Xie, H. (2004). Immunohistochemical localization of inducible and endothelial nitric oxide synthase in porcine ovaries and effects of NO on antrum formation and oocyte meiotic maturation. *Mol. Cell. Endocrinol.* 222, 93–103. doi:10.1016/j.mce.2004.04.014

Tzavlaki, K., and Moustakas, A. (2020). TGF-B signaling. *Biomolecules* 10, 487. doi:10.3390/biom10030487

Vallée, A., and Lecarpentier, Y. (2019). TGF-β in fibrosis by acting as a conductor for contractile properties of myofibroblasts. *Cell & Biosci.* 9, 98. doi:10.1186/s13578-019-0362-3

Van Linthout, S., Miteva, K., and Tschöpe, C. (2014). Crosstalk between fibroblasts and inflammatory cells. *Cardiovasc Res.* 102, 258–269. doi:10.1093/cvr/cvu062

Vega, M., Urrutia, L., Iñiguez, G., Gabler, F., Devoto, L., and Johnson, M. C. (2000). Nitric oxide induces apoptosis in the human corpus luteum *in vitro*. *Mol. Hum. Reprod.* 6, 681–687. doi:10.1093/molehr/6.8.681

Vonnahme, K. A., Redmer, D. A., Borowczyk, E., Bilski, J. J., Luther, J. S., Johnson, M. L., et al. (2006). Vascular composition, apoptosis, and expression of angiogenic factors in the corpus luteum during prostaglandin F2alpha-induced regression in sheep. *Reproduction* 131, 1115–1126. doi:10.1530/rep.1.01062

Walewska, E., Wołodko, K., Skarzynski, D., Ferreira-Dias, G., and Galvão, A. (2019). The interaction between nodal, hypoxia-inducible factor 1 alpha, and thrombospondin 1 promotes luteolysis in equine corpus luteum. *Front. Endocrinol. (Lausanne)* 10, 667. doi:10.3389/fendo.2019.00667

Wang, F., Riley, J. C. M., and Behrman, H. R. (1993). Immunosuppressive levels of glucocorticoid block extrauterine luteolysins in the rat. *Biol. Reproduction* 49, 66–73. doi:10.1095/biolreprod49.1.66

Watts, S. W. (2007). "Intrinsic regulation of the vasculature," in *xPharm: The comprehensive pharmacology reference*. Editors S. J. ENNA and D. B. BYLUND (New York: Elsevier).

Wiegel, R. E., Karsten, M. J. H., Reijnders, I. F., Van Rossem, L., Willemsen, S. P., Mulders, A., et al. (2021). Corpus luteum number and the maternal renin-angiotensin-aldosterone system as determinants of utero-placental (vascular) development: the rotterdam periconceptional cohort. *Reprod. Biol. Endocrinol.* 19, 164. doi:10.1186/s12958-021-00843-9

Wiltbank, M., Gallagher, K., Christensen, A., Brabec, R., and Keyes, P. (1990). Physiological and immunocytochemical evidence for a new concept of blood flow regulation in the corpus luteum. *Biol. Reproduction* 42, 139–149. doi:10.1095/biolreprod42.1.139

Wiltbank, M., Lopez, H., Sartori, R., Sangsritavong, S., and Gümen, A. (2006). Changes in reproductive physiology of lactating dairy cows due to elevated steroid metabolism. *Theriogenology* 65, 17–29. doi:10.1016/j.theriogenology.2005.10.003

Woad, K. J., and Robinson, R. S. (2016). Luteal angiogenesis and its control. *Theriogenology* 86, 221–228. doi:10.1016/j.theriogenology.2016.04.035

Wulff, C., Wilson, H., Largue, P., Duncan, W. C., Armstrong, D. G., and Fraser, H. M. (2000). Angiogenesis in the human corpus luteum: localization and changes in angiopoietins, tie-2, and vascular endothelial growth factor messenger ribonucleic acid. *J. Clin. Endocrinol. Metabolism* 85, 4302–4309. doi:10.1210/jcem.85.11.6942

Yamashita, H., Kamada, D., Shirasuna, K., Matsui, M., Shimizu, T., Kida, K., et al. (2008). Effect of local neutralization of basic fibroblast growth factor or vascular endothelial growth factor by a specific antibody on the development of the corpus luteum in the cow. *Mol. Reproduction Dev.* 75, 1449–1456. doi:10.1002/mrd.20878

Yanagisawa, M., Kurihara, H., Kimura, S., Tomobe, Y., Kobayashi, M., Mitsui, Y., et al. (1988). A novel potent vasoconstrictor peptide produced by vascular endothelial cells. *Nature* 332, 411–415. doi:10.1038/332411a0

Yin, M., and Pacifici, M. (2001). Vascular regression is required for mesenchymal condensation and chondrogenesis in the developing limb. *Dev. Dyn.* 222, 522–533. doi:10.1002/dvdy.1212

Yoshimatsu, Y., Wakabayashi, I., Kimuro, S., Takahashi, N., Takahashi, K., Kobayashi, M., et al. (2020). TNF-α enhances TGF-β-induced endothelial-to-mesenchymal transition via TGF-β signal augmentation. *Cancer Sci.* 111, 2385–2399. doi:10.1111/cas.14455

Yoshimura, Y. (1997). The ovarian renin–angiotensin system in reproductive physiology. *Front. Neuroendocrinol.* 18, 247–291. doi:10.1006/frne.1997.0152

Yu, Y., Leng, Y., Song, X., Mu, J., Ma, L., Yin, L., et al. (2023). Extracellular matrix stiffness regulates microvascular stability by controlling endothelial paracrine signaling to determine pericyte fate. *Arterioscler. Thromb. Vasc. Biol.* doi:10.1161/ATVBAHA.123.319119

Zalman, Y., Klipper, E., Farberov, S., Mondal, M., Wee, G., Folger, J. K., et al. (2012). Regulation of angiogenesis-related prostaglandin f2alpha-induced genes in the bovine corpus luteum. *Biol. Reproduction* 86, 92. doi:10.1095/biolreprod.111.095067

Zeisberg, E. M., Potenta, S., Xie, L., Zeisberg, M., and Kalluri, R. (2007). Discovery of endothelial to mesenchymal transition as a source for carcinoma-associated fibroblasts. *Cancer Res.* 67, 10123–10128. doi:10.1158/0008-5472.CAN-07-3127

Zheng, J., Redmer, D. A., and Reynolds, L. P. (1993). Vascular development and heparin-binding growth factors in the bovine corpus luteum at several stages of the estrous cycle. *Biol. Reproduction* 49, 1177–1189. doi:10.1095/biolreprod49.6.1177

frontiers | Frontiers in Physiology

TYPE Original Research
PUBLISHED 16 November 2023
DOI 10.3389/fphys.2023.1288907

OPEN ACCESS

EDITED BY
Hong Zheng,
University of South Dakota, United States

REVIEWED BY
Zhiying Shan,
Michigan Technological University, United States
Yang Yu,
The University of Iowa, United States

*CORRESPONDENCE
Han-Jun Wang,
hanjunwang@unmc.edu

†These authors have contributed equally to this work

RECEIVED 05 September 2023
ACCEPTED 30 October 2023
PUBLISHED 16 November 2023

CITATION
Kitzerow O, Suder P, Shukry M, Lisco SJ, Zucker IH and Wang H-J (2023), Systemic mapping of organ plasma extravasation at multiple stages of chronic heart failure. *Front. Physiol.* 14:1288907. doi: 10.3389/fphys.2023.1288907

Systemic mapping of organ plasma extravasation at multiple stages of chronic heart failure

Oliver Kitzerow[1,2†], Paul Suder[2†], Mohanad Shukry[2], Steven J. Lisco[2], Irving H. Zucker[3] and Han-Jun Wang[2*]

[1]Department of Genetics Cell Biology and Anatomy, University of Nebraska Medical Center, Omaha, NE, United States, [2]Department of Anesthesiology, University of Nebraska Medical Center, Omaha, NE, United States, [3]Department of Cellular and Integrative Physiology, University of Nebraska Medical Center, Omaha, NE, United States

Introduction: Chronic Heart failure (CHF) is a highly prevalent disease that leads to significant morbidity and mortality. Diffuse vasculopathy is a commonmorbidity associated with CHF. Increased vascular permeability leading to plasma extravasation (PEx) occurs in surrounding tissues following endothelial dysfunction. Such micro- and macrovascular complications develop over time and lead to edema, inflammation, and multi-organ dysfunction in CHF. However, a systemic examination of PEx in vital organs among different time windows of CHF has never been performed. In the present study, we investigated time-dependent PEx in several major visceral organs including heart, lung, liver, spleen, kidney, duodenum, ileum, cecum, and pancreas between sham-operated and CHF rats induced by myocardial infarction (MI).

Methods: Plasma extravasation was determined by colorimetric evaluation of Evans Blue (EB) concentrations at 3 days, ~10 weeks and 4 months following MI.

Results: Data show that cardiac PEx was initially high at day 3 post MI and then gradually decreased but remained at a moderately high level at ~10 weeks and 4 months post MI. Lung PEx began at day 3 and remained significantly elevated at both ~10 weeks and 4 months post MI. Spleen PExwas significantly increased at ~10 weeks and 4 months but not on day 3 post MI. Liver PEx occurred early at day 3 and remain significantly increased at ~10 weeks and 4 months post MI. For the gastrointestinal (GI) organs including duodenum, ileum and cecum, there was a general trend that PEx level gradually increased following MI and reached statistical significance at either 10 weeks or 4 months post MI. Similar to GI PEx, renal PEx was significantly elevated at 4 months post MI.

Discussion: In summary, we found that MI generally incites a timedependent PEx of multiple visceral organs. However, the PEx time window for individual organs in response to the MI challenge was different, suggesting that different mechanisms are involved in the pathogenesis of PEx in these vital organs during the development of CHF.

KEYWORDS

inflammation, chronic heart failure, pancreas, gastro-intestinal dysfunction, pulmonary hypertension

Introduction

Chronic heart failure (CHF) is a highly prevalent disease that drastically increases morbidity and mortality of patients (Roger, 2021). It is estimated that CHF impacts over 37 million people worldwide and is the leading cause of hospitalization among adults and the elderly (Ziaeian and Fonarow, 2016). CHF occurs secondary to earlier cardiac and vascular disorders such as hypertension, myocardial infarction (MI), or myocarditis (Kemp and Conte, 2012). Post-MI timelines of cardiac inflammation and fibrosis have been extensively analyzed as have their effects on cardiac morphology and function (Cleutjens et al., 1995; Sutton and Sharpe, 2000; Frangogiannis, 2012; Prabhu et al., 2016; Talman and Ruskoaho, 2016). What remains unknown are the influences of CHF on extracardiac organs at different timepoints during the disease. Assessing extracardiac organ function will provide a more comprehensive understanding of pathogenesis and comorbidities of CHF and promote the development of novel therapies. In this study, we performed permanent coronary ligation MI to investigate the impact of early, middle, and late stages of CHF on thoracic and abdominal organ plasma extravasation (PEx) in rats.

All cells require nutrients and a means of removing waste. In higher organisms, these functions are primarily carried out by the circulatory system. Although the vascular system is considered closed, it must be adequately permeable to allow for the exchange of nutrients and waste products. Under basal vascular permeability (BVP), molecules are exchanged in the capillaries and consist largely of water, gases, glucose, and slight amounts of plasma proteins (McDonald et al., 1999; Nagy et al., 2008). Permeability can be described in 2 other pathological forms: acute vascular hyperpermeability (AVH) and chronic vascular hyperpermeability (CVH), both of which contribute to the pathogenesis of PEx. In the instances of AVH or CVH, extravasated fluid, known as exudate, is protein rich, approaching concentrations levels of plasma. Notably, AVH is self-limiting, but chronic exposure to factors that increase permeability results in profound changes in venular structure such as pericytes detachment and endothelial thinning. The result is an enlarged highly permeable venule with profound exudate. The subsequent protein accumulation and osmotic pressure in the interstitium drives fluid retention and promotes edema. In addition, plasma proteins can interact with tissue factors to induce migration and activation of mesenchymal and inflammatory cells (Colvin and Dvorak, 1975; Dvorak et al., 1979). These actions can limit the diffusion of nutrients and elimination of waste and ultimately impair organ function. Therefore, determining PEx of a given tissue or organ can potentially serve as a guide for organ health. However, the time course of PEx in individual organs at the different stages of CHF has not been previously established. In this study, we utilized EB to assess the degree of PEx. EB binds and stains albumin, so tissues undergoing PEx are stained bluish purple due to the entrapped EB-albumin complex within their parenchyma. Concentrations of EB can then be calculated to determine relative levels of PEx and predict the course of hyperpermeability. The goals of this study were to quantify the levels of PEx in various organs at multiple timepoints after the induction of MI in hopes to determine the effects of multiple stages of CHF on extracardiac organ permeability.

Methods

All animal experimentation was approved by the Institutional Animal Care and Use Committee of the University of Nebraska Medical Center and performed in accordance with the National Institutes of Health's Guide for Use and Care of Laboratory Animals and in accordance with the ARRIVE guidelines (Kilkenny et al., 2012; Institute of Laboratory Animal Resources, 2021). Experiments were performed on adult, male Sprague-Dawley rats purchased from the Charles River Laboratories (Wilmington, MA). Food and water were supplied *ad libitum*, and rats were kept on 12-h light/dark cycles.

Rat model of chronic heart failure

Rats (180–200 g) were chosen at random to undergo either MI surgery or sham surgery. CHF was produced by left coronary artery ligation as previously described (Hong et al., 2021). Sham-operated rats were prepared in the same manner but did not undergo coronary artery ligation. Briefly, the rat was ventilated at a rate of 60 breaths/min with 2%–3% isoflurane during the surgical procedure. A left thoracotomy was performed through the fifth intercostal space, the pericardium was opened, the heart was exteriorized, and the left anterior descending coronary artery was ligated. For post procedure pain management, Buprenorphine SR (1.5 mg/kg) was subcutaneously injected immediately after surgery. All sham rats survived, and~70% of rats survived from coronary artery ligation surgery. At the end of terminal experiments, infarct size (IS) was measured by taking the ratio of the infarct area to whole left ventricle (LV) minus septum in rats 10 weeks or 4 months post sham/MI. In rats 3 days post sham/MI, we did not measure IS because the scar has not formed although each infarcted heart exhibited a pale ischemic region.

Tissue plasma extravasation and quantification of Evans Blue

Rats were anesthetized with urethane (800 mg/kg ip) and α-chloralose (40 mg/kg ip). EB, 20 mg/kg (10 mg/mL, dissolved in heparinized saline) was administered intravenously through the femoral vein. After 10 min, anesthetized rats were euthanized by transcardiac perfusion with Phosphate Buffered Saline (0.01 M, pH 7.4). Organ tissues including lungs, heart, kidney, liver, pancreas, duodenum, ileum, cecum, and spleen were excised, weighed, and photographed. Additional dissection of infarcted hearts was performed to separate regions of the infarct. The left ventricle was dissected into scar, peri-scar tissue that was adjacent the scar, and remote tissues. Then, samples were placed in 2 mL of N,N′-dimethyl formamide, homogenized, and incubated at 50°C water bath for 24 h. Samples were then centrifuged (1 min, 14,000 rpm) and the EB content in the supernatant was determined in a 96-well microplate reader (infinite M200, TECAN, Männedorf, CH, Switzerland) using a fluorescence excitation wavelength of 620 nm (bandwidth 10 nm) and an emission wavelength of 680 nm (bandwidth 40 nm) (100 μL

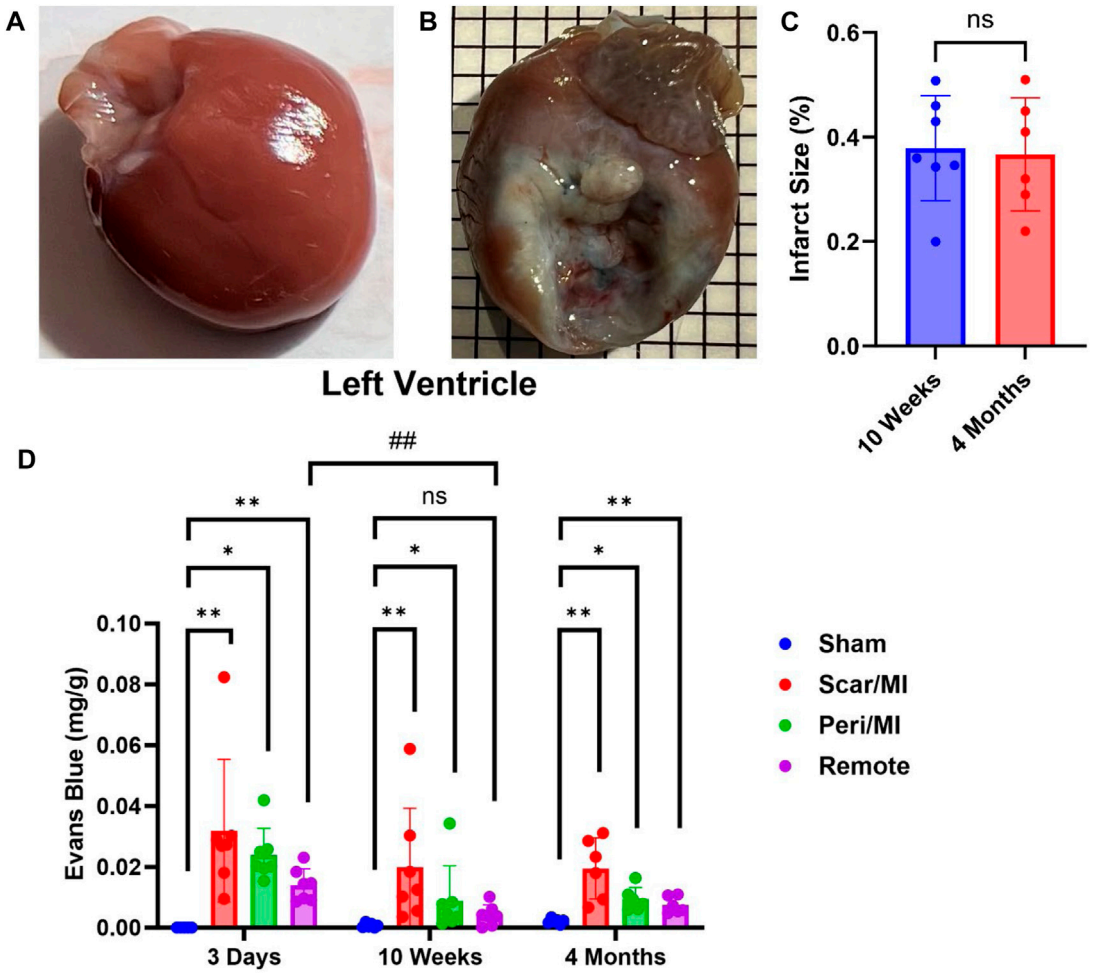

FIGURE 1
Time-dependent PEx in the heart post sham/MI. 10 weeks post MI shows scar formation and PEx visualized by the tissue content of EB in the MI **(B)** heart but not sham **(A)**. Extent of scar area is shown in **(C)**. Time course of PEx in various regions of the left ventricle in control and MI animals **(D)** Mean ± SD. n = 5-8 per group. Comparing MI with Sham group $p < 0.05$ (*) and $p < 0.005$ (**). Comparing timepoints within MI group $p < 0.005$ (##).

sample per well). Extravasation of EB was expressed as mg EB/g of tissue, by comparing the experimental values with a known standard.

Statistics

Statistical evaluation was analyzed using GraphPad Prism (GraphPad Software, San Diego, CA. Version 9.4.1). Normality was first determined using the Shapiro-Wilk test with an alpha set at 0.05. If organ data sets were not normally distributed, Mann-Whitney tests were utilized to determine differences between sham and MI groups. Unpaired t-tests were used when data sets were normally distributed. The comparison of PEx between each timepoint for MI rats was done using one-way ANOVA with tukey's multiple comparison test with $p < 0.05$ being statistically significant. Differences between two groups (Sham and MI) were defined at $p < 0.05$ being statistically significant.

Results

Evaluation of cardiac PEx at different stages of CHF

Infarcted rats at 10 weeks (i.e., middle stage of CHF) and 4 months (i.e., late stage of CHF) post MI showed significant scaring of the left ventricle compared to sham operated rats (IS at 10 weeks post MI: 37.8% ± 9.3%; IS at 4 months post MI: 36.7% ± 9.9%) (Figure 1C). All regions of the left ventricle experienced significant PEx with the scar tissue undergoing the most. At 10 weeks the remote region was significantly decreased compared to 3 days and did not show significant PEx when compared to sham. The Peri-MI region experiences PEx through 3 days and up to 4 months when compared to control. Surprisingly, the scar tissue showed the same pattern to a greater extent (Figure 1). These data demonstrate that PEx in cardiac tissues occurs at all stages of CHF, but the level at which it occurs depends on stage of CHF and proximity to the area of effect.

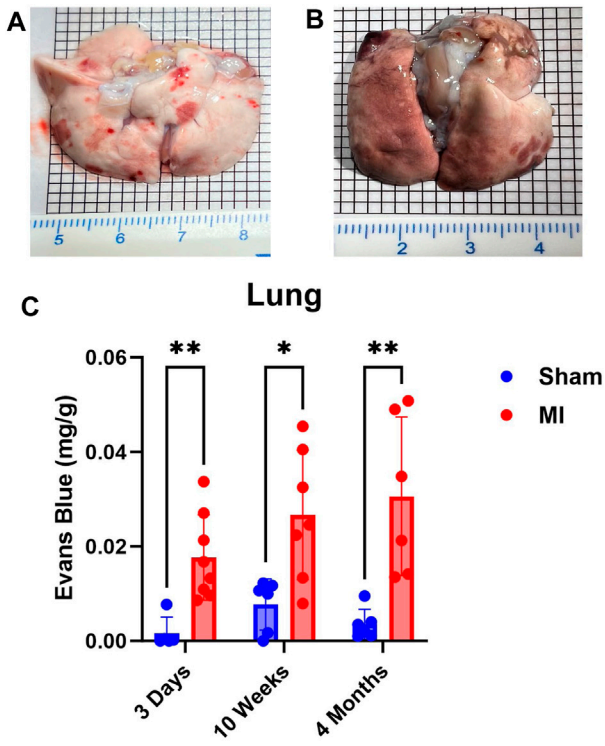

FIGURE 2
Time-dependent PEx in the lungs post sham/MI. Representative images of sham **(A)** and MI **(B)** lungs treated with EB at 10 weeks post-surgery. Time course of PEx in the lung post MI **(B)** and sham surgery **(C)**. Mean ± SD. n = 5-8 per group. Comparing MI with Sham group $p < 0.05$ (*) and $p < 0.005$ (**).

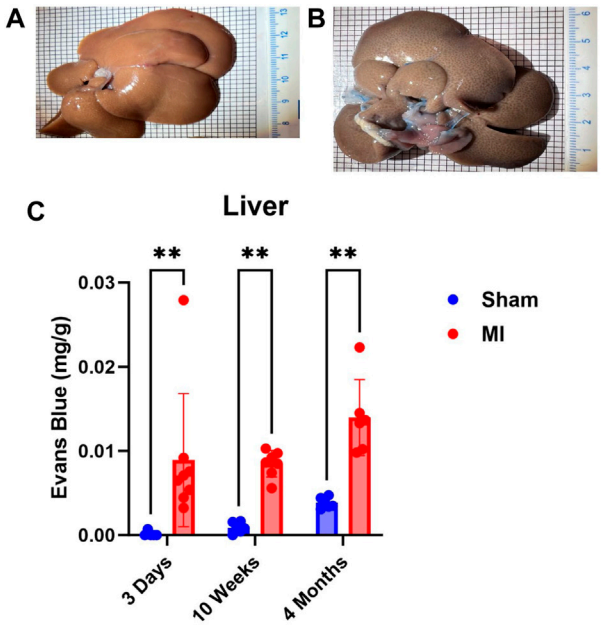

FIGURE 3
Time-dependent PEx in the liver post sham/MI. Representative images of sham **(A)** and MI **(B)** liver treated with EB at 10 weeks post-surgery. Time course of PEx in the liver PEx in sham and MI animals post-surgery **(C)**. Mean ± SD. n = 5-8 per group. Comparing MI with Sham group $p < 0.005$ (**).

Evaluation of lung PEx at different stages of CHF

Next, we examined lung PEx at different stages of CHF. Due to the relative proximity of the lung to the heart and their interconnected functions, we hypothesized the lung would mirror the temporal PEx patterns as the heart. As expected, the lungs started showing significant levels of PEx at 3 days post MI. Significant levels of PEx were seen through 10 weeks and 4 months post MI similar to the heart (Figure 2). Contrary to the heart, PEx in the lungs did not decrease over time.

Evaluation of gastrointestinal organ PEx at different stages of CHF

Pulmonary hypertension and right-sided heart failure often precede liver dysfunction. We predicted that significant levels of liver PEx would follow lung PEx. However, significant liver PEx occurred at 3 days and continued to 4 months post MI (Figure 3). Due to the hepatic portal system, we predicted concurrent and subsequent PEx of the digestive tract. However, only the duodenum and cecum showed significant PEx, and notably at varying timepoints (Figure 4). The cecum experienced significant PEx at 10 weeks while the duodenum reached significant levels at 4 months. There appeared to be slight enhancement of PEx at 4 months post MI in ileum and cecum as well, but these were not statistically significant. The pancreas did not experience significant PEx until 10 weeks and continued through 4 months (Figure 5). In contrast to the other digestive organs, PEx of the pancreas increased significantly over time with levels tripling from 10 weeks to 4 months.

Evaluation of spleen PEx at different stages of CHF

The spleen is a secondary lymphoid organ that houses leukocytes, which can be mobilized in the event of tissue damage or infection. As such, we expected significant levels of PEx to occur acutely and chronically. Surprisingly, PEx was not observed until week 10 post MI (Figure 6). Also, much like the pancreas, PEx of the spleen worsens at 4 months post MI.

Evaluation of renal PEx at different stages of CHF

The kidney did not show significant levels of PEx at 3 days post MI (Figure 7). PEx levels were still normal at 10 weeks but increased at 4 months post MI. These data closely resemble previously documented compensatory actions of the kidney at the mid-stage of CHF (Xia et al., 2022). The late renal PEx is consistent with declined renal function at the late stage of CHF.

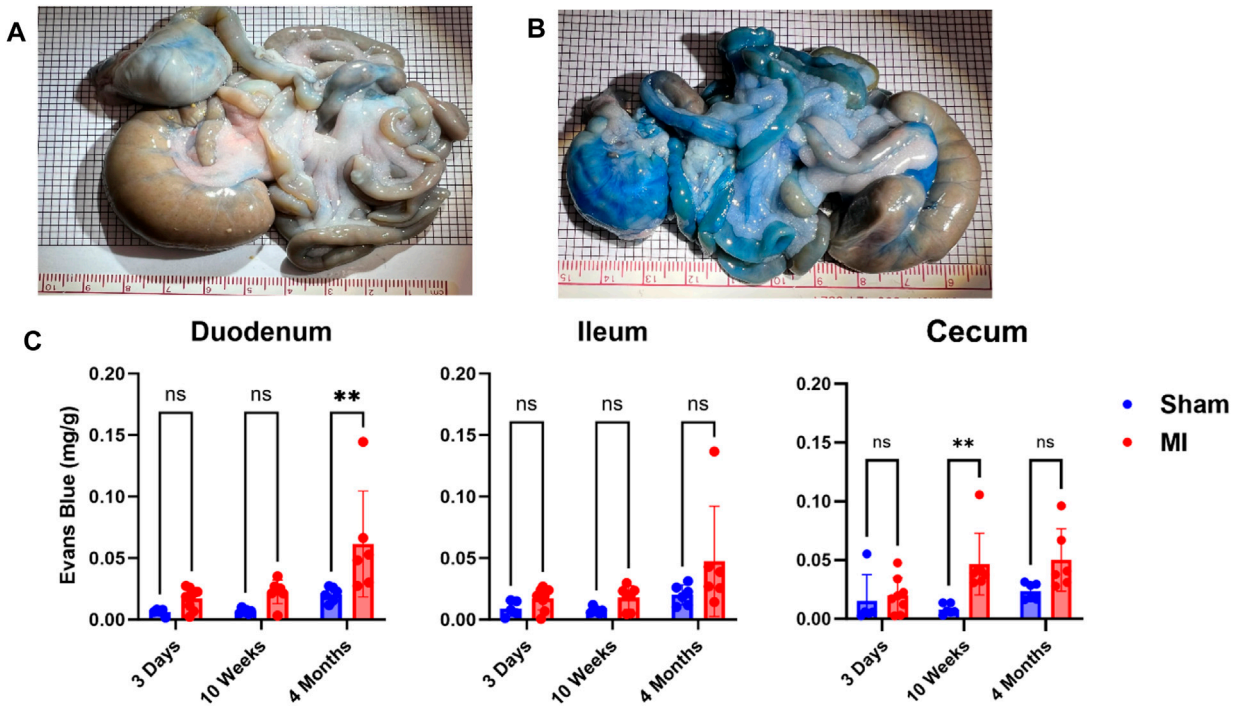

FIGURE 4
Time-dependent PEx in the gastrointestinal (GI) tract post sham/MI. Representative images of sham **(A)** and MI **(B)** GI tract treated with EB at 4 months post-surgery. Time course of PEx in the areas of the GI tract from sham and MI animals post-surgery **(C)**. Mean ± SD. n = 5-8 per group. Comparing MI with Sham group $p < 0.005$ (**).

Discussion

In this study, we examined multiorgan PEx at different stages of CHF. We used an MI model for the development of CHF in rats. MI can produce left ventricular remodeling including changes in LV size, shape, function, and cellular and molecular composition (Sutton and Sharpe, 2000). By utilizing EB, we determined divergences of PEx in thoracic and abdominal organs, the severity, and initiation and duration. In general, we found that MI induces a time-dependent increase of PEx in most visceral organs in addition to the heart. However, due to varying timepoints of PEx initiation and duration the mechanisms that promote such extravasation most likely differ among these organs.

The tight regulation of protein extravasation helps to maintain the oncotic pressure of both the blood and tissue interstitium, thus sustaining homeostasis. In general, vascular permeability (VP) is the ability of fluid to move across microvessels to allow the exchange of molecules. Basal vascular permeability describes rapid flux of small molecules such as water, salts, and gases across the endothelial barrier of capillaries. Importantly, the plasma filtrate during BVP contains very little plasma protein (McDonald et al., 1999; Nagy et al., 2008; Dvorak, 2010; Dvorak, 2021). However, during AVH or CVH, there is extensive protein extravasation with protein concentration of the exudate near plasma levels (Majno et al., 1961). In the events of AVH, the protein exudate can be beneficial in that it promotes angiogenesis and induces migration and activation of inflammatory cells like neutrophils and monocytes to clear dead tissue or pathogens. Crucially, AVH is self-limiting unlike CVH which can occur from chronic exposure to permeabilizing factors in cases of tumors or chronic inflammation (Nagy et al., 2008; Dvorak, 2010). Persistent increased protein exudate is problematic because it can result in edema and increased interstitial pressure. Accumulation of interstitial fluid is damaging to tissue health because it increases the diffusion distance for nutrients and waste products, which may compromise cellular metabolism (Scallan et al., 2010). In addition, many organs are surrounded by unyielding fascial sheaths and consequently have limited ability to expand their interstitial space. This means that relatively small increments in fluid induce large increases in interstitial pressure. Furthermore, if hyperpermeability is left to persist and edema increases, the vascular transmural pressure gradient decreases and capillaries can be physically compressed, thereby reducing tissue perfusion needed for nutrient and waste exchange. Chronically elevated extracardiac PEx after MI as demonstrated in our study highlights the clinical significance of assessing multiorgan health after MI especially upon development of CHF. The extent of extravasation of plasma solvent and solute depends on pressure and concentration gradients, hemodynamic forces, intrinsic permeability of the vascular wall (Dvorak, 2010), and inflammatory status of a given tissue (McDonald et al., 1999). By extrapolating PEx using EB concentration, we can account for the sum total of all these factors, however, we cannot be certain which mechanism is primarily responsible for the observed PEx of an organ.

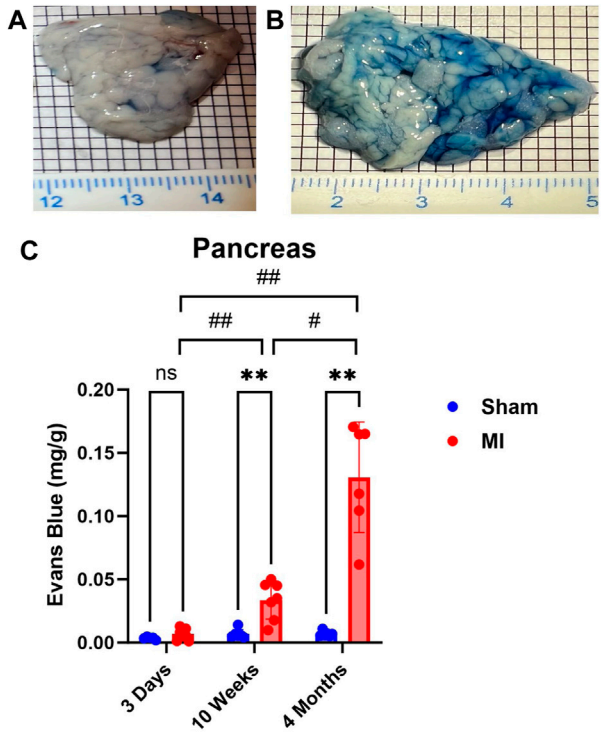

FIGURE 5
Time-dependent PEx in the pancreas post sham/MI. Representative images of sham **(A)** and MI **(B)** pancreas treated with EB at 10 weeks post-surgery. Time course of PEx in the areas of the GI tract from sham and MI animals post-surgery **(C)**. Mean ± SD. n = 5-8 per group. Comparing MI with Sham group $p < 0.005$ (**). Comparing timepoints within MI group $p < 0.05$ (#) and $p < 0.005$ (##).

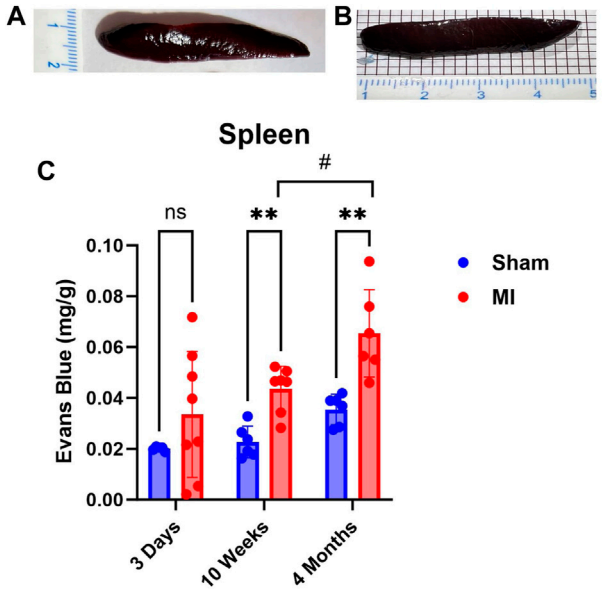

FIGURE 6
Time-dependent PEx in the spleen post sham/MI. Representative images show PEx in the spleen at 10 weeks post sham/MI **(A,B)**. Time course of PEx in the spleen from sham and MI animals post-surgery **(C)**. Mean ± SD. n = 5-8 per group. Comparing MI with Sham group $p < 0.005$ (**). Comparing timepoints within MI group $p < 0.05$ (#).

Chronic heart failure can occur secondary to earlier cardiac events like MI (Kemp and Conte, 2012). The initial infarct causes early inflammatory activation which is a necessary event for the transition to later reparative stages (Guo and Dipietro, 2010; Kain et al., 2014; Prabhu et al., 2016). The reparative stage begins around 72 h in mice (Dewald et al., 2004) and is marked with significant collagen deposition (Cleutjens et al., 1995) and myofibroblast activation (Sun and Weber, 1996) that lead to the development of fibrotic tissue (Sun and Weber, 2000; Sun et al., 2002; Dewald et al., 2004) and continued scar development. These adverse changes culminate in LV remodeling and ultimately hemodynamic perturbances that include elevated cardiac filling pressures, reduced cardiac output, and central venous congestion that are characteristic of CHF (Verbrugge et al., 2020). Based on these considerations, we predicted that our MI rat model would cause inflammatory-induced AVH in the heart and lungs while hemodynamic alterations characteristic of CHF would drive CVH in all organs.

Our rat data closely correspond with murine findings in that PEx of all regions of the heart peaked at 3 days with levels diminishing thereafter, suggesting resolution of inflammation and the initiation of repair. Of note, this may be a species-specific response; dogs demonstrated a more delayed response, with the reparative stage not beginning until 7 days (Dewald et al., 2004). Of intertest, PEx is significantly reduced in the remote region at 10 weeks but reemerges at 4 months which may be linked to the development of CHF and continued remodeling of the heart.

Our data indicate that PEx of the infarcted area is not resolved 4 months after MI. We believe that the initial PEx (3 days) is a direct result of cardiac inflammation and that chronic PEx is the result of cardiac remodeling. Angiogenic factors like vascular endothelial growth factor (VEGF), which have been shown to increase VP (Nagy et al., 2008), are highly expressed in the peripheral zone of the infarct following MI. Subsequently, the peripheral zone becomes highly vascularized just 3-days post MI (Sun et al., 2002; Rog-Zielinska et al., 2016) and remains highly vascularized over 8 weeks (Kalk et al., 1997; Sun and Weber, 2000) suggesting angiogenesis. Neovascularization would support and contribute to the creation of dense fibrillar collagen networks that are found in the infarct scar 4 weeks after MI (Sun et al., 2002). Unlike other tissues the heart demonstrates continued collagen deposition (Cleutjens et al., 1995) and myofibroblast activation (Sun and Weber, 1996) for prolonged periods of time–up to several months in rats–that would require nutrients from newly created vascular beds. We speculate that blood flow and exudate in the peripheral zone may diffuse into the fibrotic scar. Little is known about the capacity of vessels to deliver nutrients and diffusion of such nutrients to the fibrotic scar, but our data indicate that PEx of the infarct is not resolved 4 months after MI.

Given the lungs anatomic and physiological proximity to the heart, it can be reasoned that the lungs would be the first and most severely impacted extracardiac organ following an MI. Our data corroborate with this line of thinking evidenced by significant acute pulmonary PEx. Inconsistent to the heart, the lung did not

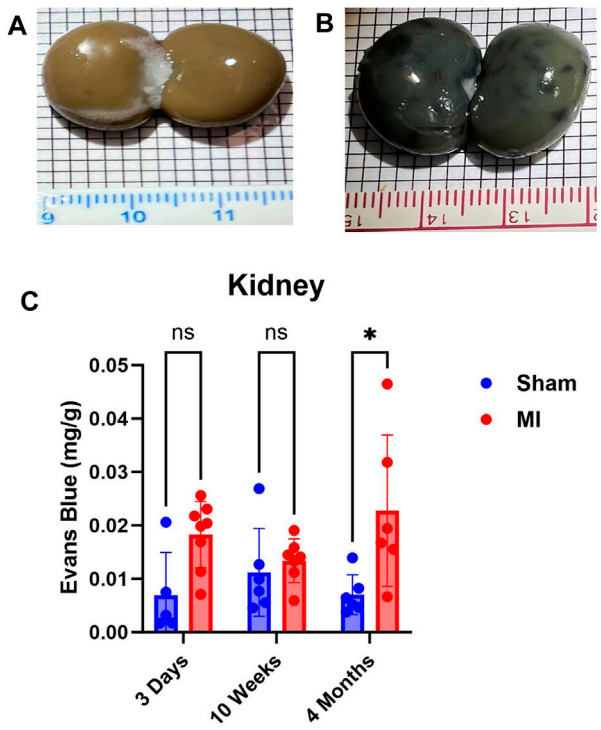

FIGURE 7
Time-dependent renal PEx post sham/MI. Representative images show PEx in the kidney at 4 months post sham/MI surgery **(A, B)**. Time course of PEx in the kidney from sham and MI animals post-surgery **(C)**. Mean ± SD. n = 5-8 per group. Comparing MI with Sham group $p < 0.05$ (*).

experience diminishment of PEx over time. It may even be increasing, but due to lack of statistical significance we cannot be certain.

As far as lung PEx is concerned, we believe the same general mechanisms are in play: initial inflammation followed by hemodynamic perturbance. Small infarcts that do not lead to elevated left ventricular end diastolic pressure induced neutrophil infiltration into the lung (Yan et al., 2014). This suggests that cardiac damage is sufficient to promote lung inflammation. However, as time goes on, diminished heart function and left-sided heart failure lead to pulmonary hypertension and an increase in pulmonary arterial wedge pressure (PAWP) (Kuebler et al., 1999; Konstam et al., 2018) both of which have deleterious effects on pulmonary function including increased plasma exudate and edema. Pulmonary hypertension can also progress to poorer right ventricular reserve, and when coupled with an increase in PAWP, will drastically worsen lung congestion (Reddy et al., 2019). Lymph flow may increase by a factor of 20–30 under sustained conditions of increased filtration attributable to elevated capillary pressure (Uhley et al., 1962). However, the increased levels of chronic PEx indicate pathologic VP that could overwhelm the lymphatic system. Even if high levels of edema are absent, small accumulations of interstitial fluid within the lungs will dramatically impair gas exchange and potentially interfere with other organ systems evidenced by the fact that lung injury can induce extrapulmonary organ PEx (Kitzerow et al., 2022).

The interplay of the heart and kidney cannot be understated; the kidneys provide clearance of waste products, maintenance of volume and electrolyte homeostasis, and modify neuroendocrine activities. Our data show elevated PEx in the kidney occurring at 4 months post MI. These data are consistent with the trend of renal pro-inflammatory/injury markers post MI (Xia et al., 2022). The lack of PEx at 10 weeks post MI may be due to a renal compensatory response that seeks to normalize cardiac output and arterial pressure post MI. The compensatory stages of heart failure may normalize kidney PEx, but upon CHF and development of elevated central venous pressure (CVP), PEx resumes due to elevated hydrostatic pressure in renal post-capillary venules. Unlike other abdominal organs, the kidney is intimately encased in a fibrous capsule causing additional plasma leakage and interstitial pressure particularly damaging and producing accelerated and irreversible loss of nephrons (Schroten et al., 2016) and promoting renal failure.

The current study shows that PEx of the intestines and pancreas occurs after liver PEx begins, 3 days post MI. This suggests that liver dysfunction precedes and may contribute to dysfunction of other digestive organs. Of the GI tract, only the duodenum and cecum demonstrated significant levels of PEx at 4 months and 10 weeks, respectively, while the ileum did not. Interestingly, the pancreas was the only digestive organ that presented significant worsening of PEx as time progressed and exhibited the highest levels of PEx of any organ including the heart. Each of these organs possesses fenestrated capillaries (Milici et al., 1985; Griffin and Gao, 2017; Burganova et al., 2021) so anatomical capillary structure does not explain the observed differences.

CHF is associated with chronic pancreatitis (Nikolic et al., 2019; Hiraiwa et al., 2022), congestive hepatopathy (Seeto et al., 2000; Sundaram and Fang, 2016), protein-losing enteropathy (Chan et al., 1999), malnutrition, and loss of appetite. Due to its development in the chronic stages of CHF we believe that PEx is caused, in part, by CVP elevation. The liver is especially sensitive to increased CVP (Seeto et al., 2000) due to the hepatic portal system. Elevated CVP increases the hydrostatic pressure of post-capillary venules and promotes VP and protein exudate in the liver because of their connections to the portal system, the intestines, pancreas, and spleen. Increased CVP also increases liver lymph flux which stresses the retroperitoneal lymphatic system (Itkin et al., 2020) which can rupture intestinal lacteals and further promote gut edema (Sundaram and Fang, 2016). Acute PEx may not occur in the gut due to its relatively high tolerance to reductions in blood flow and resistance to hypoxia (Seeto et al., 2000; Zheng et al., 2015) implying that these tissues most likely do not exhibit severe oxidative or pro-inflammatory responses that increase VP due to acutely diminished cardiac output. However, severe intestinal hypoperfusion and mucosal ischemia, have been shown to increase bacterial translocation and serum endotoxins (Niebauer et al., 1999; Krack et al., 2004) suggesting increased vascular permeability. Although the peritoneal cavity has high expansive abilities, unrestrained transcapillary filtration leads to exudation of interstitial fluid into the gut lumen (Granger, 1981) and, together with pancreatic

exocrine deficiency often seen in CHF (Xia et al., 2017), could explain malabsorption and loss of appetite.

The spleen exhibits significant PEx starting at 10 weeks. Levels rise significantly higher at 4 months. We expected the spleen to show PEx at 3 days due to the immune interactions between the spleen and heart. There appears to be an upward trend, but unlike the other organs, the normal spleen demonstrates relatively high levels of PEx. Even looking at the spleen macroscopically, sham and MI look very similar.

Spleen activity after MI has received much attention due to the spleen's importance in the development of leukocytes and its ability to respond to distant tissue injury (Swirski et al., 2009). In the case of MI, cardiac tissue damage has been shown to trigger the release of splenic immune cells, which contribute to cardiac remodeling and heart failure (Van Linthout and Tschope; Prabhu, 2018; Tian et al., 2016). Elevated VP increases mobilization of immune cells. Because VP and PEx are interrelated, we hypothesized that PEx would be enhanced 3 days following MI. Swirski et al. (Swirski et al., 2009), demonstrated splenic immune mobilization 1 day after MI, suggesting that VP may only be momentarily enhanced. However, splenic PEx is not only heightened at 4 months but increasing, which may portend an inflammatory response. Chronic heart failure has been shown to induce splenomegaly as measured by volume (Fujinami et al., 2018) and mass (Tonelli et al., 2013), and stimulate white pulp and marginal zone hypertrophy (Prabhu, 2018). Alternatively, the chronic production of splenic PEx may be the result of elevated CVP much like the other abdominal organs. As discussed above, portal hypertension can induce increases in hydrostatic pressure of post-capillary venules leading to PEx and edema. Due to their lymphatic connections via the periaortic nodes (Mikhael and Khan, 2022), liver lymph pathology can also contribute to spleen PEx.

Limitations

One of the hallmarks of CHF is elevated CVP. However, CVP was not measured in our permanent MI model, so we can only speculate that elevated CVP contributed to increased levels of PEx in each organ. In addition, lymphatics play an important role in clearing extravasated materials as well as contributing to the exudate. By measuring circulatory PEx by EB we are not able to determine the extent to which lymphatic efflux contributes to overall organ extravasate. In addition, by using EB to extrapolate PEx, we cannot determine the exact mechanisms that are occurring and driving the observed PEx of an organ. Lastly, all experiments were conducted in adult male SD rats. Further studies are required to elucidate if divergences in multiorgan PEx after MI occur due to sex differences.

Conclusion

Vascular permeability is critical for any organ function since the tight regulation of protein extravasation helps to maintain homeostasis. Persistent increased protein exudate limits the diffusion efficiency of nutrients and waste, increases interstitial pressure that can collapse capillaries and ultimately impair organ function. Increased vascular permeability could also cause organ inflammation or edema. Plasma extravasation in varying degrees is present in all organs following MI. Due to varying timepoints of PEx initiation and intervals, the mechanisms that promote extravasation, such as cardiac inflammation, hypoperfusion, or venous pressure most likely differ among organs. This is the first study to our knowledge documenting the time varying nature of PEx following MI and the development of CHF. We believe that PEx could be an independent risk factor to predict the MI-induced cardiac and extracardiac organ dysfunction.

Data availability statement

The raw data supporting the conclusion of this article will be made available by the authors, without undue reservation.

Ethics statement

The animal study was approved by the Institutional Animal Care and Use Committee of the University of Nebraska Medical Center. The study was conducted in accordance with the local legislation and institutional requirements.

Author contributions

OK: Data curation, Formal Analysis, Investigation, Methodology, Validation, Visualization, Writing–original draft. PS: Data curation, Formal Analysis, Investigation, Methodology, Validation, Visualization, Writing–review and editing. MS: Conceptualization, Formal Analysis, Resources, Supervision, Validation, Visualization, Writing–review and editing. SL: Data curation, Formal Analysis, Investigation, Project administration, Resources, Supervision, Visualization, Writing–review and editing. IZ: Conceptualization, Formal Analysis, Resources, Supervision, Visualization, Writing–review and editing. H-JW: Conceptualization, Data curation, Formal Analysis, Funding acquisition, Investigation, Methodology, Project administration, Resources, Supervision, Validation, Writing–review and editing.

Funding

The author(s) declare financial support was received for the research, authorship, and/or publication of this article. This study was supported by NIH grant R01 HL-152160 and in part, by NIH grants R01 HL-169205-01 and R01 HL126796. H-JW is also supported by Margaret R. Larson Professorship in Anesthesiology. IZ is supported, in part, by the Theodore F. Hubbard Professorship for Cardiovascular Research. OK is supported by UNMC John & Louise Skala Fellowship & G.S. Assistantship.

Conflict of interest

The authors declare that the research was conducted in the absence of any commercial or financial relationships that could be construed as a potential conflict of interest.

The author(s) declared that they were an editorial board member of Frontiers, at the time of submission. This had no impact on the peer review process and the final decision.

Publisher's note

References

Burganova, G., Bridges, C., Thorn, P., and Landsman, L. (2021). The role of vascular cells in pancreatic beta-cell function. *Front. Endocrinol. (Lausanne)* 12, 667170. doi:10.3389/fendo.2021.667170

Chan, F. K., Sung, J. J., Ma, K. M., Leung, Y. L., and Yeung, V. T. (1999). Protein-losing enteropathy in congestive heart failure: diagnosis by means of a simple method. *Hepatogastroenterology* 46, 1816–1818.

Cleutjens, J. P., Verluyten, M. J., Smiths, J. F., and Daemen, M. J. (1995). Collagen remodeling after myocardial infarction in the rat heart. *Am. J. Pathol.* 147, 325–338.

Colvin, R. B., and Dvorak, H. F. (1975). Fibrinogen/fibrin on the surface of macrophages: detection, distribution, binding requirements, and possible role in macrophage adherence phenomena. *J. Exp. Med.* 142, 1377–1390. doi:10.1084/jem.142.6.1377

Dewald, O., Ren, G., Duerr, G. D., Zoerlein, M., Klemm, C., Gersch, C., et al. (2004). Of mice and dogs: species-specific differences in the inflammatory response following myocardial infarction. *Am. J. Pathol.* 164, 665–677. doi:10.1016/S0002-9440(10)63154-9

Dvorak, H. F. (2010). Vascular permeability to plasma, plasma proteins, and cells: an update. *Curr. Opin. Hematol.* 17, 225–229. doi:10.1097/MOH.0b013e3283386638

Dvorak, H. F. (2021). Reconciling VEGF with VPF: the importance of increased vascular permeability for stroma formation in tumors, healing wounds, and chronic inflammation. *Front. Cell Dev. Biol.* 9, 660609. doi:10.3389/fcell.2021.660609

Dvorak, H. F., Orenstein, N. S., Carvalho, A. C., Churchill, W. H., Dvorak, A. M., Galli, S. J., et al. (1979). Induction of a fibrin-gel investment: an early event in line 10 hepatocarcinoma growth mediated by tumor-secreted products. *J. Immunol.* 122, 166–174. doi:10.4049/jimmunol.122.1.166

Frangogiannis, N. G. (2012). Regulation of the inflammatory response in cardiac repair. *Circ. Res.* 110, 159–173. doi:10.1161/CIRCRESAHA.111.243162

Fujinami, M., Kondo, H., Yufu, K., Shinohara, T., Ishii, Y., Teshima, Y., et al. (2018). Association between the baseline peripheral blood monocyte counts, the size of spleen, and the response to cardiac resynchronization therapy. *J. Cardiol.* 71, 299–304. doi:10.1016/j.jjcc.2017.09.004

Granger, D. N. (1981). Intestinal microcirculation and transmucosal fluid transport. *Am. J. Physiol.* 240, G343–G349. doi:10.1152/ajpgi.1981.240.5.G343

Griffin, C. T., and Gao, S. (2017). Building discontinuous liver sinusoidal vessels. *J. Clin. Invest.* 127, 790–792. doi:10.1172/JCI92823

Guo, S., and Dipietro, L. A. (2010). Factors affecting wound healing. *J. Dent. Res.* 89, 219–229. doi:10.1177/0022034509359125

Hiraiwa, H., Okumura, T., and Murohara, T. (2022). The cardiosplenic axis: the prognostic role of the spleen in heart failure. *Heart Fail Rev.* 27, 2005–2015. doi:10.1007/s10741-022-10248-4

Hong, J., Gao, L., Cai, Y., Lazartigues, E., and Wang, H. J. (2021). Voltage-gated potassium channel dysfunction in dorsal root ganglia contributes to the exaggerated exercise pressor reflex in rats with chronic heart failure. *Am. J. Physiol. Heart Circ. Physiol.* 321, H461–H474. doi:10.1152/ajpheart.00256.2021

Institute of Laboratory Animal Resources (2021). Guide for laboratory animal facilities and Care. *ILAR J.* 62 (3), 345–358. doi:10.1093/ilar/ilac012

Itkin, M., Rabinowitz, D., and Hur, S. (2020). Liver lymphatic imaging and interventions: resurrection of the forgotten knowledge. *Semin. Interv. Radiol.* 37, 318–323. doi:10.1055/s-0040-1713638

Kain, V., Prabhu, S. D., and Halade, G. V. (2014). Inflammation revisited: inflammation versus resolution of inflammation following myocardial infarction. *Basic Res. Cardiol.* 109, 444. doi:10.1007/s00395-014-0444-7

Kalkman, E. A., van Haren, P., Saxena, P. R., and Schoemaker, R. G. (1997). Regionally different vascular response to vasoactive substances in the remodelled infarcted rat heart; aberrant vasculature in the infarct scar. *J. Mol. Cell Cardiol.* 29, 1487–1497. doi:10.1006/jmcc.1997.0388

Kemp, C. D., and Conte, J. V. (2012). The pathophysiology of heart failure. *Cardiovasc Pathol.* 21, 365–371. doi:10.1016/j.carpath.2011.11.007

Kilkenny, C., Browne, W. J., Cuthill, I. C., Emerson, M., and Altman, D. G. (2012). Improving bioscience research reporting: the ARRIVE guidelines for reporting animal research. *Osteoarthr. Cartil.* 20, 256–260. doi:10.1016/j.joca.2012.02.010

Kitzerow, O., Zucker, I. H., Lisco, S. J., and Wang, H. J. (2022). Timeline of multi-organ plasma extravasation after bleomycin-induced acute lung injury. *Front. Physiol.* 13, 777072. doi:10.3389/fphys.2022.777072

Konstam, M. A., Kiernan, M. S., Bernstein, D., Bozkurt, B., Jacob, M., Kapur, N. K., et al. (2018). Evaluation and management of right-sided heart failure: a scientific statement from the American heart association. *Circulation* 137, e578–e622. doi:10.1161/CIR.0000000000000560

Krack, A., Richartz, B. M., Gastmann, A., Greim, K., Lotze, U., Anker, S. D., et al. (2004). Studies on intragastric PCO2 at rest and during exercise as a marker of intestinal perfusion in patients with chronic heart failure. *Eur. J. Heart Fail* 6, 403–407. doi:10.1016/j.ejheart.2004.03.002

Kuebler, W. M., Ying, X., Singh, B., Issekutz, A. C., and Bhattacharya, J. (1999). Pressure is proinflammatory in lung venular capillaries. *J. Clin. Invest.* 104, 495–502. doi:10.1172/JCI6872

Majno, G., Palade, G. E., and Schoefl, G. I. (1961). Studies on inflammation. II. The site of action of histamine and serotonin along the vascular tree: a topographic study. *J. Biophys. Biochem. Cytol.* 11, 607–626. doi:10.1083/jcb.11.3.607

McDonald, D. M., Thurston, G., and Baluk, P. (1999). Endothelial gaps as sites for plasma leakage in inflammation. *Microcirculation* 6, 7–22. doi:10.1111/j.1549-8719.1999.tb00084.x

Mikhael, M., and Khan, Y. S. (2022). *StatPearls*.

Milici, A. J., L'Hernault, N., and Palade, G. E. (1985). Surface densities of diaphragmed fenestrae and transendothelial channels in different murine capillary beds. *Circ. Res.* 56, 709–717. doi:10.1161/01.res.56.5.709

Nagy, J. A., Benjamin, L., Zeng, H., Dvorak, A. M., and Dvorak, H. F. (2008). Vascular permeability, vascular hyperpermeability and angiogenesis. *Angiogenesis* 11, 109–119. doi:10.1007/s10456-008-9099-z

Niebauer, J., Volk, H. D., Kemp, M., Dominguez, M., Schumann, R. R., Rauchhaus, M., et al. (1999). Endotoxin and immune activation in chronic heart failure: a prospective cohort study. *Lancet* 353, 1838–1842. doi:10.1016/S0140-6736(98)09286-1

Nikolic, S., Dugic, A., Steiner, C., Tsolakis, A. V., Haugen Löfman, I. M., Löhr, J. M., et al. (2019). Chronic pancreatitis and the heart disease: still *terra incognita*? *World J. Gastroenterol.* 25, 6561–6570. doi:10.3748/wjg.v25.i44.6561

Prabhu, S. D. (2018). The cardiosplenic Axis is essential for the pathogenesis of ischemic heart failure. *Trans. Am. Clin. Climatol. Assoc.* 129, 202–214.

Prabhu, S. D., and Frangogiannis, N. G. (2016). The biological basis for cardiac repair after myocardial infarction: from inflammation to fibrosis. *Circ. Res.* 119, 91–112. doi:10.1161/CIRCRESAHA.116.303577

Reddy, Y. N. V., Obokata, M., Wiley, B., Koepp, K. E., Jorgenson, C. C., Egbe, A., et al. (2019). The haemodynamic basis of lung congestion during exercise in heart failure with preserved ejection fraction. *Eur. Heart J.* 40, 3721–3730. doi:10.1093/eurheartj/ehz713

Roger, V. L. (2021). Epidemiology of heart failure: a contemporary perspective. *Circ. Res.* 128, 1421–1434. doi:10.1161/CIRCRESAHA.121.318172

Rog-Zielinska, E. A., Norris, R. A., Kohl, P., and Markwald, R. (2016). The living scar--cardiac fibroblasts and the injured heart. *Trends Mol. Med.* 22, 99–114. doi:10.1016/j.molmed.2015.12.006

Scallan, J., Huxley, V. H., and Korthuis, R. J. (2010). *Capillary fluid exchange: regulation, functions, and pathology integrated systems Physiology: from molecule to function to disease*.

Schroten, N. F., Damman, K., Valente, M. A. E., Smilde, T. D., van Veldhuisen, D. J., Navis, G., et al. (2016). Long-term changes in renal function and perfusion in heart failure patients with reduced ejection fraction. *Clin. Res. Cardiol.* 105, 10–16. doi:10.1007/s00392-015-0881-9

Seeto, R. K., Fenn, B., and Rockey, D. C. (2000). Ischemic hepatitis: clinical presentation and pathogenesis. *Am. J. Med.* 109, 109–113. doi:10.1016/s0002-9343(00)00461-7

Sun, Y., Kiani, M. F., Postlethwaite, A. E., and Weber, K. T. (2002). Infarct scar as living tissue. *Basic Res. Cardiol.* 97, 343–347. doi:10.1007/s00395-002-0365-8

Sun, Y., and Weber, K. T. (1996). Angiotensin converting enzyme and myofibroblasts during tissue repair in the rat heart. *J. Mol. Cell Cardiol.* 28, 851–858. doi:10.1006/jmcc.1996.0080

Sun, Y., and Weber, K. T. (2000). Infarct scar: a dynamic tissue. *Cardiovasc Res.* 46, 250–256. doi:10.1016/s0008-6363(00)00032-8

Sundaram, V., and Fang, J. C. (2016). Gastrointestinal and liver issues in heart failure. *Circulation* 133, 1696–1703. doi:10.1161/CIRCULATIONAHA.115.020894

Sutton, M. G., and Sharpe, N. (2000). Left ventricular remodeling after myocardial infarction: pathophysiology and therapy. *Circulation* 101, 2981–2988. doi:10.1161/01.cir.101.25.2981

Swirski, F. K., Nahrendorf, M., Etzrodt, M., Wildgruber, M., Cortez-Retamozo, V., Panizzi, P., et al. (2009). Identification of splenic reservoir monocytes and their deployment to inflammatory sites. *Science* 325, 612–616. doi:10.1126/science.1175202

Talman, V., and Ruskoaho, H. (2016). Cardiac fibrosis in myocardial infarction-from repair and remodeling to regeneration. *Cell Tissue Res.* 365, 563–581. doi:10.1007/s00441-016-2431-9

Tian, Y., Pan, D., Chordia, M. D., French, B. A., Kron, I. L., and Yang, Z. (2016). The spleen contributes importantly to myocardial infarct exacerbation during post-ischemic reperfusion in mice via signaling between cardiac HMGB1 and splenic RAGE. *Basic Res. Cardiol.* 111, 62. doi:10.1007/s00395-016-0583-0

Tonelli, A. R., Yadav, R., Gupta, A., Arrossi, A. V., Heresi, G. A., and Dweik, R. A. (2013). Spleen size in idiopathic and heritable pulmonary arterial hypertension. *Respiration* 85, 391–399. doi:10.1159/000339423

Uhley, H. N., Leeds, S. E., Sampson, J. J., and Friedman, M. (1962). Role of pulmonary lymphatics in chronic pulmonary edema. *Circ. Res.* 11, 966–970. doi:10.1161/01.res.11.6.966

Van Linthout, S., and Tschope, C. (2017). Inflammation - cause or consequence of heart failure or both? *Curr. Heart Fail Rep.* 14, 251–265. doi:10.1007/s11897-017-0337-9

Verbrugge, F. H., Guazzi, M., Testani, J. M., and Borlaug, B. A. (2020). Altered hemodynamics and end-organ damage in heart failure: impact on the lung and kidney. *Circulation* 142, 998–1012. doi:10.1161/CIRCULATIONAHA.119.045409

Xia, T., Chai, X., and Shen, J. (2017). Pancreatic exocrine insufficiency in patients with chronic heart failure and its possible association with appetite loss. *PLoS One* 12, e0187804. doi:10.1371/journal.pone.0187804

Xia, Z., Vellichirammal, N. N., Han, L., Gao, L., Boesen, E. I., Schiller, A. M., et al. (2022). Cardiac spinal afferent denervation attenuates renal dysfunction in rats with cardiorenal syndrome type 2. *JACC Basic Transl. Sci.* 7, 582–596. doi:10.1016/j.jacbts.2022.02.008

Yan, X., Hegab, A. E., Endo, J., Anzai, A., Matsuhashi, T., Katsumata, Y., et al. (2014). Lung natural killer cells play a major counter-regulatory role in pulmonary vascular hyperpermeability after myocardial infarction. *Circ. Res.* 114, 637–649. doi:10.1161/CIRCRESAHA.114.302625

Zheng, L., Kelly, C. J., and Colgan, S. P. (2015). Physiologic hypoxia and oxygen homeostasis in the healthy intestine. A review in the theme: cellular responses to hypoxia. *Am. J. Physiol. Cell Physiol.* 309, C350–C360. doi:10.1152/ajpcell.00191.2015

Ziaeian, B., and Fonarow, G. C. (2016). Epidemiology and aetiology of heart failure. *Nat. Rev. Cardiol.* 13, 368–378. doi:10.1038/nrcardio.2016.25

frontiers | Frontiers in Physiology

TYPE Mini Review
PUBLISHED 09 January 2024
DOI 10.3389/fphys.2023.1344885

OPEN ACCESS

EDITED BY
Meijing Wang,
Indiana University Bloomington, United States

REVIEWED BY
Jia Yao,
Emory University, United States
Wei Jaing,
Sichuan University, China

*CORRESPONDENCE
William C. W. Chen,
William.Chen@usd.edu

RECEIVED 26 November 2023
ACCEPTED 26 December 2023
PUBLISHED 09 January 2024

CITATION
Chowdhury MA, Zhang JJ, Rizk R and Chen WCW (2024), Stem cell therapy for heart failure in the clinics: new perspectives in the era of precision medicine and artificial intelligence. *Front. Physiol.* 14:1344885.
doi: 10.3389/fphys.2023.1344885

Stem cell therapy for heart failure in the clinics: new perspectives in the era of precision medicine and artificial intelligence

Mohammed A. Chowdhury[1,2,3], Jing J. Zhang[1], Rodrigue Rizk[4] and William C. W. Chen[1]*

[1]Division of Basic Biomedical Sciences, Sanford School of Medicine, University of South Dakota, Vermillion, SD, United States, [2]Department of Public Health and Health Sciences, Health Sciences Ph.D. Program, School of Health Sciences, University of South Dakota, Vermillion, SD, United States, [3]Department of Cardiology, North Central Heart, Avera Heart Hospital, Sioux Falls, SD, United States, [4]Department of Computer Science, University of South Dakota, Vermillion, SD, United States

Stem/progenitor cells have been widely evaluated as a promising therapeutic option for heart failure (HF). Numerous clinical trials with stem/progenitor cell-based therapy (SCT) for HF have demonstrated encouraging results, but not without limitations or discrepancies. Recent technological advancements in multiomics, bioinformatics, precision medicine, artificial intelligence (AI), and machine learning (ML) provide new approaches and insights for stem cell research and therapeutic development. Integration of these new technologies into stem/progenitor cell therapy for HF may help address: 1) the technical challenges to obtain reliable and high-quality therapeutic precursor cells, 2) the discrepancies between preclinical and clinical studies, and 3) the personalized selection of optimal therapeutic cell types/populations for individual patients in the context of precision medicine. This review summarizes the current status of SCT for HF in clinics and provides new perspectives on the development of computation-aided SCT in the era of precision medicine and AI/ML.

KEYWORDS

stem cells, heart failure, cell therapy, precision medicine, artificial intelligence, machine learning, clinical trial, regenerative medicine

Introduction

Heart failure (HF) typically arises from prolonged cardiomyopathy, a chronic and progressive pathological condition characterized by weakening, loss, and/or stiffening of the heart muscle (i.e., myocardium) (Dassanayaka and Jones, 2015). Without proper intervention, cumulative reductions in the cardiac capacity to pump blood likely lead to HF or even death. Unfortunately, HF is irreversible and incurable because human hearts do not have sufficient innate regenerative capacity to restore severe myocardial damage (Uygur and Lee Richard, 2016). HF has become a major global healthcare burden that progressively deteriorates the physiological capability of the affected population and significantly impacts their quality of life (Savarese et al., 2022). In the United States alone, HF affects around 2.5% and 1.7% of all men and women, respectively (Tsao et al., 2022). Importantly, the overall age-adjusted mortality rate for HF has notably increased from 2.36 to 3.16 per 100,000 people over the recent two decades (1999–2019) (Jain et al., 2022).

TABLE 1 Summary of recent clinical trials with stem cell therapy for heart failure. This table summarizes the key parameters and findings of major human trials with stem/progenitor cell therapy for heart failure since 2015.

Trial Name Author Year of Publication Trial Phase	Administration Route and Type of Stem Cells	Type of HF (Pt #)	Randomization and Sample Size	Average Age (% Male)	Average EF	NYHS Class	Key Findings
REGENERATE-DCM Hamshere et al. (2015) Phase II	Intracoronary administration of autologous BMC	NICM	S/C Saline:15 S/C G-CSF:15 IC BM serum:15 IC BMC: 15	56 (63%)	36%	≥II	At 3 months post-treatment, the IC BMC therapy group showing 1) 5.37% increase in LVEF: 38.3% ± 13.0% vs. 32.9% ± 16.5% (p = 0.0138) for up to 1 year. 2) Decrease in NYHA classification, reduced plasma NT-proBNP,increased exercise capacity, and improved quality of life. 3) No notable change in LVEF in remaining intervention groups
MiHeart Study Martino et al. (2015) Phase II/II	Intracoronary administration of autologous BMNC	NICM	Placebo: 78 IC BMNC: 82	56 (73%)	24%	III/IV	At 12 months post-treatment, no significant differences between the intervention and placebo groups for LVEF, LVESV, LVEDV, and mortality rate
MPC-HF Perin et al. (2015) Phase II	Transendocardial administration of allogenic MSC	ISCM(38) and NICM (7)	25M MPC: 20 75M MPC: 20 150M MPC: 20 (15 treated and 5 mock control 5 mock control each per group)	62 (97%)	31%	II/III	1) No difference between the groups for adverse events, clinically significant immune response, survival probability, MACE-free probability, and all-cause mortality. 2) Significant reduction in HF-related MACE (HF hospitalization, successfully resuscitated cardiac death, or cardiac death) in the 150M MPC group compared to all other groups (p = 0.025)
MSC-HF trial Mathiasen et al. (2020) Phase II	Intracoronary administration of autologous BM derived MSC	ISCM	Placebo: 20 MSC: 40	66 (36%)	28%	II/III	At 3 months post-treatment, the MSC therapy group showing: 1) Significant reduction in LVESV (−7.6 mL, p = 0.001). 2) No significant change in LVEF, stroke volume, and myocardial mass
REGENERATE-AMI Choudry et al. (2016) Phase II	Intracoronary administration of allogenic BMC	ISCM	BMC: 55 Placebo: 45	56 (84%)	48%	≥I	1) At 1 year, a greater myocardial salvage index by MRI in the BMC-treated group, compared with placebo (p = 0.048). 2) No difference in rare major adverse events between groups. 3) At the 5-year follow-up, there was no difference in the clinical outcomes between the two groups. Mathur et al. (2022)
IMPACT-CABG Noiseux et al. (2016) Phase II	Intramyocardial administration of autologous BM derived CD133+ Cells	ISCM	Intervention: 19 Placebo: 14	66 (89.5%)	40%	II-IV	1) At 6 months post-treatment, improvements in LVEF and LV volumes in all patients by MRI with no significant difference between the two groups. 2) One death and four cases of transient renal insufficiency during the 6-month follow-up period
Ixmyelocel-T for ISCM Patel et al. (2016) Phase IIB	Intramyocardial administration of autologous Ixmyelocel-T (BM deribed-CD90$^+$ MSC and Cd 45+CD14+macrophages	ISCM	Ixmyelocel-T: 66 Placebo: 60		35%	III/IV	At 12 months post-treatment, the Ixmyelocel-T therapy comparing to the placebo group: 37% reduction in cardiac events (risk ratio: 0.63 [95% CI 0.42–0.97]; p = 0.0344). Less serious adverse events (53% vs 75%, p = 0.0197)

(Continued on following page)

10.3389/fphys.2023.1344885

TABLE 1 (*Continued*) Summary of recent clinical trials with stem cell therapy for heart failure. This table summarizes the key parameters and findings of major human trials with stem/progenitor cell therapy for heart failure since 2015.

Trial Name Author Year of Publication Trial Phase	Administration Route and Type of Stem Cells	Type of HF (Pt #)	Randomization and Sample Size	Average Age (% Male)	Average EF	NYHS Class	Key Findings
CHART-1 Study Teerlink et al. (2017) Phase II/III	Intramyocardial administration of autologous cardiopoietic MSC	ISCM	Cardiopoietic MSC (C3BS- CQR-1): 120 Sham procedure: 151	62 (89%)	27%	II-IV	1) At 12 months post-treatment, the cardiopoietic MSC group showing decreases in LVEDV by 17 mL ($p = 0.006$) and increases in LVESV by 12 mL ($p = 0.017$). 2)The treatment group with a moderate number of repeated injections (>16 to <20) exhibiting the largest reverse remodeling
PERFECT Steinhoff et al. (2017) Phase III	Intramyocardial administration of autologous BM derived CD133+ stem cells	ISCM	CD133+ SC: 41 Placebo: 41	63 (85%)	32%	I-IV	1) At 180 days post-treatment, no notable difference in survival, adverse events, or change in LVEF by MRI from baseline. 2) Increased Erythropoeitin ($p = 0.02$) and SH2B3 mRNA expression ($p = 0.073$) in preoperative peripheral blood of the responders (ΔLVEF≥ 5% after 180 days); reduced CD133+ EPC ($p = 0.005$) and thrombocytes ($p = 0.004$) in the preoperative peripheral blood of the non-responders. 3) Preoperative discrimination with 80% (responders) and 84% (non-responders) accuracy after 10-fold cross-validation by machine learning-identified 20 biomarker response parameters
REGENERATE-IHD Choudhury et al. (2017) Phase II	Intramyocardial and intracoronary administration of autologous BMSC with G- CSF	ISCM	Peripheral: S/C G-CSF: 15 S/C Placebo: 15 Intramyocardial: IM BMC: 15 S/C Placebo: 15 Intracoronoary: IC BMC: 15 IC Placebo: 15	61 (100%)	30%	II-IV	1) At 1 year post-treatment, significant improvement in LVEF of 4.99% by MRI with intramyocardial BMC therapy ($p = 0.038$); no difference in LVEF in all other groups. 2) Reduced NT-proBNP at 6 months and a reduction in NYHA class at 1 year with intramyocardial BMC therapy
Muscle-derived SC with connexin-43 gene overexpression for HF Gwizdala et al. (2017) Phase I	Intramyocardial administration of allogenic engineered muscle derived stem/progentor cells	ISCM (11) and NICM (2)	13	61 (92%)	25%	II/III	At 6 months, compared to the baseline: 1) Improved exercise capacity: NYHA (3 ± 0 vs. 1.8 ± 0.7, $p = 0.003$), exercise duration (388.7 ± 141.8 s vs. 462.1 ± 176.7 s, $p = 0.025$), peak O2 consumption (14.4 ± 4.0 vs. 15.8 ± 3.7 mL/kg.min, $p = 0.022$), and O2 pulse (10.6 ± 2.9 vs. 18.9 ± 22.6 mLO2/heart rate, $p = 0.012$). 2) Improvement in the levels of BNP, LVEF, and LVED. 3) Significant improvement in the mean unipolar voltage amplitudes in the injected segments (9.6 ± 2.6 vs. 11.6 ± 3.5 mV, $p = 0.014$) and the entire LV (8.8 ± 2.8 vs. 10.2 ± 3.4mV, $p = 0.041$). 4) No deaths reported; one subject with ventricular tachycardia

(Continued on following page)

10.3389/fphys.2023.1344885

TABLE 1 (*Continued*) Summary of recent clinical trials with stem cell therapy for heart failure. This table summarizes the key parameters and findings of major human trials with stem/progenitor cell therapy for heart failure since 2015.

Trial Name Author Year of Publication Trial Phase	Administration Route and Type of Stem Cells	Type of HF (Pt #)	Randomization and Sample Size	Average Age (% Male)	Average EF	NYHS Class	Key Findings
TRIDENT study Florea et al. (2017) Phase II	Transendocardial administration of allogenic BM derived MSC	ISCM	20M-MSC: 15 100M-MSC: 15	66 (90%)	36%	I-III	At 12 months post-treatment: 1) Similar reduction in scar size in both groups by CT. 2) Increase in LVEF only with 100M-MSC Tx (by 3.7U, $p = 0.04$).3) Improved NYHA class in the 20M-MSC (35.7%) and 100M-MSC (42.9%) groups 4) Increased proBNP in the 20M-MSC group (0.32 log pg/mL $p = 0.039$), but not in the 100M-MSC group (−0.07 log pg/mL)
RIMECARD Trial Bartolucci et al. (2017) Phase I/II	Peripheral infusion of allogenic umbilical cord derived MSC	ISCM (21) and NICM (9)	UC-MSC: 15 Placebo: 15	57 (80%)	33%	I-III	At 3, 6, and 12 months post-treatment, the US-MSC group had: significant improvement in LVEF compared to baseline (+7.07 ± 6.22% vs. +1.85 ± 5.60%; $p = 0.028$) improvements of NYHA class ($p = 0.0167$ vs. baseline) and MLHFQ ($p<0.05$ vs. baseline). no difference in mortality, HF admissions, arrhythmias, or incident malignancy between the two groups
IV-MSC for NICMP Butler et al. (2017) Phase IIA	Peripheral infusion of allogenic ischemia-tolerant MSC (itMSC) grown in chronic hypoxia	NICM	itMSC: 10 Placebo: 12	47 (59%)	32%	II/III	No difference in mortality, adverse events, or hospitalization. No significant change in LVEF and LV volume. Increased 6-min walk distance (+36.47 m, 95% CI 5.98–66.97; $p = 0.02$) with itMSC Tx. 3) Improved Kansas City Cardiomyopathy clinical summary (+5.22, 95% CI 0.70–9.74; $p = 0.02$) and functional status scores (+5.65, 95% CI −0.11 to 11.41; $p = 0.06$) with itMSC Tx
IC BMC and MSC in HF Xiao et al. (2017) Phase II	Intracoronary administration of autologous BM mononuclear cells or MSC	NICM	BMMC: 16 BMSC: 17 Control: 20	50 (64%)	33%	II-IV	At 3 months, improvement in LVEF ($p = 0.004$), NYHA class ($p = 0.02$) and myocardial perfusion ($p = 0.019$) with BMSC Tx as well as LVEF ($p = 0.04$) and NYHA class ($p = 0.047$) with BMMC Tx. At 12 months, improvement in LVEF ($p = 0.005$), NYHA class ($p = 0.05$) and myocardial perfusion ($p = 0.038$) only with BMSC Tx. No difference in major adverse cardiovascular events between the three groups
POSEIDON-DCM Hare et al. (2017) Phase I/II	Transendocardial administration of allogenic or autologous BM derived MSC	NICM	Autologous BMSC: 19 Allogenic BMSC: 18	56 (71%)	26%	I-III	At 1 year post-treatment: 1) Increase in LVEF in allo-BMSC group by 8.0% ($p = 0.004$) compared with auto-BMSC; 2) Increase in the 6-min walk test with allo-BMSC by 37.0 m ($p = 0.04$); 3) Decrease in MLHFQ score in allo-BMSC ($p = 0.0022$); 4) Decreases in TNFα overall for both groups ($p = 0.0001$) with a greater decrease in the allo-BMSC group ($p = 0.05$); 5) No serious adverse events at 30 days; at12 months, serious adverse event rates: 63.5% in auto-BMSC and 28.2% in allo-BMSC ($p = 0.1$)

(Continued on following page)

10.3389/fphys.2023.1344885

TABLE 1 (*Continued*) Summary of recent clinical trials with stem cell therapy for heart failure. This table summarizes the key parameters and findings of major human trials with stem/progenitor cell therapy for heart failure since 2015.

Trial Name Author Year of Publication Trial Phase	Administration Route and Type of Stem Cells	Type of HF (Pt #)	Randomization and Sample Size	Average Age (% Male)	Average EF	NYHS Class	Key Findings
Repeat CD34$^+$ Vrtovec et al. (2018) Phase II	Transendocardial administration of autologous peripheral blood stem cells	NICM	Group A: Repeated stem cell treatment in 6 months: 30 Group B: Single stem cell treatment: 30	55 (88%)	31%	III	1) From baseline to 6 months, improvement in both groups: a. LVEF: +6.9 ± 3.3% in Group A, p = 0.001 and +7.1 ± 3.5% in Group B, p = 0.001. b. NT-proBNP: −578 ± 211 pg/mLin Group A, p = 0.02 and −633 ± 305 pg/mL in Group B, p = 0.01. c. 6-min walk test: +87 ± 21 m in Group A, p = 0.03 and +92 ± 25 m in Group B, p = 0.02)
RECARDIO Bassetti et al. (2018) Phase I	Intramyocardial administration of autologous BM derived CD133+ cells	ISCM	10	69 (100%)	38%	II-IV	1) At 6 months, improved baseline myocardial perfusion in: Summed stress scores (from 18.2 ± 8.6 to 13.8 ± 7.8, p = 0.05). Difference stress scores (from 12.0 ± 5.3 to 6.1 ± 4.0, p = 0.02). Improvement at 6 months compared to baseline in Canadian Cardiovascular Society ($p \leq 0.001$) and NYHA classes (p = 0.007). Positive correlation between changes in summed stress score and ATMP-CD133 release of proangiogenic cytokines HGF (r = 0.80, p = 0.009) and PDGF-bb (r = 0.77, p = 0.01). Negative correlation between changes in summed stress score and the proinflammatory cytokines RANTES (r = −0.79, p = 0.01) and IL-6 (r = −0.76, p = 0.02)
MPC in LVAD Yau et al. (2019) Phase II	Intramyocardial administration of allogenic MPC	ISCM (70) and NICM (89)	MPC: 106 Control: 53	55 (88.7%)	15%	II-IV	No difference between the groups in terms of successful temporary weaning from LVAD after 6 months of randomization, rate of adverse events, rate of readmission, and 1-year mortality
HUC-HEART Trial Ulus et al. (2020) Phase I/II	Intramyocardial administration of allogenic umbilical derived MSC vs BM mononuclear cells	ISCM	Control: 16 BM-MNC: 12 Umbilical MSC: 25	59 (100%)	35%	I/II	At the 6-month follow-up: decline in NT-proBNP levels compared to baseline in both cell-treated groups. At the 6- to 12-month follow-up: increase in LVEF (5.4%) and stroke volume (19.7%) only in the umbilical MSC group. Decreasing necrotic myocardium by 2.3% in the control, 4.5% in the BM-MNC group, and 7.7% in the umbilical MSC group. Increase in the 6-min walking test in the control (14.4%) and the umbilical MSC group (23.1%)
CCTRN SENECA Trial Bolli et al. (2020) Phase I	Intramyocardial administration of allogenic BM derived MSC	NICM	MSC: 14 Placebo: 17	54 (24%)	33%	II/III	No significant difference in clinical outcomes between the two groups
Collagen scaffold MSC in HF He et al. (2020) Phase I	Intramyocardial administration of allogenic MSC with cell-laden hydrogel scaffold	ISCM	CABG + Cell + Hy drogel: 18 CABG + Cell: 17 Control: 15	62 (78%)	<10%	III/IV	No significant difference in serious adverse events. At 12 months post-treatment, cardiac MRI showing significant reduction in the mean infarct size only in the collagen/cell group: −3.1% (95% CI, −6.20% to −0.02%, p = 0.05)

(Continued on following page)

10.3389/fphys.2023.1344885

TABLE 1 (*Continued*) Summary of recent clinical trials with stem cell therapy for heart failure. This table summarizes the key parameters and findings of major human trials with stem/progenitor cell therapy for heart failure since 2015.

Trial Name Author Year of Publication Trial Phase	Administration Route and Type of Stem Cells	Type of HF (Pt #)	Randomization and Sample Size	Average Age (% Male)	Average EF	NYHS Class	Key Findings
ALLSTAR Makkar et al. (2020) Phase II	Intracoronary administration of allogenic cardiosphere derived cells	ISCM	CDC: 90 Placebo: 44	55 (84.4%)	40%	I/II	A1 month post-treatment, no primary safety endpoint events. At 6-month follow-up, no change in scar size percentage. At 6-month follow-up, CDC-treated patients showing notable reductions in LVEDV (p = 0.02), LVESV (p = 0.02), and NT-proBNP (p = 0.02)
CCTRN CONCERT-HF Bolli et al. (2021) Phase II	Intracoronary administration of autologous bone marrow derived MSC and c-kit + CPC	ISCM	MSC + CPC: 33 MSC: 29 CPC: 31 Placebo: 32	62 (87%)	28%	II/III	Lowest HF-related major adverse cardiac events in the CPC- treated group compared to placebo (−22%, p = 0.043) Significantly improved QOL scores in the MSC-alone group (p = 0.05) and the MSC + CPC group (p = 0.023) vs. placebo. No significant difference among groups in LVEF, LV volumes, scar size, 6-min walking distance, and peak O2 consumption
Danish Trial Qayyum et al. (2023a) Phase II	Intramyocardial administration of allogenic adipose derived MSC	ISCM	ASC: 54 Placebo: 27	67 (81%)	34%	II	No significant change in LVESV, LVEDV, LVEF, NYHA class and 6 min walk test between groups
SCIENCE Trial Qayyum et al. (2023b) Phase II	Intramyocardial administration of allogenic adipose derived MSC	ISCM	ASC: 90 Placebo: 43	66 (93%)	32%	II/III	No significant differences between groups in LVESV, LVEDV, LVEF, NYHA class, 6-min walk test, NT-proBNP, CRP, or QOL.
MPC in HF Perin et al. (2023) Phase III	Transendocardial administration of allogenic BM derived MSC	ISCM (319) and NICM (244)	BMSC: 283 Control: 282	63 (78%)	28%	II/III	At 12 months post-treatment, BMSC group vs. control group (analysis population: n = 537): Increasing LVEF, especially in patients with inflammation. Decrease in the risk of TTFE for MI or stroke by 58% (cause- specific HR: 0.42, 95% CI: 0.23–0.76). Red uction in the risk of TTFE for the 3-point MACE by: 28% (HR: 0.72, 95% CI: 0.51–1.03) Reducing risks of MI/stroke and the 3-point MACE by 75% and 38%, respectively, in patients with inflammation (hsCRP≥2 mg/L)

Legend Abbreviations.
ATMP: Autologous advanced therapy medicinal product BM: bone marrow.
BMC: Bone marrow-derived cells BMNC: Bone marrow mononuclear cells CI: confidence interval.
CRP: C-reactive protein CT: Computed tomography EF: ejection fraction.
EPC: endothelial progenitor cell.
G-CSF: Granulocyte colony-stimulating factor HF: heart failure.
hsCRP: High-sensitivity C-reactive protein IC: intracoronary.
ISCM: Ischemic cardiomyopathy LV: left ventricule.
LVEF: Left ventricular ejection fraction LVESV: Left ventricular end-systolic volume LVEDV: Left ventricular end-diastolic volume M: million.
MACE: Major adverse cardiovascular events MSC: mesenchymal stem cells.
MLHFQ: Minnesota Living with Heart Failure Questionnaire MRI: magnetic resonance imaging.
NICM: Non-ischemic cardiomyopathy.
NT-proBNP: N-terminal pro-B-type natriuretic peptide Pt: Participants.
QOL: quality of life.
RANTES: regulated on activation, normal T cell expressed and secreted; also known as Chemokine (C-C motif) ligand 5 (CCL5). ProBNP: pro-B-type natriuretic peptide.
S/C: subcutaneous.
TNFα: Tumor necrosis factor-α TTFE: Time-to-first-event.
Tx: Treatment.

10.3389/fphys.2023.1344885

The current medical regimen for clinical Stage C symptomatic HF includes a combination of vasodilators, beta blockers, sodium-glucose cotransporter-2 inhibitors, mineralocorticoid receptor antagonists, and diuretics (Heidenreich et al., 2022). Regardless of the recommended medical treatment, about 5% of HF patients develop Stage D HF or end-stage heart disease that requires either heart transplantation or mechanical support with a left ventricular (LV) assist device (LVAD) (Costanzo et al., 2008). However, these advanced therapies for end-stage HF have their individual limitations. For example, there is a constant shortage of matching hearts for transplantation as well as a higher incidence of sudden cardiac death in heart transplant recipients compared to the general population (Colvin et al., 2022; Bonnet et al., 2023). Patients with LVAD are at an increased risk for thromboembolic complications, bleeding, driveline infection, and right ventricular failure (Chaudhry et al., 2022). Thus, there is an unmet need for alternative medical approaches that fundamentally stop or revert the progression of HF pathologies as well as biologically enable the preservation and/or regrowth of functional myocardium.

Stem cells are precursor cells that have the ability to self-renew and differentiate into functionally mature, specialized cells in various human tissues (i.e., pluripotent or multipotent) (Evans and Kaufman, 1981; Pittenger et al., 2019). Numerous efforts have been poured into stem cell research over the last two decades, resulting in abundant laboratory discoveries and translational applications of distinct human stem/progenitor cell types: embryonic stem cells (ESCs), induced pluripotent stem cells (iPSCs), lineage-restricted or tissue-specific stem/progenitor cells (e.g., hematopoietic stem cells, skeletal muscle satellite cells, and intestinal stem cells) (Martello and Smith, 2014; Pizzute et al., 2015; Moradi et al., 2019), and adult mesodermal multipotent precursor cells (e.g., mesenchymal stem/stromal cells) (Pittenger et al., 2019). Many human clinical trials using stem cell-based regenerative therapy for treating HF have thus arisen from promising basic stem cell research and demonstrated encouraging results (Table 1). (Hare et al., 2012; Perin et al., 2012; Heldman et al., 2014; Hare et al., 2017; Teerlink et al., 2017) In this review, we will summarize the current status of stem/progenitor cell therapy for HF, persistent challenges and possible solutions, as well as the future perspectives of stem cell-based cardiac regenerative medicine in the era of precision medicine and artificial intelligence (AI) (Figure 1).

The clinical scope of stem cells in heart failure

Bone marrow-derived stem cells

In 2001, bone marrow-derived stem cells (BMSCs) were first transplanted into animal models of ischemic cardiac injury where the donor cells were shown to produce *de novo* myocardial and vascular structures in the peri-infarcted regions of the myocardium (Jackson et al., 2001; Orlic et al., 2001). The observed benefits were largely attributed to the paracrine release of tissue trophic factors by the donor cells, for example, VEGF and HGF promoting angiogenesis and cardiomyocyte (CM) survival, respectively (Gnecchi et al., 2005; Mabotuwana et al., 2022).

Human phase 2 clinical trials, such as FOCUS CCTRN and TAC-HFT, were conducted in patients with ischemic cardiomyopathy (ICM) who received multiple transendocardial injections of bone marrow mononuclear cells (BMMCs) in the infarcted territory. However, the results failed to demonstrate any significant improvement in LV chamber size, ejection fraction (EF), or quality of life (Perin et al., 2012; Heldman et al., 2014). Similarly, the REGENERATE AMI trial studied the impact of intracoronary infusion of autologous BMMCs in patients with ICM (Choudry et al., 2016). Despite the encouraging results at the 1-year follow-up that showed significant decreases in the infarct size and improved myocardial salvage indices in the intervention group, the 5-year follow-up did not exhibit improved clinical outcomes, suggesting short-term benefits of intracoronary BMMC infusion (Mathur et al., 2022). Interestingly, analysis of pre-transplant bone marrow (BM) samples of patients who responded to autologous BMMC therapy in the FOCUS CCTRN trial showed a higher frequency of CXCR4+ and B cells and fewer monocytes/macrophages and endothelial colony-forming cells in their BM compared to non-responders (Taylor et al., 2016). Therefore, the presence of certain subset(s) of BM progenitor and/or immune cell populations may indicate the potency of donor cells for autologous BMMC therapy (Taylor et al., 2016). The CardiAMP trial utilized the abovementioned concept and screened their subject's BM cell potency by flow cytometry prior to the enrollment (Johnston et al., 2018; Raval et al., 2021). Subjects with ICM and favorable BM cellular composition were selected for the trial and underwent BM aspiration, followed by an enrichment process to separate the nucleated cell fraction from the plasma phase using a density-tuned dual buoy column; the enriched BM aspirate was then injected into the infarcted myocardium (Raval et al., 2021). The 12-month follow-up data on 10 patients reported significant improvement in 6-min walk distances and trends towards improved NYHA class, LVEF, and quality of life (Raval et al., 2021).

Mesenchymal stem cells

Mesenchymal stem cells (MSCs) are allogeneic STRO-1/STRO-3+ cells, a subpopulation of stromal cells that express CD73, CD90, and CD105 and can be extracted from BM, adipose, and other tissues (Simmons and Torok-Storb, 1991; Haynesworth et al., 1992; Zuk et al., 2001; Karantalis and Hare, 2015). MSCs are adult multipotent precursor cells with great potential for cardiac repair since they can be easily isolated from autologous sources and rapidly expanded *ex vivo* (Pittenger et al., 1999; Halvorsen et al., 2000; Miura et al., 2003; Dominici et al., 2006; Chen et al., 2015; Melo et al., 2017). MSCs have been shown to improve cardiac function in multiple preclinical animal models of cardiac injury (Amado et al., 2005; Alfaro et al., 2008; Qi et al., 2008; Chen et al., 2013). Their primary mechanism of action for cardiac repair is paracrine secretion of multiplex tissue trophic factors that stimulate cellular repair and regeneration via angiogenesis, endothelization, anti-inflammation, and anti-fibrosis (Kocher et al., 2001; Chen et al., 2009; Abdalmula et al., 2017). The direct differentiation of MSCs into desired cardiac cell types, if any, did not appear to contribute significantly to the functional recovery observed in prior studies (van der Spoel TI. et al., 2011a; Guo et al., 2020).

The MSC-HF trial reported that ICM patients treated with multiple intramyocardial injections of autologous BM-derived MSCs exhibit progressive improvement in LV end-systolic volume (LVESV), EF, and myocardial mass 12 months after their initial treatment, even reducing hospitalization for angina in the

MSC-treated group after 4 years (Mathiasen et al., 2020). On 1-year follow-up, the DREAM-HF trial demonstrated that single-dose transendocardial injection of allogenic BM-derived MSCs improved LVEF, LVESV, LV end-diastolic volume (LVEDV) of treated HF patients, with 12% reduction in MI or stroke risk in patients with elevated high-sensitivity CRP (≥2 mg/L) (Perin et al., 2023). These results suggest that MSC treatment can improve clinical outcomes in HF patients for up to several years, especially for those with systemic inflammation.

In contrast, human clinical trials using adipose-derived MSCs for HF treatment failed to show any significant beneficial outcomes (Qayyum et al., 2023a; Qayyum et al., 2023b). Yau *et al.* reported that intramyocardially injecting allogenic BM-derived MSCs during LVAD implantation did not improve the successful weaning from LVAD, 1-year mortality, or the rate of serious adverse events (Yau et al., 2019). Currently, the STEMVAD trial (NCT03925324) is evaluating the safety and efficacy of three serial doses of allogenic MSCs by intravenous infusions in patients with end-stage HF requiring LVAD. The results of this study will help clarify the utility of MSC therapy in patients with end-stage HF.

Cardiosphere-derived cells

Cardiosphere-derived cells (CDCs) are characterized by their ability to separate from cardiac tissues and form spheroids in suspension cultures (Messina et al., 2004). They can function as adult stem/progenitor cells and have been shown to differentiate into myocytes and vascular cells in SCID beige mice (Messina et al., 2004). CDCs mainly contribute to cardiac repair by releasing paracrine factors and exosomes which inhibit cellular apoptosis and promote angiogenesis and CM proliferation (Chimenti et al., 2010; Ibrahim et al., 2014). The ALLSTAR trial evaluated the safety and efficacy of intracoronary delivery of allogenic CDCs in ICM patients with >15% scar burden (Makkar et al., 2020). At the 6-month follow-up, the intervention group showed significant reductions in LVESV, LVEDV, N-terminal pro-B-type natriuretic peptide (NT-proBNP) levels, and decreased segmental circumferential strain with MRI, but no improvement in their LV scar size, suggesting that CDCs could functionally benefit such patients but are not anti-fibrotic (Ostovaneh et al., 2021).

Induced pluripotent stem cells

In 2006, Yamanaka and colleagues first described a cocktail of four transcription factors (Oct3/4, Sox2, c-Myc, and Klf4) capable of artificially reprogramming mouse embryonic cells and adult fibroblasts into iPSCs that exhibit the self-renewability and pluripotency similar to ESCs (Takahashi and Yamanaka, 2006). iPSCs possess multiple translational advantages over ESCs: 1) no ethical concerns regarding the cellular origin; (Zheng, 2016); 2) autologous immunocompatible cell sources (if applicable), such as patient's own fibroblasts, obviating the need for immunosuppression; (Mandai et al., 2017; Schweitzer et al., 2020); 3) direct reprogramming approaches available for differentiating into desired tissue-specific cell types without going through the pluripotent stage, for example, direct reprogramming of human fibroblasts into CMs. (Qian et al., 2012). Cardiomyogenesis from iPSCs has been attempted previously (Yang et al., 2017; Wu et al., 2023); however, iPSC-derived CMs (iPSC-CMs) largely expressed fetal phenotypes and failed to efficiently function as adult CMs (Liao et al., 2021), limiting their clinical applicability. Recently, progress has been made to enhance the maturity of iPSC-CMs (Li et al., 2022; Hsueh et al., 2023). Besides, viral vectors used to reprogram fibroblasts to iPSCs may have the potential to cause cancer; (Okita et al., 2007) alternative non-viral delivery systems to induce iPSCs are under investigation, for example, the targeted nanoparticles (Anokye-Danso et al., 2011; Ye et al., 2016; Wang et al., 2020). iPSCs have the potential for clinical cell therapy in HF patients, and currently, two phase 1 trials are ongoing to assess the safety and efficacy of human allogenic iPSC-CMs in patients with ICM (ClinicalTrials.gov Identifier: NCT04945018 and NCT04696328).

Stem/progenitor cell-derived exosomes

Exosomes are extracellular vesicles that carry various proteins, lipids, and/or RNAs and play a major role in intercellular communications (Rezaie et al., 2022). Since the paracrine effect is an essential mechanism for stem/progenitor cell-mediated cardiac repair, exosomes derived from those cells that contain secretory trophic factors (e.g., pro-angiogenic and pro-survival cytokines) may constitute an alternative therapeutic approach to direct cell transplantation (Bolli et al., 2021). For instance, exosomes derived from human iPSCs had proliferative and protective effects on cardiac mesenchymal stromal cells, impacting their transcriptomic and proteomic profiles. (Bobis-Wozowicz et al., 2015). CDC-derived exosomes delivered via intramyocardial injections were shown to improve cardiac function and decrease scar size in porcine MI models (Gallet et al., 2017). A meta-analysis of ten studies using preclinical animal models of MI revealed that exosomal therapy had the potential to reduce cellular apoptosis and autophagy as well as improve cardiac function, fibrogenesis, and inflammatory response (Zheng et al., 2022).

Potential mechanisms of action of exosomal therapy in ischemic hearts include: 1) protection against myocardial reperfusion injury by reducing oxidative stress through inhibition of caspase 3/7 activation and delivery of cardioprotective microRNAs (miRs) such as miR-21 and miR-210; (Wang et al., 2015); 2) enhancement of intracellular calcium homeostasis and cardiomyocyte contraction by rescuing the expression and function of reticulum Ca2+ ATPase 2a (SERCA-2a) and ryanodine receptor 2 (RyR-2); (Li et al., 2023); and 3) improvement of cellular energy metabolism and myocardial bioenergetics without increasing the risk of arrhythmia (Gao et al., 2020). Intriguingly, besides modulating immune responses and inflammation, immune cell-derived exosomes facilitate crosstalk between immune cells and myocardial cells, which sustains ventricular function and promotes cardiac repair post-MI (Wen et al., 2021).

The use of exosomal therapy in HF patients is still under investigation, (Marbán, 2018; Duong et al., 2023), and current challenges for clinical applications include exosomal delivery, tissue targeting, and immunogenicity (Balbi and Vassalli, 2020). Moreover, exosomes may possibly carry inherent limitations or defects of their cellular origins that could impact their therapeutic efficacy (Riva et al., 2019; Andreeva et al., 2021). Thus, selecting appropriate, healthy stem/progenitor cell sources from which beneficial exosomes can be efficiently extracted is key to improving exosome-based HF therapy.

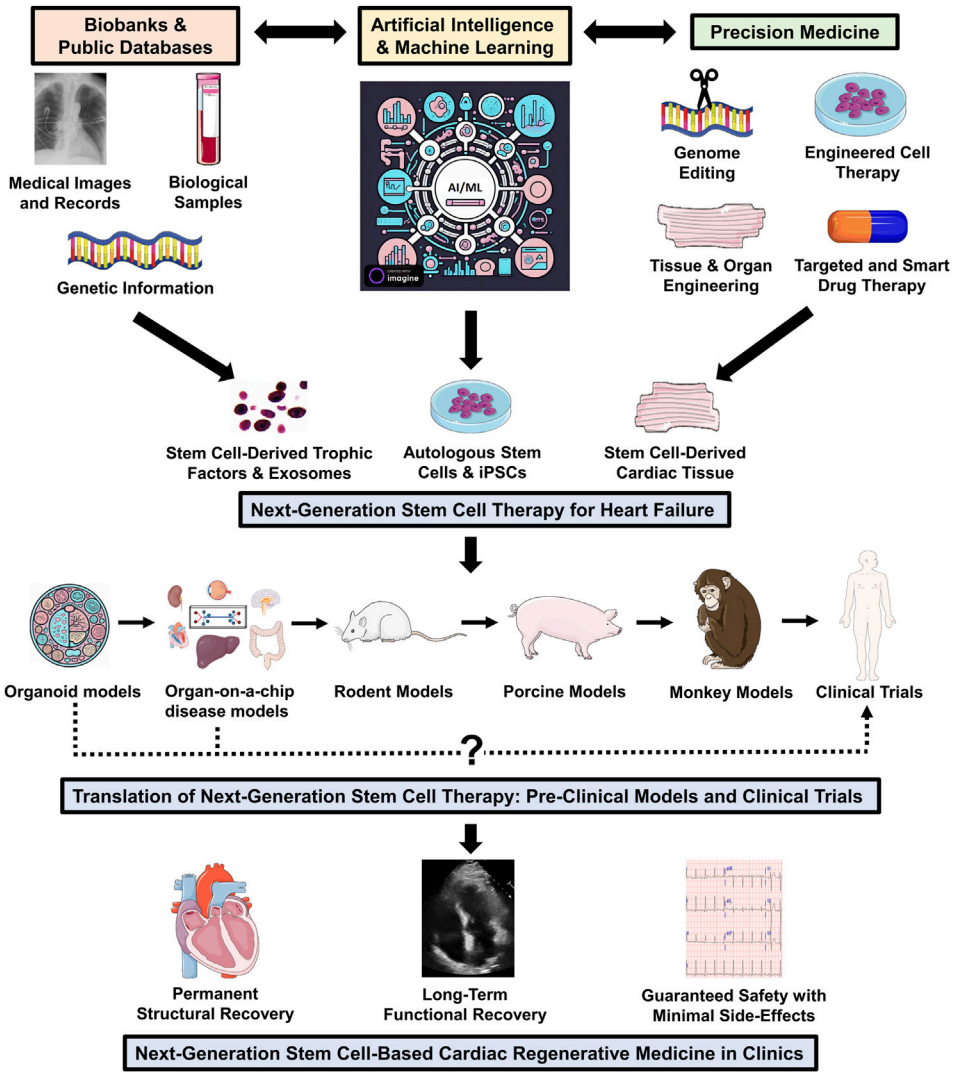

FIGURE 1
Next-generation stem/progenitor cell therapy for heart failure. To design next-generation personalized stem cell treatment for HF that ensures sustainable functional and structural recovery with minimal side effects, it is essential to integrate new components, including AI/ML, bioinformatics, and precision medicine, into stem cell research and therapeutic development. The emerging streamlined high-throughput testing platforms, such as organoid and organ-on-a-chip disease models, may greatly shorten the preclinical development phase and accelerate the progress of human trials.
The Figure was partly generated using Servier Medical Art, provided by Servier, licensed under a Creative Commons Attribution 3.0 unported license.

Challenges and alternatives for discrepancy between animal and human studies

Human trials involving stem cell therapy often fail to replicate the remarkable successes in animal models of cardiac injury (Table 1). (Rheault-Henry et al., 2021; Bolli et al., 2022; Bolli and Tang, 2022) This could be attributed to multiple reasons: 1) rodent hearts may not accurately mimic the pathophysiology of human HF because they differ from human hearts in terms of size, intrinsic heart rate, (Wessels and Sedmera, 2003), and epigenomic and transcriptomic profiles; (Lin et al., 2014); 2) a number of confounding factors that can be controlled in a laboratory experiment may not be adequately controlled in a human clinical trial, leading to differences in observed outcomes (e.g., diet and genetic background); (Hasenfuss, 1998; van der Spoel et al., 2011a); 3) inconsistent results in clinical trials may be due to the variability in study protocols between different research groups/institutions in terms of donor cell types and sources, treatment dose and duration, routes of administration, and timing of stem cell therapy. (Golpanian et al., 2015).

Besides, isolating specific stem/progenitor cells out of their native niche environment could disrupt important cell-to-cell and/or microenvironmental signaling, which may lead to suboptimal therapeutic potency including reduced cell proliferation, survival, differentiation, and/or paracrine function. (Kuchina et al., 2011). Furthermore, the cardiac disease cascade in humans is complex and consists of a dynamic process of progressive tissue ischemia, hypoxia, inflammation, and/or myocardial fibrosis, making the host environment harsh for transplanted cells to survive. Another issue is inadequate cell retention and reduced cell survival after administration because only ~11% of the delivered cells are retained in the myocardium, decreasing the overall efficiency of cell

therapy (Hou et al., 2005). Currently, the process of stem/progenitor cell homing to areas of myocardial damage is not fully understood, and strategies to improve targeted cardiac delivery are under investigation (Liesveld et al., 2020).

Also, there are variabilities among patients in terms of comorbidities, risk factors, lifestyle, and genomic differences; presently, it is not clear which type of individuals will benefit most from stem cell therapy (Patel et al., 2010; Gambini et al., 2012). Additionally, the majority of human trials used LVEF, LVESV, and LVEDV as surrogates for cardiac recovery; alternative endpoints may be needed to assess the efficacy of stem/progenitor cells since multiple clinical studies have reported improvement in subjects' quality of life and exercise tolerance without any significant increases in LVEF (Bolli et al., 2022). Thus, it may be essential to investigate alternative endpoint surrogates rather than solely relying on notable improvement in LVEF as the marker for therapeutic success (Borow et al., 2019).

There remain other challenges to solve, including 1) designing optimal cell banking strategies to maintain the therapeutic quality of donor stem/progenitor cells; 2) establishing appropriate high-throughput experimental protocols or computation algorithms to select or predict stem/progenitor cells ideal for treating a particular HF stage or pathology, respectively; and 3) building more non-invasive tools to measure how transplanted precursor cells function within the human subjects. Addressing these challenges may help improve the efficacy of stem cell therapy in human trials.

The application of stem cells in precision medicine for heart failure

Precision medicine is the anticipated future of medicine where therapy will be tailored according to the patient's genetic composition, environment, lifestyle, and risk factors (Ashley, 2016; Delpierre and Lefèvre, 2023). Stem cells can be used for a number of applications in precision medicine: 1) stem cell-derived CMs can be used to understand or simulate the pathophysiology of patient-specific cardiac conditions; (Musunuru et al., 2018) 2) cardiac diseases caused by genetic mutations can be replicated in patient-derived or engineered cell models with the assistance of the iPSC technology or genome editing tools, respectively; (Musunuru et al., 2018) 3) stem cell-derived cardiac cellular models can be used to test the efficacy and safety of personalized medication for individual patients; (Chen et al., 2016) and 4) autologous stem cell-derived cardiac cells may be used as a personalized therapeutic tool (Musunuru et al., 2018; Lightner and Chan, 2021).

Alternatively, cardiac organoid models derived from stem cells have been used to substitute animal and human subjects for the initial testing of the safety and/or efficacy in drug development, reducing animal and human morbidity and mortality (Azar et al., 2021). Thus, utilizing stem cells in precision medicine will not only improve our understanding of acquired cardiac disease (e.g., ICM and HF), (Bolli et al., 2022) inherent conditions (e.g., familial cardiomyopathies), (Jiang et al., 2021) and congenital heart defects (e.g., hypoplastic left heart syndrome, Ebstein anomaly, Fontan circulation with right ventricular dysfunction), (Tsilimigras et al., 2017) but also has the potential to be used as adjuvant treatment to current medical or surgical therapies.

Furthermore, large clinical datasets that comprise patient histories and characteristics, body fluid compositions, diagnostic results, tissue pathologies, imaging studies, and/or treatment effects may be used to identify, classify, or even predict the distinct signatures or behaviors of genome, epigenome, transcriptome, proteome, and/or phenome associated with a particular cardiac pathology in individual patients, and *vice versa* (Attia et al., 2019; Qiu et al., 2020; Segar et al., 2020; Liu et al., 2022). Also, many biological samples of patient-specific stem cells used in clinical trials are currently stored in biobanks (Musunuru et al., 2018; Annaratone et al., 2021). Combining the big data of multiomics with the cellular background and clinical information may facilitate a personalized multi-level analysis (Shi and Xu, 2019; Hu et al., 2020). Such comprehensive personalized analysis may improve our understanding of how stem cells behave and/or interact with other cell types under specific pathological conditions or disease stages (e.g., terminal-stage HF), ultimately aiding in the design of precision stem cell therapy for personalized medicine (Figure 1).

Computational tools to aid future development of stem cell-based therapeutics

The fields of AI and machine learning (ML) are rapidly expanding and contributing to various medical applications, including medical imaging, personalized medicine, and robotic-assisted surgeries (Krajcer, 2022; Haug and Drazen, 2023). AI-driven decision-making is exemplified in scenarios where algorithms can process environmental and biological inputs, such as changes in the culture media, intercellular signals, or cellular behaviors, and respond accordingly based on predefined parameters (Adlung et al., 2021). For instance, AI may autonomously detect and sustain predetermined cellular phenotypes by adjusting the conditions in human stem/progenitor cell cultures (e.g., infusing specific cytokines to stimulate cell growth or adding bicarbonate to maintain consistent pH levels), keeping the culture quality and streamlining routine wet-lab tasks (Capponi and Daniels, 2023).

AI's capability to analyze large preclinical and clinical datasets from biobanks, research data depositories, public health databases, and healthcare systems has immense implications for stem cell therapeutics in the context of precision medicine. AI/ML can be leveraged to identify common genomic traits, individual genetic polymorphism, disease-associated mutations, morphological patterns, and/or cellular functions in a personalized manner (Capponi and Daniels, 2023). This transdisciplinary knowledge helps: 1) determine the developmental stage and maturation of stem cells, (Guan et al., 2021; Kim et al., 2022) 2) assess their regenerative potentials and/or limitations, (Fischbacher et al., 2021), and 3) predict their therapeutic efficacy and/or side-effects in individual subjects. (Mota et al., 2021). For example, ML algorithms were used to identify biomarkers for predicting positive patient responses to BMSC therapy, (Steinhoff et al., 2017), characterize CMs non-invasively using video microscopy and image analysis, (Maddah and Loewke, 2014), analyze the effects of drugs on the calcium signals of iPSC-CMs, (Juhola et al., 2021), identify cell lines with/without genetic defects using

cellular images, (Kim et al., 2023), and identify neural stem cell differentiation. (Zhu et al., 2021).

Moreover, by analyzing the unique DNA methylation profiles, investigators devised a linear classification learning model to discern iPSCs, ESCs, somatic cells, and embryonal carcinoma cells, achieving 94.23% accuracy. (Nishino et al., 2021). Another group utilized convolutional neural networks (CNNs) to effectively differentiate pluripotent cells from initial differentiating cells. (Waisman et al., 2019). The training of the CNN model involved the use of light microscopic images of PSCs captured at different intervals after the induction process, including mouse-embryonic cells being induced to epiblast-like cells. (Waisman et al., 2019). Notably, the results demonstrated CNN's remarkable capability to distinguish between differentiated and undifferentiated cells with 99% accuracy.

Importantly, AI can leverage information from separate studies, extensive datasets, and stem cell biobanks to create models that predict the outcomes of stem cell therapy for specific disease states. These models can potentially be applied to enhance stem cell proliferation, optimize their functions in the host environment, and/or predict the most effective population(s) for individuals with specific phenotypes of cardiomyopathy (Capponi and Daniels, 2023). Thus, integrating AI/ML into stem cell research holds great promise for advancing precursor cell-based therapy for HF by: 1) facilitating our understanding of stem cell biology within specific cardiac disease contexts at a systems level; 2) improving the good manufacturing practice for clinical-grade cellular products; and 3) establishing personalized therapeutic prediction models for individual patients (Figure 1).

Discussion

A considerable number of recent clinical trials in stem cell therapy for HF have demonstrated its promise and substantially increased our understanding of the behaviors and working mechanisms of stem/progenitor cells in patients (Table 1). (Hamshere et al., 2015; Martino et al., 2015; Perin et al., 2015; Choudry et al., 2016; Noiseux et al., 2016; Patel et al., 2016; Bartolucci et al., 2017; Butler et al., 2017; Choudhury et al., 2017; Florea et al., 2017; Gwizdala et al., 2017; Hare et al., 2017; Steinhoff et al., 2017; Teerlink et al., 2017; Xiao et al., 2017; Bassetti et al., 2018; Vrtovec et al., 2018; Yau et al., 2019; Bolli et al., 2020; He et al., 2020; Makkar et al., 2020; Mathiasen et al., 2020; Ulus et al., 2020; Bolli et al., 2021; Qayyum et al., 2023a; Qayyum et al., 2023b; Perin et al., 2023) In the next phase of clinical stem cell research, it is critical to address the outcome discrepancy between preclinical and clinical studies and expand the scope of stem cell-based therapy to other forms of cardiomyopathy, such as chemotherapy- or arrhythmia-induced cardiomyopathy. Exploiting the power of AI/ML and computational tools will facilitate our understanding of the benefits and limitations of stem cell therapy and provide a systems perspective for properly applying stem cell therapeutics in the context of precision and personalized medicine.

Author contributions

MC: Investigation, Resources, Software, Visualization, Writing–original draft, Writing–review and editing. JZ: Investigation, Writing–original draft, Writing–review and editing. RR: Conceptualization, Investigation, Writing–original draft, Writing–review and editing. WC: Conceptualization, Funding acquisition, Investigation, Project administration, Resources, Supervision, Visualization, Writing–original draft, Writing–review and editing.

Funding

The author(s) declare financial support was received for the research, authorship, and/or publication of this article. This work was supported by the U.S. Department of Defense (W81XWH2110089 to WC), the American Heart Association Career Development Award (855260 to WC), and the University of South Dakota Sanford School of Medicine (Startup Fund to WC).

Conflict of interest

The authors declare that the research was conducted in the absence of any commercial or financial relationships that could be construed as a potential conflict of interest.

Publisher's note

All claims expressed in this article are solely those of the authors and do not necessarily represent those of their affiliated organizations, or those of the publisher, the editors and the reviewers. Any product that may be evaluated in this article, or claim that may be made by its manufacturer, is not guaranteed or endorsed by the publisher.

References

Abdalmula, A., Dooley, L. M., Kaufman, C., Washington, E. A., House, J. V., Blacklaws, B. A., et al. (2017). Immunoselected STRO-3+ mesenchymal precursor cells reduce inflammation and improve clinical outcomes in a large animal model of monoarthritis. *Stem Cell. Res. Ther.* 8 (1), 22. doi:10.1186/s13287-016-0460-7

Adlung, L., Cohen, Y., Mor, U., and Elinav, E. (2021). Machine learning in clinical decision making. *Med* 2 (6), 642–665. doi:10.1016/j.medj.2021.04.006

Alfaro, M. P., Pagni, M., Vincent, A., Atkinson, J., Hill, M. F., Cates, J., et al. (2008). The Wnt modulator sFRP2 enhances mesenchymal stem cell engraftment, granulation tissue formation and myocardial repair. *Proc. Natl. Acad. Sci. U. S. A.* 105 (47), 18366–18371. doi:10.1073/pnas.0803437105

Amado, L. C., Saliaris, A. P., Schuleri, K. H., St John, M., Xie, J. S., Cattaneo, S., et al. (2005). Cardiac repair with intramyocardial injection of allogeneic mesenchymal stem cells after myocardial infarction. *Proc. Natl. Acad. Sci. U. S. A.* 102 (32), 11474–11479. doi:10.1073/pnas.0504388102

Andreeva, O. E., Shchegolev, Y. Y., Scherbakov, A. M., Mikhaevich, E. I., Sorokin, D. V., Gudkova, M. V., et al. (2021). Secretion of mutant DNA and mRNA by the exosomes of breast cancer cells. *Molecules* 26 (9), 2499. doi:10.3390/molecules26092499

Annaratone, L., De Palma, G., Bonizzi, G., Sapino, A., Botti, G., Berrino, E., et al. (2021). Basic principles of biobanking: from biological samples to precision medicine for patients. *Virchows Arch.* 479 (2), 233–246. doi:10.1007/s00428-021-03151-0

Anokye-Danso, F., Trivedi, C. M., Juhr, D., Gupta, M., Cui, Z., Tian, Y., et al. (2011). Highly efficient miRNA-mediated reprogramming of mouse and human somatic cells to pluripotency. *Cell. Stem Cell.* 8 (4), 376–388. doi:10.1016/j.stem.2011.03.001

Ashley, E. A. (2016). Towards precision medicine. *Nat. Rev. Genet.* 17 (9), 507–522. doi:10.1038/nrg.2016.86

Attia, Z. I., Noseworthy, P. A., Lopez-Jimenez, F., Asirvatham, S. J., Deshmukh, A. J., Gersh, B. J., et al. (2019). An artificial intelligence-enabled ECG algorithm for the identification of patients with atrial fibrillation during sinus rhythm: a retrospective analysis of outcome prediction. *Lancet* 394 (10201), 861–867. doi:10.1016/S0140-6736(19)31721-0

Azar, J., Bahmad, H. F., Daher, D., Moubarak, M. M., Hadadeh, O., Monzer, A., et al. (2021). The use of stem cell-derived organoids in disease modeling: an update. *Int. J. Mol. Sci.* 22 (14), 7667. doi:10.3390/ijms22147667

Balbi, C., and Vassalli, G. (2020). Exosomes: beyond stem cells for cardiac protection and repair. *STEM CELLS* 38 (11), 1387–1399. doi:10.1002/stem.3261

Bartolucci, J., Verdugo, F. J., González, P. L., Larrea, R. E., Abarzua, E., Goset, C., et al. (2017). Safety and efficacy of the intravenous infusion of umbilical cord mesenchymal stem cells in patients with heart failure: a phase 1/2 randomized controlled trial (rimecard trial [randomized clinical trial of intravenous infusion umbilical cord mesenchymal stem cells on cardiopathy]). *Circ. Res.* 121 (10), 1192–1204. doi:10.1161/CIRCRESAHA.117.310712

Bassetti, B., Carbucicchio, C., Catto, V., Gambini, E., Rurali, E., Bestetti, A., et al. (2018). Linking cell function with perfusion: insights from the transcatheter delivery of bone marrow-derived CD133+ cells in ischemic refractory cardiomyopathy trial (RECARDIO). *Stem Cell. Res. Ther.* 9 (1), 235. doi:10.1186/s13287-018-0969-z

Bobis-Wozowicz, S., Kmiotek, K., Sekula, M., Kedracka-Krok, S., Kamycka, E., Adamiak, M., et al. (2015). Human induced pluripotent stem cell-derived microvesicles transmit RNAs and proteins to recipient mature heart cells modulating cell fate and behavior. *Stem Cells* 33 (9), 2748–2761. doi:10.1002/stem.2078

Bolli, R., Mitrani, R. D., Hare, J. M., Pepine, C. J., Perin, E. C., Willerson, J. T., et al. (2021). A Phase II study of autologous mesenchymal stromal cells and c-kit positive cardiac cells, alone or in combination, in patients with ischaemic heart failure: the CCTRN CONCERT-HF trial. *Eur. J. Heart Fail* 23 (4), 661–674. doi:10.1002/ejhf.2178

Bolli, R., Perin, E. C., Willerson, J. T., Yang, P. C., Traverse, J. H., Henry, T. D., et al. (2020). Allogeneic mesenchymal cell therapy in anthracycline-induced cardiomyopathy heart failure patients: the CCTRN SENECA trial. *JACC CardioOncol* 2 (4), 581–595. doi:10.1016/j.jaccao.2020.09.001

Bolli, R., Solankhi, M., Tang, X. L., and Kahlon, A. (2022). Cell therapy in patients with heart failure: a comprehensive review and emerging concepts. *Cardiovasc Res.* 118 (4), 951–976. doi:10.1093/cvr/cvab135

Bolli, R., and Tang, X. L. (2022). The sad plight of cell therapy for heart failure: causes and consequences. *J. Cardiovasc Aging* 2, 16. doi:10.20517/jca.2022.02

Bonnet, G., Coutance, G., Aubert, O., Waldmann, V., Raynaud, M., Asselin, A., et al. (2023). Sudden cardiac death after heart transplantation: a population-based study. *EP Eur.* 25 (5), euad126. doi:10.1093/europace/euad126

Borow, K. M., Yaroshinsky, A., Greenberg, B., and Perin, E. C. (2019). Phase 3 DREAM-HF trial of mesenchymal precursor cells in chronic heart failure. *Circ. Res.* 125 (3), 265–281. doi:10.1161/CIRCRESAHA.119.314951

Butler, J., Epstein, S. E., Greene, S. J., Quyyumi, A. A., Sikora, S., Kim, R. J., et al. (2017). Intravenous allogeneic mesenchymal stem cells for nonischemic cardiomyopathy: safety and efficacy results of a phase II-A randomized trial. *Circ. Res.* 120 (2), 332–340. doi:10.1161/CIRCRESAHA.116.309717

Capponi, S., and Daniels, K. G. (2023). Harnessing the power of artificial intelligence to advance cell therapy. *Immunol. Rev.* 320, 147–165. n/a(n/a). doi:10.1111/imr.13236

Chaudhry, S. P., DeVore, A. D., Vidula, H., Nassif, M., Mudy, K., Birati, E. Y., et al. (2022). Left ventricular assist devices: a primer for the general cardiologist. *J. Am. Heart Assoc.* 11 (24), e027251. doi:10.1161/JAHA.122.027251

Chen, C.-W., Montelatici, E., Crisan, M., Corselli, M., Huard, J., Lazzari, L., et al. (2009). Perivascular multi-lineage progenitor cells in human organs: regenerative units, cytokine sources or both? *Cytokine and Growth Factor Rev.* 20 (5-6), 429–434. doi:10.1016/j.cytogfr.2009.10.014

Chen, C.-W., Okada, M., Proto, J. D., Gao, X., Sekiya, N., Beckman, S. A., et al. (2013). Human pericytes for ischemic heart repair. *STEM CELLS* 31 (2), 305–316. doi:10.1002/stem.1285

Chen, I. Y., Matsa, E., and Wu, J. C. (2016). Induced pluripotent stem cells: at the heart of cardiovascular precision medicine. *Nat. Rev. Cardiol.* 13 (6), 333–349. doi:10.1038/nrcardio.2016.36

Chen, W. C. W., Baily, J. E., Corselli, M., Díaz, M. E., Sun, B., Xiang, G., et al. (2015). Human myocardial pericytes: multipotent mesodermal precursors exhibiting cardiac specificity. *STEM CELLS* 33 (2), 557–573. doi:10.1002/stem.1868

Chimenti, I., Smith, R. R., Li, T. S., Gerstenblith, G., Messina, E., Giacomello, A., et al. (2010). Relative roles of direct regeneration versus paracrine effects of human cardiosphere-derived cells transplanted into infarcted mice. *Circ. Res.* 106 (5), 971–980. doi:10.1161/CIRCRESAHA.109.210682

Choudhury, T., Mozid, A., Hamshere, S., Yeo, C., Pellaton, C., Arnous, S., et al. (2017). An exploratory randomized control study of combination cytokine and adult autologous bone marrow progenitor cell administration in patients with ischaemic cardiomyopathy: the REGENERATE-IHD clinical trial. *Eur. J. Heart Fail* 19 (1), 138–147. doi:10.1002/ejhf.676

Choudry, F., Hamshere, S., Saunders, N., Veerapen, J., Bavnbek, K., Knight, C., et al. (2016). A randomized double-blind control study of early intra-coronary autologous bone marrow cell infusion in acute myocardial infarction: the REGENERATE-AMI clinical trial. *Eur. Heart J.* 37 (3), 256–263. doi:10.1093/eurheartj/ehv493

Colvin, M., Smith, J. M., Ahn, Y., Skeans, M. A., Messick, E., Bradbrook, K., et al. (2022). OPTN/SRTR 2020 annual data report: heart. *Am. J. Transpl.* 22 (Suppl. 2), 350–437. doi:10.1111/ajt.16977

Costanzo, M. R., Mills, R. M., and Wynne, J. (2008). Characteristics of "stage D" heart failure: insights from the acute decompensated heart failure national registry longitudinal module (ADHERE LM). *Am. Heart J.* 155 (2), 339–347. doi:10.1016/j.ahj.2007.10.020

Dassanayaka, S., and Jones, S. P. (2015). Recent developments in heart failure. *Circulation Res.* 117 (7), e58–e63. doi:10.1161/CIRCRESAHA.115.305765

Delpierre, C., and Lefèvre, T. (2023). Precision and personalized medicine: what their current definition says and silences about the model of health they promote. Implication for the development of personalized health. *Front. Sociol.* 8, 1112159. doi:10.3389/fsoc.2023.1112159

Dominici, M., Le Blanc, K., Mueller, I., Slaper-Cortenbach, I., Marini, F., Krause, D., et al. (2006). Minimal criteria for defining multipotent mesenchymal stromal cells. The International Society for Cellular Therapy position statement. *Cytotherapy* 8 (4), 315–317. doi:10.1080/14653240600855905

Duong, A., Parmar, G., Kirkham, A. M., Burger, D., and Allan, D. S. (2023). Registered clinical trials investigating treatment with cell-derived extracellular vesicles: a scoping review. *Cytotherapy* 25 (9), 939–945. doi:10.1016/j.jcyt.2023.04.007

Evans, M. J., and Kaufman, M. H. (1981). Establishment in culture of pluripotential cells from mouse embryos. *Nature* 292 (5819), 154–156. doi:10.1038/292154a0

Fischbacher, B., Hedaya, S., Hartley, B. J., Wang, Z., Lallos, G., Hutson, D., et al. (2021). Modular deep learning enables automated identification of monoclonal cell lines. *Nat. Mach. Intell.* 3 (7), 632–640. doi:10.1038/s42256-021-00354-7

Florea, V., Rieger, A. C., DiFede, D. L., El-Khorazaty, J., Natsumeda, M., Banerjee, M. N., et al. (2017). Dose comparison study of allogeneic mesenchymal stem cells in patients with ischemic cardiomyopathy (the TRIDENT study). *Circ. Res.* 121 (11), 1279–1290. doi:10.1161/CIRCRESAHA.117.311827

Gallet, R., Dawkins, J., Valle, J., Simsolo, E., de Couto, G., Middleton, R., et al. (2017). Exosomes secreted by cardiosphere-derived cells reduce scarring, attenuate adverse remodelling, and improve function in acute and chronic porcine myocardial infarction. *Eur. Heart J.* 38 (3), 201–211. doi:10.1093/eurheartj/ehw240

Gambini, E., Pesce, M., Persico, L., Bassetti, B., Gambini, A., Alamanni, F., et al. (2012). Patient profile modulates cardiac c-kit(+) progenitor cell availability and amplification potential. *Transl. Res.* 160 (5), 363–373. doi:10.1016/j.trsl.2012.05.009

Gao, L., Wang, L., Wei, Y., Krishnamurthy, P., Walcott, G. P., Menasché, P., et al. (2020). Exosomes secreted by hiPSC-derived cardiac cells improve recovery from myocardial infarction in swine. *Sci. Transl. Med.* 12 (561), eaay1318. doi:10.1126/scitranslmed.aay1318

Gnecchi, M., He, H., Liang, O. D., Melo, L. G., Morello, F., Mu, H., et al. (2005). Paracrine action accounts for marked protection of ischemic heart by Akt-modified mesenchymal stem cells. *Nat. Med.* 11 (4), 367–368. doi:10.1038/nm0405-367

Golpanian, S., Schulman, I. H., Ebert, R. F., Heldman, A. W., DiFede, D. L., Yang, P. C., et al. (2015). Concise review: review and perspective of cell dosage and routes of administration from preclinical and clinical studies of stem cell therapy for heart disease. *Stem Cells Transl. Med.* 5 (2), 186–191. doi:10.5966/sctm.2015-0101

Guan, B. X., Bhanu, B., Theagarajan, R., Liu, H., Talbot, P., and Weng, N. (2021). Human embryonic stem cell classification: random network with autoencoded feature extractor. *J. Biomed. Opt.* 26 (5), 052913. doi:10.1117/1.JBO.26.5.052913

Guo, Y., Yu, Y., Hu, S., Chen, Y., and Shen, Z. (2020). The therapeutic potential of mesenchymal stem cells for cardiovascular diseases. *Cell. Death Dis.* 11 (5), 349. doi:10.1038/s41419-020-2542-9

Gwizdala, A., Rozwadowska, N., Kolanowski, T. J., Malcher, A., Cieplucha, A., Perek, B., et al. (2017). Safety, feasibility and effectiveness of first in-human administration of muscle-derived stem/progenitor cells modified with connexin-43 gene for treatment of advanced chronic heart failure. *Eur. J. Heart Fail* 19 (1), 148–157. doi:10.1002/ejhf.700

Halvorsen, Y. C., Wilkison, W. O., and Gimble, J. M. (2000). Adipose-derived stromal cells--their utility and potential in bone formation. *Int. J. Obes. Relat. Metab. Disord.* 24 (Suppl. 4), S41–S44. doi:10.1038/sj.ijo.0801503

Hamshere, S., Arnous, S., Choudhury, T., Choudry, F., Mozid, A., Yeo, C., et al. (2015). Randomized trial of combination cytokine and adult autologous bone marrow progenitor cell administration in patients with non-ischaemic dilated cardiomyopathy: the REGENERATE-DCM clinical trial. *Eur. Heart J.* 36 (44), 3061–3069. doi:10.1093/eurheartj/ehv390

Hare, J. M., DiFede, D. L., Rieger, A. C., Florea, V., Landin, A. M., El-Khorazaty, J., et al. (2017). Randomized comparison of allogeneic versus autologous mesenchymal stem cells for nonischemic dilated cardiomyopathy: POSEIDON-DCM trial. *J. Am. Coll. Cardiol.* 69 (5), 526–537. doi:10.1016/j.jacc.2016.11.009

Hare, J. M., Fishman, J. E., Gerstenblith, G., DiFede Velazquez, D. L., Zambrano, J. P., Suncion, V. Y., et al. (2012). Comparison of allogeneic vs autologous bone marrow–derived mesenchymal stem cells delivered by transendocardial injection in patients with ischemic cardiomyopathy: the POSEIDON randomized trial. *Jama* 308 (22), 2369–2379. doi:10.1001/jama.2012.25321

Hasenfuss, G. (1998). Animal models of human cardiovascular disease, heart failure and hypertrophy. *Cardiovasc. Res.* 39 (1), 60–76. doi:10.1016/s0008-6363(98)00110-2

Haug, C. J., and Drazen, J. M. (2023). Artificial intelligence and machine learning in clinical medicine, 2023. *N. Engl. J. Med.* 388 (13), 1201–1208. doi:10.1056/NEJMra2302038

Haynesworth, S. E., Goshima, J., Goldberg, V. M., and Caplan, A. I. (1992). Characterization of cells with osteogenic potential from human marrow. *Bone* 13 (1), 81–88. doi:10.1016/8756-3282(92)90364-3

He, X., Wang, Q., Zhao, Y., Zhang, H., Wang, B., Pan, J., et al. (2020). Effect of intramyocardial grafting collagen scaffold with mesenchymal stromal cells in patients with chronic ischemic heart disease: a randomized clinical trial. *JAMA Netw. Open* 3 (9), e2016236. doi:10.1001/jamanetworkopen.2020.16236

Heidenreich, P. A., Bozkurt, B., Aguilar, D., Allen, L. A., Byun, J. J., Colvin, M. M., et al. (2022). 2022 AHA/ACC/HFSA guideline for the management of heart failure: a report of the American college of cardiology/American heart association joint committee on clinical practice guidelines. *Circulation* 145 (18), e895–e1032. doi:10.1161/CIR.0000000000001063

Heldman, A. W., DiFede, D. L., Fishman, J. E., Zambrano, J. P., Trachtenberg, B. H., Karantalis, V., et al. (2014). Transendocardial mesenchymal stem cells and mononuclear bone marrow cells for ischemic cardiomyopathy: the TAC-HFT randomized trial. *Jama* 311 (1), 62–73. doi:10.1001/jama.2013.282909

Hou, D., Youssef, E. A., Brinton, T. J., Zhang, P., Rogers, P., Price, E. T., et al. (2005). Radiolabeled cell distribution after intramyocardial, intracoronary, and interstitial retrograde coronary venous delivery: implications for current clinical trials. *Circulation* 112 (9 Suppl. l), I150–I156. doi:10.1161/CIRCULATIONAHA.104.526749

Hsueh, Y.-C., Pratt, R. E., Dzau, V. J., and Hodgkinson, C. P. (2023). Novel method of differentiating human induced pluripotent stem cells to mature cardiomyocytes via Sfrp2. *Sci. Rep.* 13 (1), 3920. doi:10.1038/s41598-023-31144-3

Hu, J., Xu, J., Yu, M., Gao, Y., Liu, R., Zhou, H., et al. (2020). An integrated prognosis model of pharmacogenomic gene signature and clinical information for diffuse large B-cell lymphoma patients following CHOP-like chemotherapy. *J. Transl. Med.* 18 (1), 144. doi:10.1186/s12967-020-02311-1

Ibrahim, A. G., Cheng, K., and Marbán, E. (2014). Exosomes as critical agents of cardiac regeneration triggered by cell therapy. *Stem Cell. Rep.* 2 (5), 606–619. doi:10.1016/j.stemcr.2014.04.006

Jackson, K. A., Majka, S. M., Wang, H., Pocius, J., Hartley, C. J., Majesky, M. W., et al. (2001). Regeneration of ischemic cardiac muscle and vascular endothelium by adult stem cells. *J. Clin. Investig.* 107 (11), 1395–1402. doi:10.1172/JCI12150

Jain, V., Minhas, A. M. K., Morris, A. A., Greene, S. J., Pandey, A., Khan, S. S., et al. (2022). Demographic and regional trends of heart failure–related mortality in young adults in the US, 1999-2019. *JAMA Cardiol.* 7 (9), 900–904. doi:10.1001/jamacardio.2022.2213

Jiang, X., Chen, Y., Liu, X., Ye, L., Yu, M., Shen, Z., et al. (2021). Uncovering inherited cardiomyopathy with human induced pluripotent stem cells. *Front. Cell. Dev. Biol.* 9, 672039. doi:10.3389/fcell.2021.672039

Johnston, P. V., Duckers, H. J., Raval, A. N., Cook, T. D., and Pepine, C. J. (2018). Not all stem cells are created equal. *Circulation Res.* 123 (8), 944–946. doi:10.1161/CIRCRESAHA.118.313425

Juhola, M., Penttinen, K., Joutsijoki, H., and Aalto-Setälä, K. (2021). Analysis of drug effects on iPSC cardiomyocytes with machine learning. *Ann. Biomed. Eng.* 49 (1), 129–138. doi:10.1007/s10439-020-02521-0

Karantalis, V., and Hare, J. M. (2015). Use of mesenchymal stem cells for therapy of cardiac disease. *Circulation Res.* 116 (8), 1413–1430. doi:10.1161/CIRCRESAHA.116.303614

Kim, M., Namkung, Y., Hyun, D., and Hong, S. (2023). Prediction of stem cell state using cell image-based deep learning. *Adv. Intell. Syst.* 5 (7), 2300017. doi:10.1002/aisy.202370031

Kim, M., Namkung, Y., Hyun, D., and Hong, S. (2022). Prediction of stem cell state using cell image-based deep learning. *Adv. Intell. Syst.* 1, 2300017. doi:10.1002/aisy.202300017

Kocher, A. A., Schuster, M. D., Szabolcs, M. J., Takuma, S., Burkhoff, D., Wang, J., et al. (2001). Neovascularization of ischemic myocardium by human bone-marrow-derived angioblasts prevents cardiomyocyte apoptosis, reduces remodeling and improves cardiac function. *Nat. Med.* 7 (4), 430–436. doi:10.1038/86498

Krajcer, Z. (2022). Artificial intelligence in cardiovascular medicine: historical overview, current status, and future directions. *Tex Heart Inst. J.* 49 (2), e207527. doi:10.14503/THIJ-20-7527

Kuchina, A., Espinar, L., Garcia-Ojalvo, J., and Süel, G. M. (2011). Reversible and noisy progression towards a commitment point enables adaptable and reliable cellular decision-making. *PLoS Comput. Biol.* 7 (11), e1002273. doi:10.1371/journal.pcbi.1002273

Li, H., Wang, L., Ma, T., Liu, Z., and Gao, L. (2023). Exosomes secreted by endothelial cells derived from human induced pluripotent stem cells improve recovery from myocardial infarction in mice. *Stem Cell. Res. Ther.* 14 (1), 278. doi:10.1186/s13287-023-03462-w

Li, L., Wan, Z., Wang, R., Zhao, Y., Ye, Y., Yang, P., et al. (2022). Generation of high-performance human cardiomyocytes and engineered heart tissues from extended pluripotent stem cells. *Cell. Discov.* 8 (1), 105. doi:10.1038/s41421-022-00446-7

Liao, Y., Zhu, L., and Wang, Y. (2021). Maturation of stem cell-derived cardiomyocytes: foe in translation medicine. *Int. J. Stem Cells* 14 (4), 366–385. doi:10.15283/ijsc21077

Liesveld, J. L., Sharma, N., and Aljitawi, O. S. (2020). Stem cell homing: from physiology to therapeutics. *STEM CELLS* 38 (10), 1241–1253. doi:10.1002/stem.3242

Lightner, A. L., and Chan, T. (2021). Precision regenerative medicine. *Stem Cell. Res. Ther.* 12 (1), 39. doi:10.1186/s13287-020-02092-w

Lin, S., Lin, Y., Nery, J. R., Urich, M. A., Breschi, A., Davis, C. A., et al. (2014). Comparison of the transcriptional landscapes between human and mouse tissues. *Proc. Natl. Acad. Sci.* 111 (48), 17224–17229. doi:10.1073/pnas.1413624111

Liu, Z., Lin, G., Yan, Z., Li, L., Wu, X., Shi, J., et al. (2022). Predictive mutation signature of immunotherapy benefits in NSCLC based on machine learning algorithms. *Front. Immunol.* 13, 989275. doi:10.3389/fimmu.2022.989275

Mabotuwana, N. S., Rech, L., Lim, J., Hardy, S. A., Murtha, L. A., Rainer, P. P., et al. (2022). Paracrine factors released by stem cells of mesenchymal origin and their effects in cardiovascular disease: a systematic review of pre-clinical studies. *Stem Cell. Rev. Rep.* 18 (8), 2606–2628. doi:10.1007/s12015-022-10429-6

Maddah, M., and Loewke, K. (2014). Automated, non-invasive characterization of stem cell-derived cardiomyocytes from phase-contrast microscopy. *Med. Image Comput. Comput. Assist. Interv.* 17 (Pt 1), 57–64. doi:10.1007/978-3-319-10404-1_8

Makkar, R. R., Kereiakes, D. J., Aguirre, F., Kowalchuk, G., Chakravarty, T., Malliaras, K., et al. (2020). Intracoronary ALLogeneic heart STem cells to Achieve myocardial Regeneration (ALLSTAR): a randomized, placebo-controlled, double-blinded trial. *Eur. Heart J.* 41 (36), 3451–3458. doi:10.1093/eurheartj/ehaa541

Mandai, M., Watanabe, A., Kurimoto, Y., Hirami, Y., Morinaga, C., Daimon, T., et al. (2017). Autologous induced stem-cell-derived retinal cells for macular degeneration. *N. Engl. J. Med.* 376 (11), 1038–1046. doi:10.1056/NEJMoa1608368

Marbán, E. (2018). The secret life of exosomes: what bees can teach us about next-generation therapeutics. *J. Am. Coll. Cardiol.* 71 (2), 193–200. doi:10.1016/j.jacc.2017.11.013

Martello, G., and Smith, A. (2014). The nature of embryonic stem cells. *Annu. Rev. Cell. Dev. Biol.* 30, 647–675. doi:10.1146/annurev-cellbio-100913-013116

Martino, H., Brofman, P., Greco, O., Bueno, R., Bodanese, L., Clausell, N., et al. (2015). Multicentre, randomized, double-blind trial of intracoronary autologous mononuclear bone marrow cell injection in non-ischaemic dilated cardiomyopathy (the dilated cardiomyopathy arm of the MiHeart study). *Eur. Heart J. NICM2015* 36 (42), 2898–2904. doi:10.1093/eurheartj/ehv477

Mathiasen, A. B., Qayyum, A. A., Jørgensen, E., Helqvist, S., Kofoed, K. F., Haack-Sørensen, M., et al. (2020). Bone marrow-derived mesenchymal stromal cell treatment in patients with ischaemic heart failure: final 4-year follow-up of the MSC-HF trial. *Eur. J. Heart Fail* 22 (5), 884–892. doi:10.1002/ejhf.1700

Mathur, A., Sim, D. S., Choudry, F., Veerapen, J., Colicchia, M., Turlejski, T., et al. (2022). Five-year follow-up of intracoronary autologous cell therapy in acute myocardial infarction: the REGENERATE-AMI trial. *Esc. Heart Fail* 9 (2), 1152–1159. doi:10.1002/ehf2.13786

Melo, F. R., Bressan, R. B., Forner, S., Martini, A. C., Rode, M., Delben, P. B., et al. (2017). Transplantation of human skin-derived mesenchymal stromal cells improves locomotor recovery after spinal cord injury in rats. *Cell. Mol. Neurobiol.* 37 (5), 941–947. doi:10.1007/s10571-016-0414-8

Messina, E., De Angelis, L., Frati, G., Morrone, S., Chimenti, S., Fiordaliso, F., et al. (2004). Isolation and expansion of adult cardiac stem cells from human and murine heart. *Circ. Res.* 95 (9), 911–921. doi:10.1161/01.RES.0000147315.71699.51

Miura, M., Gronthos, S., Zhao, M., Lu, B., Fisher, L. W., Robey, P. G., et al. (2003). SHED: stem cells from human exfoliated deciduous teeth. *Proc. Natl. Acad. Sci. U. S. A.* 100 (10), 5807–5812. doi:10.1073/pnas.0937635100

Moradi, S., Mahdizadeh, H., Šarić, T., Kim, J., Harati, J., Shahsavarani, H., et al. (2019). Research and therapy with induced pluripotent stem cells (iPSCs): social, legal, and ethical considerations. *Stem Cell. Res. Ther.* 10 (1), 341. doi:10.1186/s13287-019-1455-y

Mota, S. M., Rogers, R. E., Haskell, A. W., McNeill, E. P., Kaunas, R., Gregory, C. A., et al. (2021). Automated mesenchymal stem cell segmentation and machine learning-based phenotype classification using morphometric and textural analysis. *J. Med. Imaging (Bellingham)* 8 (1), 014503. doi:10.1117/1.JMI.8.1.014503

Musunuru, K., Sheikh, F., Gupta, R. M., Houser, S. R., Maher, K. O., Milan, D. J., et al. (2018). Induced pluripotent stem cells for cardiovascular disease modeling and precision medicine: a scientific statement from the American heart association.

Circulation Genomic Precis. Med. 11 (1), e000043. doi:10.1161/HCG.0000000000000043

Nishino, K., Takasawa, K., Okamura, K., Arai, Y., Sekiya, A., Akutsu, H., et al. (2021). Identification of an epigenetic signature in human induced pluripotent stem cells using a linear machine learning model. *Hum. Cell.* 34 (1), 99–110. doi:10.1007/s13577-020-00446-3

Noiseux, N., Mansour, S., Weisel, R., Stevens, L. M., Der Sarkissian, S., Tsang, K., et al. (2016). The IMPACT-CABG trial: a multicenter, randomized clinical trial of CD133+ stem cell therapy during coronary artery bypass grafting for ischemic cardiomyopathy. *J. Thorac. Cardiovasc Surg.* 152 (6), 1582–1588. doi:10.1016/j.jtcvs.2016.07.067

Okita, K., Ichisaka, T., and Yamanaka, S. (2007). Generation of germline-competent induced pluripotent stem cells. *Nature* 448 (7151), 313–317. doi:10.1038/nature05934

Orlic, D., Kajstura, J., Chimenti, S., Jakoniuk, I., Anderson, S. M., Li, B., et al. (2001). Bone marrow cells regenerate infarcted myocardium. *Nature* 410 (6829), 701–705. doi:10.1038/35070587

Ostovaneh, M. R., Makkar, R. R., Ambale-Venkatesh, B., Ascheim, D., Chakravarty, T., Henry, T. D., et al. (2021). Effect of cardiosphere-derived cells on segmental myocardial function after myocardial infarction: ALLSTAR randomised clinical trial. *Open Heart* 8 (2), e001614. doi:10.1136/openhrt-2021-001614

Patel, A. N., Henry, T. D., Quyyumi, A. A., Schaer, G. L., Anderson, R. D., Toma, C., et al. (2016). Ixmyelocel-T for patients with ischaemic heart failure: a prospective randomised double-blind trial. *Lancet* 387 (10036), 2412–2421. doi:10.1016/S0140-6736(16)30137-4

Patel, S. A., King, C. C., Lim, P. K., Habiba, U., Dave, M., Porecha, R., et al. (2010). Personalizing stem cell research and therapy: the arduous road ahead or missed opportunity? *Curr. Pharmacogenomics Person. Med.* 8 (1), 25–36. doi:10.2174/1875692111008010025

Perin, E. C., Borow, K. M., Henry, T. D., Mendelsohn, F. O., Miller, L. W., Swiggum, E., et al. (2023). Randomized trial of targeted transendocardial mesenchymal precursor cell therapy in patients with heart failure. *J. Am. Coll. Cardiol.* 81 (9), 849–863. doi:10.1016/j.jacc.2022.11.061

Perin, E. C., Borow, K. M., Silva, G. V., DeMaria, A. N., Marroquin, O. C., Huang, P. P., et al. (2015). A phase II dose-escalation study of allogeneic mesenchymal precursor cells in patients with ischemic or nonischemic heart failure. *Circ. Res.* 117 (6), 576–584. doi:10.1161/CIRCRESAHA.115.306332

Perin, E. C., Willerson, J. T., Pepine, C. J., Henry, T. D., Ellis, S. G., Zhao, D. X. M., et al. (2012). Effect of transendocardial delivery of autologous bone marrow mononuclear cells on functional capacity, left ventricular function, and perfusion in chronic heart failure: the FOCUS-CCTRN trial. *Jama* 307 (16), 1717–1726. doi:10.1001/jama.2012.418

Pittenger, M. F., Discher, D. E., Péault, B. M., Phinney, D. G., Hare, J. M., and Caplan, A. I. (2019). Mesenchymal stem cell perspective: cell biology to clinical progress. *npj Regen. Med.* 4 (1), 22. doi:10.1038/s41536-019-0083-6

Pittenger, M. F., Mackay, A. M., Beck, S. C., Jaiswal, R. K., Douglas, R., Mosca, J. D., et al. (1999). Multilineage potential of adult human mesenchymal stem cells. *Science* 284 (5411), 143–147. doi:10.1126/science.284.5411.143

Pizzute, T., Lynch, K., and Pei, M. (2015). Impact of tissue-specific stem cells on lineage-specific differentiation: a focus on the musculoskeletal system. *Stem Cell. Rev. Rep.* 11 (1), 119–132. doi:10.1007/s12015-014-9546-8

Qayyum, A. A., Mouridsen, M., Nilsson, B., Gustafsson, I., Schou, M., Nielsen, O. W., et al. (2023a). Danish phase II trial using adipose tissue derived mesenchymal stromal cells for patients with ischaemic heart failure. *Esc. Heart Fail* 10 (2), 1170–1183. doi:10.1002/ehf2.14281

Qayyum, A. A., van Klarenbosch, B., Frljak, S., Cerar, A., Poglajen, G., Traxler-Weidenauer, D., et al. (2023b). Effect of allogeneic adipose tissue-derived mesenchymal stromal cell treatment in chronic ischaemic heart failure with reduced ejection fraction - the SCIENCE trial. *Eur. J. Heart Fail* 25 (4), 576–587. doi:10.1002/ejhf.2772

Qi, C. M., Ma, G. S., Liu, N. F., Shen, C. x., Chen, Z., Liu, X. j., et al. (2008). Transplantation of magnetically labeled mesenchymal stem cells improves cardiac function in a swine myocardial infarction model. *Chin. Med. J. Engl.* 121 (6), 544–550. doi:10.1097/00029330-200803020-00016

Qian, L., Huang, Y., Spencer, C. I., Foley, A., Vedantham, V., Liu, L., et al. (2012). *In vivo* reprogramming of murine cardiac fibroblasts into induced cardiomyocytes. *Nature* 485 (7400), 593–598. doi:10.1038/nature11044

Qiu, S., Joshi, P. S., Miller, M. I., Xue, C., Zhou, X., Karjadi, C., et al. (2020). Development and validation of an interpretable deep learning framework for Alzheimer's disease classification. *Brain* 143 (6), 1920–1933. doi:10.1093/brain/awaa137

Raval, A. N., Johnston, P. V., Duckers, H. J., Cook, T. D., Traverse, J. H., Altman, P. A., et al. (2021). Point of care, bone marrow mononuclear cell therapy in ischemic heart failure patients personalized for cell potency: 12-month feasibility results from CardiAMP heart failure roll-in cohort. *Int. J. Cardiol.* 326, 131–138. doi:10.1016/j.ijcard.2020.10.043

Rezaie, J., Feghhi, M., and Etemadi, T. (2022). A review on exosomes application in clinical trials: perspective, questions, and challenges. *Cell. Commun. Signal.* 20 (1), 145. doi:10.1186/s12964-022-00959-4

Rheault-Henry, M., White, I., Grover, D., and Atoui, R. (2021). Stem cell therapy for heart failure: medical breakthrough, or dead end? *World J. Stem Cells* 13 (4), 236–259. doi:10.4252/wjsc.v13.i4.236

Riva, P., Battaglia, C., and Venturin, M. (2019). Emerging role of genetic alterations affecting exosome biology in neurodegenerative diseases. *Int. J. Mol. Sci.* 20 (17), 4113. doi:10.3390/ijms20174113

Savarese, G., Becher, P. M., Lund, L. H., Seferovic, P., Rosano, G. M. C., and Coats, A. J. S. (2022). Global burden of heart failure: a comprehensive and updated review of epidemiology. *Cardiovasc. Res.* 118 (17), 3272–3287. doi:10.1093/cvr/cvac013

Schweitzer, J. S., Song, B., Herrington, T. M., Park, T. Y., Lee, N., Ko, S., et al. (2020). Personalized iPSC-derived dopamine progenitor cells for Parkinson's disease. *N. Engl. J. Med.* 382 (20), 1926–1932. doi:10.1056/NEJMoa1915872

Segar, M. W., Patel, K. V., Ayers, C., Basit, M., Tang, W. H. W., Willett, D., et al. (2020). Phenomapping of patients with heart failure with preserved ejection fraction using machine learning-based unsupervised cluster analysis. *Eur. J. Heart Fail.* 22 (1), 148–158. doi:10.1002/ejhf.1621

Shi, M., and Xu, G. (2019). Development and validation of GMI signature based random survival forest prognosis model to predict clinical outcome in acute myeloid leukemia. *BMC Med. Genomics* 12 (1), 90. doi:10.1186/s12920-019-0540-5

Simmons, P. J., and Torok-Storb, B. (1991). Identification of stromal cell precursors in human bone marrow by a novel monoclonal antibody, STRO-1. *Blood* 78 (1), 55–62. doi:10.1182/blood.v78.1.55.55

Steinhoff, G., Nesteruk, J., Wolfien, M., Kundt, G., Borgermann, J., et al. (2017). Cardiac function improvement and bone marrow response -: outcome analysis of the randomized PERFECT phase III clinical trial of intramyocardial CD133(+) application after myocardial infarction. *EBioMedicine* 22, 208–224. doi:10.1016/j.ebiom.2017.07.022

Takahashi, K., and Yamanaka, S. (2006). Induction of pluripotent stem cells from mouse embryonic and adult fibroblast cultures by defined factors. *Cell.* 126 (4), 663–676. doi:10.1016/j.cell.2006.07.024

Taylor, D. A., Perin, E. C., Willerson, J. T., Zierold, C., Resende, M., Carlson, M., et al. (2016). Identification of bone marrow cell subpopulations associated with improved functional outcomes in patients with chronic left ventricular dysfunction: an embedded cohort evaluation of the FOCUS-CCTRN trial. *Cell. Transpl.* 25 (9), 1675–1687. doi:10.3727/096368915X689901

Teerlink, J. R., Metra, M., Filippatos, G. S., Davison, B. A., Bartunek, J., Terzic, A., et al. (2017). Benefit of cardiopoietic mesenchymal stem cell therapy on left ventricular remodelling: results from the Congestive Heart Failure Cardiopoietic Regenerative Therapy (CHART-1) study. *Eur. J. Heart Fail* 19 (11), 1520–1529. doi:10.1002/ejhf.898

Tsao, C. W., Aday, A. W., Almarzooq, Z. I., Alonso, A., Beaton, A. Z., Bittencourt, M. S., et al. (2022). Heart disease and stroke statistics—2022 update: a report from the American heart association. *Circulation* 145 (8), e153–e639. doi:10.1161/CIR.0000000000001052

Tsilimigras, D. I., Oikonomou, E. K., Moris, D., Schizas, D., Economopoulos, K. P., and Mylonas, K. S. (2017). Stem cell therapy for congenital heart disease: a systematic review. *Circulation* 136 (24), 2373–2385. doi:10.1161/CIRCULATIONAHA.117.029607

Ulus, A. T., Mungan, C., Kurtoglu, M., Celikkan, F. T., Akyol, M., Sucu, M., et al. (2020). Intramyocardial transplantation of umbilical cord mesenchymal stromal cells in chronic ischemic cardiomyopathy: a controlled, randomized clinical trial (HUC-heart trial). *Int. J. Stem Cells* 13 (3), 364–376. doi:10.15283/ijsc20075

Uygur, A., and Lee Richard, T. (2016). Mechanisms of cardiac regeneration. *Dev. Cell.* 36 (4), 362–374. doi:10.1016/j.devcel.2016.01.018

van der Spoel, T. I., Jansen of Lorkeers, S. J., Agostoni, P., van Belle, E., Gyöngyösi, M., Sluijter, J. P. G., et al. (2011a). Human relevance of pre-clinical studies in stem cell therapy: systematic review and meta-analysis of large animal models of ischaemic heart disease. *Cardiovasc Res.* 91 (4), 649–658. doi:10.1093/cvr/cvr113

Vrtovec, B., Poglajen, G., Sever, M., Zemljic, G., Frljak, S., Cerar, A., et al. (2018). Effects of repetitive transendocardial CD34+ cell transplantation in patients with nonischemic dilated cardiomyopathy. *Circ. Res.* 123 (3), 389–396. doi:10.1161/CIRCRESAHA.117.312170

Waisman, A., La Greca, A., Möbbs, A. M., Scarafía, M. A., Santín Velazque, N. L., Neiman, G., et al. (2019). Deep learning neural networks highly predict very early onset of pluripotent stem cell differentiation. *Stem Cell. Rep.* 12 (4), 845–859. doi:10.1016/j.stemcr.2019.02.004

Wang, Y., Wang, Z., Xie, K., Zhao, X., Jiang, X., Chen, B., et al. (2020). High-efficiency cellular reprogramming by nanoscale puncturing. *Nano Lett.* 20 (7), 5473–5481. doi:10.1021/acs.nanolett.0c01979

Wang, Y., Zhang, L., Li, Y., Chen, L., Wang, X., Guo, W., et al. (2015). Exosomes/microvesicles from induced pluripotent stem cells deliver cardioprotective miRNAs and prevent cardiomyocyte apoptosis in the ischemic myocardium. *Int. J. Cardiol.* 192, 61–69. doi:10.1016/j.ijcard.2015.05.020

Wen, H., Peng, L., and Chen, Y. (2021). The effect of immune cell-derived exosomes in the cardiac tissue repair after myocardial infarction: molecular mechanisms and pre-clinical evidence. *J. Cell. Mol. Med.* 25 (14), 6500–6510. doi:10.1111/jcmm.16686

Wessels, A., and Sedmera, D. (2003). Developmental anatomy of the heart: a tale of mice and man. *Physiol. Genomics* 15 (3), 165–176. doi:10.1152/physiolgenomics.00033.2003

Wu, P., Sai, X., Li, Z., Ye, X., Jin, L., Liu, G., et al. (2023). Maturation of induced pluripotent stem cell-derived cardiomyocytes and its therapeutic effect on myocardial infarction in mouse. *Bioact. Mater* 20, 286–305. doi:10.1016/j.bioactmat.2022.05.024

Xiao, W., Guo, S., Gao, C., Dai, G., Gao, Y., Li, M., et al. (2017). A randomized comparative study on the efficacy of intracoronary infusion of autologous bone marrow mononuclear cells and mesenchymal stem cells in patients with dilated cardiomyopathy. *Int. Heart J.* 58 (2), 238–244. doi:10.1536/ihj.16-328

Yang, Y., Liu, B., Xu, J., Wang, J., Wu, J., Shi, C., et al. (2017). Derivation of pluripotent stem cells with *in vivo* embryonic and extraembryonic potency. *Cell.* 169 (2), 243–257. doi:10.1016/j.cell.2017.02.005

Yau, T. M., Pagani, F. D., Mancini, D. M., Chang, H. L., Lala, A., Woo, Y. J., et al. (2019). Intramyocardial injection of mesenchymal precursor cells and successful temporary weaning from left ventricular assist device support in patients with advanced heart failure: a randomized clinical trial. *JAMA* 321 (12), 1176–1186. doi:10.1001/jama.2019.2341

Ye, J., Ge, J., Zhang, X., Cheng, L., Zhang, Z., He, S., et al. (2016). Pluripotent stem cells induced from mouse neural stem cells and small intestinal epithelial cells by small molecule compounds. *Cell. Res.* 26 (1), 34–45. doi:10.1038/cr.2015.142

Zheng, Y. L. (2016). Some ethical concerns about human induced pluripotent stem cells. *Sci. Eng. Ethics* 22 (5), 1277–1284. doi:10.1007/s11948-015-9693-6

Zheng, Y. L., Wang, W. D., Cai, P. Y., Zheng, F., Zhou, Y. F., Li, M. M., et al. (2022). Stem cell-derived exosomes in the treatment of acute myocardial infarction in preclinical animal models: a meta-analysis of randomized controlled trials. *Stem Cell. Res. Ther.* 13 (1), 151. doi:10.1186/s13287-022-02833-z

Zhu, Y., Huang, R., Wu, Z., Song, S., Cheng, L., and Zhu, R. (2021). Deep learning-based predictive identification of neural stem cell differentiation. *Nat. Commun.* 12 (1), 2614. doi:10.1038/s41467-021-22758-0

Zuk, P. A., Zhu, M., Mizuno, H., Huang, J., Futrell, J. W., Katz, A. J., et al. (2001). Multilineage cells from human adipose tissue: implications for cell-based therapies. *Tissue Eng.* 7 (2), 211–228. doi:10.1089/107632701300062859

frontiers | Frontiers in Physiology

TYPE Original Research
PUBLISHED 21 June 2024
DOI 10.3389/fphys.2024.1401768

OPEN ACCESS

EDITED BY
Hanjun Wang,
University of Nebraska Medical Center,
United States

REVIEWED BY
Bryan K. Becker,
University of Alabama at Birmingham,
United States
Shunguang Wei,
The University of Iowa, United States

*CORRESPONDENCE
Hong Zheng,
hong.zheng@usd.edu

RECEIVED 15 March 2024
ACCEPTED 09 May 2024
PUBLISHED 21 June 2024

CITATION
Boomer SH, Liu X and Zheng H (2024), Effects of regulator of G protein signaling 2 (RGS2) overexpression in the paraventricular nucleus on blood pressure in rats with angiotensin II-induced hypertension.
Front. Physiol. 15:1401768.
doi: 10.3389/fphys.2024.1401768

Effects of regulator of G protein signaling 2 (RGS2) overexpression in the paraventricular nucleus on blood pressure in rats with angiotensin II-induced hypertension

Shane H. Boomer, Xuefei Liu and Hong Zheng*

Basic Biomedical Sciences, Sanford School of Medicine, University of South Dakota, Vermillion, SD, United States

The hypothalamic paraventricular nucleus (PVN) regulates sympathetic activity and blood pressure. The regulator of G protein signaling 2 (RGS2) is a negative G protein regulator, which selectively regulates Gαq signaling, a potential cause of hypertension. This study aimed to examine angiotensin II (ANG II)-G protein-RGS2 signaling on the central mechanisms of blood pressure control, sympathetic activation, and kidney function. The Sprague Dawley rats were infused with ANG II (200 ng/kg/min) via osmotic mini pump to induce hypertension. Adenovirus (AV) vectors encoding RGS2 was transfected into the PVN *in vivo*. By radio telemetry measurements, we found AV-RGS2 transfection to the PVN significantly attenuated the increase of mean arterial pressure in ANG II infusion rats from days 2–7 of the 2-week experiment (Day 7: ANG II + AV-RGS2 141.3 ± 10.0 mmHg vs. ANG II 166.9 ± 9.3 mmHg, $p < 0.05$). AV-RGS2 transfection significantly reduced the serum norepinephrine level and acute volume reflex and increased daily urine volume and sodium excretion in ANG II-infused hypertensive rats. AV-RGS2 transfection significantly reduced Gαq and PKC protein expressions within the PVN in ANG II infusion rats. In cultured mouse hypothalamic cells, real-time PCR study showed ANG II treatment increased mRNA expression of Gαq, Gαs, and RGS2, and AV-RGS2 treatment decreased ANG II-induced mRNA expression of Gαq and Gαs. Using confocal imagery, we found that AV-RGS2 attenuated the increase of calcium influx in ANG II-treated cells. Our results suggest that central overexpression of RGS2 in the PVN attenuated the increase of blood pressure and sympathetic outflow, and improves kidney excretory function in hypertensive rats. This may be via the alteration of ANG II-G-protein-RGS2 signaling in the central nervous system.

KEYWORDS

regulator of G-protein signaling 2, G-protein-coupled receptor, angiotensin-II, paraventricular nucleus, blood pressure, hypertension

Introduction

Hypertension is a cardiovascular disease that significantly increases associated mortality and morbidity (Chobanian et al., 2003; Wu et al., 2015). Data suggests that more than 50% of clinical hypertension cases are primary (essential) forms, often featuring a neurogenic origin (Frame et al., 2016). The hypothalamic paraventricular nucleus (PVN) is a critical central nucleus regulating sympathetic activity. Excitatory input to pre-autonomic neurons in the PVN leads to increased sympathetic outflow in animal models with hypertension (Li and Pan, 2017; Guyenet et al., 2020). The dysfunction of sympathetic modulation within the PVN contributes to fluid and electrolyte balance alterations, which are seen in animals with hypertension and chronic heart failure (Zheng et al., 2022). With its roles in stress, metabolism, growth, reproduction, and autonomic function, the PVN has been established as one of the most critical control autonomic centers in the brain (Ferguson et al., 2008; Zhang and Anderson, 2014).

The sympathetic nervous system (SNS) acts on α- and β-adrenergic receptors that are coupled to G-proteins. Specific α- and β-adrenergic receptors act on specific G-protein isoforms. α1 receptors are coupled to Gq proteins, α2 receptors are coupled to Gi proteins, and β1 and β2 receptors are coupled to Gs proteins (Vasudevan et al., 2011; Taylor and Cassagnol, 2024). Heterotrimeric G-proteins have three distinct subunits (α, β, and γ). As GTP binds, the α subunit dissociates from the β and γ subunits, triggering downstream signaling specific to the G-protein isoform. In the isoforms associated with excitatory function, the signaling cascade is an essential factor in increasing cellular activity, causing several proteins to be transcribed relating to cell cycle progression, proliferation, growth factors, metabolism, neurotrophy, and cell survival (Wang et al., 2018; Alshak and Das, 2024). With G-proteins being present within all cell types, it is plain to see their vital role in cell signaling. Understanding the regulatory mechanisms of different isoforms of G-proteins within the brain, specifically Gαq/Gαs, is essential in how they are directed to modify sympathetic activation and cardiovascular parameters.

Angiotensin II (ANG II) acts to activate type 1 (AT_1) and type 2 (AT_2) receptors, each with their corresponding mechanism. As ANG II binds to the AT_1 receptor, a conformation change ensues, allowing GTP binding, subunit dissociation, and intracellular signaling (Eguchi et al., 2018). AT_1 receptors are coupled to a Gq protein, where the α subunit will act to activate phospholipase C enzyme (Freeman and Tallant, 1994). This enzyme then acts to increase intracellular calcium through inositol triphosphate (IP3) and activate protein kinase C (PKC) through diacylglycerol (Bill and Vines, 2020). ANG II stimulates sympathetic activity, increases vasoconstriction, impacts sodium and water reabsorption in the kidneys, and influences baroreceptor sensitivity, stress responses, and cardiovascular remodeling (Fyhrquist et al., 1995).

The regulators of G-protein signaling (RGS) family regulates G protein signaling through their GTPase-activating proteins (GAP) activity. This GAP activity causes GTP to hydrolyze to GDP, thus inactivating and causing the reassociation of the three subunits (α, β, and γ), and halting the signaling cascade (Kimple et al., 2011). Further looking into RGS's activity on G-proteins and the cessation of cell signaling may be an important feature in the progression of blood pressure dysregulation. Of the RGS protein family, RGS2 regulation has been shown to be an emerging target in multiple tissues for various pathologies (McNabb et al., 2020; O'Brien et al., 2019). Studies have examined RGS2 in cognitive dysfunction, cardiac fibrosis, and pancreatic dysfunction. With little to no studies being done on the RGS2 protein on G-protein signaling on the central mechanisms of blood pressure control, we view it as important to examine how these interactions affect sympathetic reflex and the progression of hypertension. Examining the neuronal activity with cell signaling cascade changes in blood pressure management between hypertensive and normotensive subjects may be a critical link needed to help better combat this condition.

The present study aimed to test the central molecular mechanisms of RGS2 protein and its relationships with the sympathetic nervous system, as well as its roles in cardiovascular and renal function. *In vivo*, we assessed the blood pressure changes, sympathetic activation, acute volume reflex, and kidney function in chronic ANG II infusion rats with central adenovirus (AV) RGS2 transfection in the PVN. *In vitro*, we assessed the changes in G-protein with ANG II and AV-RGS2 treatment. We also examined ANG II-induced calcium flux changes as we altered the expression of RGS2 in the neuronal culture cells.

Materials and methods

Animals

For *in vivo* study, we used male Sprague-Dawley rats (treatment started at 12 weeks of age, end-of-treatment aged approximately 14–16 weeks, total animal number = 60) of *Rattus norvegicus* (Envigo and USD Animal Resource Center). The rats were housed in the Animal Resource Center at the University of South Dakota on a 12-h day/night cycle with *ad libitum* access to standard rat chow and water. All the procedures on animals were approved by the Institutional Animal Care and Use Committee of the University of South Dakota. The experiments were in accordance with the American Physiological Society and the National Institutes of Health Guide for the Care and Use of Laboratory Animals.

Anesthesia

For rat survival surgeries, the subject was placed unconscious via isoflurane gas introduced at 4%–5% in oxygen. Maintenance levels (2%–4%) of isoflurane were given, and reflexes were monitored to ensure adequate anesthetic dosage. Ventilatory rate, depth, and quality were assessed and titrated to ensure the proper anesthetic without loss of ventilation. Post-surgery, 0.1 mL buprenorphine SR (0.5 mg/mL) was given subcutaneously for analgesia. The subject was monitored following surgery for proper and timely surgical site healing.

In rat non-survival surgeries, the subject was given either urethane and α-chloralose (0.5 mL/100 g, concentration 8.8 g/50 mL), or Thiobutabarbital (Inactin Hydrate) (2 mL/kg, concentration 0.05 g/mL) via intraperitoneal injection. Reflexes

were monitored, and sacrifice occurred when reflexes were absent. Additional doses of anesthetic were given accordingly. The subject was sacrificed following the completion of the experiment.

Chronic ANG II infusion via osmotic mini pump

In this survival surgery, the osmotic mini pump (Alzet: Model 2002; Durect, CA) was inserted into the scruff of the neck of the subject. An incision was made, and blunt dissection was performed to create a cavity where the osmotic pump was placed. The osmotic pump was calibrated to deliver ANG II (Sigma, St Louis, MO) at 200 ng/kg/min over 2 weeks.

Adenoviral RGS2 (AV-RGS2) transfection in the PVN

The subject was anesthetized and placed on the stereotaxis device. An incision was made along the midline of the cranium. A small hole was drilled into the skull to allow for the insertion of the needle and delivering the injection into the PVN. To give an injection into the PVN, we moved from bregma −1.7 to −1.8 mm along the A-P axis, +/− 0.5 mm along the M-L axis and went to a depth of 7.5–8 mm from the surface of the skull. 50 nL of AV-RGS2 with co-expression of reporter mCherry (2 × 10e9, SignaGen, Frederick, MD) or AV-GFP was given bilaterally upon each injection. AV-RGS2 transfection, in relation to ANG II infusion, occurred on the same day as the osmotic minipump implantation.

Transfection evaluation was completed by RGS2 mRNA level, histological assessment confirming mCherry staining and RGS2 fluorescent signal within the PVN area. For RGS2 mRNA studies, additional rats were transfected with AV-GFP as a control. For histological studies of AV-RGS2 transfection, each subject was used as self-control. The AV-RGS2 was introduced unilaterally to the PVN region in the left hemisphere, with no virus being introduced to the right hemisphere. We compared the left *versus* right PVN by the presence and absence of AV-RGS2 coupled with mCherry fluorescence.

Radio telemetry recording of blood pressure

The telemetry unit (Model PA-C10, Data Sciences International, St. Paul, MN) was inserted into the subject by making a subdermal pocket adjacent to the femoral artery. A magnet and radio were used to activate and assess the telemetry device. With telemetry implanted, we monitored blood pressure and heart rate changes before and during ANG II infusion in conscious states for 2 weeks. Blood pressure and heart rate measurements were recorded every hour in the morning to afternoon for 1 min and averaged for each day following the conclusion of the experiment. Data was recorded and stored on the Ponemah (Data Sciences International) outfitted for the mentioned telemetry devices. Measurements were taken over 2 weeks and exported to Excel for analysis.

Metabolic parameter, sympathetic activity, and kidney function study

After 1 week of ANG II infusion and AV-RGS2 transfection, each subject was placed within a NALGENE laboratory metabolic cage (Thermal Scientific) for 24 h and provided standard rat chow and water *ad libitum*. Each cage was given standard rat chow and 250 mL of water. After 24 h, the subject was placed back into a standard rat cage. Water intake was noted. Urine was collected, and 24-h urine volume was measured. Urine was centrifuged and taken to measure sodium, norepinephrine, and creatinine concentration.

Urinary sodium concentration was measured via a flame photometer (Jenway PFP7, Cole-Parmer Ltd., Vernon Hills, IL). Urinary and serum norepinephrine (LSBio, Shirley, MA) and creatinine (Sigma) were measured via ELISA kit. With concentrations of urine sodium and norepinephrine, 24-h urine volume measurements allowed us to measure the 24-h excretion rate of sodium and norepinephrine. 24-h urine volume, urine and serum creatinine concentration, and body weight were used to calculate glomerular filtration rates (GFR) of each subject.

General procedures during acute volume reflex experiments

Tracheostomy

An incision was placed along the midline of the tracheal area, and blunt dissection was performed to reveal the cartilaginous rings of the trachea. A transverse incision on the trachea was made, and a polyethylene tube was inserted and secured. The tube was examined for adequate ventilation by assessing the fogging of the tube and normal respiratory effort, frequency, and depth.

Vascular access

An incision was placed along the femoral triangle. The femoral artery and vein pair were exposed and isolated. The femoral artery catheter was assessed for pulsatile flow within the tube, and proper readings were made on the MacLab system monitor (ADInstruments, Colorado Springs, CO). Blood pressure and heart rate measurements were recorded from the arterial catheter. Saline replacement was given through the venous catheter.

Retroperitoneal access and urostomy placement

While the subject was in a prone position, a series of incisions and blunt dissection along the lumbar region were made to access the retroperitoneal space. The ureter was isolated from surrounding tissues and cut to allow for a PE-10 tube to be inserted. Urine output was assessed by measuring the before-and-after weight of the collecting vial, calculating liquid volume, and dividing by the collection time. Following, kidney weight was also measured to evaluate the volume per time collected per gram of kidney.

Saline challenge protocol (acute volume reflex)

The subject was given Thiobutabarbital (Inactin hydrate, 2 mL/kg, concentration 0.05 g/mL) via an intraperitoneal injection. Left and right urostomies were provided, and the subject was allowed 15–30 min recovery. Baseline urine output was measured over 15-min intervals with a 1 mL/h normal saline replacement. After baseline measurements, saline replacement was increased to 10% of body weight per hour. Urine output was collected every 5 min until 30 min. Then, saline replacement was reduced to 1 mL/h, and a recovery baseline was collected at two 15-min intervals. Collection tubes were weighed before and after urine collection, allowing us to calculate urine volume from the difference in measurements. Urine flow and sodium concentration changes were noted and calculated throughout the acute experiment.

Tissue preparation and Western blot

Frozen tissue from the PVN were cut with a cryostat according to a stereotaxic atlas. The brain sections were bilaterally punched using the Palkovits and Brownstein technique (Palkovits, 1983). The punches were homogenized in 100 µL of radioimmunoprecipitation assay (RIPA) buffer containing a 1% protease inhibitor cocktail (Promega, Madison, WI) and phosphatase inhibitor cocktail (ThermoFisher Scientific). Bicinchoninic acid assay (ThermoFisher Scientific) was then completed to measure the protein concentration and calibrate each sample. 4 × loading buffer was added (1:3) to the protein samples and placed within the −80°C freezer for later use.

Western blot protocol included loading protein samples (30–40 µg) onto a sodium dodecyl sulfate polyacrylamide electrophoresis gel and subjecting them to electrophoresis for 120 min at 90 V. The gel was then transferred to a polyvinylidene difluoride membrane for 90 min at 300 milliamps. Initial blocking was completed in Tris-buffered saline with tween (TBST)-milk. Primary mouse antibodies were incubated overnight in the concentrations shown below. Secondary anti-mouse antibody conjugated to Alexa Fluor 680 (1:10000, ThermoFisher Scientific) was incubated over 1.5–2 h and then washed. Fluorescent signals of the blotted membranes were detected using a LICOR scanner (Lincoln, NE) and quantified using ImageJ from NIH. The membranes were analyzed for target protein labeling intensity *versus* a β-actin control.

The following primary antibodies were used: RGS2 (sc-100761, 1:125); Gαq (sc-136181, 1:125); Gαs (sc-135914, 1:125); PKCα (sc-8323, 1:125), PKAα (sc-28315, 1:125), and β-actin (sc-398595, 1:1000) (Santa Cruz Biotechnology, Santa Cruz, CA).

Real-time PCR

Frozen PVN tissue samples were extracted by punching and placed into TRI reagent (Molecular Research Center, Cincinnati, OH) and homogenized for 10–15 s. RNA extractive of each punched tissue was dissolved in DNase/RNase-free water, and reverse transcription was completed. The sample of cDNA was used in quantitative real-time PCR (Applied Biosystems, ThermoFisher Scientific) to have a quantitative measurement for the primers used. The melting curve was analyzed to ensure the quality of the quantitative real-time PCR experiment. RNA primers include RGS2, Gαq and Gαs, with β-actin used as a housekeeping primer. Relative expression of target gene was calculated with delta-deltaCt method, which related expression of the target gene to expression of a housekeeping gene (β-actin).

The following primer sequences were used: RGS2-Sense Strand - GCC TGA TGG AGA ACA ACT CTT A; RGS2-Antisense Strand - TCA TCT CAC ACC CTG CTT TC; GNAq-Sense Strand - GCC TGC ATC AGT CAG TAT GT; GNAq-Antisense Strand - GGC TTT CTA GAG CAA GGG ATA G; GNAs-Sense Strand - AGA GGA GAA AGG AGG AGA AGA A; GNAs-Antisense Strand - GCC TCT GTA GCA GGA AGT TAA G; β-actin-Sense Strand - GAG GTA TCC TGA CCC TGA AGT A; β-actin-Antisense Strand - GCT CGA AGT CTA GAG CAA CAT AG.

Cryostat sectioning and immunohistochemistry

Under deep anesthesia with isoflurane, the subject was perfused through the left cardiac ventricle with heparinized saline followed by 4% paraformaldehyde. The brain was removed, post-fixed with paraformaldehyde, and then placed in 30% sucrose. Brain sections of the PVN (each section 30 µm thick) were cut with a cryostat according to a stereotaxic atlas and preserved in cryoprotectant.

Immunohistochemistry steps included a blocking step (1 h in 10% donkey serum), primary antibody incubation (anti-RGS2, 1:200, MABC1220, Millipore, Sigma) (overnight in 1% donkey serum in PBS-Triton), and secondary antibody incubation (Alexa Fluor 488 donkey anti-mouse secondary antibody, 1:200, 2 h, Jackson ImmunoResearch, West Grove, PA). After washing, the sections were then placed on slides, dried, and covered with a Vectashield mounting medium (Vector Laboratory, Burlingame, CA). Immunofluorescence of RGS2 and mCherry within the PVN (sections from −1.7 mm to −1.8 mm to bregma) were viewed by a Leica fluorescence microscope and captured by a digital camera (Leica, Germany).

Hypothalamic cell culture

For the cell culture studies, a hypothalamic cell line (mHypoA-POMC/GFP-1, CLU500, CELLutions Biosystems Inc., ON, Canada) was used. We used the mHypoA-POMC cell line as they are a hypothalamic cell line, and they have a common protein expression to other hypothalamic cell lines. However, their unique protein expression (responsible for their neuroendocrine function) should also be considered. We had indiscriminate targeting of the PVN, so all PVN neurons, including POMC neurons, are potentially impacted.

A culture medium of 1% penicillin/streptomycin in Dulbecco's Modified Eagle Medium (DMEM) was used with fetal bovine serum to grow the cells within the culture flask.

Cell cultures were maintained until they reached 60%–70% confluency, and then the cells were plated for the ANG II and AV-RGS2 treatment studies.

Cells were plated for 24–48 h and then starved for another 24 h. Following this, we treated the individual plates with their assigned treatment. Treatments had varying final concentrations of ANG II (6.25, 12.5, 25, 50,100 μM) in DMEM. Each dish contained 5 mL of DMEM. Viral transfection was achieved by adding 50 μL AV-RGS2 (stocking concentration: 10e8, final concentration: 10e6) for −24 h. Cells were scraped from the plates, collected, and used for the mRNA studies. Alongside the ANG II treatments, an additional dish of starved cells was used as a control. This control was treated with 100 μL of only DMEM, while the treated cells had varying concentrations of ANG II in 100 μL DMEM. Gene expression targets were compared to β-actin controls.

Calcium imaging

For calcium imaging, mHypoA-POMC/GFP-1 cells were pre-incubated with or without AV-RGS2 for 24 h at 37°C in an 8-well Ibidi slide chamber (Ibidi United States, Inc., Fitchburg, Wisconsin). Each well contains 300 μL of DMEM. Viral transfection was achieved by adding 3 μL AV-RGS2 (final concentration: 1e7). After incubation, the cells were loaded with Fluo-3 (5 μM, stocking: 150 μM, add 10 μL into 300 μL medium) (ThermoFisher Scientific) for 30 min at 37°C. At the end of the incubation, cells were washed with DMEM to remove extracellular Fluo-3 and add fresh DMEM (300 μL). Cells were then placed on the stage of a laser confocal microscope (Leica). The confocal calcium image with green fluorescence was taken when the neurons were challenged with ANG II (Final concentration: 1 mM). Fluo-3 was excited by light at 488 nm, and fluorescence was measured at wavelengths of >515 nm using a ×100 objective. Raw data was imported into an Excel file for analysis.

Statistical analysis

The controls for the *in vivo* experiments included Sprague-Dawley rats without ANG II treatment, and ANG II infusion without AV-RGS2. When comparing to the PVN injection of AV-RGS2, we subjected a control Sprague-Dawley rat to AV-GFP PVN injection. Controls for the *in vitro* experiments include a plate of cells treated only with DMEM medium.

Statistical significance in before-and-after treatments was determined by Student's paired *t*-test. Student's t-test was used to calculate differences in samples with two groups. Experiments with 3 groups was analyzed by one-way ANOVA, followed by the appropriate *post hoc* analysis. Two-way ANOVA was used to evaluate the effects of two factors (treatment and time).

Data was assessed prior to parametric analysis if the assumptions of parametric analysis were met. If assumptions were violated, appropriate measures were taken to correct these violations. If the violations remain, nonparametric analysis tools were used instead. Statistical significance was accepted when $p < 0.05$. All data were presented as means ± SE. Data was assessed using Prism 9 (GraphPad Software, La Jolla, CA).

Results

General data

Male Sprague-Dawley rats were used and had a mean body weight of −395 g at the time of tissue collection ranging between 14 and 16 weeks of age. Chronic ANG II infusion and AV-RGS2 transfection did not significantly change the body weight among the groups.

Adenoviral gene transfer of RGS2 within the PVN

We evaluated the efficacy of AV-RGS2 gene transfer in the PVN by comparing RGS2 mRNA levels of the PVN. We completed bilateral adenovirus PVN injections in 12 male Sprague-Dawley rats. 6 rats were transfected with AV-GFP as controls, and the other 6 were transfected with AV-RGS2. Post-transfection tissue collection occurred at 3, 7, and 14 days with two rats in each group for each adenovirus transfection. Analysis of our Sprague-Dawley rat strain showed that the PVN had significantly increased RGS2 mRNA expression in AV-RGS2 transfected rats compared to the AV-GFP transfected rats (Figure 1A). RGS2 showed peak mRNA expression on the 3rd day, with increased expressions at weeks 1 and 2 of the experiment compared to the AV-GFP injected rats. Overall, there was an increase in RGS2 gene expression over the 3 timepoints (Figure 1B).

5 Sprague Dawley rats were unilaterally transfected with AV-RGS2 in the PVN in the left hemisphere, with the right hemisphere being self-control. We compared left *versus* right PVN by the presence and absence of AV-RGS2 coupled with mCherry fluorescent protein. The mCherry and RGS2 fluorescent signal was increased 3-, 6-, 9-, 12-, and 15 days post-transfection. Figure 1C shows the images acquired with mCherry, RGS2, and merged staining within the PVN at 6 days post-transfection.

Effect of AV-RGS2 on arterial pressure in conscious ANG II infusion rats

Baseline blood pressure and heart rate measurements were taken over multiple days after telemetry device insertion recovery and before ANG II infusion (Mean blood pressure: 111.2 +/− 2.3 mmHg). Chronic ANG II infusion significantly increased blood pressure over 2-week (First week: 166.9 +/− 9.3 mmHg; Second week: 188.6 +/− 6.5 mmHg). AV-RGS2 transfection in the PVN significantly attenuated the increase of blood pressure in the ANG II + RGS2 group compared to the ANG II group from day 2 to day 7 (Figure 2A). No differences were noted between when the virus was given, and they showed a similar increase to the hypertensive phenotype occurring early in the 2nd week of the telemetry experiment. The results shown below are in order of the ANG II + AV-RGS2 and ANG II group, respectively (in mmHg). Day 2: 123.4 +/− 7.7 vs. 145.3 +/− 8.0, $p < 0.05$; Day 3: 132.3 +/− 6.4 vs. 155.5 +/− 10.7, $p < 0.05$; Day 4: 136.7 +/− 10.1 vs. 157.4 +/− 8.0, $p < 0.05$; Day 5: 139.3 +/− 9.5 vs. 158.7 +/− 6.0, $p < 0.05$; Day 6: 140.3 +/− 7.0 vs. 160.3 +/− 4.6, $p < 0.05$; Day 7: 141.3 +/− 10.0 vs.

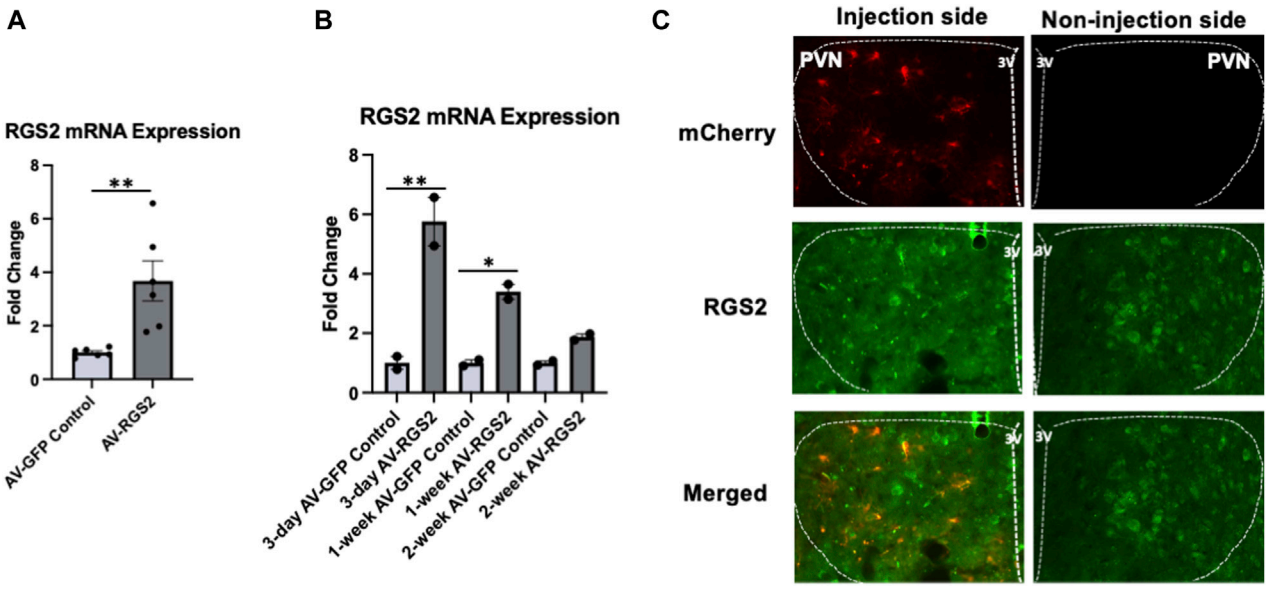

FIGURE 1
(A) The mRNA expression changes of RGS2 within the PVN with AV-GFP or AV-RGS2 transfection, *n* = 6/group. **(B)** The mRNA expression changes of RGS2 within the PVN over time with AV-RGS2 or AV-GFP transfection. RGS2 showed peak expression on the 3rd day, with increased expressions at weeks 1 and 2 of the experiment compared to the AV-GFP injected rats. Four subjects were used for each time point (2 AV-RGS2, 2 AV-GFP). **p < 0.05, **p < 0.01 signifies within groups.* **(C)** Histological assessment of AV-RGS2 with mCherry (red) transfection and RGS2 (green) in the PVN area at 6-day post-transfection, X400. *n* = 5. 3V: third ventricle.

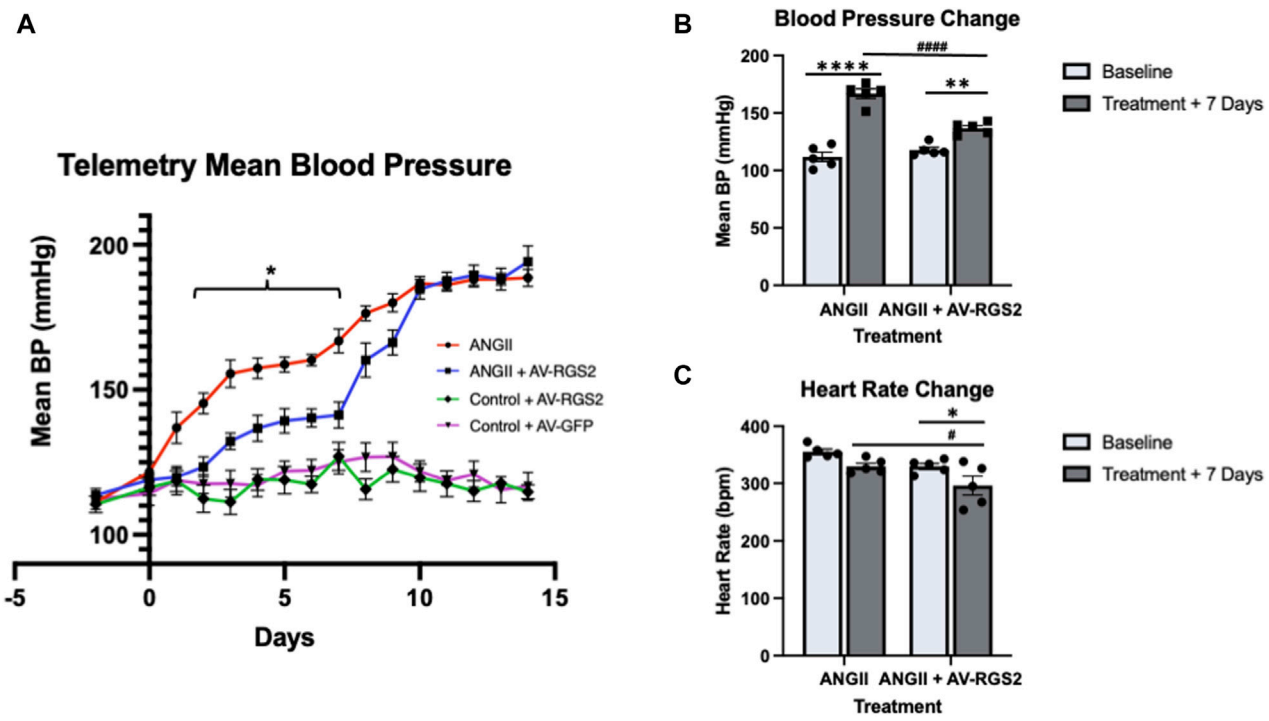

FIGURE 2
(A) The mean blood pressure (BP) changes over a 2-week period. Days 2 through 7 showed a significant reduction of blood pressure in the ANG II + AV-RGS2 groups compared to the ANG II group. **p < 0.05 signifies between groups.* **(B, C)**: Depict changes in blood pressure and heart rate at 7-day treatment from baseline. **p < 0.05, **p < 0.01, ****p < 0.0001 signifies within groups, #p < 0.01, ####p < 0.0001 signifies between groups, n* = 4–5/group.

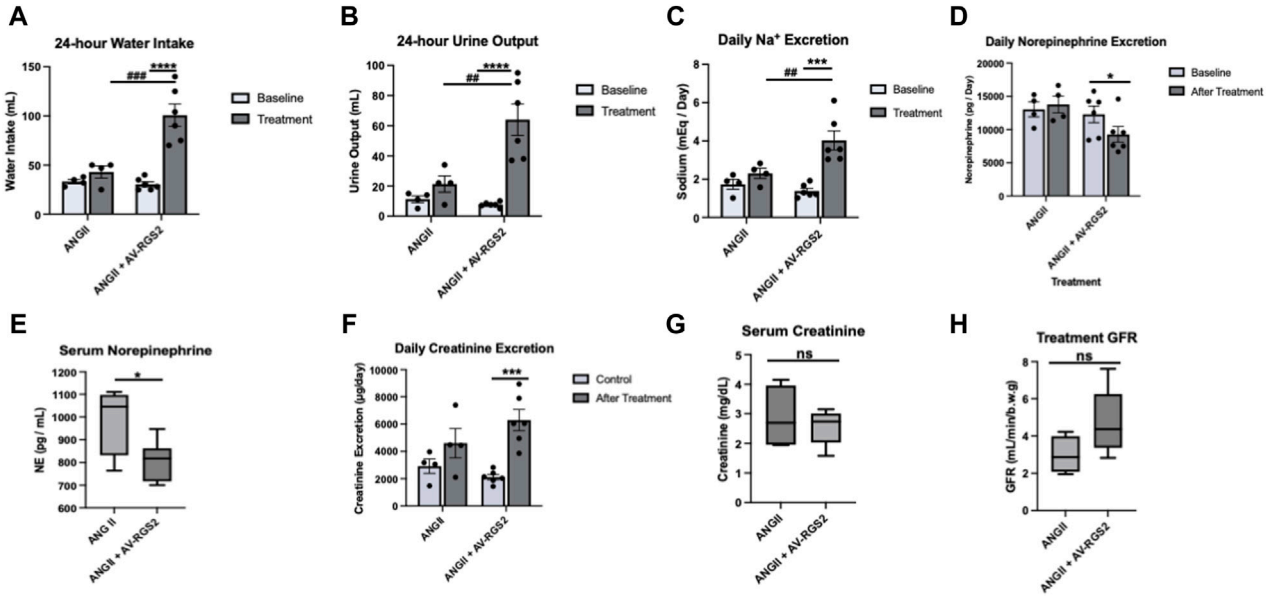

FIGURE 3
Metabolic changes in ANG II-induced hypertensive rats with or without AV-RGS2 introduced to the PVN. Water intake **(A)**, urine output **(B)**, and urine sodium excretion **(C)** before and after treatment in ANG II and ANG II + AV-RGS2 groups. **(D, E)** showed the changes in serum and urine norepinephrine concentration. **(F–H)** showed the changes in urine excretion and serum concentration of creatinine and GFR. *$p < 0.05$, ***$p < 0.001$, ****$p < 0.0001$ signifies within groups, ##$p < 0.01$, ###$p < 0.001$ signifies between groups. n = 4–6/group.

166.9 +/− 9.3, $p < 0.05$. There were no significant differences of blood pressure from day 8 to the end of the experiment. There were no significant differences comparing the normotensive control groups with AV-GFP and AV-RGS2. Day 7 mean blood pressure and heart rate changes from baseline are shown in Figures 2B,C, respectively. There was a significant increase in blood pressure from baseline in both ANG II and ANG II + AV-RGS2 groups. However, the changes in blood pressure in the ANG II + AV-RGS2 group were attenuated compared to those in the group that received ANG II infusion alone. There was a significant decrease in heart rate in the ANG II + AV-RGS2 group *versus* ANG II infusion alone group.

Effect of AV-RGS2 on the metabolic parameters, sympathetic activity, and kidney function in conscious ANG II infusion rats

We measured water intake and urine output over 24 h. Water consumption for the ANG II + AV-RGS2 group measured at 100.7 +/− 11.4 mL, which was significantly higher than its pre-treatment baseline (30.5 +/− 2.4 mL, $p < 0.0001$) and the ANG II group (43.0 +/− 6.0 mL, $p < 0.001$) (Figure 3A). Urine output for the ANG II + AV-RGS2 group measured at 64.0 +/− 10.5 mL, which was significantly higher than its pre-treatment baseline (7.6 +/− 0.7 mL, $p < 0.0001$) and the ANG II group (21.4 +/− 5.4 mL, $p = 0.001$) (Figure 3B). Daily sodium excretion significantly increased after treatment in the ANG II + AV-RGS2 group compared to the baseline (4.0 +/− 0.5 vs. 1.4 +/− 0.1 mEq/day, $p < 0.0001$) (Figure 3C). Daily sodium excretion in the ANG II + AV-RGS2 group was significantly increased compared to the ANG II group (4.0 +/− 0.5 vs. 2.0 +/− 0.3 mEq/day, $p < 0.01$).

To evaluate sympathetic activity, assessment of 24-h urine norepinephrine excretion (as sympathetic index) showed that the ANG II + AV-RGS2 group was significantly decreased after treatment compared to the ANG II group (9262.9 +/− 1171.8 vs. 12293.5 +/− 1257.7 pg/day, $p < 0.05$) (Figure 3D). Daily urinary norepinephrine excretion in the ANG II group tended to increase but not reach statistical significance (13021.6 +/− 1119.6 vs. 13783.2 +/− 1267.9 pg/mL, $p > 0.05$). The ANG II + AV-RGS2 group had significantly decreased serum norepinephrine concentration compared to the ANG II group (806.7 +/− 36.0 vs. 991.4 +/− 77.3 pg/mL, $p < 0.05$) (Figure 3E).

To evaluate kidney function, we found that daily urine creatinine excretion was significantly increased in the ANG II + AV-RGS2 group compared to the pre-treatment values (6290.3 +/− 762.1 µg/day vs. 2124.5 +/− 192.8 µg/day, $p < 0.001$) (Figure 3F). Serum creatinine concentration in the ANG II + AV-RGS2 group tended to lower than the ANG II group, but not significantly different between the two groups ($p > 0.05$) (Figure 3G). Calculated glomerular filtration rates tended to be increased in the ANG II + AV-RGS2 group compared to the ANG II group but did not reach significance ($p > 0.05$) (Figure 3H).

Effect of AV-RGS2 on the acute volume reflex in ANG II infusion rats

Average urine flow and sodium excretion in the acute volume reflex experiment under anesthesia was depicted in Figures 4A,B. There was a significant increased baseline urine volume in the ANG II and ANG II + AV-RGS2 groups compared to the control ($p < 0.05$). The urine flow and sodium excretion responses to saline

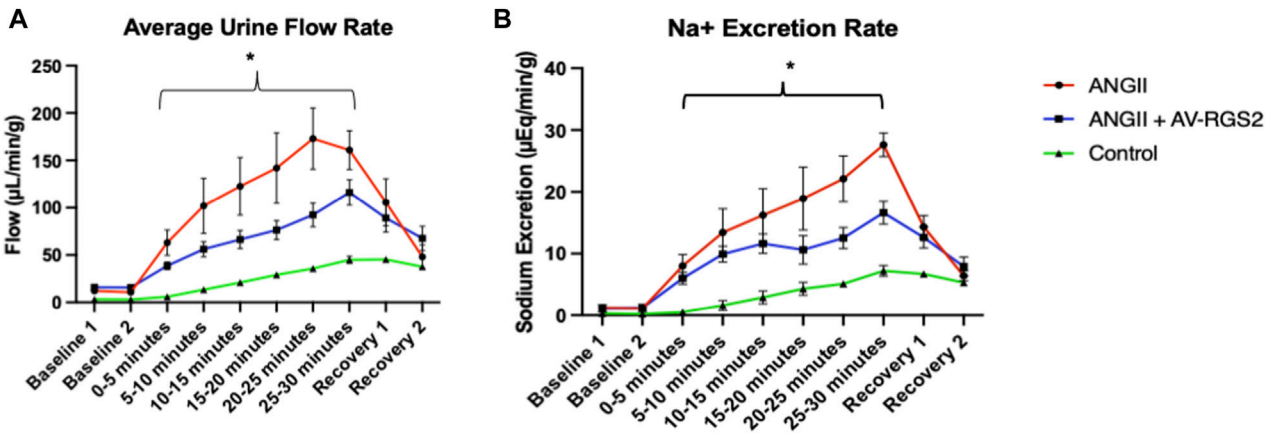

FIGURE 4
(A) The urine flow rate changes when subjected to a 10% body weight per hour saline challenge, measured in uL of urine per minute per gram of kidney. **(B)** The sodium excretion rate with 10% body weight per hour saline challenge, measured in uEq of per minute per gram of kidney. Baseline and Recovery was measured over 15-min intervals. Samples are measured over 5-min intervals. *$p < 0.05$ compared to the AV-RGS2 and control groups. n = 3–4/group.

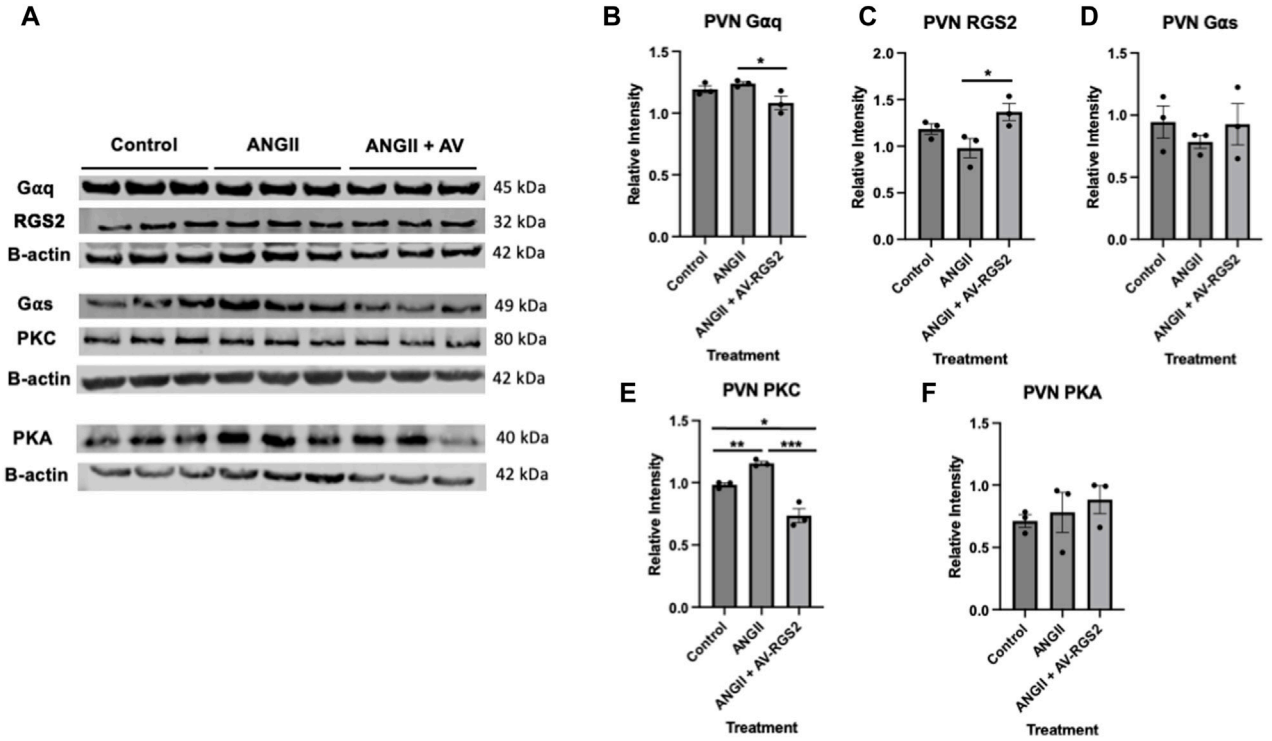

FIGURE 5
(A) The gel images were obtained from the Western blot experiment and used for the data analysis. **(B–F)** Protein expressions of Gαq, RGS2, Gαs, PKC and PKA in the PVN with the introduction of AV-RGS2. *$p < 0.05$, **$p < 0.01$, ***$p < 0.001$ signifies between groups. n = 3/group.

challenge significantly increased in both ANG II and ANG II + AV-RGS2 groups *($p < 0.05$)*. However, AV-RGS2 significantly attenuated the urine flow and sodium excretion responses challenged with saline infusion compared to the ANG II infusion group *($p < 0.05$)*.

PVN tissue Western blot assessment

Figure 5A shows the gel images obtained from the Western blot experiment and used for the data analysis. Assessment of G-proteins and downstream effectors show that Gαq, not Gαs, was significantly

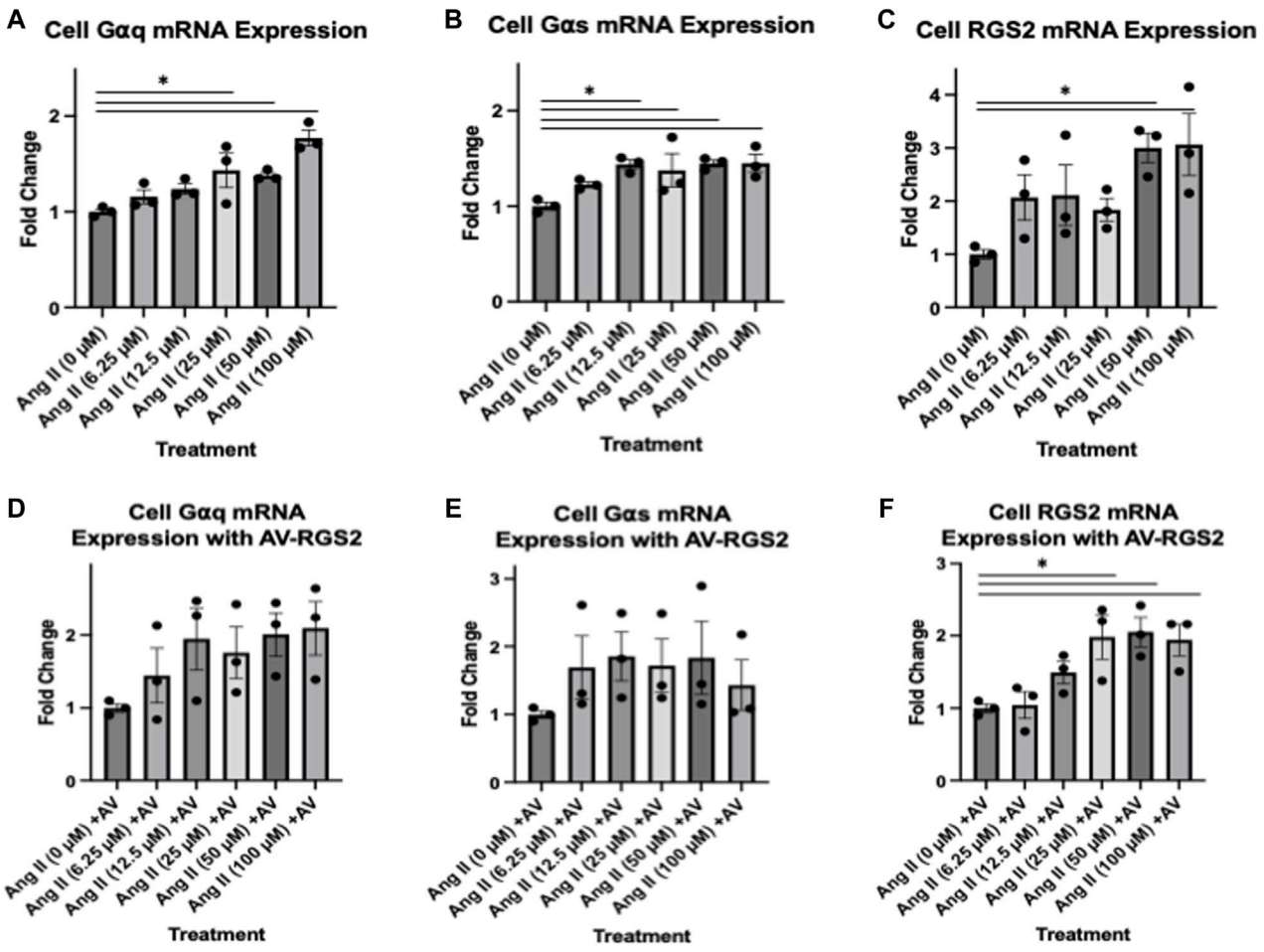

FIGURE 6
(A–C) The changes in mRNA expression in cell culture with treatment of varying concentrations of ANG II. **(D–F)**: Treatments with ANG II with AV-RGS2. There was an increase in mRNA expression as the concentration of ANG II increases. The addition of AV-RGS2 attenuated the fold change seen with ANG II. *$p < 0.05$ compared to the control without ANG II. n = 3/group.

decreased in the ANG II + AV-RGS2 compared to the ANG II infusion group ($p < 0.05$) (Figures 5B,D). RGS2 expression in the PVN was shown to be significantly increased in the ANG II + AV-RGS2 compared to the ANG II group ($p < 0.05$) (Figure 5C). We also found that G-protein downstream effector PKC in the ANG II group was significantly increased compared to the control ($p < 0.05$). PKC protein expression were significantly attenuated with AV-RGS2 transfection compared to the ANG II group ($p < 0.05$) (Figure 5E). However, there was no significant change in protein kinase A (PKA) expression in the PVN after AV-RGS2 transfection ($p > 0.05$) (Figure 5F).

Effect of AV-RGS2 on ANG II-induced G-protein mRNA expression in the hypothalamic cell line

Real-time PCR analysis showed that treatment of ANG II had a graded increase in Gαq (Figure 6A), Gαs (Figure 6B) and RGS2 (Figure 6C) from control, as the concentration of ANG II increased. The collected data had a positive trend and reached statistical significance with ANG II treatment ($p < 0.05$). In the setting of cell cultures treated with ANG II with AV-RGS2, Gαq and Gαs mRNA levels were not significantly different compared to the control ($p > 0.05$) (Figures 6D,E), while RGS2 mRNA showed a similar graded increase (Figure 6F), suggesting AV-RGS2 treatment attenuated the upregulation of G-protein gene expression seen in ANG II treatment.

Calcium imaging

Treatment of cells with ANG II causes the activation of PKC and influx of calcium into the cytoplasm, which then can be pictured via fluorescence. As RGS2 deactivates the receptor activated by ANG II, we expect to see a reduction of calcium fluorescence in cells treated with ANG II and transfected with AV-RGS2. Confocal imaging was shown in Figure 7A, and fluorescence analysis was displayed in Figure 7B. Analysis showed that AV-RGS2 transfected cells treated with ANG II demonstrated attenuated fluo-3 fluorescence signal compared to the cells only treated with ANG II. Cells treated with AV-RGS2 showed a significant decrease in fluorescence in both duration and intensity.

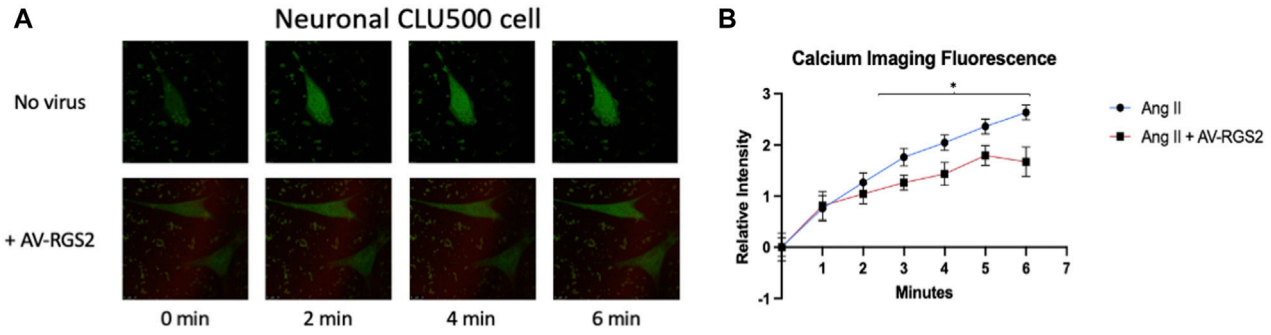

FIGURE 7
(A) The progression of fluorescence over 8 min in cells treated in DMEM with a final concentration of 1 mM ANG II, with/without AV-RGS2 transfection. **(B)** The calculated relative intensity compared to the baseline. Cells treated with AV-RGS2 showed a significant decrease in fluorescence in both duration and intensity. *n* = 3 per group. λ = 488 nm **p < 0.05 compared to the control (ANG II without AV-RGS2).*

Discussion

In this study, AV-RGS2 transfection to the PVN significantly attenuated the increase of mean arterial pressure in ANG II infusion rats from days 2–7 of the 2-week experiment. AV-RGS2 significantly decreased the serum norepinephrine concentration, 24-h urine norepinephrine excretion, and acute volume reflex. AV-RGS2 also increased daily urine volume, water consumption, and sodium excretion in ANG II-infused hypertensive rats. AV-RGS2 transfection within the PVN significantly lower the Gαq and PKC protein expressions within the PVN in ANG II infusion rats. In hypothalamic cells, AV-RGS2 attenuated ANG II-induced mRNA expression of Gαq, Gαs. We also found a attenuated calcium influx in ANG II-treated cells with AV-RGS2 transfection. This data supports the effects of RGS2 in the PVN on blood pressure, sympathetic outflow, and kidney function in hypertensive rats.

Various studies have shown the importance of G-proteins and their impact on cellular signaling (Sriram and Insel, 2018). Of the RGS protein family, RGS2 regulation has been shown to be an emerging target in multiple tissues for various pathologies (McNabb et al., 2020; O'Brien et al., 2019). It is important to investigate the actions of RGS proteins, specifically RGS2, on Gαq signaling. The activity of RGS2 on G-protein signaling and the cessation of cell signaling may be an important feature in the progression of blood pressure dysregulation. One study shows that a reduced expression of RGS2 within the placenta may contribute to the development of preeclampsia (Perschbacher et al., 2020). RGS2 is also shown to have a role in vascular function, with a reduced expression of RGS2 in the vasculature contributing to hypertension (Osei-Owusu and Blumer, 2015). Additionally, RGS2 maintains a role in renal hemodynamics and contributes to overall renal function (Osei-Owusu et al., 2015).

Other studies have mainly focused on the peripheral mechanisms of RGS2. Still, no studies have shown the central roles of RGS2 and how it impacts blood pressure regulation and kidney function through sympathetic activity modulation. With little to no studies being done on the RGS2 protein on G-protein signaling on the central mechanisms of blood pressure control, we view it as important to examine how these interactions affect sympathetic reflex and the progression of hypertension. Examining the neuronal activity with cell signaling cascade changes in blood pressure management between hypertensive and normotensive subjects may be a critical link needed to help better combat this condition.

We elected to use ANG II infusion to induce a hypertensive state in our rat model. We used ANG II infusion and PVN AV-RGS2 transfection rats in a second group. ANG II infusion quickly induced a hypertensive phenotype in this model. ANG II infusion rats with PVN AV-RGS2 transfection had significantly attenuated the increase of blood pressure compared to the ANG II group. This confirms that overexpression of RGS2 in the PVN attenuates the rise in blood pressure caused by ANG II. The attenuation of the increase of blood pressure in the PVN AV-RGS2 group also suggests that the PVN is a critical central nucleus regulating blood pressure, and RGS2 impacts blood pressure regulation within the PVN.

Our present study shows we can directly alter RGS2 mRNA expression with AV-RGS2 transfection in a rat model, confirmed by mRNA measurement and histological assessment. As expected with adenovirus transfection, there was an acute increase in mRNA expression of RGS2 after 3 days of transfection; then the RGS2 mRNA level gradually decreased over the next 2 weeks. The decreasing level of RGS2 might be because of the immune system clearing the adenovirus transfection. Our hemodynamic study showed that the AV-RGS2 transfection to the PVN significantly reduced mean arterial pressure in ANG II infusion rats in the first week of the 2-week ANG II infusion period. This was consistent with the mRNA study, showing the reduced efficacy of AV-RGS2 transfection after 7 days.

Studies suggest that the dysfunction of sympathetic modulation within the PVN contributes to fluid and electrolyte unbalance and kidney excretory dysfunction, which is seen in hypertension and chronic heart failure (Zheng et al., 2022). Our metabolic study showed urine output and water consumption were increased in the ANG II + AV-RGS2 combined treatment group compared to the ANG II infusion and control groups. This may be caused by an alteration in sympathetic activity from the AV-RGS2 transfection. One characteristic of hypertension is the conservation of sodium. In addition, we saw that daily urine excretion was significantly increased in the ANG II + AV-RGS2 combined treatment model, suggesting sodium retention was relieved by the introduction of AV-RGS2 in the PVN in hypertensive rats.

To examine sympathetic activity changes, 24-h urine norepinephrine excretion was examined. As expected, the

excretion rates showed that AV-RGS2 decreased overall norepinephrine excretion. Serum norepinephrine was significantly increased in the ANG II infusion model, which suggested alterations in sympathetic activity. To measure kidney function, urine and serum creatinine concentrations were evaluated and used to determine glomerular filtration. The trends suggest kidney function was improved with the ANG II and AV-RGS2 combined treatment compared to the ANG II infusion model. The data suggests a mild-to-moderate change in kidney function with AV-RGS2 transfection, which was expected as the upregulation of RGS2 impacted overall sympathetic activity and, thus, kidney function in ANG II-induced hypertension.

The PVN is a critical site for the coordination and integration of neurogenic and hormonal actions on the cardiovascular system and the kidney, in response to changes in blood volume (volume reflex) and sodium concentration/osmolality in the body. Several lines of evidence provide credence for the critical role of the parvocellular neurons of the PVN in the neural regulation of fluid balance (Li et al., 2003; Coote, 2005). The specific details of the pathways within the central nervous system and the specific neurotransmitter substances involved in the volume reflex arc have been investigated to some extent. In the experiment to evaluate volume reflex, we saw that the urine flow rate and sodium excretion rates were significantly increased in the ANG II infusion group compared to the control group. ANG II with AV-RGS2 transfection group had attenuated diuresis and natriuresis compared to the ANG II infusion group. These differences suggest that RGS2 alters volume reflex and ANG II-induced fluid responsiveness from the central nervous system.

Furthermore, we examined molecular interactions involving G-protein activation and the activation of downstream effector proteins. ANG II binds to a Gq-protein-coupled receptor, which RGS2 selectively regulates. G-protein activation triggers numerous responses throughout the organism. Gq-protein activates PKC and mobilizes Ca^{2+} by activating phospholipase C, which hydrolyzes PIP3, cleaving it into DAG and IP3 (Mizuno and Itoh, 2009). Gs-protein activates adenylate cyclase activity, which contributes to cAMP production, activating PKA. Gi-protein inhibits this pathway by inhibiting adenylate cyclase (Sassone-Corsi, 2012). This signaling cascade is an important factor of heightened cellular activity, causing several proteins to be transcribed relating to cell cycle progression, proliferation, growth factors, metabolism, neurotrophy, and cell survival (Wang et al., 2018). With G-proteins being present within all cell types, it is plain to see their vital role in cell signaling. Understanding brain G-protein subunits, specifically Gαq/Gαs, is important in how they are directed to alter sympathetic activation and cardiovascular parameters. With this, we elected to evaluate the changes in G-protein and downstream signaling in the PVN as we manipulated ANG II and RGS2.

Our PVN tissue protein analysis showed decreased changes in Gαq but not Gαs with AV-RGS2 transfection, further aiding our statement regarding RGS2 selectivity for Gq-protein interaction. As a downstream effector protein of Gq-protein activation, PKC significantly increased with ANG II infusion and decreased with AV-RGS2 transfection compared to the ANG II infusion group. This is expected as RGS2 returns to active Gαq to its inactive state, halting the downstream actions directly involving PKC. In addition, we evaluated changes in PKA, which is downstream of Gs-protein activation. No changes were present in PKA protein expression in the PVN.

To further examine the role of RGS2 on the ANG II-G-protein signaling in our mouse hypothalamic cell line, we found increased G-protein mRNA expression as ANG II treatment concentration increased. AV-RGS2 treatment reduced the G-protein mRNA expression induced by ANG II treatment. These *in vitro* studies further support that RGS2 interacts with G-proteins and returns them to an inactive state, halting the downstream signaling cascade expected with ANG II-G-protein activation. Further, ANG II acts on a signaling pathway that is expected to increase intracellular calcium, so we should expect an increase in calcium flux by adding ANG II. RGS2 should decrease the duration and intensity of calcium flux by limiting the action of ANG II by Gq-protein deactivation. We used confocal microscopy to measure calcium flux in cells treated with or without AV-RGS2 in response to ANG II. We have demonstrated that AV-RGS-treated cells had a significantly reduced fluorescence compared to those without AV-RGS2 treatment. This suggests an attenuation in calcium flux in the AV-RGS2 treated group, which is the expected result when Gq-protein activation time is decreased with increases in RGS2 protein.

Perspectives

Our results describe a novel role of RGS2 in the PVN for regulating blood pressure, sympathetic activation, and kidney function in hypertension. These findings show that the action of RGS2 on ANG II-induced Gq-protein activation modulates blood pressure, sympathetic activation, and kidney function in hypertension. Our study provides new insights into the central regulation of blood pressure and potential targets to treat hypertension.

Limitations and alternative approaches

Many factors influence the overall blood pressure control of an organism. In this study, we are investigating only few impacting factors of blood pressure regulation. In addition, among the receptors and proteins investigated, many isoforms and subtypes of these receptors have differing ligand-receptor interactions and downstream signaling. While between organisms, the tissue-specific receptors are generally conserved, there are subtle differences that may impact overall results. Further investigation is needed to better understand how acting of specific receptors or proteins can have off-target effects. The jump between rodent and human models of hypertension may contribute to a variation of results. Some models of hypertension do not accurately display a phenotype that can be characterized as essential hypertension, which may impact results, especially when comparing essential hypertension in humans.

Additional limitations include our use of an adenovirus as a vector, which has a higher immunogenic response in comparison to adeno-associated virus, which may contribute to unwanted physiological responses. We also used only male models, and thus, sex as a biological variable must be noted. Additional female subjects would have to be used to exclude sex as a biological variable in addition to ANG II infusion and AV-RGS2 transfection. In addition, we used daily sodium excretion from urine to assess sodium handling, while true sodium balance must take account for sodium intake. However, no

considerable changes in food intake were noted. Finally, we used some controls for our telemetry study, yet we did not have an ANG II infusion with AV-GFP control to determine vector impacts on ANGII infusion. These limitations will be considered in future studies.

Data availability statement

The original contributions presented in the study are included in the article/Supplementary Material, further inquiries can be directed to the corresponding author.

Ethics statement

All the procedures on animals were approved by the Institutional Animal Care and Use Committee of the University of South Dakota. The experiments were in accordance with the American Physiological Society and the National Institutes of Health Guide for the Care and Use of Laboratory Animals. The study was conducted in accordance with the local legislation and institutional requirements.

Author contributions

SB: Conceptualization, Data curation, Formal Analysis, Investigation, Methodology, Software, Writing–original draft, Writing–review and editing. XL: Conceptualization, Data curation, Formal Analysis, Investigation, Methodology, Software, Supervision, Writing–original draft. HZ: Conceptualization, Funding acquisition, Methodology, Project administration, Resources, Supervision, Validation, Visualization, Writing–review and editing.

Funding

The author(s) declare that financial support was received for the research, authorship, and/or publication of this article. This work was supported by funding from the National Institute of Health (R01-DK-129311), the GRISE fellowship from the National Institute of Health (T32GM-136503), and the Sanford School of Medicine at the University of South Dakota.

Acknowledgments

We want to acknowledge the personnel in the Animal Resource Center at USD for their contributions to the project and the assurance of the welfare of the animal models used throughout the study. We would also like to acknowledge Jessie Freeling in the Physiology Core at USD for her expertise and aid with surgical interventions. Additionally, we would like to thank Dr. Scott Pattison for his help with confocal imaging.

Conflict of interest

The authors declare that the research was conducted in the absence of any commercial or financial relationships that could be construed as a potential conflict of interest.

Publisher's note

Supplementary material

The Supplementary Material for this article can be found online at: https://www.frontiersin.org/articles/10.3389/fphys.2024.1401768/full#supplementary-material

References

Alshak, M. N., and Das, J. M. (2024). "Neuroanatomy, sympathetic nervous system," in *StatPearls* (Treasure Island (FL): StatPearls Publishing LLC).

Bill, C. A., and Vines, C. M. (2020). Phospholipase C. *Adv. Exp. Med. Biol.* 1131, 215–242. doi:10.1007/978-3-030-12457-1_9

Chobanian, A. V., Bakris, G. L., Black, H. R., Cushman, W. C., Green, L. A., Izzo, J. L., Jr., et al. (2003). Seventh report of the joint national committee on prevention, detection, evaluation, and treatment of high blood pressure. *Hypertension* 42 (6), 1206–1252. doi:10.1161/01.HYP.0000107251.49515.c2

Coote, J. H. (2005). A role for the paraventricular nucleus of the hypothalamus in the autonomic control of heart and kidney. *Exp. Physiol.* 90 (2), 169–173. doi:10.1113/expphysiol.2004.029041

Eguchi, S., Kawai, T., Scalia, R., and Rizzo, V. (2018). Understanding angiotensin II type 1 receptor signaling in vascular pathophysiology. *Hypertension* 71 (5), 804–810. doi:10.1161/hypertensionaha.118.10266

Ferguson, A. V., Latchford, K. J., and Samson, W. K. (2008). The paraventricular nucleus of the hypothalamus - a potential target for integrative treatment of autonomic dysfunction. *Expert Opin. Ther. Targets* 12 (6), 717–727. doi:10.1517/14728222.12.6.717

Frame, A. A., Carmichael, C. Y., and Wainford, R. D. (2016). Renal afferents. *Curr. Hypertens. Rep.* 18 (9), 69. doi:10.1007/s11906-016-0676-z

Freeman, E. J., and Tallant, E. A. (1994). Vascular smooth-muscle cells contain AT1 angiotensin receptors coupled to phospholipase D activation. *Biochem. J.* 304, 543–548. doi:10.1042/bj3040543

Fyhrquist, F., Metsärinne, K., and Tikkanen, I. (1995). Role of angiotensin II in blood pressure regulation and in the pathophysiology of cardiovascular disorders. *J. Hum. Hypertens.* 9 (5), S19–S24.

Guyenet, P. G., Stornetta, R. L., Souza, G., Abbott, S. B. G., and Brooks, V. L. (2020). Neuronal networks in hypertension: recent advances. *Hypertension* 76 (2), 300–311. doi:10.1161/hypertensionaha.120.14521

Kimple, A. J., Bosch, D. E., Giguère, P. M., and Siderovski, D. P. (2011). Regulators of G-protein signaling and their Gα substrates: promises and challenges in their use as drug discovery targets. *Pharmacol. Rev.* 63 (3), 728–749. doi:10.1124/pr.110.003038

Li, D. P., and Pan, H. L. (2017). Glutamatergic regulation of hypothalamic presympathetic neurons in hypertension. *Curr. Hypertens. Rep.* 19 (10), 78. doi:10.1007/s11906-017-0776-4

Li, Y. F., Mayhan, W. G., and Patel, K. P. (2003). Role of the paraventricular nucleus in renal excretory responses to acute volume expansion: role of nitric oxide. *Am. J. Physiol. Heart Circ. Physiol.* 285 (4), H1738–H1746. doi:10.1152/ajpheart.00727.2002

McNabb, H. J., Zhang, Q., and Sjögren, B. (2020). Emerging roles for regulator of G protein signaling 2 in (Patho)physiology. *Mol. Pharmacol.* 98 (6), 751–760. doi:10.1124/molpharm.120.000111

Mizuno, N., and Itoh, H. (2009). Functions and regulatory mechanisms of Gq-signaling pathways. *Neurosignals* 17 (1), 42–54. doi:10.1159/000186689

O'Brien, J. B., Wilkinson, J. C., and Roman, D. L. (2019). Regulator of G-protein signaling (RGS) proteins as drug targets: progress and future potentials. *J. Biol. Chem.* 294 (49), 18571–18585. doi:10.1074/jbc.REV119.007060

Osei-Owusu, P., and Blumer, K. J. (2015). Regulator of G Protein signaling 2: a versatile regulator of vascular function. *Prog. Mol. Biol. Transl. Sci.* 133, 77–92. doi:10.1016/bs.pmbts.2015.02.001

Osei-Owusu, P., Owens, E. A., Jie, L., Reis, J. S., Forrester, S. J., Kawai, T., et al. (2015). Regulation of renal hemodynamics and function by RGS2. *PLoS One* 10 (7), e0132594. doi:10.1371/journal.pone.0132594

Palkovits, M. (1983). Punch sampling biopsy technique. *Methods Enzymol.* 103, 368–376. doi:10.1016/s0076-6879(83)03025-6

Perschbacher, K. J., Deng, G., Sandgren, J. A., Walsh, J. W., Witcher, P. C., Sapouckey, S. A., et al. (2020). Reduced mRNA expression of RGS2 (regulator of G protein signaling-2) in the placenta is associated with human preeclampsia and sufficient to cause features of the disorder in mice. *Hypertension* 75 (2), 569–579. doi:10.1161/hypertensionaha.119.14056

Sassone-Corsi, P. (2012). The cyclic AMP pathway. *Cold Spring Harb. Perspect. Biol.* 4 (12), a011148. doi:10.1101/cshperspect.a011148

Sriram, K., and Insel, P. A. (2018). G protein-coupled receptors as targets for approved drugs: how many targets and how many drugs? *Mol. Pharmacol.* 93 (4), 251–258. doi:10.1124/mol.117.111062

Taylor, B. N., and Cassagnol, M. (2024). "Alpha-adrenergic receptors," in *StatPearls* (Treasure Island (FL): StatPearls Publishing LLC).

Vasudevan, N. T., Mohan, M. L., Goswami, S. K., and Naga Prasad, S. V. (2011). Regulation of β-adrenergic receptor function: an emphasis on receptor resensitization. *Cell Cycle* 10 (21), 3684–3691. doi:10.4161/cc.10.21.18042

Wang, H., Xu, J., Lazarovici, P., Quirion, R., and Zheng, W. (2018). cAMP response element-binding protein (creb): a possible signaling molecule link in the pathophysiology of schizophrenia. *Front. Mol. Neurosci.* 11, 255. doi:10.3389/fnmol.2018.00255

Wu, C. Y., Hu, H. Y., Chou, Y. J., Huang, N., Chou, Y. C., and Li, C. P. (2015). High blood pressure and all-cause and cardiovascular disease mortalities in community-dwelling older adults. *Med. Baltim.* 94 (47), e2160. doi:10.1097/md.0000000000002160

Zhang, D. Y., and Anderson, A. S. (2014). The sympathetic nervous system and heart failure. *Cardiol. Clin.* 32 (1), 33–45. doi:10.1016/j.ccl.2013.09.010

Zheng, H., Katsurada, K., Nandi, S., Li, Y., and Patel, K. P. (2022). A critical role for the paraventricular nucleus of the hypothalamus in the regulation of the volume reflex in normal and various cardiovascular disease states. *Curr. Hypertens. Rep.* 24 (7), 235–246. doi:10.1007/s11906-022-01187-4

frontiers | Frontiers in Physiology

TYPE Original Research
PUBLISHED 22 July 2024
DOI 10.3389/fphys.2024.1401774

OPEN ACCESS

EDITED BY
Rohit Ramchandra,
The University of Auckland, New Zealand

REVIEWED BY
Ibrahim M. Salman,
Case Western Reserve University, United States
Gary C. Mouradian,
Medical College of Wisconsin, United States

*CORRESPONDENCE
Han-Jun Wang,
hanjunwang@unmc.edu

RECEIVED 15 March 2024
ACCEPTED 08 July 2024
PUBLISHED 22 July 2024

CITATION
Kamra K, Zucker IH, Schultz HD and Wang H-J (2024), Chemoreflex sensitization occurs in both male and female rats during recovery from acute lung injury.
Front. Physiol. 15:1401774.
doi: 10.3389/fphys.2024.1401774

Chemoreflex sensitization occurs in both male and female rats during recovery from acute lung injury

Kajal Kamra[1,2], Irving H. Zucker[1], Harold D. Schultz[1] and Han-Jun Wang[1,2]*

[1]Department of Cellular and Integrative Physiology, University of Nebraska Medical Center, Omaha, NE, United States, [2]Department of Anesthesiology, University of Nebraska Medical Center, Omaha, NE, United States

Introduction: Sex-specific patterns in respiratory conditions, such as asthma, COPD, cystic fibrosis, obstructive sleep apnea, and idiopathic pulmonary fibrosis, have been previously documented. Animal models of acute lung injury (ALI) have offered insights into sex differences, with male mice exhibiting distinct lung edema and vascular leakage compared to female mice. Our lab has provided evidence that the chemoreflex is sensitized in male rats during the recovery from bleomycin-induced ALI, but whether sex-based chemoreflex changes occur post-ALI is not known. To bridge this gap, the current study employed the bleomycin-induced ALI animal model to investigate sex-based differences in chemoreflex activation during the recovery from ALI.

Methods: ALI was induced using a single intra-tracheal instillation of bleomycin (bleo, 2.5 mg/Kg) (day 1). Resting respiratory frequency (f_R) was measured at 1-2 days pre-bleo, day 7 (D7) post-bleo, and 1 month (1 mth) post-bleo. The chemoreflex responses to hypoxia (10% O_2, 0% CO_2) and normoxic-hypercapnia (21% O_2, 5% CO_2) were measured before bleo administration (pre-bleo) and 1 mth post-bleo using whole-body plethysmography. The apnea-hypopnea Index (AHI), post-sigh apneas, and sighs were measured at each time point.

Results: There were no significant differences in resting f_R between male and female rats at the pre-bleo time point or in the increase in resting f_R at D7 post-bleo. At 1 mth post-bleo, the resting f_R was partially restored in both sexes but the recovery towards normal ranges of resting f_R was significantly lower in male rats. The AHI, post-sigh apneas, and sighs were not different between male and female rats pre-bleo and 1 mth post-bleo. However, at D7 post-bleo, the male rats exhibited a higher AHI than female rats. Both male and female rats exhibited a sensitized chemoreflex in response to hypoxia and normoxic-hypercapnia with no significant differences between sexes.

Conclusion: A sex difference in resting ventilatory parameters occurs post ALI with a prolonged increase in resting f_R and larger AHI in male rats. On the other hand, we did not find any sex differences in the chemoreflex sensitization that occurs at 1 mth post-bleo. This work contributes to a better understanding of sex-based variations in lung disorders.

KEYWORDS

acute respiratory distress syndrome, acute lung injury, bleomycin, chemoreflex, sex-based differences

1 Introduction

In studies involving vertebrate animals and humans, the consideration of "sex" as a critical biological variable is essential throughout the design, analysis, and reporting of research (Lee, 2018). Sex-related differences in lung development are apparent throughout life, affected by factors like variations in lung growth and maturity, as well as the influence of sex hormones (Carey et al., 2007; Silveyra et al., 2021). Pulmonary diseases such as respiratory distress syndrome, bronchiolitis, pneumonia, chronic obstructive pulmonary disease (COPD), obstructive sleep apnea (OSA), and the SARS-CoV-2 epidemic have reported sex differences (Silveyra et al., 2021).

Acute lung injury (ALI) and its severe form, acute respiratory distress syndrome (ARDS) caused by the disruption of the normal capillary endothelial barrier leads to impacting ventilatory control (Young et al., 2019). Acute respiratory failure, responsible for 10% of ICU admissions with significant mortality and morbidity, affects approximately 200,000 new cases annually in the US alone (Mowery et al., 2020). Epidemiological research on sex differences in all-cause ARDS presents contradictory findings, with some studies indicating a substantial correlation between ARDS incidence, mortality, and sex (Moss and Mannino, 2002; Agarwal et al., 2006; Phua et al., 2009; Lemos-Filho et al., 2013; Chen et al., 2015). Structural and functional variations in lung and airway development, influenced by genetic, epigenetic, hormonal, and environmental factors, contribute to these disparities (Silveyra et al., 2021). Notably, pre-term birth in males is associated with a greater disadvantage (Bancalari and Jain, 2019). Sex hormones, particularly testosterone and estrogen, play a role in influencing immune-related cells, macrophage polarization, airway smooth muscle cells, and inflammation (Becerra-Díaz et al., 2018). Clinical studies show that male infants are more susceptible to lower respiratory tract infections, bronchiolitis, respiratory distress syndrome, and bronchopulmonary dysplasia (Liptzin et al., 2015). In contrast, male children are more prone to asthma, while women exhibit a higher exacerbation risk in chronic obstructive pulmonary disease (COPD) and a lower likelihood of obstructive sleep apnea (OSA) compared to men (Han et al., 2018). Sex differences have also been studied in different models of ALI by several groups. Most importantly, all those studies focused on lung pathology post-ALI. A potential sex difference in the neural control of breathing post-ALI has not been investigated.

Carotid bodies (CBs), peripheral chemoreceptors found at the common carotid artery bifurcation, are stimulated by hypoxemia brought on by ALI. As a basic defensive response to return blood gas concentrations to normal, these chemoreceptors detect changes in pH and blood gas levels. The enhancement of sympathetic drive by acute or chronic CB activation is a well-established phenomenon. Excessive sympathetic output can cause cardiac arrhythmias, cardio-renal syndrome, metabolic syndrome, Type 2 diabetes, and impaired cardiac activity (Mark, 1995; Marcus et al., 2014; Moreira et al., 2015; Li, 2022). Previously, our laboratory has provided evidence of increased chemosensitivity during recovery from ALI in male rats (Kamra et al., 2022). Nevertheless, there remains a knowledge gap regarding the comparisons of male *vs.* female chemoreflex changes during the recovery from ALI. The current study utilizes a bleomycin-induced ALI animal model to investigate sex-based differences in chemoreflex activation under ALI conditions.

2 Methods

2.1 Ethical approval

Animals were housed in a temperature-controlled environment (22°C–25°C) with a 12 h light-dark cycle and *ad libitum* access to food and water, by standards set by the National Institutes of Health Guidelines for the Care and Use of Laboratory Animals. All experimental protocols were approved by the Institutional Animal Care and Use Committee (IACUC) of the University of Nebraska Medical Center (protocol ID no. 17-006-03 FC).

2.2 Animals

Eighteen adult (eight male and ten female) Sprague-Dawley rats (2 - 3 months old) were used for these experiments. They were allowed to acclimate for 3 days to their new environment before the experiment. All animal experimentation (collection of ventilatory parameters during rest and hypoxic/hypercapnic gas exposure) was performed during the day (9:00–16:00 h). Delivery of bleomycin sulfate (bleo) was performed within the Department of Comparative Medicine. At the end of the experimental protocol, all animals were humanely euthanized with an overdose of pentobarbital sodium (150 mg/kg, IV). Euthanasia was confirmed by the removal of vital organs. An experimental timeline is shown in Figure 1.

2.3 Drugs and chemicals

Bleo was purchased from Enzo Life Sciences (New York, United States). Bleo was dissolved in saline for intra-tracheal administration. This procedure was performed within the Department of Comparative Medicine.

2.4 Rat model of lung injury

Rats were randomized into two experimental groups and evaluated at three time points- 1-2 days before instillation (pre-bleo), day 7 (D7) post-bleo, and 1 month (1 mth) post-bleo instillation as follows: male bleo-treated rats (n = 8) and female bleo-treated rats (n = 10). Bleo (2.5 mg/kg) was instilled on day 0 intratracheally under 2% - 3% isoflurane anesthesia.

2.5 Breathing and ventilatory chemoreflex function

Unrestrained whole-body plethysmography was utilized to measure ventilatory parameters-respiratory rate (f_R), tidal volume (V_t) and minute ventilation (V_E) in conscious rats by using signals from a differential-pressure transducer (DLP 2.5, Harvard Apparatus), amplified, and connected to a PC via an acquisition system (PowerLab 35 Series) managed by LabChart (v8.1.5) software (ADInstruments, Colorado Springs, United States). Rats were acclimated to the plethysmograph chamber for 1 h each for two consecutive days before

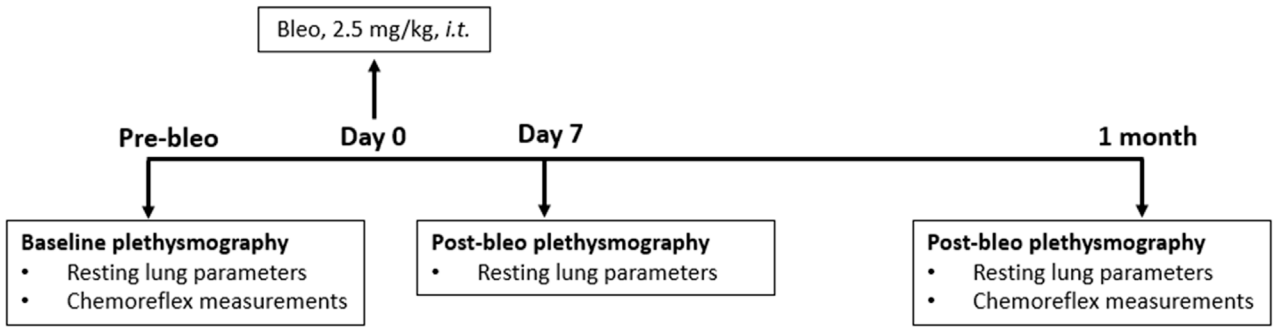

FIGURE 1
Timeline showing the experimental design.

TABLE 1 Mean body weight and mean change in body weight (in grams) for male and female dose bleo rats.

	Body weight (grams)		
	W0 pre-bleo	Day 7 post-bleo	1 mth post-bleo
Male rats (n = 8)	410 ± 59	394 ± 63	510 ± 47 **
Female rats (n = 10)	187 ± 27	175 ± 17	243 ± 19 **

Values are mean ± SD; Bleo indicates bleomycin. **$p < 0.0001$ *vs.* W0 (Week 0) pre-bleo.

recordings. Respiratory parameters were not recorded during the acclimatization sessions. The plethysmography chambers used for this study were custom-made (Midwest Plastics Inc., Nebraska, United States) and were 10, 10.5, and 20 cm in height, width, and length, respectively. The volume channel (i.e., flow integration) was calibrated by pushing 5 mL of air using a syringe before the start of the recording. During recordings, a constant flow of gas at 3 L/min was maintained to avoid an increase in humidity, temperature, and CO_2 levels using a manually operated flow meter (Precision Medical, Northampton, PA, United States). The body weight (in grams) of rats was recorded before each experiment. In the resting state, rats were exposed to normoxia (21% O_2, 0% CO_2) for baseline measurements followed by two different gas challenges-hypoxia (10% O_2, 0% CO_2) and normoxic hypercapnia (21% O_2, 5% CO_2) balanced by N_2. The order of the gas challenge was randomized and was maintained for 5 minutes. The last 1-min-long segment without any artifacts was used for analysis. A normoxic exposure of a minimum of 10 min or more was used in between challenges. All resting ventilatory parameters considered for analysis were recorded when the rats were awake and stationary (no activity-related events were included in the analysis in the LabChart8 raw data file). V_E was calculated as the product of f_R and V_t. V_t and V_E were normalized to body weight. All data values were extracted from LabChart8 raw data files. A 30-min recording without artifacts was recorded for all rats while they breathed room air. This was used to measure all resting ventilatory parameters and to manually extract apneas, hypopneas, sighs, and post-sigh apneas from LabChart 8 raw data files. Apneas were defined as the cessation of breathing for at least three respiratory cycles, as determined by the respiratory rate for the prior 10 s; hypopneas were defined as reductions in breath amplitude 50% of the average cycle amplitude of the preceding 10 s of regular breathing; post-sigh apneas were defined as the cessation of breathing for at least three respiratory cycles immediately after a sigh. Apneas and hypopneas were expressed as Apnea-Hypopnea Index (AHI, events/hour). Sighs and post-sigh apneas were also expressed as events/hour.

2.6 Statistical analysis

Data analysis in text, tables, and figures are presented as mean ± SD. Statistical evaluation was analyzed using GraphPad Prism (GraphPad Software, San Diego, CA. Version 8). For the chemoreflex comparisons, two-way ANOVA with Bonferroni corrections (male vs. Female and Pre-Bleo vs. Post-Bleo) was used with $p \leq 0.05$ being statistically significant. Body weight and baseline respiratory parameters at multiple time points post-Bleo were compared by using two-way Repeated Measurement (RM) ANOVA with $p \leq 0.05$ being statistically significant.

3 Results

3.1 Effect of bleomycin on body weight in male and female rats post-ALI

Body weights were measured in all rats at pre-bleo administration and post-bleo administration at D7 and 1 mth. Body weight did not change in either male or female rates during the first 7 days post-bleo (Table 1). At 1-mth post-bleo, male and female rats significantly increased body weight by 99 ± 74 g ($p < 0.0001$) and 56 ± 24 g, $p < 0.0001$), respectively (Table 1).

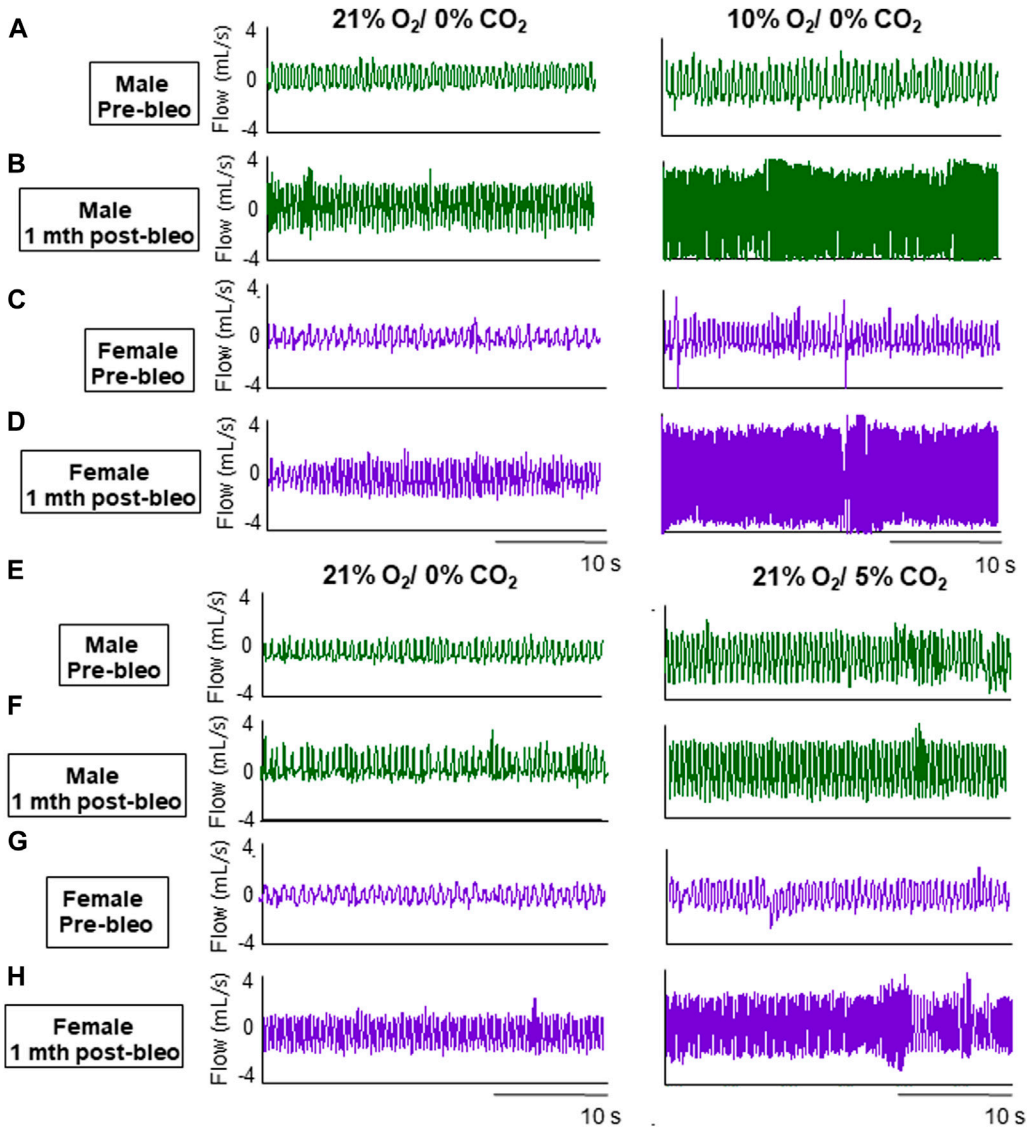

FIGURE 2
Representative ventilator tracings at normoxia, 10% hypoxia, and 5% normoxic-hypercapnia were obtained in a male and a female rat.

3.2 Sex-based differences in baseline respiratory parameters between male and female rats post-ALI

As noted in Figures 2A, C, E, G, male and female rats showed a steady normal resting f_R pattern pre-bleo with average f_R similar between groups (male rats = 95 ± 15 bpm; female rats = 86 ± 11 bpm (Table 2). However, as expected, consistent with our previously published data, both male (280 ± 70 bpm, $p < 0.0001$) and female (240 ± 43 bpm, $p < 0.0001$) rats exhibited a significant increase in resting f_R post-bleo treatment at D7 after receiving bleo compared to the pre-bleo time point (Table 2). This increase in f_R was partially restored at 1 mth post-bleo treatment in both groups (male = 141 ± 44 bpm ($p = 0.0004$, D7 *vs.* 1 mth post-bleo) and female = 104 ± 23 bpm ($p < 0.0001$, D7 *vs.* 1 mth post-bleo) (Table 2; Figures 2B, D, F, H). The comparison of f_R between male and female rats at 1 mth post-bleo time point was significantly different ($p = 0.03$) with male rats having a higher resting f_R than female rats (male *vs.* female: 141 ± 44 bpm *vs.* 104 ± 23 bpm). In male rats, the V_t and V_E were significant differences in D7 post-bleo when compared to pre-bleo time points. The female group also showed no significant differences in $V_{t,}$ however, V_E was significantly increased at D7 post-bleo and 1 mth-post-bleo when compared to pre-bleo ($p < 0.0001$, female rats: pre-bleo *vs.* D7 post-bleo).

3.3 Sex-based differences in the occurrence of apneic events between male and female rats post ALI

The 30-minute-raw data recorded during normoxic gas exposure were utilized to manually extract apneas from male and female rats at three time points-pre-bleo, D7 post-bleo, and 1 mth post-bleo. Male and female rats showed a significant difference

TABLE 2 Mean resting ventilatory parameters for male and female bleo rats.

		Male rats (n = 8)	Female rats (n = 10)
Resting f_R (BPM)	Pre-bleo	95 ± 15	86 ± 11
	D7 post-bleo	280 ± 70 ***	240 ± 43 ***
	I-mth post-bleo	141 ± 44 $ *	104 ± 23
Resting V_t (mL/Kg)	Pre-bleo	0.45 ± 0.15	0.63 ± 0.27
	D7 post-bleo	0.31 ± 0.1 $$ **	0.57 ± 0.18
	I-mth post-bleo	0.38 ± 0.05 $$$	0.75 ± 0.19
Resting V_E (mL/min/Kg)	Pre-bleo	40 ± 9.8	50 ± 27.6
	D7 post-bleo	85 ± 27 $$ **	143 ± 52 ***
	I-mth post-bleo	57 ± 20.76	74 ± 24 *

Values are mean ± SD; bleo indicates bleomycin. $ (all time points *vs.* pre-bleo); * (Male *vs.* Female rats).

($p = 0.02$) in the occurrence of apneas throughout the experimental timeline. The changes pre- and post-bleo were also seen to be significantly different ($p = 0.002$) (Figure 3A).

The post-sigh apneas were significantly different between male vs. female rats ($p = 0.02$). These differences however were not seen to be affected by bleo treatment (pre-vs. post-bleo, $p = 0.08$) (Figure 3B). The occurrence of sighs did not change significantly at all three time points for either sex and for pre-vs. post-bleo, revealing no sex differences for sighs during the acute and recovery phase of ALI (Figure 3C).

3.4 Sex-based differences in the chemoreflex sensitivity between male and female rats during the recovery from ALI

The chemoreflex responses to 10% hypoxia and 5% normoxic-hypercapnia were assessed by measuring the absolute difference between 21% O_2/0% CO_2 and 10% O_2/0% CO_2 or 21% O_2/5% CO_2-induced responses. At pre-bleo, both male and female rats exhibited similar increases in f_R and V_E in response to 10% hypoxia (Figures 4A, C, E). At 1 mth post-bleo, there was a significant increase in chemosensitivity (Figures 4B, F) with no differences in chemoreflex activation between male *vs.* female groups of rats (Figures 4B, F). The changes in V_t in response to 10% hypoxia were not statistically significant for either male *vs.* female groups of rats (Figures 4C, D).

Similarly, in response to 5% normoxic-hypercapnia, both male and female rats showed similar changes in f_R and V_E at pre-bleo time points (Figures 5A, E). Like 10% hypoxia, both groups showed a significant increase in chemoreflex activation at 1 mth post-bleo with no difference between sexes (Figures 5B, F). The changes in V_t in response to 5% normoxic-hypercapnia were not statistically significant for either male *vs.* female groups of rats (Figures 5C, D).

4 Discussion

In this study, we examined the resting breathing parameters (f_R, AHI, sighs, post sigh apneas) during both the acute phase (D7) and recovery phase (1 mth) of ALI, and the chemoreflex sensitization during the recovery from ALI in male and female rats. The key findings of this study are summarized as follows: 1) There were no significant differences in the resting breathing parameters (f_R, AHI, sighs, post sigh apneas) between male and female rats. At the D7 post-bleo, resting f_R was significantly increased in both male and female rats but tended to increase by a larger degree in male rats. At 1 mth post-bleo, the resting f_R was partially restored in both sexes but the recovery towards normal ranges of resting f_R was significantly lower in male rats. At D7 post-bleo, the males exhibited significantly more events/hour of AHI compared to females. 2) At the pre-bleo time point, both male and female groups showed similar chemoreflex responses in f_R to 10% hypoxia and 5% normoxic-hypercapnia. During recovery from ALI at 1 mth post-bleo, the chemoreflex sensitivity in response to hypoxia and normoxic-hypercapnia did not exhibit sex-based differences.

Animal models, such as the two-hit model involving acid instillation followed by overventilation, have provided histological evidence of sex differences in ALI, with male mice exhibiting distinct lung edema and vascular leakage compared to female mice (Erfinanda et al., 2021). Another study observed higher levels of airway inflammation and hyperresponsiveness in male mice (Carey et al., 2007). Lingappan et al. investigated sex-specific differences in lung injury induced by hyperoxic exposure in neonate mice (Lingappan et al., 2016). They found that male neonate mice exhibited a greater cytokine response and pulmonary angiogenesis arrest compared to females (Lingappan et al., 2016). They observed similar patterns in adult male mice compared to females (Lingappan et al., 2016). On the other hand, several other studies from LPS-induced ALI models showed no significant sex difference in lung pathology. For instance, Nguyen et al. reported no differences in pulmonary injury and abnormal lung development between male and female mice exposed to early postnatal systemic LPS challenge (Nguyen et al., 2019). They also reported findings that suggest a similar innate response to early neonatal LPS exposure and the resulting pulmonary sequelae in male and female mice (Nguyen et al., 2019). Another study demonstrated no sex-based differences in LPS-induced TLR4 expression in the adult rat lung (Du et al., 2005).

A previous study from our lab using a bleo-induced ALI adult rat model demonstrated a significant increase in resting f_R in male ALI rats at D7 post-bleo administration (Kamra et al., 2022). The present study demonstrated no significant difference in this

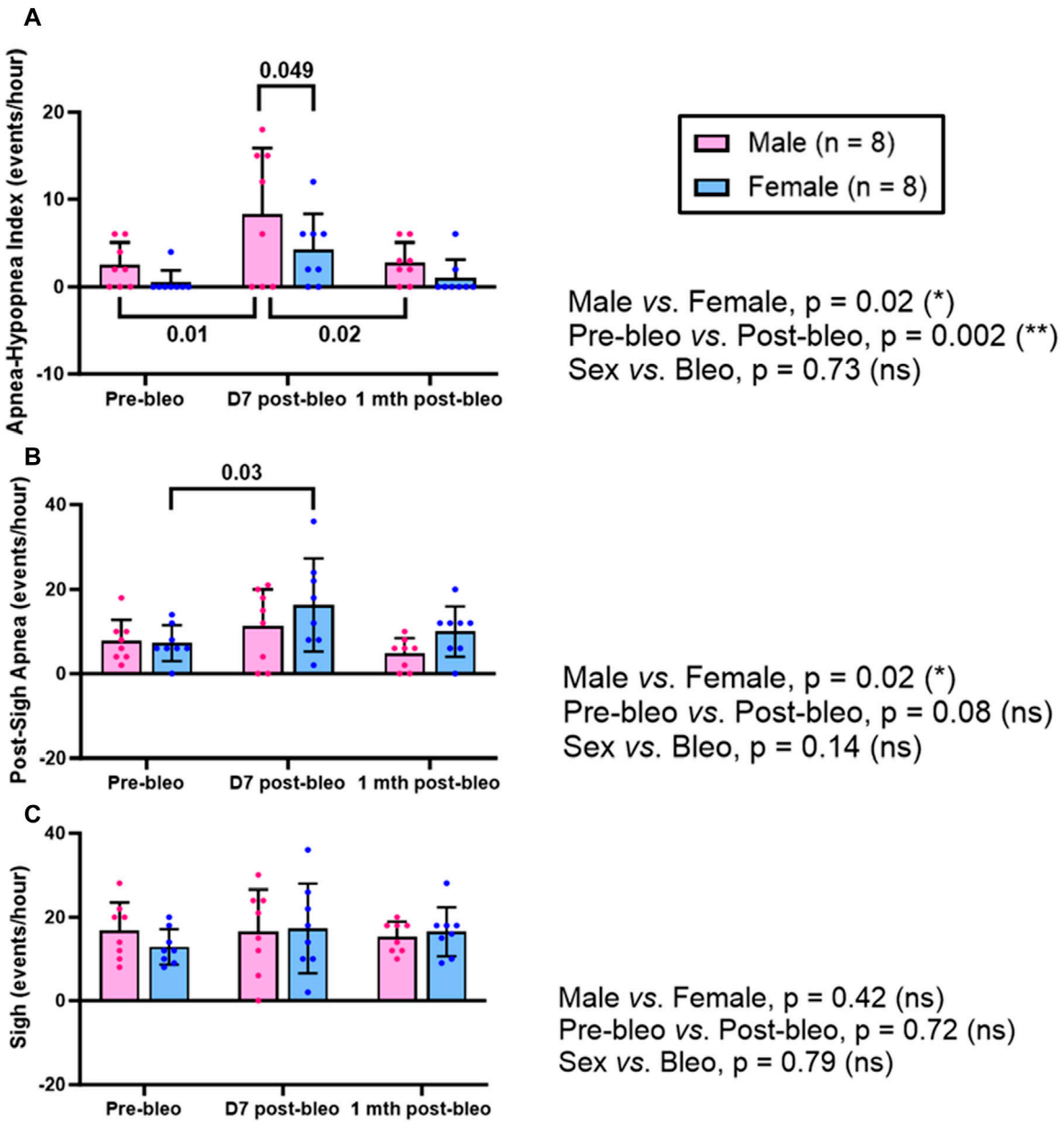

FIGURE 3
Effects of sex, bleomycin (pre-*vs.* post-bleo) and the interaction between the sex and treatment for **(A)** Apnea-hypopnea index (AHI), **(B)** Post-sigh apnea occurrence, and **(C)** Sigh occurrence in male (n = 8) and female (n = 8) rats. Two-way ANOVA, repeated measures, Values are mean ± SD.

increase in resting f_R at D7 post-bleo between male and female rats. However, a trend of comparatively higher resting f_R was seen in adult male ALI rats at D7 post-bleo compared to female ALI rats. More importantly, the recovery from increased resting f_R in male rats at 1 mth post-bleo was significantly slower than in female rats. This may be due to the protective effects of female sex hormones (Speyer et al., 2005; Carey et al., 2007; Erfinanda et al., 2021). It is known that female neonate mice demonstrated a better antioxidant defense mechanism against hyperoxia-induced reactive oxygen species (ROS) (Vento et al., 2009; Tondreau et al., 2012). Estrogen's antioxidant, vasodilatory, and anti-inflammatory properties contribute to a lower risk of cardiovascular diseases in females (Xiang et al., 2021).

In addition, we also documented a significant increase in the occurrence of apneas and hypopneas in male ALI rats at the D7 post-bleo time point. This increase was significantly increased in male rats at this time point compared to female bleo rats that also exhibited a trend towards higher apneic incidences. The post-sigh apneas were significantly higher at D7 post-bleo in female rats while the male rats exhibited a trend to show an increase. Consistent with our AHI data, clinical evidence also suggests that obstructive sleep apnea is documented to be higher in males than in females (Lin et al., 2008). In our study, we see this significant increase in apneic events at the D7 post-bleo time point as lung injury is at its peak during this period, after the first and only insult of bleo (Kamra et al., 2022). It is known that the

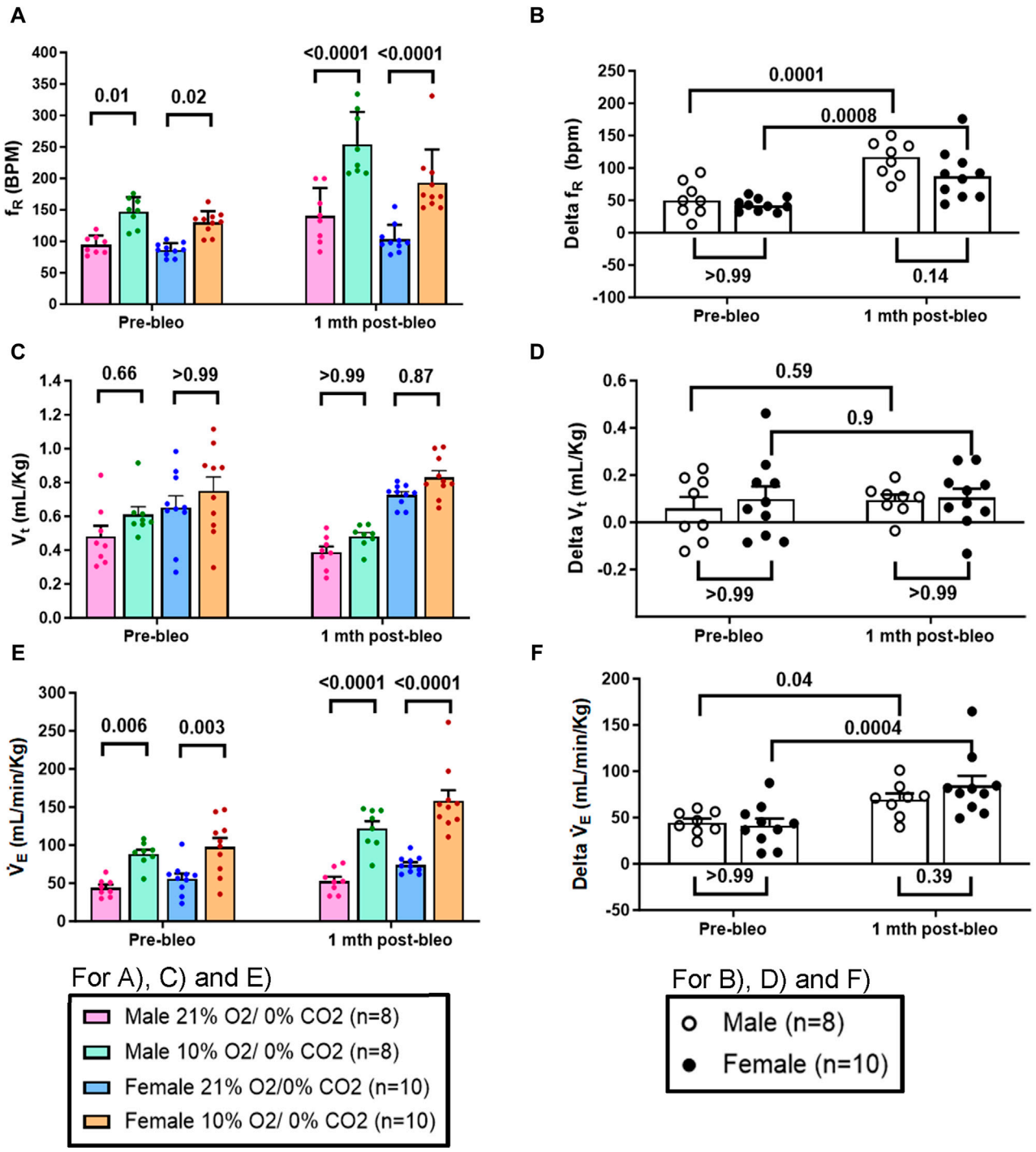

FIGURE 4
Effect of bleomycin on ventilatory parameters in male (n = 8) and female (n = 10) rats in response to chemoreflex activation with 10% O2/0% CO2. Two-way ANOVA, Values are mean ± SD: **(A)** Respiratory rate (f_R) at normoxia *vs.* hypoxia; **(B)** Delta f_R (Delta is the absolute difference between the response at normoxia and hypoxia); **(C)** Tidal volume (V_t) at normoxia *vs.* hypoxia; **(D)** Delta V_t; **(E)** Minute ventilation ($\dot{V}_E$) at normoxia *vs.* hypoxia; **(F)** Delta $\dot{V}_E$.

occurrence of apneas and hypopneas are among many factors associated with increased sympathetic nerve activity, inflammation, and intermittent hypoxia, and may be caused by respiratory control instability (Javaheri et al., 2017).

Previously, we reported evidence of enhanced chemoreflex response to hypoxia and normoxic-hypercapnia in the recovery phase (1 mth post-bleo) in male ALI rats (Kamra et al., 2022). However, a potential sex difference in chemoreflex sensitivity during the recovery of ALI was not examined. The data from the present study in male and female rats corroborate the findings from our previous study in male ALI rats of chemoreflex sensitization with recovery from ALI. We now show no statistically significant

10.3389/fphys.2024.1401774

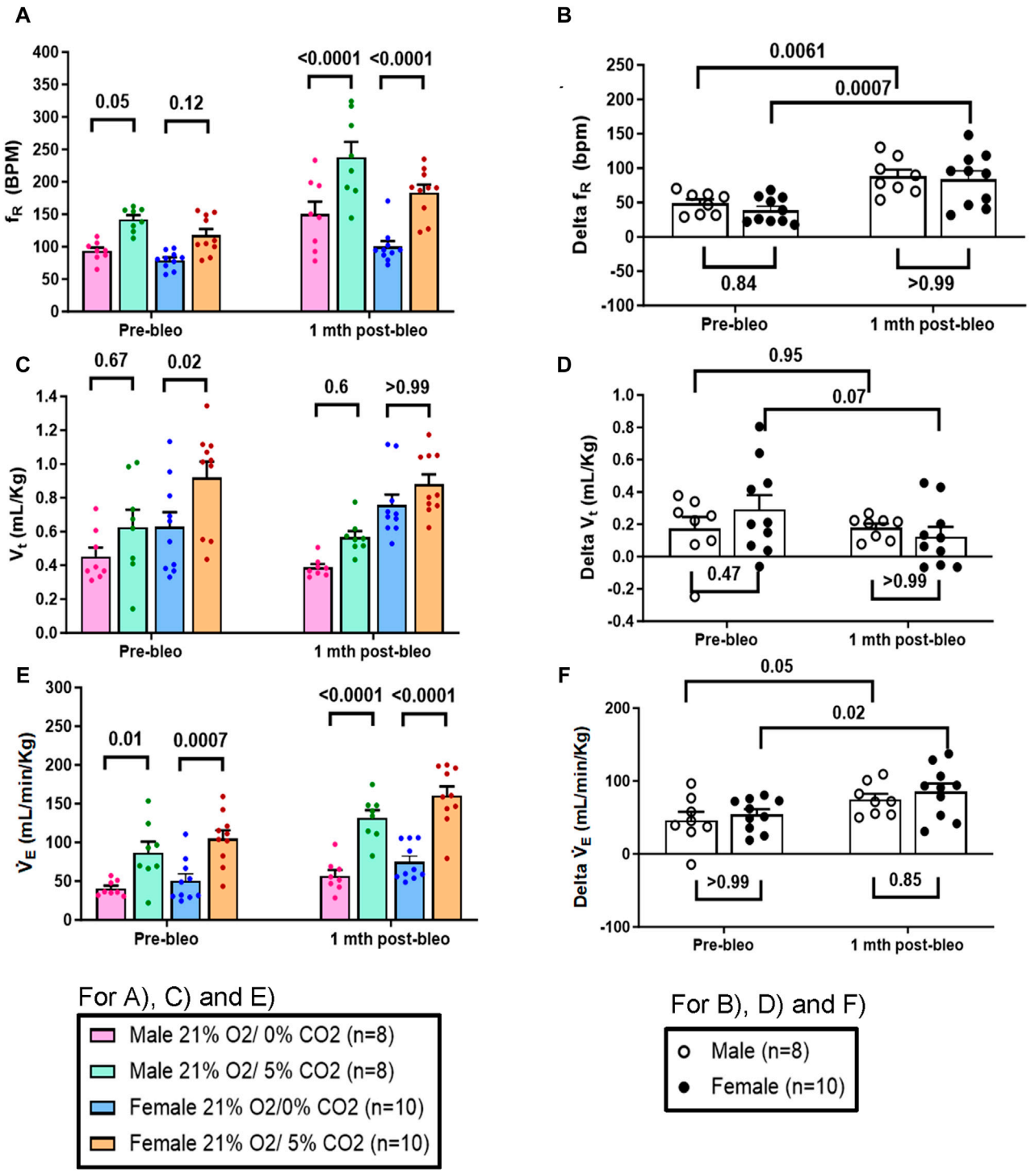

FIGURE 5
Effect of bleomycin on ventilatory parameters in male (n = 8) and female (n = 10) rats in response to 21% O2/5% CO2. Two-way ANOVA, Values are mean ± SD: **(A)** Respiratory rate (f_R) at normoxia *vs.* normoxic-hypercapnia; **(B)** Delta f_R (Delta is the absolute difference between the response at normoxia and normoxic-hypercapnia); **(C)** Tidal volume (V_t) at normoxia *vs.* normoxic-hypercapnia; **(D)** Delta V_t; **(E)** Minute ventilation (V_E) at normoxia *vs.* normoxic-hypercapnia; **(F)** Delta V_E.

differences in chemoreflex sensitization in male vs. female rats during the recovery of ALI.

Supportive evidence of no sex differences in chemosensitivity was presented by Usselman et al. who examined the effect of sex on chemoreflex regulation of muscle sympathetic nerve activity in young healthy men and women who were not using any form of hormonal contraception (Usselman et al., 2015). They observed similar sympathetic responses to chemoreflex activation in men and women (Usselman et al., 2015). Interestingly, in rats exposed to CIH, another study showed there are sex differences in respiratory-related

sympathetic nerve discharge that characterize differences in the respiratory modulation of sympathetic activity after CIH (Souza et al., 2018).

Independent of sex hormones, these data in juvenile rats (Souza et al., 2018) demonstrate sexual dimorphism in the reconfiguration of respiratory and pre-sympathetic network interactions after CIH (Souza et al., 2018). It is interesting to note that in the current study, at 1 mth post-bleo, the recovery of resting f_R was significantly faster in female bleo rats than in male bleo rats. The generation of resting f_R is controlled both by intrinsic respiratory drive and thoracic neural receptors. It is possible that in the case of female bleo-rats, the female sex hormone exhibited protective effects in the reflexes controlling the resting f_R generation (Behan et al., 2003; Zhang et al., 2020). However, at the same time point (1 mth post-bleo), we note that the chemoreflex activation in response to both hypoxia and normoxic-hypercapnia was not different between the sexes. The peripheral and central chemoreceptors contribute to the integrated receptor input in the pons and medulla to modify the generation of rhythmic breathing during non-normoxic conditions. The effect of sex hormones on these chemoreceptors and whether estrogen has any protective effects on the respiratory rhythm generator is not well understood. It is noteworthy that sex-based differences in chemoreflex were not measured at the D7 post-bleo timepoint in the current study. According to our earlier research, male rats with moderate ALI tend to exhibit a significantly blunted chemoreflex response to hypoxia or normoxic-hypercapnia at this timepoint, whereas those with severe ALI generally have a more sensitive chemoreflex response (Kamra et al., 2022). The reasons for this disparity in chemoreflex sensitivity between male rats with moderate and severe ALI at D7—blunted versus sensitized—remain unclear. However, we observed that during the ALI recovery period, or 1-month post-ALI, both moderate and severe ALI rats developed a sensitized chemoreflex. Given that both moderate and severe ALI rats showed consistent chemoreflex sensitization at this chronic time window, we chose to focus on the recovery period in the current study due to the complex changes in chemoreflex sensitivity between these groups at the D7 post-ALI timepoint.

5 Conclusion

In conclusion, our study highlighted noteworthy sex differences in terms of resting f_R, with a pronounced increase observed in males at the 1 mth post-bleo time point. Moreover, sex-specific variations were identified in acute AHI (at the D7 post-bleo), emphasizing the importance of sex as a determinant in respiratory responses. Interestingly, the chemoreflex response exhibited consistency across sexes during both pre-bleo and recovery from ALI (1-mth post-bleo). These findings point to a need for a broader understanding of sex-based variations in lung disorders and underscore the importance of considering sex as a crucial factor in respiratory research. Further exploration of these mechanisms is warranted to advance our knowledge and refine therapeutic strategies tailored to the unique aspects of male and female respiratory physiology.

Data availability statement

The raw data supporting the conclusions of this article will be made available by the authors, without undue reservation.

Ethics statement

The animal study was approved by the Institutional Animal Care and Use Committee (IACUC) of the University of Nebraska Medical Center. The study was conducted in accordance with the local legislation and institutional requirements.

Author contributions

KK: Data curation, Investigation, Methodology, Project administration, Validation, Writing–original draft, Writing–review and editing. IZ: Conceptualization, Methodology, Supervision, Writing–review and editing. HS: Conceptualization, Methodology, Supervision, Writing–review and editing. H-JW: Conceptualization, Funding acquisition, Investigation, Methodology, Project administration, Resources, Supervision, Visualization, Writing–review and editing.

Funding

The author(s) declare that financial support was received for the research, authorship, and/or publication of this article. This study was supported by NIH grant R01 HL-152160-01 and in part, by NIH grants R01 HL171602-01, HL-169205-01 and R21 HL170127-01. HW is also supported by Margaret R. Larson Professorship in Anesthesiology. IZ is supported, in part, by the Theodore F. Hubbard Professorship for Cardiovascular Research.

Conflict of interest

The authors declare that the research was conducted in the absence of any commercial or financial relationships that could be construed as a potential conflict of interest.

The author(s) declared that they were an editorial board member of Frontiers, at the time of submission. This had no impact on the peer review process and the final decision.

Publisher's note

References

Agarwal, R., Aggarwal, A. N., Gupta, D., Behera, D., and Jindal, S. K. (2006). Etiology and outcomes of pulmonary and extrapulmonary acute lung injury/ARDS in a respiratory ICU in North India. *Chest* 130 (3), 724–729. doi:10.1378/chest.130.3.724

Bancalari, E., and Jain, D. (2019). Bronchopulmonary dysplasia: 50 years after the original description. *Neonatology* 115 (4), 384–391. doi:10.1159/000497422

Becerra-Díaz, M., Strickland, A. B., Keselman, A., and Heller, N. M. (2018). Androgen and androgen receptor as enhancers of M2 macrophage polarization in allergic lung inflammation. *J. Immunol.* 201 (10), 2923–2933. doi:10.4049/jimmunol.1800352

Behan, M., Zabka, A. G., Thomas, C. F., and Mitchell, G. S. (2003). Sex steroid hormones and the neural control of breathing. *Respir. physiology Neurobiol.* 136 (2-3), 249–263. doi:10.1016/s1569-9048(03)00086-7

Carey, M. A., Card, J. W., Voltz, J. W., Germolec, D. R., Korach, K. S., and Zeldin, D. C. (2007). The impact of sex and sex hormones on lung physiology and disease: lessons from animal studies. *Am. J. Physiology-Lung Cell. Mol. Physiology* 293 (2), L272–L278. doi:10.1152/ajplung.00174.2007

Chen, W., Chen, Y. Y., Tsai, C. F., Chen, S. C. C., Lin, M. S., Ware, L. B., et al. (2015). Incidence and outcomes of acute respiratory distress syndrome: a nationwide registry-based study in Taiwan, 1997 to 2011. *Medicine* 94 (43), e1849. doi:10.1097/MD.0000000000001849

Du, X., Yao, Y., Li, R., Shen, C., and Yin, H. (2005). Influence of sexual difference on expression of toll-like receptor 4 and myeloid differential protein-2 mRNA in the lung in septic rats. *Zhongguo Wei Zhong Bing Ji Jiu Yi Xue* 17 (12), 726–728.

Erfinanda, L., Ravindran, K., Kohse, F., Gallo, K., Preissner, R., Walther, T., et al. (2021). Oestrogen-mediated upregulation of the Mas receptor contributes to sex differences in acute lung injury and lung vascular barrier regulation. *Eur. Respir. J.* 57 (1), 2000921. doi:10.1183/13993003.00921-2020

Han, M. K., Arteaga-Solis, E., Blenis, J., Bourjeily, G., Clegg, D. J., DeMeo, D., et al. (2018). Female sex and gender in lung/sleep health and disease. Increased understanding of basic biological, pathophysiological, and behavioral mechanisms leading to better health for female patients with lung disease. *Am. J. Respir. Crit. care Med.* 198 (7), 850–858. doi:10.1164/rccm.201801-0168WS

Javaheri, S., Barbe, F., Campos-Rodriguez, F., Dempsey, J. A., Khayat, R., et al. (2017). Sleep apnea: types, mechanisms, and clinical cardiovascular consequences. *J. Am. Coll. Cardiol.* 69 (7), 841–858. doi:10.1016/j.jacc.2016.11.069

Kamra, K., Karpuk, N., Adam, R., Zucker, I. H., Schultz, H. D., and Wang, H. J. (2022). Time-dependent alteration in the chemoreflex *post*-acute lung injury. *Front. Physiology* 13, 2214. doi:10.3389/fphys.2022.1009607

Lee, S. K. (2018). Sex as an important biological variable in biomedical research. *BMB Rep.* 51 (4), 167–173. doi:10.5483/bmbrep.2018.51.4.034

Lemos-Filho, L. B., Mikkelsen, M. E., Martin, G. S., Dabbagh, O., Adesanya, A., Gentile, N., et al. (2013). Sex, race, and the development of acute lung injury. *Chest* 143 (4), 901–909. doi:10.1378/chest.12-1118

Li, Y.-L. (2022). Stellate ganglia and cardiac sympathetic overactivation in heart failure. *Int. J. Mol. Sci.* 23 (21), 13311. doi:10.3390/ijms232113311

Lin, C. M., Davidson, T. M., and Ancoli-Israel, S. (2008). Gender differences in obstructive sleep apnea and treatment implications. *Sleep. Med. Rev.* 12 (6), 481–496. doi:10.1016/j.smrv.2007.11.003

Lingappan, K., Jiang, W., Wang, L., and Moorthy, B. (2016). Sex-specific differences in neonatal hyperoxic lung injury. *Am. J. Physiology-Lung Cell. Mol. Physiology* 311 (2), L481–L493. doi:10.1152/ajplung.00047.2016

Liptzin, D. R., Landau, L. I., and Taussig, L. M. (2015). Sex and the lung: observations, hypotheses, and future directions. *Pediatr. Pulmonol.* 50 (12), 1159–1169. doi:10.1002/ppul.23178

Marcus, N. J., Del Rio, R., and Schultz, H. D. (2014). Central role of carotid body chemoreceptors in disordered breathing and cardiorenal dysfunction in chronic heart failure. *Front. physiology* 5, 438. doi:10.3389/fphys.2014.00438

Mark, A. Y. L. (1995). Sympathetic dysregulation in heart failure: mechanisms and therapy. *Clin. Cardiol.* 18 (S1), I-3-I–I8. doi:10.1002/clc.4960181303

Moreira, M. C. S., Pinto, I. S. J., Mourão, A. A., Fajemiroye, J. O., Colombari, E., Reis, Â. A. S., et al. (2015). Does the sympathetic nervous system contribute to the pathophysiology of metabolic syndrome? *Front. physiology* 6, 234. doi:10.3389/fphys.2015.00234

Moss, M., and Mannino, D. M. (2002). Race and gender differences in acute respiratory distress syndrome deaths in the United States: an analysis of multiple-cause mortality data (1979–1996). *Crit. care Med.* 30 (8), 1679–1685. doi:10.1097/00003246-200208000-00001

Mowery, N. T., Terzian, W. H., and Nelson, A. C. (2020). Acute lung injury. *Curr. problems Surg.* 57 (5), 100777. doi:10.1016/j.cpsurg.2020.100777

Nguyen, L., Castro, O., De Dios, R., Sandoval, J., McKenna, S., and Wright, C. J. (2019). Sex-differences in LPS-induced neonatal lung injury. *Sci. Rep.* 9 (1), 8514. doi:10.1038/s41598-019-44955-0

Phua, J., Badia, J. R., Adhikari, N. K. J., Friedrich, J. O., Fowler, R. A., Singh, J. M., et al. (2009). Has mortality from acute respiratory distress syndrome decreased over time? A systematic review. *Am. J. Respir. Crit. care Med.* 179 (3), 220–227. doi:10.1164/rccm.200805-722OC

Silveyra, P., Fuentes, N., and Rodriguez Bauza, D. E. (2021). Sex and gender differences in lung disease. *Lung Inflamm. Health Dis.* 1304, 227–258. doi:10.1007/978-3-030-68748-9_14

Souza, G. M. P., Amorim, M. R., Moraes, D. J. A., and Machado, B. H. (2018). Sex differences in the respiratory-sympathetic coupling in rats exposed to chronic intermittent hypoxia. *Respir. Physiology Neurobiol.* 256, 109–118. doi:10.1016/j.resp.2017.09.003

Speyer, C. L., Rancilio, N. J., McClintock, S. D., Crawford, J. D., Gao, H., Sarma, J. V., et al. (2005). Regulatory effects of estrogen on acute lung inflammation in mice. *Am. J. Physiology-Cell Physiology* 288 (4), C881–C890. doi:10.1152/ajpcell.00467.2004

Tondreau, M. Y., Boucher, E., Simard, M., Tremblay, Y., and Bilodeau, J. F. (2012). Sex-specific perinatal expression of glutathione peroxidases during mouse lung development. *Mol. Cell. Endocrinol.* 355 (1), 87–95. doi:10.1016/j.mce.2012.01.022

Usselman, C. W., Gimon, T. I., Nielson, C. A., Luchyshyn, T. A., Coverdale, N. S., Van Uum, S. H. M., et al. (2015). Menstrual cycle and sex effects on sympathetic responses to acute chemoreflex stress. *Am. J. Physiology-Heart Circulatory Physiology* 308 (6), H664–H671. doi:10.1152/ajpheart.00345.2014

Vento, M., Aguar, M., Escobar, J., Arduini, A., Escrig, R., Brugada, M., et al. (2009). Antenatal steroids and antioxidant enzyme activity in preterm infants: influence of gender and timing. *Antioxidants redox Signal.* 11 (12), 2945–2955. doi:10.1089/ars.2009.2671

Xiang, D., Liu, Y., Zhou, S., Zhou, E., and Wang, Y. (2021). Protective effects of estrogen on cardiovascular disease mediated by oxidative stress. *Oxidative Med. Cell. Longev.* 2021 (1), 5523516. doi:10.1155/2021/5523516

Young, B. P., Loparo, K. A., Dick, T. E., and Jacono, F. J. (2019). Ventilatory pattern variability as a biometric for severity of acute lung injury in rats. *Respir. physiology Neurobiol.* 265, 161–171. doi:10.1016/j.resp.2019.03.009

Zhang, L., Ou, X., Zhu, T., and Lv, X. (2020). Beneficial effects of estrogens in obstructive sleep apnea hypopnea syndrome. *Sleep Breath.* 24, 7–13. doi:10.1007/s11325-019-01896-2

frontiers | Frontiers in Cellular Neuroscience

TYPE Original Research
PUBLISHED 06 November 2024
DOI 10.3389/fncel.2024.1496930

OPEN ACCESS

EDITED BY
Pierre Szepetowski,
INSERM U901 Institut de Neurobiologie de la Méditerranée, France

REVIEWED BY
Ernesto Griego,
Albert Einstein College of Medicine, United States
Zhongjiao Jiang,
University at Buffalo, United States
Igor Medina,
Institut National de la Santé et de la Recherche Médicale (INSERM), France

*CORRESPONDENCE
Luye Qin
✉ Luye.Qin@usd.edu

RECEIVED 16 September 2024
ACCEPTED 25 October 2024
PUBLISHED 06 November 2024

CITATION
Ma K, Zhang D, McDaniel K, Webb M, Newton SS, Lee FS and Qin L (2024) A sexually dimorphic signature of activity-dependent BDNF signaling on the intrinsic excitability of pyramidal neurons in the prefrontal cortex.
Front. Cell. Neurosci. 18:1496930.
doi: 10.3389/fncel.2024.1496930

A sexually dimorphic signature of activity-dependent BDNF signaling on the intrinsic excitability of pyramidal neurons in the prefrontal cortex

Kaijie Ma[1], Daoqi Zhang[1], Kylee McDaniel[2], Maria Webb[3], Samuel S. Newton[1], Francis S. Lee[4] and Luye Qin[1]*

[1]Division of Basic Biomedical Sciences, Sanford School of Medicine, University of South Dakota, Vermillion, SD, United States, [2]Department of Biotechnology, Mount Marty University, Yankton, SD, United States, [3]School of Health Sciences, University of South Dakota, Vermillion, SD, United States, [4]Department of Psychiatry, Department of Pharmacology, Sackler Institute for Developmental Psychobiology, Weill Cornell Medicine, New York, NY, United States

Autism spectrum disorder (ASD) is a group of neurodevelopmental disorders with strong genetic heterogeneity and more prevalent in males than females. We and others hypothesize that diminished activity-dependent neural signaling is a common molecular pathway dysregulated in ASD caused by diverse genetic mutations. Brain-derived neurotrophic factor (BDNF) is a key growth factor mediating activity-dependent neural signaling in the brain. A common single nucleotide polymorphism (SNP) in the pro-domain of the human *BDNF* gene that leads to a methionine (Met) substitution for valine (Val) at codon 66 (Val66Met) significantly decreases activity-dependent BDNF release without affecting basal BDNF secretion. By using mice with genetic knock-in of this human BDNF methionine (Met) allele, our previous studies have shown differential severity of autism-like social deficits in male and female $BDNF^{+/Met}$ mice. Pyramidal neurons are the principal neurons in the prefrontal cortex (PFC), a key brain region for social behaviors. Here, we investigated the impact of diminished activity-dependent BDNF signaling on the intrinsic excitability of pyramidal neurons in the PFC. Surprisingly, diminished activity-dependent BDNF signaling significantly increased the intrinsic excitability of pyramidal neurons in male mice, but not in female mice. Notably, significantly decreased thresholds of action potentials were observed in male $BDNF^{+/Met}$ mice, but not in female $BDNF^{+/Met}$ mice. Voltage-clamp recordings revealed that the sodium current densities were significantly increased in the pyramidal neurons of male $BDNF^{+/Met}$ mice, which were mediated by increased transcriptional level of *Scn2a* encoding sodium channel $Na_V 1.2$. Medium after hyperpolarization (mAHP), another important parameter to determine intrinsic neuronal excitability, is strongly associated with neuronal firing frequency. Further, the amplitudes of mAHP were significantly decreased in male $BDNF^{+/Met}$ mice only, which were mediated by the downregulation of *Kcnn2* encoding small conductance calcium-activated potassium channel 2 (SK2). This study reveals a sexually dimorphic signature of diminished activity-dependent BDNF signaling on the intrinsic neuronal excitability of pyramidal neurons in the PFC, which provides possible cellular and molecular mechanisms underpinning the sex differences in idiopathic ASD patients and human autism victims who carry BDNF Val66Met SNP.

KEYWORDS

activity-dependent neural signaling, BDNF, Val66Met polymorphism, intrinsic neuronal excitability, sex

1 Introduction

ASD is highly genetically heterogeneous and caused by both inherited and *de novo* gene mutations (Simons Foundation Autism Research Initiative, SFARI) (Satterstrom et al., 2020; Homozygosity Mapping Collaborative for Autism et al., 2014). We and others hypothesize that diminished activity-dependent neural signaling is a common molecular pathway dysregulated in ASD caused by diverse genetic mutations (Ebert and Greenberg, 2013; Yap and Greenberg, 2018). Brain-derived neurotrophic factor (BDNF) is synthesized and secreted in response to neuronal activity, which is a key molecule mediating activity-dependent neural signaling and has particular roles in synaptic transmission, synaptic connections, neurotransmitter release, and synaptic plasticity during postnatal neuronal development (Song et al., 2017; Greenberg et al., 2009; Chao, 2003). A common single nucleotide polymorphism (SNP) in the pro-domain of the human *BDNF* gene that leads to a methionine (Met) substitution for valine (Val) at amino acid 66 (Val66Met) significantly reduces dendritic trafficking, synaptic localization of the protein, and decreases up to 30% of activity-dependent BDNF release without affecting basal BDNF secretion (Chen et al., 2006; Egan et al., 2003). This human BDNF Val66Met SNP has been linked to psychiatric diseases, including anxiety (Chen et al., 2006; Egan et al., 2003; Notaras et al., 2015). Human studies showed that the BDNF Val66Met SNP was significantly associated with children with ASD in the Korean population (Yoo et al., 2014). Abnormal cortical developmental was observed in autism children harboring BDNF Val66Met SNP (Raznahan et al., 2009). By using mice with genetic knock-in of this human BDNF methionine (Met) allele, our recent studies have shown that diminished activity-dependent BDNF signaling differentially induces autism-like social deficits in males and females, and that males appear to be more severe than females (Ma et al., 2023).

In humans and rodents, the prefrontal cortex (PFC) is a hub brain region critical for "high-level" executive functions, including social behavior and cognition (Arnsten and Rubia, 2012; Davidson, 2002; Qin et al., 2019; Qin et al., 2018). Ours and others' studies have demonstrated that *Shank3*-deficiency significantly diminished NMDA receptors- and AMPA (α-amino-3-hydroxy-5-methyl-4-isoxazolepropionic acid) receptors-mediated glutamatergic synaptic transmission in the PFC, which caused social deficits in mouse models (Duffney et al., 2015; Wang et al., 2016; Qin et al., 2018). Increased neural activity in the PFC is a key pathogenesis of social deficits in ASD (Lee et al., 2017; Gao and Penzes, 2015; Yizhar et al., 2011; Spratt et al., 2019). Pyramidal neurons are the principal neurons in the PFC, which send out long-distance glutamatergic excitation to the subcortical regions (Murugan et al., 2017; Zhong et al., 2022; Zhong et al., 2020). Intrinsic neuronal excitability is the capability of a neuron to generate action potentials in response to integrative synaptic inputs such as somatic current injections, which is determined primarily by the densities and functions of voltage-gated ion channels (Zhang and Linden, 2003). The changes in intrinsic neuronal excitability are thought to play an important role in learning and memory (Chen et al., 2020), and social deficits in autism mouse models (Spratt et al., 2019; Zhang et al., 2021; Tatsukawa et al., 2019; Eaton et al., 2021; Spratt et al., 2021; Khandelwal et al., 2021). However, little is known about the impact of activity-dependent BDNF signaling on the intrinsic neuronal excitability of pyramidal neurons in the PFC.

According to the latest data from the Autism and Developmental Disabilities Monitoring (ADDM) network (CDC: Centers for Diseases Control and Prevention), one in 36 8-year-old children have been identified with ASD in 2020. Males are four times more likely to be diagnosed with ASD than females. To highlight the need to investigate the neural mechanisms of ASD in both sexes (Shansky and Woolley, 2016), in this study, we characterized the impact of diminished activity-dependent BDNF signaling on the intrinsic neuronal excitability of pyramidal neurons in the PFC by using male and female $BDNF^{+/+}$ and $BDNF^{+/Met}$ mice.

2 Materials and methods

2.1 Animal care and husbandry

The use of animals and procedures performed were approved by the Institutional Animal Care and Use Committee of Sanford School of Medicine, University of South Dakota. A mouse model with genetic knock-in of a human BDNF Met variant was created, and the procedures for heterozygote breeding and genotyping were described previously (Chen et al., 2006). These mice were backcrossed more than 12 generations into the C57BL/6 strain. Animals were group-housed ($n = 4–5$) in standard cages and were kept on a 12-h light–dark cycle in a temperature-controlled room. Food and water were available *ad libitum*. Experiments were performed in male and female $BDNF^{+/Met}$ mice and sex- and age- matched WT littermates $BDNF^{+/+}$, which were derived from heterozygous $BDNF^{+/Met}$ breeding pairs.

2.2 Brain slice preparation

Coronal brain slices containing PFC were prepared from 2 months old male and female $BDNF^{+/+}$ and $BDNF^{+/Met}$ mice as described previously (Qin et al., 2019; Qin et al., 2018; Qin et al., 2021). In brief, mice were anesthetized with isoflurane and rapidly decapitated. Brains were immediately removed, iced, and cut into 300 µm slices by a Vibratome (Leica VP1000S, Leica Microsystems Inc.). Brain slices were then incubated at 33°C in artificial cerebrospinal fluid (ACSF) (in mM: 130 NaCl, 26 NaHCO3, 3 KCl, 5 MgCl2, 1.25 NaH2PO4, 1 CaCl2, 10 glucose, pH 7.4, 300 mOsm) for 1 h and then kept for 1–4 h at room temperature (20–21°C) bubbling with 95% O2, 5% CO2.

2.3 Whole cell patch-clamp recordings

For recordings, the brain slice was positioned in a perfusion chamber attached to the fixed stage of an upright microscope (Olympus) and submerged in continuously flowing oxygenated ACSF (in mM: 130 NaCl, 26 NaHCO3, 1 CaCl2, 5 MgCl2, 3 KCl, 1.25 NaH2PO4, 10 glucose, pH 7.4, 300 mOsm). Layer V pyramidal neurons in the PFC were visualized with infrared differential interference contrast video microscopy. Recordings were performed with a multi-Clamp 700B amplifier (Molecular Devices), and data were acquired using pClamp 11.2 software, filtered at 1 kHz and sampling rate at 10 kHz with an Axon Digidata 1550B plus HumSilencer digitizer (Molecular Devices). Recording electrodes were pulled from borosilicate glass capillaries (1.5/0.86 mm OD/ID)

with a micropipette puller (Sutter Instrument, model P-97, Novato, CA). The resistances of patch electrodes were 4–6 MΩ when filled with internal solution.

Whole-cell current-clamp recordings were used to measure action potentials. The brain slice was bathed in a modified ACSF with low (0.5 mM) MgCl2 to elevate neuronal activity, which more closely mimics the ionic composition of the brain interstitial fluid *in situ*. AMPA (*α*-amino-3-hydroxy-5-methyl-4-isoxazolepropionic acid) (20 mM CNQX) and $GABA_A$ (g-aminobutyric acid) receptors blockers (20 mM bicuculline) were added in action potentials recordings as in our previous studies (Qin et al., 2021). The pipettes were filled with an intracellular solution (in mM): 124 K-gluconate, 1 MgCl2, 6 KCl, 5 EGTA, 10 HEPES, 0.5 CaCl2, and 12 phosphocreatine, 5 MgATP, 0.5 Na2GTP, 0.2 Leupeptin, pH 7.2–7.3, 265–270 mOsm. To label the neurons under recording, the internal solution was supplemented with 0.05% sulforhodamine B. Slices were then fixed with 4% paraformaldehyde for 30 min, washed 3 times in PBS (pH 7.4). The neuronal images were acquired with a Leica TCS SP8 confocal microscope.

Seal formation and membrane rupture were done in a voltage-clamp mode at holding potential of −70 mV. Resting membrane potentials were measured immediately on break-in. A series of 250 ms current pulses (from −20 to 130 pA, 10 pA increments) were elicited to obtain action potential firing trains while the neurons were held at a fixed potential of −70 mV.

Rheobase was the minimal electric current required to elicit an action potential when current was injected into a neuron holding at −70 mV. The first spike latency was the time interval between the beginning of the current step and the occurrence of the first action potential elicited by minimal electric current. The voltage threshold of action potential was defined as the voltage where the value of dV/dt first exceeded 10 mV/ms at the first spike elicited by minimal electric current. The amplitude of medial after hyperpolarization (mAHP) was measured as the difference between the threshold and the peak of the most negative followed the action potentials after the first action potential (regular spiking neurons) or after short-bursts (intrinsic bursting neurons) elicited by 100 pA current injection (Wu et al., 2016).

The input resistance (r) was determined by injecting a − 100 pA, 250 ms hyperpolarizing current into the neuron holding at −70 mV. The membrane time constant (τ) was calculated using a single exponential fit of the voltage change in response to −100 pA hyperpolarizing current injection with 250 ms duration. The cell capacitance (c) was calculated under a current-clamp mode using the formula $c = r/\tau$, where c was membrane capacitance, r was cell membrane resistance, and τ was membrane time constant (Sun et al., 2020).

Whole-cell voltage-clamp recordings were used to measure sodium currents. The brain slice was bathed in ACSF. Recording pipette contained the following internal solution (in mM: 100 CsCl, 10 tetraethylammonium chloride (TEA-Cl), 5 4-aminopyridine (4-AP), 10 HEPES, 4 NaCl, 1 MgCl2, 5 EGTA, 12 phosphocreatine, 5 MgATP, 0.5 Na2GTP, 0.2 Leupeptin, pH 7.2–7.3, 265–270 mOsm) (Milescu et al., 2010). Neurons were held at −70 mV and stepped to a range of potentials (−70 to +50 mV, 10 mV increments) for 100 ms each. Current densities (current/capacitance) were plotted as a function of depolarizing potential to generate current densities-voltage curves. All electrophysiological recordings were performed at room temperature (21–22°C). During recordings, neurons with leak currents >200 pA were discarded. Series resistance (Rs) was compensated to 80–90%. Cells having series resistance >10 MΩ or change above 20% throughout the experiments were excluded from analysis (Sontheimer and Ransom, 2002; Manz et al., 2021). The leakage current amplitudes were subtracted offline from the current peaks, and the capacitive transients were not cancelled (Surges et al., 2006). The amplitude of sodium current was measured as the difference between the onset of depolarization (after capacitive transient) and the peak of inward current.

2.4 Quantitative real-time RT-PCR

Total RNA was isolated from mouse PFC punches using Trizol reagent (Invitrogen) and treated with DNase I (Invitrogen) to remove genomic DNA. Then the iScriptTM cDNA synthesis Kit (Bio-Rad) was used to obtain cDNA from the tissue mRNA. Quantitative real time PCR was carried out using the iCycler iQ™ RealTime PCR Detection System and iQ™ Supermix (Bio-Rad) according to the manufacturer's instructions. In brief, GAPDH was used as the housekeeping gene for quantitation of the expression of target genes in samples from male and female $BDNF^{+/+}$ and $BDNF^{+/Met}$ mice. Fold changes in the target genes were determined by: Fold change = $2^{-\Delta(\Delta CT)}$, where $\Delta CT = C_T$ (target) - C_T(GAPDH), and $\Delta(\Delta C_T) = \Delta C_T$ (another group) - ΔC_T (male $BDNF^{+/+}$). C_T (threshold cycle) is defined as the fractional cycle number at which the fluorescence reaches 10X of the standard deviation of the baseline. A total reaction mixture of 20 mL was amplified in a 96-well thin-wall PCR plate (Bio-Rad) using the following PCR cycling parameters: 95°C for 5 min followed by 40 cycles of 95°C for 45 s, 55°C for 45 s, and 72°C for 45 s. Primers for all target genes are listed in Table 1.

2.5 Statistical analysis

Data were analyzed with GraphPad Prism 10 (GraphPad) and Clampfit 11.2 (Molecular Devices, Sunnyvale, CA). For statistical significance, experiments with more than two groups were assessed with two-way or three-way ANOVA, followed by *post hoc* Bonferroni tests for multiple comparisons. All values were presented as mean ± SEM. $p < 0.05$ was considered statistically different.

3 Results

3.1 Diminished activity-dependent BDNF signaling significantly increases the intrinsic excitability of pyramidal neurons in the PFC of male mice, but not in female mice

To examine the impact of diminished activity-dependent BDNF signaling on the intrinsic excitability of pyramidal neurons in the PFC, we performed a whole-cell patch clamp to evoke action potentials by injecting a series of constant currents while holding the membrane potential at -70 mV. Given that deep layer glutamatergic pyramidal neurons in PFC showed the clearest deficits in autistic children (Stoner

TABLE 1 List of primers used in qPCR experiments.

Target Gene	Forward	Reverse	Gene reference
Gapdh	gacaactcactcaagattgtcag	atggcatggactgtggtcatgag	NM_001289726.1
Scn1a	agcttcaacttcttcaccag	tgggccattttcatcatcat	NM_001313997.1
Scn2a	ccttgctgctattgaacaac	cctgcttccaagtcactatt	NM_001099298.3
Scn3a	agaatctcttgctgctatcg	agcttccaagtcactgtttg	NM_001355166.1
Scn8a	ctttcatctacggggacatc	gcgctaaatctgaagagagt	NM_001077499.2
Hcn1	ggtcaacaaattctccctcc	agtcactgtacggatggata	NM_010408.3
Hcn2	cccaaggtttcgttctcat	aattggcgctgcaggaag	NM_008226.2
Hcn3	tactgggatctcatcatgct	cagagaggacattgaagacg	NM_008227.2
Hcn4	gtcagcagggttttggatta	cacgggtatgatgatcagatt	NM_001081192.3
Kcnn1	atacaccaaggagtcactct	caagaacagctggatctctc	NM_001363407.2
Kcnn2	aacagctctgacatggaaac	cttgtcctggctctgttg	NM_001312905.2
Kcnn3	ctggtctgttgcactcttc	tggtcattgagatttagctgg	NM_080466.2
Kcnn4	ctgagatgttgtggttcctg	ccacaataagacaaaggagga	NM_008433.5
Kcnq2	ttagtcttctcctgccttgt	cacaaagtactcaacaccga	NM_010611.3
Kcnq3	aagtcaccttggcgctag	gttgttcctcttgactggg	NM_152923.3
Kcnq4	tgtctgtactgtccaccat	atatactccaagccaaagacc	NM_001081142.3
Kcnq5	ctgtacaacgtgctggag	ttttgtatgctcagggatgg	NM_001160139.1

et al., 2014), pyramidal neurons in layer V were selected for electrophysiological measurements. As shown in Figure 1A, pyramidal neurons can be reliably identified by electrophysiological recordings according to our previous studies (Qin et al., 2018; Qin et al., 2021). Pyramidal neurons have been classified into different subclasses based upon their spiking patterns (Franceschetti et al., 1998; Griego et al., 2022). We identified regularly spiking (RS) and intrinsic bursting (IB) pyramidal neurons in male and female BDNF$^{+/+}$ and BDNF $^{+/Met}$ mice, which is consistent with others' studies (Franceschetti et al., 1998; Griego et al., 2022; Hedrick and Waters, 2011). In male BDNF$^{+/+}$ mice, 50% (8/16 neurons) of the recorded pyramidal neurons exhibited a regular spiking (RS) pattern in response to a series of depolarizing current steps and 50% (8/16 neurons) of them exhibited short bursts (two to five closely-spaced action potentials) (intrinsic bursting, IB) pattern. The proportion of these two types' pyramidal neurons remained similar in female BDNF$^{+/+}$ (RS, 56%, 9/16 neurons; IB, 44, 7/16 neurons), male BDNF $^{+/Met}$ (RS, 50%, 8/16 neurons; IB, 50%, 8/16 neurons) and female BDNF$^{+/Met}$ mice (RS: 50%, 10/20 neurons; IB: 50%, 10/20 neurons). The input–output curve was conducted by gradually increasing the stimulus intensity of the depolarizing pulse (10 pA, 250 ms). The number of action potentials in regular spiking and intrinsic bursting pyramidal neurons was significantly increased with the incremented injected currents in male and female BDNF$^{+/+}$ and BDNF$^{+/Met}$ mice. The regular spiking and intrinsic bursting pyramidal neurons from male BDNF$^{+/Met}$ mice displayed similar trends of higher number of evoked action potentials, but not significantly, compared to male and female BDNF$^{+/+}$, and female BDNF$^{+/Met}$ mice (Supplementary Figure S1). Then, we combined the regular spiking and intrinsic bursting pyramidal neurons together in each group. The number of evoked action potentials was significantly higher in the total pyramidal neurons of PFC from male BDNF$^{+/Met}$ mice, but not female BDNF$^{+/Met}$ mice, compared to male and female BDNF$^{+/+}$ mice ($F_{\text{Genotype (1, 64)}} = 3.7$, $p = 0.059$, $F_{\text{Sex (1, 64)}} = 2.8$, $p = 0.099$, $F_{\text{Genotype and Sex interaction (1, 64)}} = 5.4$, $p = 0.024$, three-way ANOVA) (Figures 1B,C). Therefore, regular spiking and intrinsic bursting pyramidal neurons were pooled together in each group in this study. These results suggest that diminished activity-dependent BDNF signaling has a sexual dimorphic effect on the intrinsic excitability of pyramidal neurons in the PFC.

3.2 Diminished activity-dependent BDNF signaling significantly alters properties of action potential of pyramidal neurons in male mice, but not in female mice

To further determine the mechanisms of diminished activity-dependent BDNF signaling increased intrinsic excitability of pyramidal neurons in male mice, we examined the key parameters reflecting the action potential properties of pyramidal neurons in male and female BDNF$^{+/+}$ and BDNF$^{+/Met}$ mice. As shown in Figures 2A–E, diminished activity-dependent BDNF signaling significantly decreased rheobase in male, but not in female mice, the minimal electric current required to elicit an action potential when current was injected into a neuron (male BDNF$^{+/+}$: 72.5 ± 5.6 pA; female BDNF$^{+/+}$: 71.6 ± 4.9 pA; male BDNF$^{+/Met}$: 50.6 ± 3.3; female BDNF$^{+/Met}$: 70.3 ± 3.9 pA. n = 16–20 neurons/4–5 mice/group. $F_{\text{Genotype (1, 64)}} = 6.7$, $p = 0.012$; $F_{\text{Sex (1, 64)}} = 4.3$, $p = 0.042$; $F_{\text{Genotype and Sex interaction (1, 64)}} = 5.2$, $p = 0.025$, two-way ANOVA). Male BDNF$^{+/Met}$ mice showed significantly shortened first spike latency, the period from the beginning of stimulus to the occurrence of first action potential (male BDNF$^{+/+}$: 180.2 ± 10 ms; female BDNF$^{+/+}$: 187.1 ± 9.8 ms; male BDNF$^{+/Met}$: 133.2 ± 12.4 ms; female BDNF$^{+/Met}$: 181.3 ± 9.2 ms. n = 16–20 neurons/4–5 mice/group. $F_{\text{Genotype (1, 64)}} = 6.4$, $p = 0.01$, $F_{\text{Sex (1, 64)}} = 7.0$, $p = 0.01$, $F_{\text{Genotype and Sex interaction (1, 64)}} = 3.9$, $p = 0.05$, two-way ANOVA). The threshold of action potential reflects how easily a neuron turns synaptic inputs into an action potential. The thresholds of action

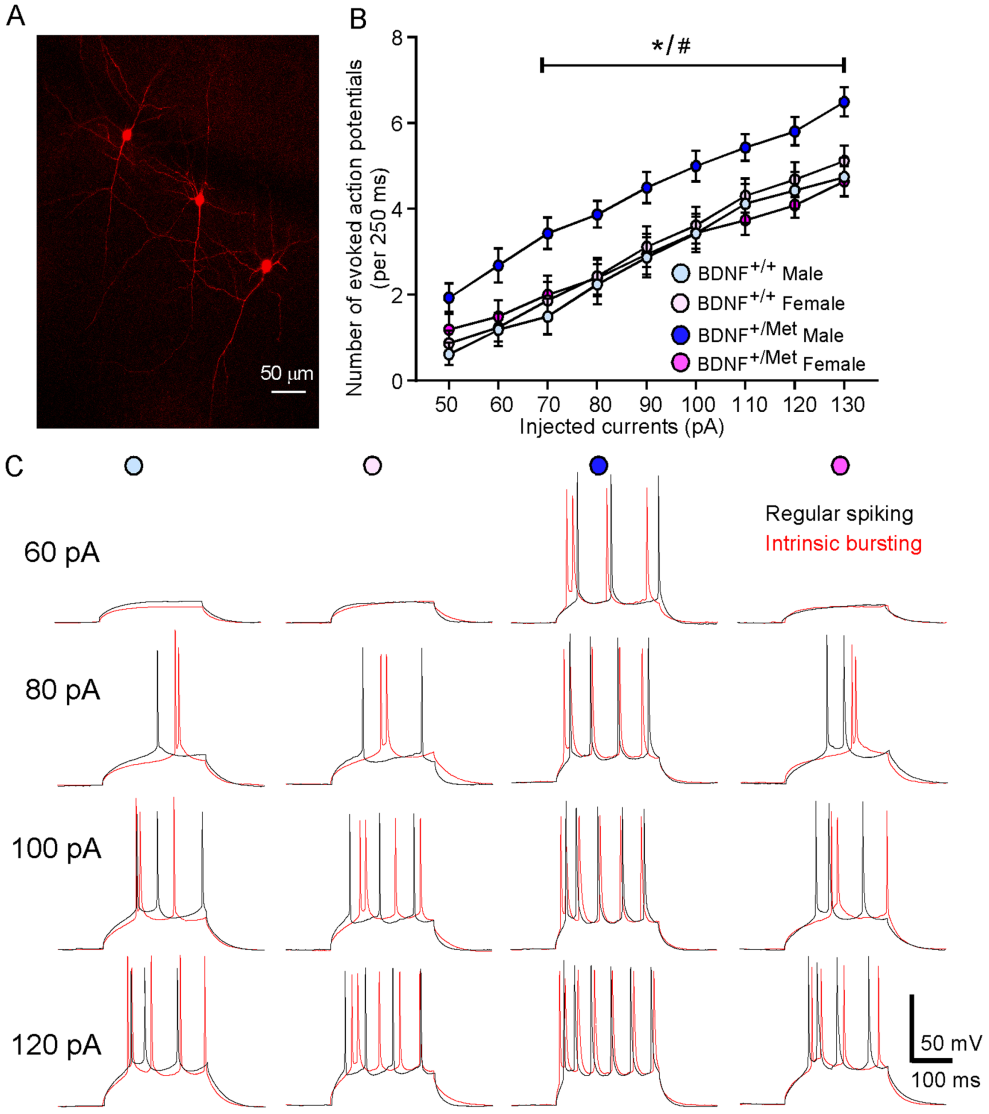

FIGURE 1
Diminished activity-dependent BDNF signaling significantly increases intrinsic neuronal excitability of pyramidal neurons in the PFC of male mice, but not in female mice. **(A)** A representative confocal image showing layer V pyramidal neurons used for recording. **(B)** Quantification of the number of evoked action potentials in response to injected currents in the pyramidal neurons of PFC from $BDNF^{+/+}$ and $BDNF^{+/Met}$ mice. $n = 16–20$ neurons/4–5 mice/group. **(C)** Representative action potential traces from regular spiking (black) and intrinsic bursting (red) pyramidal neurons. $*p < 0.05$, $BDNF^{+/Met}$ versus $BDNF^{+/+}$; $\#p < 0.05$, male versus female, three-way ANOVA.

potentials were significantly lower in the pyramidal neurons from male $BDNF^{+/Met}$ mice, but not from female mice, compared to male and female $BDNF^{+/+}$ mice (male $BDNF^{+/+}$: -44.6 ± 1.1 mV; female $BDNF^{+/+}$: -45.0 ± 0.6 mV; male $BDNF^{+/Met}$: -48.5 ± 0.5 mV; female $BDNF^{+/Met}$: -45.7 ± 0.5 mV. n = 16–20 neurons/4–5 mice/group. $F_{\text{Genotype }(1, 64)} = 10.4$, $p = 0.002$, $F_{\text{Sex }(1, 64)} = 2.9$, $p = 0.09$, $F_{\text{Genotype and Sex interaction }(1, 64)} = 5.2$, $p = 0.03$, two-way ANOVA). Medium afterhyperpolarization (mAHP) affects the threshold of action potential and neuronal firing activity (Bean, 2007; Dwivedi and Bhalla, 2021). The amplitudes of mAHP were significantly smaller in the pyramidal neurons from male $BDNF^{+/Met}$ mice, but not from female mice, compared to male and female $BDNF^{+/+}$ mice (male $BDNF^{+/+}$: -6.2 ± 0.4 mV; female $BDNF^{+/+}$: -6.6 ± 0.3 mV; male $BDNF^{+/Met}$: -4.5 ± 0.2 s; female $BDNF^{+/Met}$: -6.3 ± 0.3 s. n = 16–20 neurons/4–5 mice/group. $F_{\text{Genotype }(1, 64)} = 9.7$, $p = 0.003$, $F_{\text{Sex }(1, 64)} = 13.2$, $p = 0.0006$, $F_{\text{Genotype and Sex interaction }(1, 64)} = 4.7$, $p = 0.03$, two-way ANOVA). These results demonstrate that diminished activity-dependent BDNF signaling differentially alters the properties of action potential in the pyramidal neurons from male and female mice, which mediates the sex effect of diminished activity-dependent BDNF signaling on the intrinsic excitability of pyramidal neurons.

3.3 Diminished activity-dependent BDNF signaling has no effects on passive membrane properties

The passive intrinsic properties of neurons are highly related to the ability of neurons to generate action potentials (Chen et al., 2020). Next, we examined the impact of diminished activity-dependent BDNF signaling on the passive membrane properties of

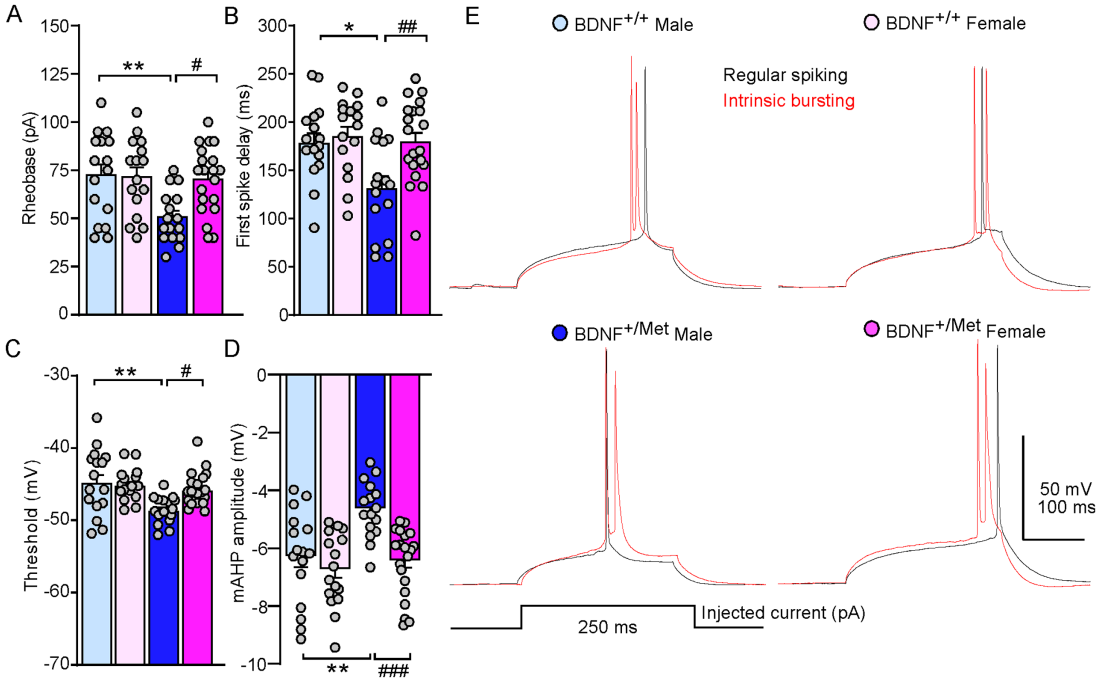

FIGURE 2
Diminished activity-dependent BDNF signaling differentially alters properties of action potential of pyramidal neurons in the PFC of males and females. Bar graphs showing rheobase **(A)**, first spike delay **(B)**, threshold **(C)**, and mAHP **(D)** in the pyramidal neurons of PFC from male and female BDNF$^{+/+}$ and BDNF$^{+/Met}$ mice. *$p < 0.05$, **$p < 0.01$, BDNF$^{+/Met}$ versus BDNF$^{+/+}$; #$p < 0.05$, ##$p < 0.01$, ###$p < 0.001$, male versus female, $n = 16$–20 neurons/4–5 mice/group, two-way ANOVA. **(E)** Representative traces of the first spike elicited with minimum electric current in regular spiking (black) and intrinsic bursting (red) pyramidal neurons.

pyramidal neurons in male and female mice. The passive membrane properties were determined by injecting a small hyperpolarizing current into the soma of neurons (100 pA). As shown in Supplementary Figure S2, there were no differences of resting membrane potentials, cell capacitance, input resistance, and Tau between male and female BDNF$^{+/+}$ mice and BDNF$^{+/Met}$ mice. These results demonstrated that diminished activity-dependent BDNF signaling has no effects on the passive membrane properties of pyramidal neurons in male and female mice, which indicates there are no significant differences in morphology of layer V pyramidal neurons in the PFC of male and female BDNF$^{+/+}$ and BDNF$^{+/Met}$ mice (Isokawa, 1997).

3.4 Diminished activity-dependent BDNF signaling increases the expression of *Scn2a* and voltage-gated sodium currents in male, but not in female mice

Voltage-gated sodium channels play an essential role in generation and propagation of action potentials (Goldin et al., 2000). To determine whether diminished activity-dependent BDNF signaling increases the sodium currents in male mice, we evaluated the amplitudes of sodium currents in the pyramidal neurons of male and female BDNF$^{+/+}$ and BDNF$^{+/Met}$ mice in a voltage-clamp mode. The membrane potential was held at −70 mV. The total inward currents were recorded in response to voltage steps from −70 to +50 mV (10 mV step increase, 100 ms). As shown in current density curves and representative traces (Figures 3A–C), the peak inward currents were triggered at −50 mV. The inward currents were abolished in the presence of tetrodotoxin (TTX, 0.5 μM). The peak current densities were significantly increased in the pyramidal neurons from male BDNF$^{+/Met}$ mice, compared to female BDNF$^{+/Met}$ and BDNF$^{+/+}$ mice (male BDNF$^{+/+}$: −64.5 ± 1.5 pA/pF; female BDNF$^{+/+}$: −68.9 ± 2.1 pA/pF; male BDNF$^{+/Met}$: −92.5 ± 1.9 pA/pF; female BDNF$^{+/Met}$: −71.4 ± 1.3 pA/pF, n = 16 neurons/4 mice/group, $F_{\text{Genotype (1, 60)}} = 76.0$, $p < 0.0001$; $F_{\text{Sex (1, 60)}} = 22.9$, $p < 0.0001$, $F_{\text{Genotype and Sex interaction (1, 60)}} = 52.9$, $p < 0.0001$). Among the 9 known members, Nav1.1, Nav1.2, Nav 1.3, and Nav1.6 are highly expressed in the central nervous system (Lai and Jan, 2006), which are composed by α and *β* subunits. To determine which sodium channel contributes to the decreased thresholds of action potentials in the pyramidal neurons from male BDNF$^{+/Met}$ mice, we examined the transcriptional level of α subunits of these four sodium channels, given that the a subunit forms a pore that conducts sodium. As shown in Figure 3D, the mRNA levels of *Scn2a* (encoding Nav 1.2) were significantly higher in PFC lysates from male BDNF$^{+/Met}$ mice ($F_{\text{Genotype (1, 64)}} = 11.6$, $p = 0.002$, $F_{\text{Sex (1, 64)}} = 14.6$, $p = 0.0007$, $F_{\text{Genotype and Sex interaction (1, 64)}} = 15.4$, $p = 0.005$), while the mRNA levels of *Scn1a* (encoding Nav 1.1), *Scn3a* (encoding Nav 1.3), and *Scn8a* (encoding Nav 1.6) were largely unchanged. These results suggest the increased *Scn2a* contributes to the higher sodium currents and decreased thresholds of action potentials in male BDNF$^{+/Met}$ mice.

10.3389/fncel.2024.1496930

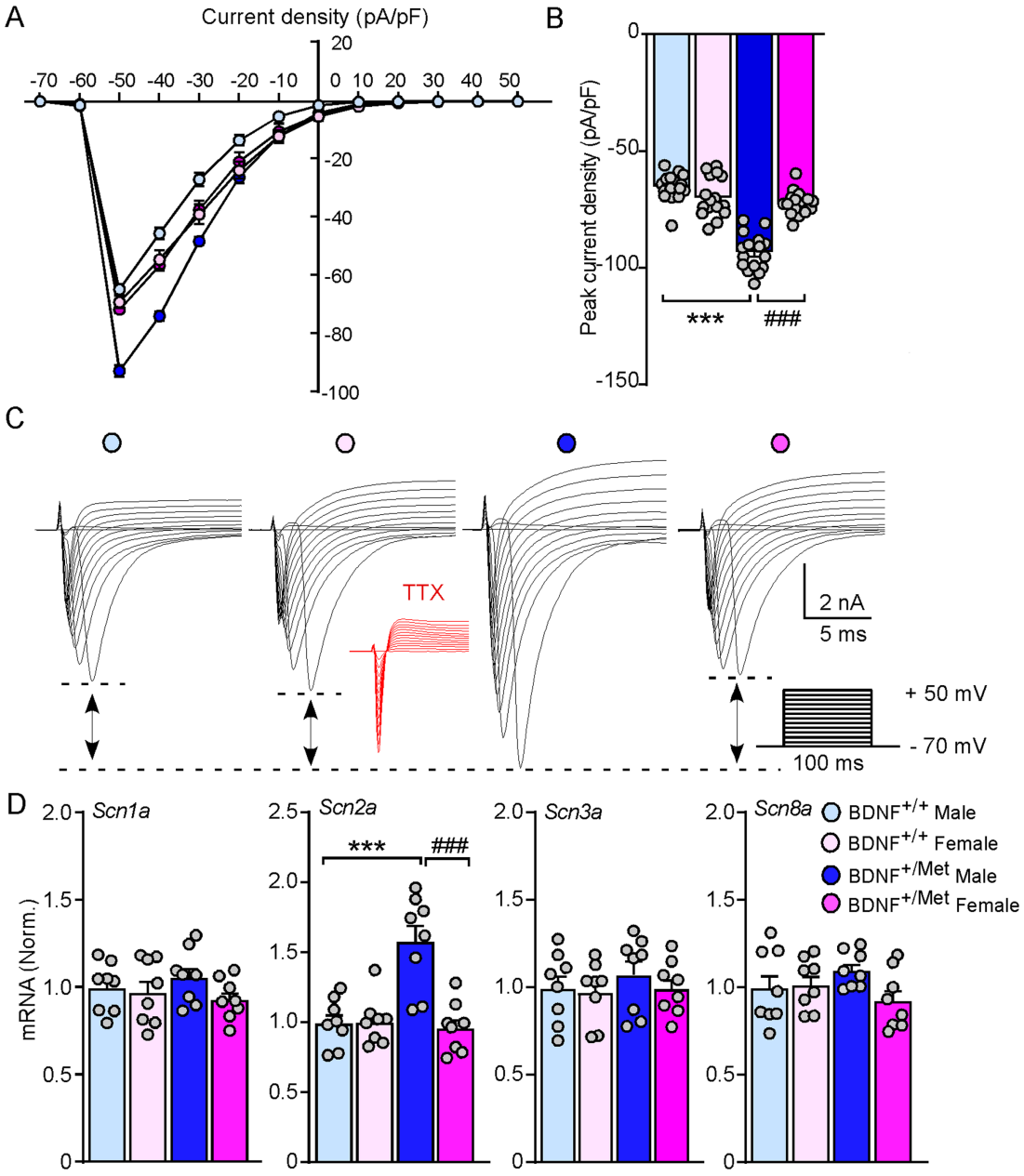

FIGURE 3
Diminished activity-dependent BDNF signaling significantly increases voltage-gated sodium currents and the expression of *Scn2a* in male mice, but not in female mice. **(A)** Current density-voltage relationship showing sodium current density in the pyramidal neurons from PFC of BDNF$^{+/+}$ and BDNF$^{+/Met}$ mice. $n = 16$ neurons/4 mice/group. **(B)** Bar graph showing the peak current density in the pyramidal neurons from PFC of BDNF$^{+/+}$ and BDNF$^{+/Met}$ mice. ***$p < 0.001$, BDNF$^{+/Met}$ versus BDNF$^{+/+}$; ###$p < 0.001$, male versus female, $n = 16$ neurons/4 mice/group, two-way ANOVA. **(C)** Representative traces of voltage-gated sodium currents recorded in response to voltage steps from −70 to +50 mV in the pyramidal neurons from PFC of BDNF$^{+/+}$ and BDNF$^{+/Met}$ mice. Inset: TTX (0.5 μM) abolished the inward currents. **(D)** Quantitative real-time PCR showing the mRNA levels of *Scn1a*, *Scn2a*, *Scn3a*, and *Scn8a* in the PFC of BDNF$^{+/+}$ and BDNF$^{+/Met}$ mice. ***$p < 0.001$, BDNF$^{+/Met}$ versus BDNF$^{+/+}$; ###$p < 0.001$, male versus female, $n = 8$ mice/group, two-way ANOVA.

3.5 Diminished activity-dependent BDNF signaling selectively decreases the transcriptional level of *Kcnn2* in male mice, but not in female mice

Medium afterhyperpolarization (mAHP) is mainly mediated by small conductance calcium activated potassium channels (SK), voltage-gated potassium channels 7 (KCNQ), and hyperpolarization activated cyclic nucleotide (HCN) channels (Dwivedi and Bhalla, 2021; Mateos-Aparicio et al., 2014; Gu et al., 2005). To find out which ion channels mediate the smaller mAHP in pyramidal neurons from male BDNF$^{+/Met}$ mice (Figure 2E), we examined the transcriptional levels of *Kcnn1-4* (encoding SK1-4 channels), *Kcnq2-5* (encoding KCNQ channels), and *Hcn1-4* (encoding HCN1-4 channels) in the PFC. As shown in Figure 4, the mRNA levels of *kcnn2* (encoding SK2) were significantly decreased in PFC lysates from male BDNF$^{+/Met}$ mice

($F_{\text{Genotype (1, 28)}} = 12.5$, $p = 0.0015$; $F_{\text{Sex (1, 28)}} = 5.6$, $p = 0.025$), while the mRNA levels of *Kcnn1*, *Kcnn3*, *Kcnn4, Kcnq2-5* and *Hcn1-4* were largely unchanged. These results suggest that the decreased *Kcnn2* is responsible for the smaller mAHP in male BDNF$^{+/Met}$ mice.

4 Discussion

In this study, we characterized the impact of diminished activity-dependent BDNF signaling on the intrinsic excitability of pyramidal neurons in the PFC by using mice with knock-in of a human BDNF Met allele. Our results showed that diminished activity-dependent BDNF signaling increased intrinsic excitability of pyramidal neurons in male mice, but not in female mice. Furthermore, diminished activity-dependent BDNF signaling significantly increased the expression of *Scn2a* and decreased the expression of *Kcnn2* in male mice only, which decreased the thresholds of action potentials and facilitated the propagation of firing. We provide the first preclinical evidence that diminished activity-dependent BDNF signaling has a sexually dimorphic effect on the intrinsic excitability of pyramidal neurons in the PFC.

The high incidence of epilepsy in ASD patients indicates that the elevated excitability of pyramidal neurons is a major pathogenic factor in ASD (Blackmon et al., 2016; Sansa et al., 2011; Frye et al., 2013; Viscidi et al., 2013; Jeste and Tuchman, 2015). Increased intrinsic excitability of pyramidal neurons was found in the cortical neuronal culture by blocking neuronal activity by adding TTX, which was prevented by co-application of BDNF (Desai et al., 1999a; Desai et al., 1999b). In the present study, we found the evoked action potentials were significantly increased in the pyramidal neurons of PFC from male, but not female BDNF$^{+/Met}$ mice, indicating the critical role of activity-dependent BDNF in homeostatic regulation of intrinsic excitability of pyramidal neurons. Additionally, the thresholds and mAHP of action potentials were significantly lower in male BDNF$^{+/Met}$ mice. The higher AP frequencies, lower thresholds, and smaller mAHP of action potentials in male BDNF$^{+/Met}$ mice indicate that activity-dependent BDNF differentially regulates intrinsic neuronal excitability in males and females.

One critical question is the underlying molecular mechanisms. The increased intrinsic excitability of pyramidal neurons in male BDNF$^{+/Met}$ mice may occur through different ionic mechanisms. Voltage-gated sodium channels are one of the most important ion channels, which are crucial for the thresholds of action potentials. We found an upregulation of the sodium currents in pyramidal neurons of male BDNF$^{+/Met}$ mice. Consistent with others' report (Sontheimer and Ransom, 2002), the sodium currents showed abruptly activated large inward currents with voltage steps to −50 mV, which indicated intrinsic signs of poor voltage control in brain slices recordings. Activity deprivation increased the sodium currents without affecting activation nor inactivation characteristics of sodium channels (Desai et al., 1999b), which indicates diminished activity-dependent BDNF signaling will not alter the kinetic characteristics of sodium channels in male mice, though a voltage-independent change on open-channel probability cannot be ruled out (Li et al., 1992). Further studies are needed via minimizing the uncontrolled space-clamp axonal currents by applying a depolarizing pre-pulse before each voltage step (Milescu et al., 2010; Griego et al., 2022) or dissociated pyramidal neurons from PFC, given that somatic sodium currents are under good voltage control. Nav1.2 (encoded by *Scn2a*) is one of several sodium channels involved in initiation and propagation of action potentials in neurons (Sanders et al., 2018) and expressed predominantly in pyramidal cells (Spratt et al., 2019). The transcription of *Scn2a* is selectively upregulated in the PFC of male BDNF$^{+/Met}$ mice. Nav1.2 is expressed in other cell types, such as interneurons (Yamagata et al., 2017), and glia cells (Pappalardo et al., 2016) in the PFC. The combined transcriptional and electrophysiological evidence strongly suggests the upregulated Nav1.2 mediates the increased sodium currents in the pyramidal neurons of male BDNF$^{+/Met}$ mice.

mAHP is another parameter used to determine the intrinsic neuronal excitability, which is a hyperpolarized phase after a single or a train of action potentials and lasts 50 ~ 300 ms (Chen et al., 2020). mAHP is predominantly mediated by small conductance calcium-activated potassium (SK) channels, although voltage-gated potassium channels 7 (Kv7) and hyperpolarization-activated cyclic nucleotide-gated (HCN) channels have also been shown to contribute to the mAHP (Dwivedi and Bhalla, 2021; Gu et al., 2005).

SK channels are small-conductance calcium-activated potassium channels that are widely expressed in neurons and influence neuronal firing frequency (Faber and Sah, 2007; Sun et al., 2020). There are four family members in the SK channels, which are SK1, SK2, SK3, and SK4, encoded by *Kcnn1*, *Kcnn2*, *Kcnn3*, and *Kcnn4*, respectively. Activation of SK channels by calcium influx can modulate the frequency of action potential through rapid potassium efflux, which leads membrane repolarization/hyperpolarization. Alterations in SK channels have also been reported in various brain diseases. Humans carrying loss-of-function *KCNN2* mutations have been linked with ASD (Nam et al., 2023; Alonso-Gonzalez et al., 2019; Grove et al., 2019). Downregulation of SK2 was associated with augmented reticular thalamic bursting and seizures in *Scn1a*-Dravet syndrome (Ritter-Makinson et al., 2019). However, increased *Kcnn2* decreased intrinsic excitability of cortical pyramidal neurons in a PTEN-associated autism mouse model (Garcia-Junco-Clemente et al., 2013). Intellectual disability and developmental delay symptoms have been reported in patients carrying *KCNN3* variants (Bauer et al., 2019; Gripp et al., 2021; Schwarz et al., 2022). We found that diminished activity-dependent BDNF signaling selectively decreases *Kcnn2*, but *not Kcnn1*, *Kcnn3,* and *Kcnn4.*

Kcnq genes encode five family members of the Kv7 channels (Kv7.1–Kv7.5), which are a group of low-threshold voltage-gated potassium channels known as "M-channel" (Brown and Passmore, 2009). Four of them (*Kcnq2-5*) are expressed in the nervous system. Kv7.2 and Kv7.3 (encoded by *Kcnq2/3*) are the principal molecular components of M-channels, which are expressed on both excitatory and inhibitory neurons and constrain repetitive neuronal firing (Gu et al., 2005; Brown and Passmore, 2009; Delmas and Brown, 2005). Mutations of *KCNQ2/3* cause ASD and benign familial neonatal epilepsy (Satterstrom et al., 2020; Homozygosity Mapping Collaborative for Autism et al., 2014; Piro et al., 2019; Soldovieri et al., 2014; Maljevic and Lerche, 2014; Wang et al., 2020). *Kcnq2* deficiency in pyramidal neurons increased neuronal excitability, resulting in epilepsy (Peters et al., 2005; Soh et al., 2014). However, diminished activity-dependent BDNF signaling has no effect on the expressions of *Kcnq2-5*.

HCN channels are encoded by four genes (*Hcn1–4*), which can be activated typically at potentials below −50 mV and open at the resting membrane potential, conducting an inward cation current

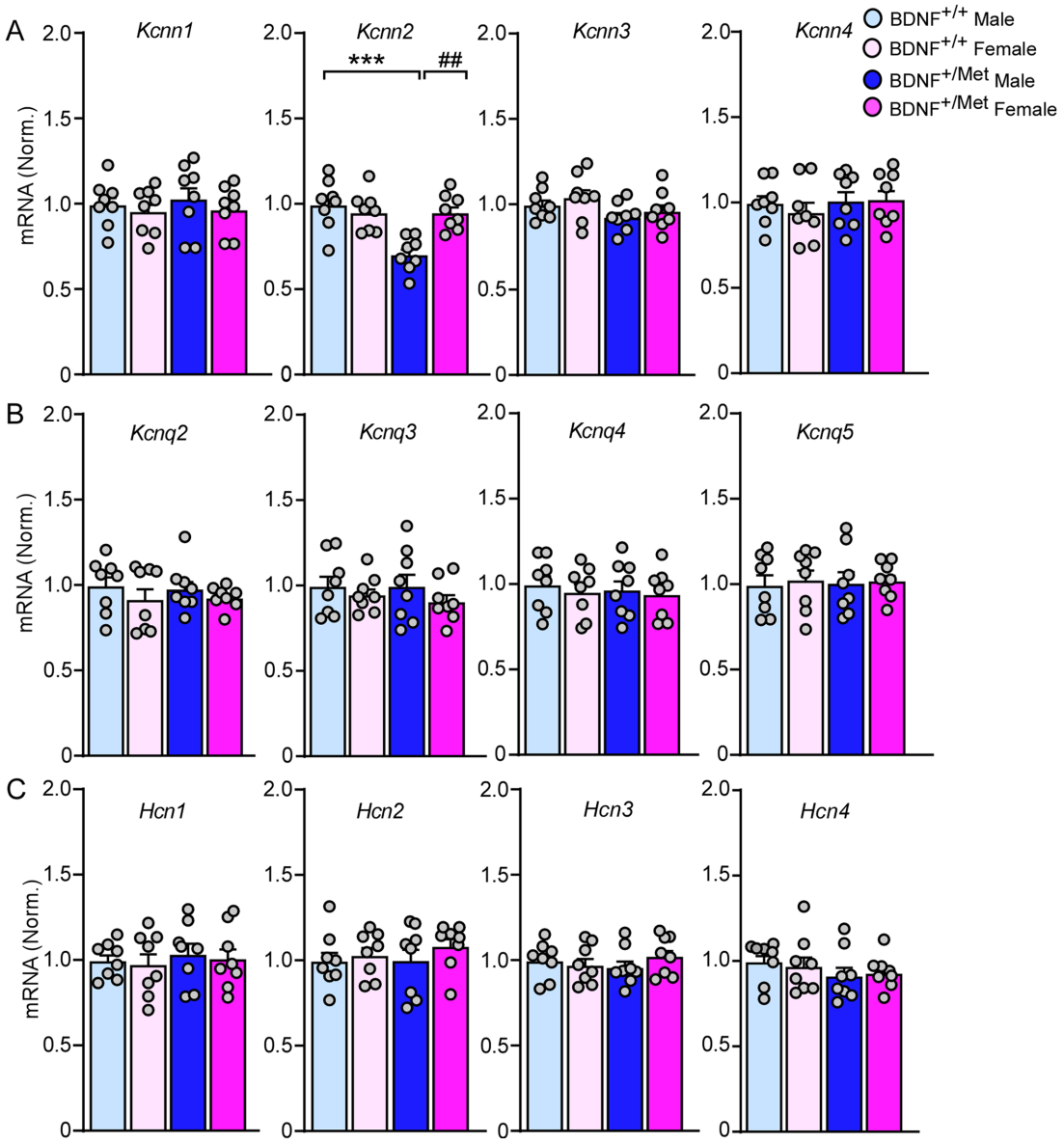

FIGURE 4
The impact of diminished activity-dependent BDNF signaling on the expression of SK channels, KCNQ channels, and HCN channels in the PFC. Quantitative real-time PCR showing the mRNA levels of SK channels **(A)**, KCNQ channels **(B)**, and HCN channels **(C)** in the PFC of BDNF$^{+/+}$ and BDNF$^{+/Met}$ mice. ***$p < 0.001$, BDNF$^{+/Met}$ versus BDNF$^{+/+}$; ##$p < 0.01$, male versus female, $n = 8$ mice/group, two-way ANOVA.

(I_h) (Biel et al., 2009; Mishra and Narayanan, 2023; Santoro and Shah, 2020). In the mouse brain, HCN1 and HCN2 are predominantly expressed in the presynaptic synapse, soma, dendrites, and axon initial segments of layer V pyramidal neurons in the frontal cortex (Santoro and Shah, 2020), where they regulate glutamate release (Huang and Trussell, 2014) and generation of action potentials (Ko et al., 2016). The hyperexcitability of layer V pyramidal neurons in the anterior cingulate cortex was associated with a decrease in I_h (Santello and Nevian, 2015). *HCN1/2* are implicated in early infantile epileptic encephalopathy and absence seizures (Crunelli et al., 2023; Ludwig et al., 2003; Nava et al., 2014). In this study, there were no differences in the expressions of *Hcn1-4* between BDNF$^{+/+}$ and BDNF$^{+/Met}$ mice.

Therefore, diminished activity-dependent BDNF signaling selectively decreased the expression of *Kcnn2*, but *not Kcnn1*, *Kcnn3*, *Kcnn4*, Kv7 channels, and HCN channels, which indicates SK2 mediates the decreased mAHP in male BDNF$^{+/Met}$ mice.

There are several limitations in this study. First, the causal link between upregulated *Scn2a,* decreased *Kccn2* and increased intrinsic excitatory in pyramidal neurons of male BDNF$^{+/Met}$ mice is unknown. Selectively knockdown *Scn2a* and overexpression of *Kcnn2* in the pyramidal neurons of male BDNF$^{+/Met}$ mice will confirm this causal link in our future studies. Female C57Bl/6J mice exhibited higher glutamatergic transmission in the PFC compared to males (Knouse et al., 2022). Second, the contribution of synaptic inputs on the neuronal excitability of pyramidal neurons in the PFC, and the impact of diminished activity-dependent BDNF signaling on the principle neurons in the other brain regions, need to be further investigated, which may mediate the anxiety, autism-like social deficits, and sex-specific effect of diminished activity-dependent BDNF signaling

on spatial memory (Ma et al., 2023). Third, the molecular mechanisms underlying the increased *Scn2a* and decreased *Kcnn2* in the PFC of male BDNF$^{+/Met}$ mice are difficult to decipher at this moment, which will be investigated in future studies.

In summary, using a knock-in mouse model of the human BDNF Val66 Met SNP, the present study demonstrates that the increased *Scn2a* and decreased *Kcnn2* account for the sex effect of diminished activity-dependent BDNF signaling on the intrinsic excitability of pyramidal neurons in the PFC. The sex differences of intrinsic excitability of pyramidal neurons in the PFC of male and female BDNF$^{+/Met}$ mice may partially contribute to the severe autism-like behavioral deficits in male BDNF$^{+/Met}$ mice (Ma et al., 2023) and support that males are more vulnerable to having ASD (Giarelli et al., 2010; Werling and Geschwind, 2013). Targeting *Scn2a* and *Kcnn2* is a potential therapy for male ASD patients with or without BDNF Val66Met SNP.

Data availability statement

The raw data supporting the conclusions of this article will be made available by the authors, without undue reservation.

Ethics statement

The animal study was approved by Institutional Animal Care and Use Committee of Sanford School of Medicine, University of South Dakota. The study was conducted in accordance with the local legislation and institutional requirements.

Author contributions

KMa: Conceptualization, Data curation, Formal analysis, Investigation, Methodology, Resources, Writing – review & editing. DZ: Formal analysis, Writing – review & editing. KMc: Formal analysis, Writing – review & editing. MW: Formal analysis, Writing – review & editing. SN: Funding acquisition, Writing – review & editing. FL: Funding acquisition, Writing – review & editing. LQ: Conceptualization, Funding acquisition, Data curation, Formal analysis, Investigation, Methodology, Resources, Project administration, Supervision, Validation, Writing – original draft, Writing – review & editing.

Funding

The author(s) declare that financial support was received for the research, authorship, and/or publication of this article. This work is supported by startup funding from Sanford School of Medicine, University of South Dakota (LQ), Sanford School of Medicine Faculty Research Grant (LQ), South Dakota Board of Regents Competitive Research Grant (LQ), NIH R21 MH134106 (LQ), NIH P20 GM103443 (KMc), NIH R01 MH106640 (SSN), and NIH R01 MH123154 (FL).

Acknowledgments

We are grateful to Dr. Sunghee Cho (Burke Neurological Institute, Weill Medical College of Cornell University) for the mice with knock-in of a human BDNF Met variant.

Conflict of interest

The authors declare that the research was conducted in the absence of any commercial or financial relationships that could be construed as a potential conflict of interest.

The author(s) declared that they were an editorial board member of Frontiers, at the time of submission. This had no impact on the peer review process and the final decision.

Publisher's note

Supplementary material

The Supplementary material for this article can be found online at: https://www.frontiersin.org/articles/10.3389/fncel.2024.1496930/full#supplementary-material

SUPPLEMENTARY FIGURE S1
Quantification of the number of evoked action potentials in response to injected currents in the regular spiking pyramidal neurons **(A)** and intrinsic bursting pyramidal neurons **(B)** of PFC from BDNF$^{+/+}$ and BDNF$^{+/Met}$ mice. A: *n* = 8-10 neurons/4-5 mice/group; B: n = 7-10 neurons/4-5 mice/group.

SUPPLEMENTARY FIGURE S2
Diminished activity-dependent BDNF signaling has no effect on the passive membrane properties of pyramidal neurons in male and female mice. *n* = 16-20 neurons/4-5 mice per group. **(A)** Resting potential, **(B)** Capacitance, **(C)** Input resistance, **(D)** Membrane time constant (τ), and **(E)** Representative traces in response to -100 pA hyperpolarizing current injection with 250 ms duration in the pyramidal neurons from PFC of BDNF$^{+/+}$ and BDNF$^{+/Met}$ mice.

References

Alonso-Gonzalez, A., Calaza, M., Rodriguez-Fontenla, C., and Carracedo, A. (2019). Novel gene-based analysis of ASD GWAS: insight into the biological role of associated genes. *Front. Genet.* 10:733. doi: 10.3389/fgene.2019.00733

Arnsten, A. F., and Rubia, K. (2012). Neurobiological circuits regulating attention, cognitive control, motivation, and emotion: disruptions in neurodevelopmental psychiatric disorders. *J. Am. Acad. Child Adolesc. Psychiatry* 51, 356–367. doi: 10.1016/j.jaac.2012.01.008

Bauer, C. K., Schneeberger, P. E., Kortüm, F., Altmüller, J., Santos-Simarro, F., Baker, L., et al. (2019). Gain-of-function mutations in KCNN3 encoding the small-conductance ca(2+)-activated K(+) channel SK3 cause Zimmermann-Laband syndrome. *Am. J. Hum. Genet.* 104, 1139–1157. doi: 10.1016/j.ajhg.2019.04.012

Bean, B. P. (2007). The action potential in mammalian central neurons. *Nat. Rev. Neurosci.* 8, 451–465. doi: 10.1038/nrn2148

Biel, M., Wahl-Schott, C., Michalakis, S., and Zong, X. (2009). Hyperpolarization-activated cation channels: from genes to function. *Physiol. Rev.* 89, 847–885. doi: 10.1152/physrev.00029.2008

Blackmon, K., Bluvstein, J., MacAllister, W. S., Avallone, J., Misajon, J., Hedlund, J., et al. (2016). Treatment resistant epilepsy in Autism Spectrum disorder: increased risk for females. *Autism Res.* 9, 311–320. doi: 10.1002/aur.1514

Brown, D. A., and Passmore, G. M. (2009). Neural KCNQ (Kv7) channels. *Br. J. Pharmacol.* 156, 1185–1195. doi: 10.1111/j.1476-5381.2009.00111.x

Chao, M. V. (2003). Neurotrophins and their receptors: a convergence point for many signalling pathways. *Nat. Rev. Neurosci.* 4, 299–309. doi: 10.1038/nrn1078

Chen, L., Cummings, K. A., Mau, W., Zaki, Y., Dong, Z., Rabinowitz, S., et al. (2020). The role of intrinsic excitability in the evolution of memory: significance in memory allocation, consolidation, and updating. *Neurobiol. Learn. Mem.* 173:107266. doi: 10.1016/j.nlm.2020.107266

Chen, Z. Y., Jing, D., Bath, K. G., Ieraci, A., Khan, T., Siao, C. J., et al. (2006). Genetic variant BDNF (Val66Met) polymorphism alters anxiety-related behavior. *Science* 314, 140–143. doi: 10.1126/science.1129663

Crunelli, V., David, F., Morais, T. P., and Lorincz, M. L. (2023). HCN channels and absence seizures. *Neurobiol. Dis.* 181:106107. doi: 10.1016/j.nbd.2023.106107

Davidson, R. J. (2002). Anxiety and affective style: role of prefrontal cortex and amygdala. *Biol. Psychiatry* 51, 68–80. doi: 10.1016/S0006-3223(01)01328-2

Delmas, P., and Brown, D. A. (2005). Pathways modulating neural KCNQ/M (Kv7) potassium channels. *Nat. Rev. Neurosci.* 6, 850–862. doi: 10.1038/nrn1785

Desai, N. S., Rutherford, L. C., and Turrigiano, G. G. (1999a). BDNF regulates the intrinsic excitability of cortical neurons. *Learn. Mem.* 6, 284–291. doi: 10.1101/lm.6.3.284

Desai, N. S., Rutherford, L. C., and Turrigiano, G. G. (1999b). Plasticity in the intrinsic excitability of cortical pyramidal neurons. *Nat. Neurosci.* 2, 515–520. doi: 10.1038/9165

Duffney, L. J., Zhong, P., Wei, J., Matas, E., Cheng, J., Qin, L., et al. (2015). Autism-like deficits in Shank3-deficient mice are rescued by targeting actin regulators. *Cell Rep.* 11, 1400–1413. doi: 10.1016/j.celrep.2015.04.064

Dwivedi, D., and Bhalla, U. S. (2021). Physiology and therapeutic potential of SK, H, and M medium AfterHyperPolarization ion channels. *Front. Mol. Neurosci.* 14:658435. doi: 10.3389/fnmol.2021.658435

Eaton, M., Zhang, J., Ma, Z., Park, A. C., Lietzke, E., Romero, C. M., et al. (2021). Generation and basic characterization of a gene-trap knockout mouse model of Scn2a with a substantial reduction of voltage-gated sodium channel Na(v) 1.2 expression. *Genes Brain Behav.* 20:e12725. doi: 10.1111/gbb.12725

Ebert, D. H., and Greenberg, M. E. (2013). Activity-dependent neuronal signalling and autism spectrum disorder. *Nature* 493, 327–337. doi: 10.1038/nature11860

Egan, M. F., Kojima, M., Callicott, J. H., Goldberg, T. E., Kolachana, B. S., Bertolino, A., et al. (2003). The BDNF val66met polymorphism affects activity-dependent secretion of BDNF and human memory and hippocampal function. *Cell* 112, 257–269. doi: 10.1016/S0092-8674(03)00035-7

Faber, E. S., and Sah, P. (2007). Functions of SK channels in central neurons. *Clin. Exp. Pharmacol. Physiol.* 34, 1077–1083. doi: 10.1111/j.1440-1681.2007.04725.x

Franceschetti, S., Sancini, G., Panzica, F., Radici, C., and Avanzini, G. (1998). Postnatal differentiation of firing properties and morphological characteristics in layer V pyramidal neurons of the sensorimotor cortex. *Neuroscience* 83, 1013–1024. doi: 10.1016/S0306-4522(97)00463-6

Frye, R. E., Rossignol, D., Casanova, M. F., Brown, G. L., Martin, V., Edelson, S., et al. (2013). A review of traditional and novel treatments for seizures in autism spectrum disorder: findings from a systematic review and expert panel. *Front. Public Health* 1:31. doi: 10.3389/fpubh.2013.00031

Gao, R., and Penzes, P. (2015). Common mechanisms of excitatory and inhibitory imbalance in schizophrenia and autism spectrum disorders. *Curr. Mol. Med.* 15, 146–167. doi: 10.2174/1566524015666150303003028

Garcia-Junco-Clemente, P., Chow, D. K., Tring, E., Lazaro, M. T., Trachtenberg, J. T., and Golshani, P. (2013). Overexpression of calcium-activated potassium channels underlies cortical dysfunction in a model of PTEN-associated autism. *Proc. Natl. Acad. Sci. USA* 110, 18297–18302. doi: 10.1073/pnas.1309207110

Giarelli, E., Wiggins, L. D., Rice, C. E., Levy, S. E., Kirby, R. S., Pinto-Martin, J., et al. (2010). Sex differences in the evaluation and diagnosis of autism spectrum disorders among children. *Disabil. Health J.* 3, 107–116. doi: 10.1016/j.dhjo.2009.07.001

Goldin, A. L., Barchi, R. L., Caldwell, J. H., Hofmann, F., Howe, J. R., Hunter, J. C., et al. (2000). Nomenclature of voltage-gated sodium channels. *Neuron* 28, 365–368. doi: 10.1016/S0896-6273(00)00116-1

Greenberg, M. E., Xu, B., Lu, B., and Hempstead, B. L. (2009). New insights in the biology of BDNF synthesis and release: implications in CNS function. *J. Neurosci.* 29, 12764–12767. doi: 10.1523/JNEUROSCI.3566-09.2009

Griego, E., Santiago-Jiménez, G., and Galván, E. J. (2022). Systemic administration of lipopolysaccharide induces hyperexcitability of prelimbic neurons via modulation of sodium and potassium currents. *Neurotoxicology* 91, 128–139. doi: 10.1016/j.neuro.2022.05.010

Gripp, K. W., Smithson, S. F., Scurr, I. J., Baptista, J., Majumdar, A., Pierre, G., et al. (2021). Syndromic disorders caused by gain-of-function variants in KCNH1, KCNK4, and KCNN3-a subgroup of K(+) channelopathies. *Eur. J. Hum. Genet.* 29, 1384–1395. doi: 10.1038/s41431-021-00818-9

Grove, J., Ripke, S., Als, T. D., Mattheisen, M., Walters, R. K., Won, H., et al. (2019). Identification of common genetic risk variants for autism spectrum disorder. *Nat. Genet.* 51, 431–444. doi: 10.1038/s41588-019-0344-8

Gu, N., Vervaeke, K., Hu, H., and Storm, J. F. (2005). Kv7/KCNQ/M and HCN/h, but not KCa2/SK channels, contribute to the somatic medium after-hyperpolarization and excitability control in CA1 hippocampal pyramidal cells. *J. Physiol.* 566, 689–715. doi: 10.1113/jphysiol.2005.086835

Hedrick, T., and Waters, J. (2011). Spiking patterns of neocortical L5 pyramidal neurons in vitro change with temperature. *Front. Cell. Neurosci.* 5:1. doi: 10.3389/fncel.2011.00001

Homozygosity Mapping Collaborative for Autismde Rubeis, S., He, X., Goldberg, A. P., Poultney, C. S., Samocha, K., et al. (2014). Synaptic, transcriptional and chromatin genes disrupted in autism. *Nature* 515, 209–215. doi: 10.1038/nature13772

Huang, H., and Trussell, L. O. (2014). Presynaptic HCN channels regulate vesicular glutamate transport. *Neuron* 84, 340–346. doi: 10.1016/j.neuron.2014.08.046

Isokawa, M. (1997). Membrane time constant as a tool to assess cell degeneration. *Brain Res. Brain Res. Protoc.* 1, 114–116. doi: 10.1016/S1385-299X(96)00016-5

Jeste, S. S., and Tuchman, R. (2015). Autism Spectrum disorder and epilepsy: two sides of the same coin? *J. Child Neurol.* 30, 1963–1971. doi: 10.1177/0883073815601501

Khandelwal, N., Cavalier, S., Rybalchenko, V., Kulkarni, A., Anderson, A. G., Konopka, G., et al. (2021). FOXP1 negatively regulates intrinsic excitability in D2 striatal projection neurons by promoting inwardly rectifying and leak potassium currents. *Mol. Psychiatry* 26, 1761–1774. doi: 10.1038/s41380-020-00995-x

Knouse, M. C., McGrath, A. G., Deutschmann, A. U., Rich, M. T., Zallar, L. J., Rajadhyaksha, A. M., et al. (2022). Sex differences in the medial prefrontal cortical glutamate system. *Biol. Sex Differ.* 13:66. doi: 10.1186/s13293-022-00468-6

Ko, K. W., Rasband, M. N., Meseguer, V., Kramer, R. H., and Golding, N. L. (2016). Serotonin modulates spike probability in the axon initial segment through HCN channels. *Nat. Neurosci.* 19, 826–834. doi: 10.1038/nn.4293

Lai, H. C., and Jan, L. Y. (2006). The distribution and targeting of neuronal voltage-gated ion channels. *Nat. Rev. Neurosci.* 7, 548–562. doi: 10.1038/nrn1938

Lee, E., Lee, J., and Kim, E. (2017). Excitation/inhibition imbalance in animal models of Autism Spectrum disorders. *Biol. Psychiatry* 81, 838–847. doi: 10.1016/j.biopsych.2016.05.011

Li, M., West, J. W., Lai, Y., Scheuer, T., and Catterall, W. A. (1992). Functional modulation of brain sodium channels by cAMP-dependent phosphorylation. *Neuron* 8, 1151–1159. doi: 10.1016/0896-6273(92)90135-Z

Ludwig, A., Budde, T., Stieber, J., Moosmang, S., Wahl, C., Holthoff, K., et al. (2003). Absence epilepsy and sinus dysrhythmia in mice lacking the pacemaker channel HCN2. *EMBO J.* 22, 216–224. doi: 10.1093/emboj/cdg032

Ma, K., Taylor, C., Williamson, M., Newton, S. S., and Qin, L. (2023). Diminished activity-dependent BDNF signaling differentially causes autism-like behavioral deficits in male and female mice. *Front. Psych.* 14:1182472. doi: 10.3389/fpsyt.2023.1182472

Maljevic, S., and Lerche, H. (2014). Potassium channel genes and benign familial neonatal epilepsy. *Prog. Brain Res.* 213, 17–53. doi: 10.1016/B978-0-444-63326-2.00002-8

Manz, K. M., Siemann, J. K., McMahon, D. G., and Grueter, B. A. (2021). Patch-clamp and multi-electrode array electrophysiological analysis in acute mouse brain slices. *STAR Protoc.* 2:100442. doi: 10.1016/j.xpro.2021.100442

Mateos-Aparicio, P., Murphy, R., and Storm, J. F. (2014). Complementary functions of SK and Kv7/M potassium channels in excitability control and synaptic integration in rat hippocampal dentate granule cells. *J. Physiol.* 592, 669–693. doi: 10.1113/jphysiol.2013.267872

Milescu, L. S., Bean, B. P., and Smith, J. C. (2010). Isolation of somatic Na+ currents by selective inactivation of axonal channels with a voltage prepulse. *J. Neurosci.* 30, 7740–7748. doi: 10.1523/JNEUROSCI.6136-09.2010

Mishra, P., and Narayanan, R. (2023). The enigmatic HCN channels: a cellular neurophysiology perspective. *Proteins*. 1–21. doi: 10.1002/prot.26643

Murugan, M., Jang, H. J., Park, M., Miller, E. M., Cox, J., Taliaferro, J. P., et al. (2017). Combined social and spatial coding in a descending projection from the prefrontal cortex. *Cell* 171, 1663–77.e16. doi: 10.1016/j.cell.2017.11.002

Nam, Y. W., Downey, M., Rahman, M. A., Cui, M., and Zhang, M. (2023). Channelopathy of small- and intermediate-conductance ca(2+)-activated K(+) channels. *Acta Pharmacol. Sin.* 44, 259–267. doi: 10.1038/s41401-022-00935-1

Nava, C., Dalle, C., Rastetter, A., Striano, P., de Kovel, C. G., Nabbout, R., et al. (2014). De novo mutations in HCN1 cause early infantile epileptic encephalopathy. *Nat. Genet.* 46, 640–645. doi: 10.1038/ng.2952

Notaras, M., Hill, R., and van den Buuse, M. (2015). The BDNF gene Val66Met polymorphism as a modifier of psychiatric disorder susceptibility: progress and controversy. *Mol. Psychiatry* 20, 916–930. doi: 10.1038/mp.2015.27

Pappalardo, L. W., Black, J. A., and Waxman, S. G. (2016). Sodium channels in astroglia and microglia. *Glia* 64, 1628–1645. doi: 10.1002/glia.22967

Peters, H. C., Hu, H., Pongs, O., Storm, J. F., and Isbrandt, D. (2005). Conditional transgenic suppression of M channels in mouse brain reveals functions in neuronal excitability, resonance and behavior. *Nat. Neurosci.* 8, 51–60. doi: 10.1038/nn1375

Piro, E., Nardello, R., Gennaro, E., Fontana, A., Taglialatela, M., Donato Mangano, G., et al. (2019). A novel mutation in KCNQ3-related benign familial neonatal epilepsy: electroclinical features and neurodevelopmental outcome. *Epileptic Disord.* 21, 87–91. doi: 10.1684/epd.2019.1030

Qin, L., Ma, K., Wang, Z. J., Hu, Z., Matas, E., Wei, J., et al. (2018). Social deficits in Shank3-deficient mouse models of autism are rescued by histone deacetylase (HDAC) inhibition. *Nat Neurosci.* 21, 564–575. doi: 10.1038/s41593-018-0110-8

Qin, L., Ma, K., and Yan, Z. (2019). Chemogenetic activation of prefrontal cortex in Shank3-deficient mice ameliorates social deficits, NMDAR hypofunction, and Sgk2 downregulation. *iScience* 17, 24–35. doi: 10.1016/j.isci.2019.06.014

Qin, L., Williams, J. B., Tan, T., Liu, T., Cao, Q., Ma, K., et al. (2021). Deficiency of autism risk factor ASH1L in prefrontal cortex induces epigenetic aberrations and seizures. *Nat. Commun.* 12:6589. doi: 10.1038/s41467-021-26972-8

Raznahan, A., Toro, R., Proitsi, P., Powell, J., Paus, T., Bolton, P., et al. (2009). A functional polymorphism of the brain derived neurotrophic factor gene and cortical anatomy in autism spectrum disorder. *J. Neurodev. Disord.* 1, 215–223. doi: 10.1007/s11689-009-9012-0

Ritter-Makinson, S., Clemente-Perez, A., Higashikubo, B., Cho, F. S., Holden, S. S., Bennett, E., et al. (2019). Augmented reticular thalamic bursting and seizures in Scn1a-Dravet syndrome. *Cell Rep.* 26, 54–64.e6. doi: 10.1016/j.celrep.2018.12.018

Sanders, S. J., Campbell, A. J., Cottrell, J. R., Moller, R. S., Wagner, F. F., Auldridge, A. L., et al. (2018). Progress in understanding and treating SCN2A-mediated disorders. *Trends Neurosci.* 41, 442–456. doi: 10.1016/j.tins.2018.03.011

Sansa, G., Carlson, C., Doyle, W., Weiner, H. L., Bluvstein, J., Barr, W., et al. (2011). Medically refractory epilepsy in autism. *Epilepsia* 52, 1071–1075. doi: 10.1111/j.1528-1167.2011.03069.x

Santello, M., and Nevian, T. (2015). Dysfunction of cortical dendritic integration in neuropathic pain reversed by serotoninergic neuromodulation. *Neuron* 86, 233–246. doi: 10.1016/j.neuron.2015.03.003

Santoro, B., and Shah, M. M. (2020). Hyperpolarization-activated cyclic nucleotide-gated channels as drug targets for neurological disorders. *Annu. Rev. Pharmacol. Toxicol.* 60, 109–131. doi: 10.1146/annurev-pharmtox-010919-023356

Satterstrom, F. K., Kosmicki, J. A., Wang, J., Breen, M. S., De Rubeis, S., An, J. Y., et al. (2020). Large-scale exome Sequencing study implicates both developmental and functional changes in the neurobiology of Autism. *Cell* 180, 568–84.e23. doi: 10.1016/j.cell.2019.12.036

Schwarz, M., Ryba, L., Křepelová, A., Moslerová, V., Zelinová, M., Turnovec, M., et al. (2022). Zimmermann-Laband syndrome in monozygotic twins with a mild neurobehavioral phenotype lacking gingival overgrowth-a case report of a novel KCNN3 gene variant. *Am. J. Med. Genet. A* 188, 1083–1087. doi: 10.1002/ajmg.a.62616

Shansky, R. M., and Woolley, C. S. (2016). Considering sex as a biological variable will be valuable for neuroscience research. *J. Neurosci.* 36, 11817–11822. doi: 10.1523/JNEUROSCI.1390-16.2016

Soh, H., Pant, R., LoTurco, J. J., and Tzingounis, A. V. (2014). Conditional deletions of epilepsy-associated KCNQ2 and KCNQ3 channels from cerebral cortex cause differential effects on neuronal excitability. *J. Neurosci.* 34, 5311–5321. doi: 10.1523/JNEUROSCI.3919-13.2014

Soldovieri, M. V., Boutry-Kryza, N., Milh, M., Doummar, D., Heron, B., Bourel, E., et al. (2014). Novel KCNQ2 and KCNQ3 mutations in a large cohort of families with benign neonatal epilepsy: first evidence for an altered channel regulation by syntaxin-1A. *Hum. Mutat.* 35, 356–367. doi: 10.1002/humu.22500

Song, M., Martinowich, K., and Lee, F. S. (2017). BDNF at the synapse: why location matters. *Mol. Psychiatry* 22, 1370–1375. doi: 10.1038/mp.2017.144

Sontheimer, H., and Ransom, C. B. (2002). "Whole-cell patch-clamp recordings" in Patch-clamp analysis. eds. W. Walz, A. A. Boulton and G. B. Baker (New Jersey: Humana Press), 35–68.

Spratt, P. W. E., Alexander, R. P. D., Ben-Shalom, R., Sahagun, A., Kyoung, H., Keeshen, C. M., et al. (2021). Paradoxical hyperexcitability from Na(V)1.2 sodium channel loss in neocortical pyramidal cells. *Cell Rep.* 36:109483. doi: 10.1016/j.celrep.2021.109483

Spratt, P. W. E., Ben-Shalom, R., Keeshen, C. M., Burke, K. J., Clarkson, R. L., Sanders, S. J., et al. (2019). The Autism-associated gene Scn2a contributes to dendritic excitability and synaptic function in the prefrontal cortex. *Neuron* 103, 673–85.e5. doi: 10.1016/j.neuron.2019.05.037

Stoner, R., Chow, M. L., Boyle, M. P., Sunkin, S. M., Mouton, P. R., Roy, S., et al. (2014). Patches of disorganization in the neocortex of children with autism. *N. Engl. J. Med.* 370, 1209–1219. doi: 10.1056/NEJMoa1307491

Sun, Q., Jiang, Y. Q., and Lu, M. C. (2020). Topographic heterogeneity of intrinsic excitability in mouse hippocampal CA3 pyramidal neurons. *J. Neurophysiol.* 124, 1270–1284. doi: 10.1152/jn.00147.2020

Sun, J., Liu, Y., Baudry, M., and Bi, X. (2020). SK2 channel regulation of neuronal excitability, synaptic transmission, and brain rhythmic activity in health and diseases. *Biochim. Biophys. Acta, Mol. Cell Res.* 1867:118834. doi: 10.1016/j.bbamcr.2020.118834

Surges, R., Brewster, A. L., Bender, R. A., Beck, H., Feuerstein, T. J., and Baram, T. Z. (2006). Regulated expression of HCN channels and cAMP levels shape the properties of the h current in developing rat hippocampus. *Eur. J. Neurosci.* 24, 94–104. doi: 10.1111/j.1460-9568.2006.04880.x

Tatsukawa, T., Raveau, M., Ogiwara, I., Hattori, S., Miyamoto, H., Mazaki, E., et al. (2019). Scn2a haploinsufficient mice display a spectrum of phenotypes affecting anxiety, sociability, memory flexibility and ampakine CX516 rescues their hyperactivity. *Mol. Autism.* 10:15. doi: 10.1186/s13229-019-0265-5

Viscidi, E. W., Triche, E. W., Pescosolido, M. F., McLean, R. L., Joseph, R. M., Spence, S. J., et al. (2013). Clinical characteristics of children with autism spectrum disorder and co-occurring epilepsy. *PLoS One* 8:e67797. doi: 10.1371/journal.pone.0067797

Wang, X., Bey, A. L., Katz, B. M., Badea, A., Kim, N., David, L. K., et al. (2016). Altered mGluR5-Homer scaffolds and corticostriatal connectivity in a Shank3 complete knockout model of autism. *Nat. Commun.* 7:11459. doi: 10.1038/ncomms11459

Wang, T., Hoekzema, K., Vecchio, D., Wu, H., Sulovari, A., Coe, B. P., et al. (2020). Large-scale targeted sequencing identifies risk genes for neurodevelopmental disorders. *Nat. Commun.* 11:4932. doi: 10.1038/s41467-020-18723-y

Werling, D. M., and Geschwind, D. H. (2013). Sex differences in autism spectrum disorders. *Curr. Opin. Neurol.* 26, 146–153. doi: 10.1097/WCO.0b013e32835ee548

Wu, X. B., Liang, B., and Gao, Y. J. (2016). The increase of intrinsic excitability of layer V pyramidal cells in the prelimbic medial prefrontal cortex of adult mice after peripheral inflammation. *Neurosci. Lett.* 611, 40–45. doi: 10.1016/j.neulet.2015.11.030

Yamagata, T., Ogiwara, I., Mazaki, E., Yanagawa, Y., and Yamakawa, K. (2017). Nav1.2 is expressed in caudal ganglionic eminence-derived disinhibitory interneurons: mutually exclusive distributions of Nav1.1 and Nav1.2. *Biochem. Biophys. Res. Commun.* 491, 1070–1076. doi: 10.1016/j.bbrc.2017.08.013

Yap, E. L., and Greenberg, M. E. (2018). Activity-regulated transcription: bridging the gap between neural activity and behavior. *Neuron* 100, 330–348. doi: 10.1016/j.neuron.2018.10.013

Yizhar, O., Fenno, L. E., Prigge, M., Schneider, F., Davidson, T. J., O'Shea, D. J., et al. (2011). Neocortical excitation/inhibition balance in information processing and social dysfunction. *Nature* 477, 171–178. doi: 10.1038/nature10360

Yoo, H. J., Yang, S. Y., Cho, I. H., Park, M., and Kim, S. A. (2014). Polymorphisms of BDNF gene and autism spectrum disorders: family based association study with korean trios. *Psychiatry Investig.* 11, 319–324. doi: 10.4306/pi.2014.11.3.319

Zhang, J., Chen, X., Eaton, M., Wu, J., Ma, Z., Lai, S., et al. (2021). Severe deficiency of the voltage-gated sodium channel Na(V)1.2 elevates neuronal excitability in adult mice. *Cell Rep.* 36:109495. doi: 10.1016/j.celrep.2021.109495

Zhang, W., and Linden, D. J. (2003). The other side of the engram: experience-driven changes in neuronal intrinsic excitability. *Nat. Rev. Neurosci.* 4, 885–900. doi: 10.1038/nrn1248

Zhong, P., Cao, Q., and Yan, Z. (2022). Selective impairment of circuits between prefrontal cortex glutamatergic neurons and basal forebrain cholinergic neurons in a tauopathy mouse model. *Cereb. Cortex* 32, 5569–5579. doi: 10.1093/cercor/bhac036

Zhong, P., Qin, L., and Yan, Z. (2020). Dopamine differentially regulates response dynamics of prefrontal cortical principal neurons and interneurons to Optogenetic stimulation of inputs from ventral tegmental area. *Cereb. Cortex* 30, 4402–4409. doi: 10.1093/cercor/bhaa027

frontiers | Frontiers in Physiology

TYPE Original Research
PUBLISHED 15 January 2025
DOI 10.3389/fphys.2024.1481460

OPEN ACCESS

EDITED BY
Paras Kumar Mishra,
University of Nebraska Medical Center,
United States

REVIEWED BY
Bochra Tourki,
USF Health, United States
Mallikarjun Patil,
University of Alabama at Birmingham,
United States

*CORRESPONDENCE
William C. W. Chen,
william.chen@usd.edu

RECEIVED 15 August 2024
ACCEPTED 26 December 2024
PUBLISHED 15 January 2025

CITATION
Zhang JJ, Rizk R, Li X, Lee BG, Matthies ML, Bietz KA, Kim K, Huard J, Wang Y and Chen WCW (2025) Interleukin-10 exhibit dose-dependent effects on macrophage phenotypes and cardiac remodeling after myocardial infarction.
Front. Physiol. 15:1481460.
doi: 10.3389/fphys.2024.1481460

Interleukin-10 exhibit dose-dependent effects on macrophage phenotypes and cardiac remodeling after myocardial infarction

Jing J. Zhang[1], Rodrigue Rizk[2], Xiaoping Li[1], Brandon G. Lee[3], Mason L. Matthies[1], Kennedy A. Bietz[1], Kang Kim[3,4,5], Johnny Huard[6], Yadong Wang[7] and William C. W. Chen[1]*

[1]Division of Basic Biomedical Sciences, Sanford School of Medicine, University of South Dakota, Vermillion, SD, United States, [2]Department of Computer Science, University of South Dakota, Vermillion, SD, United States, [3]Department of Bioengineering, Swanson School of Engineering, University of Pittsburgh, Pittsburgh, PA, United States, [4]Center for Ultrasound Molecular Imaging and Therapeutics, Department of Medicine, University of Pittsburgh School of Medicine, Pittsburgh, PA, United States, [5]McGowan Institute for Regenerative Medicine, University of Pittsburgh, Pittsburgh, PA, United States, [6]The Linda & Mitch Center for Regenerative and Personalized Medicine, Steadman Philippon Research Institute, Vail, CO, United States, [7]The Biofoundry, Department of Biomedical Engineering, Cornell University, Ithaca, NY, United States

Introduction: Interleukin-10 (IL-10) is a potent immunomodulatory cytokine widely explored as a therapeutic agent for diseases, including myocardial infarction (MI). High-dose IL-10 treatment may not achieve expected outcomes, raising the question of whether IL-10 has dose-dependency, or even uncharted side-effects from overdosing. We hypothesized that IL-10 has dose-dependent effects on macrophage (Mφ) phenotypic transition and cardiac remodeling after MI.

Methods: Using RAW264.7 monocyte models, we examined whether administering differential doses of exogenous IL-10 (0–1,000 ng/mL) perturbs classic M1 (pro-inflammatory) and M2 (anti-inflammatory) phenotypes of polarized Mφ or even alters the phenotypic transition of prospective M1 and M2 polarization. We then investigated the impact of single intramyocardial IL-10 administration on cardiac function, structure, and inflammation post-MI, using a mouse MI model.

Results: Compared with 0-ng/mL control, 250-ng/mL IL-10 had the strongest overall effects in decreasing M1 and increasing M2 phenotypes on polarized Mφ while ≥500-ng/mL IL-10 dampened M1 polarization and augmented native IL-10 secretion more effectively than low doses *in vitro*. Echocardiography revealed that the 250-ng group had consistently higher contractile function and lower left ventricular (LV) dilatation than the saline control over 6 weeks while ≥1,000-ng groups exhibited transient lower LV ejection fraction at 5 days post-MI *in vivo*. Moreover, different doses of IL-10 differentially modulated myocardial gene expression, phagocytic cell infiltration at the infarct, LV fibrosis, and revascularization post-MI, with some, but not all, doses exerting beneficial effects.

Discussion: Our study suggested that IL-10 has an effective dose range on Mφ phenotypes, and intramyocardial IL-10 treatment may trigger cardioprotective or unwanted effects post-MI in a dose-dependent manner.

KEYWORDS

interleukin-10, ischemic heart disease, myocardial infarction, immunomodulation, macrophage phenotype, cardiac remodeling

Introduction

In 2023, cardiovascular disease (CVD) caused roughly 20.5 million deaths worldwide, representing an 18.5% increase in the CVD-associated death rate compared to that of 2010 (Tsao et al., 2023). The role of tissue inflammatory responses in cardiac remodeling and functional recovery following myocardial damage has been widely investigated in recent years (Epelman et al., 2015; Frangogiannis, 2015; Santos-Zas et al., 2018; Halade and Lee, 2022). The early-phase inflammatory responses are primarily initiated and propagated by the innate immune system soon after myocardial injury and typically involve multiple secretory cytokines that mediate a variety of pathophysiological activities within and around the damaged tissue, such as cell death, myocardial fibrosis, metabolic homeostasis, and tissue regeneration (Halade and Lee, 2022; Frangogiannis, 2014; Pluijmert et al., 2021). For example, the expression of tumor necrosis factor (TNF)-α, a critical pro-inflammatory cytokine, significantly increases in the failing myocardium (Schumacher and Naga Prasad, 2018). Interleukin-6 (IL-6) is a versatile cytokine that is notably elevated and primarily activates pro-inflammatory responses after acute myocardial infarction (AMI) (Anderson et al., 2013). On the other hand, interleukin-10 (IL-10) is a pleiotropic cytokine that exhibits broad immunoregulatory and anti-inflammatory activities (Iyer and Cheng, 2012; Saraiva et al., 2020; Carlini et al., 2023; York et al., 2024). IL-10 not only inhibits the expression of the essential pro-inflammatory cytokines, including TNF-α, interleukin-1β (IL-1β), and IL-6 but also reduces the production of macrophage (Mφ)-derived reactive oxygen species (ROS) and nitric oxide (NO) (Saraiva et al., 2020).

In the cardiac milieu, the decrease of IL-10 expression over time following MI has been associated with reduced long-term cardiac function (Kaur et al., 2006). The increased plasma levels of anti-inflammatory mediators following intravenous immunoglobulin administration, including IL-10, notably correlated with augmented left ventricle (LV) contractile function in patients with congestive heart failure (Gullestad et al., 2001). Moreover, daily subcutaneous administrations of recombinant human IL-10 (rhIL-10, 10 μg/animal/day) significantly improved the survival of mice suffering from viral myocarditis, attenuated myocardial lesions, and suppressed pro-inflammatory cytokine production (Nishio et al., 1999). In a rat model of AMI, subcutaneous injections of rhIL-10 (75 μg/kg/day) continuously for 4 weeks resulted in significantly enhanced LV function, decreased serum levels of pro-inflammatory cytokines/chemokines such as TNF-α, IL-6 and monocyte chemoattractant protein-1 (MCP-1), and reduced myocardial macrophage infiltration (Stumpf et al., 2008). It was further demonstrated that systemic administrations of mouse IL-10 (50 μg/kg, 5 times post-MI) in a mouse AMI model significantly reduced inflammatory responses, improved LV function, and mitigated cardiac remodeling (Krishnamurthy et al., 2009). Two major mechanistic pathways haven been identified to contribute to the IL-10-mediated therapeutic benefits: inhibiting cardiac fibrosis through human antigen R/matrix metallopeptidase 9 (HuR/MMP-9) suppression and increased myocardial capillary density through signal transducer and activator of transcription 3 (STAT3) activation (Krishnamurthy et al., 2009; Haghikia et al., 2014). Thus, IL-10 treatment has a potential to modulate myocardial inflammatory responses and benefit cardiac structural and functional recovery post-MI (Jung et al., 2017; Tesoro et al., 2022).

Mφ are versatile innate immune cells that play key roles in the initiation, propagation, and resolution of myocardial inflammation after MI (Bruton et al., 2022; Gao et al., 2021; Kim et al., 2021). Both resident and recruited Mφ contribute to the clearance of the dead cells and cellular debris, the initiation of the repair process, and the modulation of the inflammatory responses (Zhang et al., 2021; Wu and Lu, 2019; Salina et al., 2022). These Mφ are classically categorized into two broad functional groups with distinct phenotypes: M1 or inflammatory Mφ that are pro-inflammatory and primarily contribute to the initiation and propagation of the post-injury inflammatory responses, and M2 or noninflammatory Mφ that largely participate in the resolution of inflammation as well as tissue repair and recovery (Yunna et al., 2020; Cheng and Rong, 2018; Ni et al., 2021; Jian et al., 2023). Failure of the Mφ participation in the post-injury immune responses resulted in impaired healing and chronic inflammation (Zuo et al., 2023; Krzyszczyk et al., 2018; Ganesh and Ramkumar, 2020). IL-10 has been shown to play a pivotal role in limiting the injury-induced inflammatory responses and facilitating the Mφ phenotypic switch from inflammatory to anti-inflammatory (Saraiva and O'Garra, 2010; Ip et al., 2017). IL-10 treatment can modulate macrophage polarization, reducing their secretion of pro-inflammatory cytokines and enhancing their contribution to cardiac tissue repair post-MI (Krishnamurthy et al., 2009; Jung et al., 2017). Nevertheless, despite its promise, the therapeutic potential of direct intramyocardial administration of IL-10 remains untested.

Furthermore, the large, repeated therapeutic doses of IL-10 required for the subcutaneous or systemic administration in prior studies not only increase the risks of potential unwanted or off-target effects but also substantially raise the cost of the treatment (Asadullah et al., 2003). For example, dramatically elevated serum IL-10 in patients has been reported to play pro-inflammatory and immune-activating roles in COVID-19 pathogenesis, suggesting the unwanted effects of overly high circulating IL-10 concentrations (Lu et al., 2021; Zhao et al., 2020; Han et al., 2020). To facilitate preclinical and clinical translation of IL10-based therapeutics for ischemic heart disease, in this study, we addressed the knowledge gap between the therapeutic dosage of IL-10, immune modulation, cardiac repair, and possible unwanted effects. We hypothesized

that the Mφ phenotype polarization could be programmed with appropriate doses of IL-10 to favor tissue repair and that early localized administration of IL-10 into the ischemic myocardium could ameliorate myocardial inflammation, cardiac remodeling, and LV dysfunction, leading to enhanced cardiac structural and functional recovery post-MI. To test our hypotheses, the current study explored dose-dependent effects of IL-10 on programming classic macrophage phenotypes and assessed the therapeutic potential of an early, single-dose intramyocardial injection of IL-10 in a mouse MI model.

Materials and methods

Induction of macrophage polarization *in vitro*

We used RAW264.7 murine monocyte/Mφ cell line as a model for evaluating the polarization of Mφ phenotypes. To induce M1 polarization, RAW264.7 cells were treated with 20 ng/mL recombinant murine interferon-gamma (mIFNγ; 315-05, PeproTech, Cranbury, NJ, United States) for 24 h. To induce M2 polarization, RAW264.7 cells were treated with 20 ng/mL recombinant murine interleukin-4 (mIL-4; 214-14, PeproTech) for 48 h. Cellular morphology was observed and imaged daily post-induction with the EVOS M7000 microscope (ThermoFisher Scientific, Waltham, MA, United States). Flow cytometry was used to confirm the outcome of the induction. For M1 polarization, we labeled cells with a primary rat anti-mouse CD86 antibody conjugated with Alexa Fluor 488 (105,017, BioLegend, San Diego, CA, United States). For M2 polarization, we labeled cells with a primary rat anti-mouse CD206 (MMR) antibody conjugated with Alexa Fluor 488 (141,709, BioLegend, San Diego, CA, United States).

Dose-dependent effects of IL-10 on macrophage phenotypes *in vitro*

To examine the phenotypic effects of differential dosage of IL-10 on the classic M1/M2 polarization of Mφ *in vitro*, we used rhIL-10 (200-10, PeproTech). We chose rhIL-10 because it is functionally active on both murine and human cells, according to the manufacturer's instructions and previous literature (Nishio et al., 1999; Stumpf et al., 2008). We implemented two distinct experimental protocols to investigate the impact of IL-10 on 1) phenotypes of established Mφ polarization or 2) prospective programming of Mφ polarization. In protocol #1, naïve RAW 264.7 cells were first induced with mIFNγ and mIL-4 for 24 and 48 h to establish the classic M1 and M2 phenotypes, respectively, followed by individual treatment with different doses of IL-10 (0, 25, 100, 250, 500, and 1,000 ng/mL) for 24 h. In protocol #2, naïve RAW 264.7 cells were co-stimulated with a phenotype-polarizing agent (mIFNγ for M1 or mIL-4 for M2) in conjunction with one of the six IL-10 doses (0, 25, 100, 250, 500, or 1,000 ng/mL) for 36 h. Cellular morphology was observed and imaged daily with the EVOS M7000 microscope. Flow cytometry and cytokine secretion were used to quantify the phenotypic and functional outcomes of these experiments, respectively.

Flow cytometry

Cells labeled with fluorescence-conjugated primary antibodies were analyzed with an Accuri C6 flow cytometer, equipped with 405, 488, and 561 nm lasers (BD Biosciences, San Jose, CA, United States). Ten thousand events per sample were collected for analysis. Sphero rainbow calibration particles with eight peaks (RCP-30-5A, Spherotech, Lake Forest, IL, United States) were used for instrument normalization and MEFL calculation. Briefly, RAW264.7 cells were detached by scraping, washed and resuspended in phosphate-buffered saline (PBS), and quantified using a Countess 3 FL automatic hemocytometer (AMQAF 2000, Thermo Fisher Scientific Cellular Analysis, Eugene, OR, United States). The cell concentration was then adjusted to 1×10^6 cells/mL before incubating them for 20 min on ice with fluorescence-conjugated primary antibodies against specific cell lineage markers that were diluted in FACS buffer (PBS with 1% bovine serum albumin) and protected from light. Cells were then washed twice with PBS to remove excessive antibodies and resuspended in 500 µL of FACS buffer for analysis. For each sample, 10,000 events were collected to ensure statistical significance of the data. Flow cytometry data were analyzed and quantified with FlowJo (FlowJo LLC, Ashland, OR, United States) and represented in histograms (single parameter).

Enzyme-Linked Immunosorbent Assay

Enzyme-Linked Immunosorbent Assay (ELISA) was performed to quantify the amounts of TNF-α and murine IL-10 (mIL-10) in the cell culture supernatants that were secreted by the induced RAW264.7 cells treated with different doses of IL-10. The sandwich ELISA development kits specific for capturing murine TNF-α (900-T54) and mIL-10 (900-T53) were used with ELISA TMB Buffer Kit (900-T00) (all from PeproTech) for the colorimetric detection in prepare 96-well standard ELISA microplates (Greiner Bio-One North America, Monroe, NC, United States). ELISA was performed following the manufacturer's instructions. Absorbance readings at 450 nm were recorded with an EnSpire Multilabel Reader (Perkin Elmer, Shelton, CT, United States).

Experimental animals

The Institutional Animal Care and Use Committee (IACUC) at the University of Pittsburgh (UPitt) and University of South Dakota (USD) approved the animal usage and surgical procedures performed in this study (UPitt IACUC Protocol 12010140 and USD IACUC Protocol 03-01-22-25D). A total of 73 male 10–12 weeks old BALB/cJ mice (Jackson Laboratory, Bar Harbor, ME, United States) were used for this study.

Intramyocardial injection of IL-10 in acute myocardial infarction model

The same rhIL-10 employed *in vitro* was also used for *in vivo* studies. The induction of AMI and intramyocardial injections were

performed as we previously described (Figure 3A) (Xiang et al., 2011; Chen et al., 2013; Chu et al., 2013) Briefly, after the induction of anesthesia with 4% isoflurane gas, mice were intubated and inhalationally anesthetized with 2% isoflurane gas throughout the surgery. MI was microscopically induced by permanent ligation of the left anterior descending (LAD) coronary artery. Mice were then randomly assigned to one of the six IL-10 treatment groups: 25, 100, 250, 500, 1,000, and 2000 ng of rhIL-10 (all diluted in 30 μL of sterile 0.9% saline). Ten minutes after the induction of MI, injections were microscopically performed at three sites of the ischemic myocardium (at the center and two borders of the infarct area, each receiving 10 μL solution). Control mice received 30 μL saline (Baxter Healthcare, Deerfield, IL, United States) at the same three sites, following the same procedures.

Echocardiography

Echocardiographic studies were performed by a blinded investigator repeatedly before surgery and at 5 days, 2 weeks, and 6 weeks post-surgery to assess the cardiac function as described previously (Chen et al., 2013; Chu et al., 2013; Okada et al., 2012). Concisely, mice were initially anesthetized with 2% isoflurane gas and subsequently maintained at 1%–1.5% isoflurane gas throughout the echocardiographic study. Mice were then immobilized on a heated stage equipped with electrocardiography. Heart rate, respiratory rate, and body temperature were continuously monitored and maintained. Echocardiographic parameters were measured using high-frequency ultrasound scanners (Vevo 770 and 2,100 at the Center for Ultrasound Molecular Imaging and Therapeutics, University of Pittsburgh Medical Center, and Vevo 3,100 at the University of South Dakota (USD) Animal Resource Center; both from FUJIFILM VisualSonics Inc., Canada). End-systolic dimension (ESD) and end-diastolic dimensions (EDD) were determined from the short-axis images of the LV using M-mode. At least eight consecutive beats were measured. End-systolic area (ESA) and end-diastolic area (EDA) were measured from short-axis images of the LV using B-mode. Contractile parameters, including LV fractional shortening (LVFS) and LV ejection fraction (LVEF), were determined as previously described (Manning et al., 1994; Pollick et al., 1995; Wandt et al., 1999). Mice that were sacrificed for histological analyses or died prior to the end point of 6 weeks post-injection were excluded from the echocardiographic studies.

Histological and immunohistochemical analyses

Animals were sacrificed at 6 weeks post-surgery. Hearts were harvested and arrested in diastole by immediately immersing in 1 M potassium chloride (KCl) and processed as previously reported (Xiang et al., 2011; Chen et al., 2013; Chu et al., 2013). Hearts were flash-frozen in 2-methylbutane (Sigma-Aldrich, St. Louis, MO, United States) that was pre-cooled in liquid nitrogen or dry ice. Frozen hearts were stored at −80°C and subsequently serially cryosectioned at 8-μm thickness from the apex to the ligation level (approximately 0.5 mm in length). Heart slices at 1-mm thickness were collected immediately below the ligation level for molecular analyses from randomly selected heart samples. Each series contains 18–24 heart sections, which are roughly 200 μm apart natively and collected on one glass slide. Sections were fixed in a pre-cooled (−20°C) mixture of methanol and acetone (1:1) for 5 min or in 4% paraformaldehyde for 8 min at room temperature (RT) immediately prior to staining (all from Sigma-Aldrich). For immunohistochemistry, non-specific antibody binding was blocked with 10% donkey or goat serum for 1–2 h at RT and, if necessary, with the Mouse-on-Mouse (M.O.M.) antibody staining kit (Vector Laboratories, Burlingame, CA, United States). For evaluation of chronic inflammation, sections were incubated overnight at 4°C with rat anti-mouse CD68 primary antibody (1: 200, Abcam, Cambridge, MA, United States), followed by goat anti-rat-Alexa488 IgG (1:400, Life Technologies, Grand Island, NY, United States). To examine vascular endothelial cells (ECs) and smooth muscle cells (SMCs), sections were first incubated overnight at 4°C with rat anti-mouse CD31 (platelet endothelial cell adhesion molecule, PECAM-1) antibody (1:100, Becton-Dickinson Biosciences, Franklin Lakes, NJ, United States), followed by donkey anti-rat-Alexa594 IgG (1:400, Life Technologies) at RT for 1 h, and subsequently incubated with mouse anti-alpha smooth muscle actin-FITC (1:100, Sigma-Aldrich). Nuclei were stained with Hoechst 33,342 diluted in PBS (1:1,000, Life Technologies) at RT for 5 min.

Quantification of chronic inflammation and revascularization

To evaluate chronic inflammation within the infarct region, immunofluorescent staining of anti-mouse CD68 was performed on the serial cryosections of flash-frozen mouse hearts. The macrophage infiltration index, indicated by the number of $CD68^+$ phagocytic cells per mm^2, was subsequently estimated by averaging $CD68^+$ cell counts in 6-8 randomly selected images of the entire infarct region of each heart at the mid-infarct level. To quantify revascularization in the heart, double immunofluorescent staining with antibodies against a mouse EC marker, CD31, and a mammalian SMC marker, αSMA, was sequentially performed on the serial cryosections of mouse hearts. The capillary density, indicated by the number of $CD31^+$ capillary ECs per mm^2, was subsequently estimated by averaging $CD31^+$ cell counts in 6 randomly selected images of the infarct region or peri-infarct area of each heart at the mid-infarct level; the SMC density, indicated by the number of perivascular (i.e., adjacent to $CD31^+$ ECs) αSMA + cells per mm^2, was subsequently computed by averaging αSMA + cell counts in 6 randomly selected images of the infarct region or peri-infarct area of each heart at the mid-infarct level, as described previously (Chen et al., 2013; Okada et al., 2012). All images were analyzed using ImageJ.

Measurement of cardiac fibrosis

Masson's trichrome staining kit (IMEB, San Marcos, CA, United States) was used to reveal collagen deposition on heart serial cryosections, following the manufacturer's instructions. The

TABLE 1 Primer sequences for quantitative real-time PCR (qPCR) analysis.

Gene symbol	Forward primer (5′→ 3′)	Reverse primer (5′→ 3′)
GAPDH	AGGTCGGTGTGAACGGATTTG	TGTAGACCATGTAGTTGAGGTCA
IL1-beta	GCAACTGTTCCTGAACTCAACT	ATCTTTTGGGGTCCGTCAACT
IFN-gamma	ATGAACGCTACACACTGCATC	CCATCCTTTTGCCAGTTCCTC
IL-6	TAGTCCTTCCTACCCCAATTTCC	TTGGTCCTTAGCCACTCCTTC
iNOS	CACCAAGCTGAACTTGAGCGA	CCATAGGAAAAGACTGCACCGA
TNF-alpha	CCCTCACACTCAGATCATCTTCT	GCTACGACGTGGGCTACAG
Axl	TGAGCCAACCGTGGAAAGAG	AGGCCACCTTATGCCGATCTA
MerTk	ACCCAGTTGCTAGAGAGCTG	TGGTGAGTCTGTCTCCGGTAA
Vsig4	AGAGGCTACAGGCAAGTTTTG	GGAGTCACGTAGGAAGATGGT
CX3CL1	CGCGTTCTTCCATTTGTGTA	TGGGATTCGTGAGGTCATCT
Arg1	GGAAAGCCAATGAAGAGCTG	GATGCTTCCAACTGCCAGAC
CD206	GGTCTATGGAACCACGGATG	TGCCCAGTAAGGAGTACATGG
mIL-10	CGACTCCTTAATGCAGGACT	TTGATTTCTGGGCCATGC
α-SMA	GTCCCAGACATCAGGGAGTAA	TCGGATACTTCAGCGTCAGGA
Hyal3	TCTGTGGTATGGAATGTACCCT	TTTTGGCCGTGAAAATGTTGG
VEGF	GCACATAGAGAGAATGAGCTTCC	CTCCGCTCTGAACAAGGCT
CD163	ATGGGTGGACACAGAATGGTT	CAGGAGCGTTAGTGACAGCAG
Postn	CCTGCCCTTATATGCTCTGCT	AAACATGGTCAATAGGCATCACT
PDGF	AGGTATGTATCCACACATGCGT	AGTTCCTGTTGGTTTCATCTCG
Col1a1	GCTCCTCTTAGGGGCCACT	CCACGTCTCACCATTGGGG
CD64	AGGTTCCTCAATGCCAAGTGA	GCGACCTCCGAATCTGAAGA

area of the collagen deposition (indicating cardiac fibrosis) and the area of the entire left ventricular cardiac tissue (including the septal area and excluding void space in the chamber cavity) were measured using a digital image analyzer (ImageJ). Fibrotic area fraction was estimated as the ratio of fibrotic tissue to the entire cross-sectional area of left ventricular tissue and averaged from 6 randomly selected sections at comparable infarct levels per heart.

Quantitative polymerase chain reaction analysis

Quantitative polymerase chain reaction (qPCR) was performed to quantify relative expression levels of key genes in the infarcted hearts 5 days after the induction of MI. The SYBR Green Master Mix for qPCR (A25741; Applied Biosystems, Waltham, MA, United States) was used with forward and reverse primer pairs (Integrated DNA Technologies, Newark, NJ, United States) for the qPCR gene expression analysis (Table 1). Glyceraldehyde-3-phosphate dehydrogenase (GAPDH) was used as the endogenous control gene for delta Ct calculation. Genes investigated include: TNF-α, IL-6, IFNγ, inducible nitric oxide synthase (iNOS), IL-1β, mIL-10, mannose receptor (CD206), arginase 1 (Arg1), AXL receptor tyrosine kinase (Axl), T-cell membrane protein 4 (Tim4), MER proto-oncogene tyrosine kinase (MerTK), chemokine (C-X3-C motif) ligand 1 (CX3CL1), vascular endothelial growth factor-A (VEGF-A), hyaluronidase 3 (Hyal3), alpha smooth muscle actin (α-SMA), v-set immunoglobulin domain-containing 4 (Vsig4), Fc-gamma receptor 1 (CD64), scavenger receptor cysteine-rich type 1 protein M130 (CD163), platelet-derived growth factor (PDGF), periostin (Postn), and type I collagen (Col1a1) (Jung et al., 2017). The fold change in gene expression was calculated using the $2^{(-\Delta\Delta Ct)}$ method (n = 5 per group).

Statistical analysis

All measured data are presented as mean ± standard error (SE). Statistical differences between groups were analyzed by one-way analysis of variance (ANOVA) or two-way repeated ANOVA (for repeated echocardiographic measurements) with a 95% confidence interval. Statistical significance was set at $p \leqq 0.05$. For multiple comparisons *post hoc* analysis, Bonferroni or Dunnett test was performed for one-way ANOVA, and Tukey test was performed for two-way ANOVA. Statistical analyses were performed with GraphPad Prism 10 statistics software (Dotmatics, Boston, MA, United States).

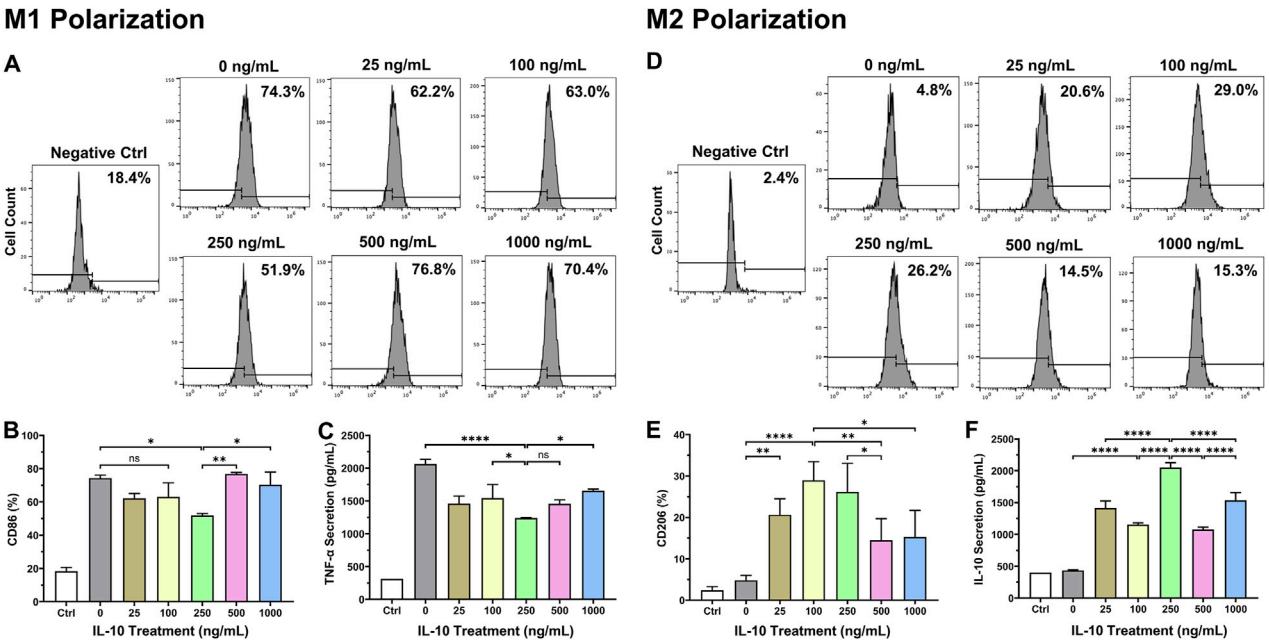

FIGURE 1
Dose-dependent effects of IL-10 on polarized macrophage phenotypes. To investigate dose-dependent effects of IL-10 on the phenotypes of polarized Mφ, naïve RAW264.7 cells were first differentiated into the classic M1 and M2 phenotypes with mIFNγ and mIL-4, respectively, followed by treatment with titrated IL-10 (0, 25, 100, 250, 500, or 1,000 ng/mL) for 24 h. We then analyzed M1 and M2 phenotypic changes by labeling cells with **(A, B)** anti-CD86 (classic M1 marker) and **(D, E)** anti-CD206 (classic M2 marker) antibodies, respectively, before subjecting cells to flow cytometry. **(A)** Representative graphs with averaged ratios of $CD86^+$ cells from each IL-10 treatment group. **(B)** Quantification of the flow cytometry data (n = 3 per group). Only the 250 group showed significantly lower CD86 expression than the 0 group ($p = 0.0148$). The 500 and 1,000 groups had significantly higher CD86 expression than the 250 group ($p < 0.01$ and $p < 0.05$, respectively). **(C)** Detection of mTNF-α secretion by polarized M1 cells after hIL-10 treatment using ELISA. The 250 group consistently exhibited significantly lower TNF-α secretion than the 0, 100, and 1,000 groups ($p < 0.0001$, $p = 0.0478$, and $p = 0.0146$, respectively). **(D)** Representative graphs with averaged ratios of CD206+ cells from each IL-10 treatment group. **(E)** Quantification of the flow cytometry data (n = 3 per group). The 25, 100, and 250 groups showed significantly higher CD206 expression than the 0 group ($p = 0.007$, $p < 0.0001$, and $p = 0.0003$, respectively). The 500 and 1,000 groups expressed much less CD206 than the 100 ($p = 0.0078$ and $p = 0.0123$) and 250 groups ($p = 0.0425$ and $p = 0.0654$), respectively. **(F)** Detection of native mIL-10 secretion by polarized M2 cells after hIL-10 treatment using ELISA. All IL-10 treatment groups exhibited significantly higher mIL-10 secretion than the 0 group (all $p < 0.0001$). Wildtype naïve RAW264.7 cells served as the negative controls (Ctrl). Note: *$p < 0.05$, **$p < 0.01$, ***$p < 0.001$, and ****$p < 0.0001$; ns: not statistically significant.

Data availability

The authors declare that all relevant data supporting the findings of this study are available within the paper and its supplementary Information. Source data files for the quantitative data generated in this study are available upon request.

Results

IL-10 exhibits dose-dependent modulations on polarized macrophage phenotypes

To assess the efficacy of IL-10 for modulating the phenotypes of polarized Mφ, we first differentiated naïve RAW264.7 monocytes to classic M1 and M2 Mφ with mIFNγ and mIL-4, respectively (Supplemental Figure 1). We then treated polarized Mφ individually with differential doses of IL-10 (0, 25, 100, 250, 500, and 1,000 ng/mL) for 24 h. Flow cytometry analysis showed that the 250 group has significantly lower CD86 (classic M1 marker) expression when compared with no IL-10 treatment (0 ng/mL); the 500 and 1,000 groups have notably higher CD86 expression when compared with the 250 group (Figures 1A, B). The ELISA assay revealed that M1 Mφ in the 250 group secreted notably less pro-inflammatory cytokine murine TNF-α (mTNF-α) when compared with 0, 100, and 1,000 groups (Figure 1C). On the other hand, the 25, 100, and 250 groups had the highest CD206 (classic M2 marker) expression when compared with no IL-10 treatment while the 500 and 1,000 groups had ~45–50% and ~40–45% lower CD206 expression than the 100 and 250 groups, respectively (Figures 1D, E). The ELISA assay showed that all IL-10 treated groups have substantially increased secretion of native murine IL-10 (mIL-10), with the 250 group showing the highest mIL-10 secretion (Figure 1F), consistent with our flow cytometry data. No antibody cross-reaction between mIL-10 and exogenous hIL-10 was observed (Supplemental Figure 2). These results suggest that one can induce drifting of established Mφ phenotypes from the pro-inflammatory/destructive toward the anti-inflammatory/resolutive by administering appropriate doses of IL-10 (Yunna et al., 2020).

IL-10 programs macrophage polarization in a dose-dependent manner

To investigate how different exogenous IL-10 doses would impact the Mφ polarization process, we co-stimulated naïve RAW264.7 monocyte differentiation with one of the six doses of IL-

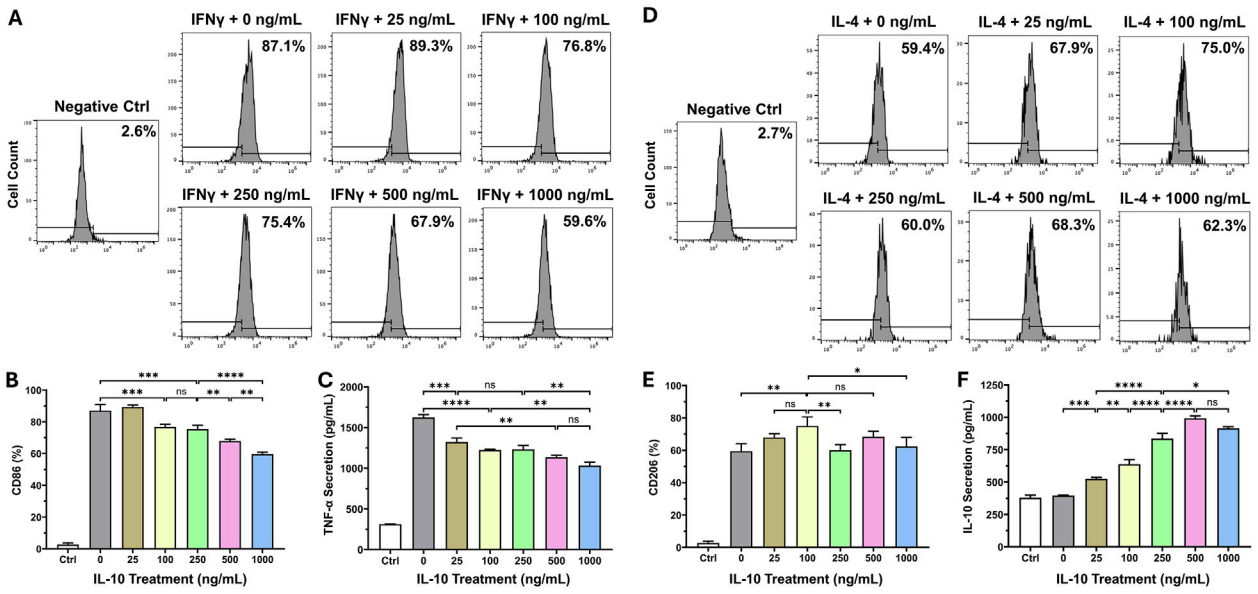

FIGURE 2
Dose-dependent effects of IL-10 on macrophage polarization. To study the effect of exogenous IL-10 treatment with differential doses on the Mφ polarization process, we differentiated naïve RAW264.7 monocytes with a standard polarizing agent (mIFNγ for M1 and mIL-4 for M2) and one of the six doses of IL-10: 0, 25, 100, 250, 500, and 1,000 ng/mL simultaneously for 36 h. We analyzed the manifestation of classic M1 and M2 phenotypes with flow cytometry by labeling cells with **(A, B)** anti-CD86 and **(D, E)** anti-CD206 antibodies, respectively. **(A)** Representative graphs with averaged ratios of CD86$^+$ cells from each IL-10 treatment group. **(B)** Quantification of the flow cytometry data (n = 3 per group). All groups had significantly lower CD86 expression than the 0 group (all $p < 0.001$), except the 25 group ($p > 0.05$). **(C)** Detection of mTNF-α secretion by polarized M1 cells after hIL-10 treatment using ELISA. All groups had significantly less TNF-α secretion when compared with the 0 group (all $p < 0.001$). **(D)** Representative graphs with averaged ratios of CD206+ cells from each IL-10 treatment group. **(E)** Quantification of the flow cytometry data (n = 3 per group). The 100 group showed significantly higher CD206 expression than the 0, 250, and 1,000 groups ($p = 0.0047$, $p = 0.0065$, and $p = 0.0229$, respectively). **(F)** Detection of native mIL-10 secretion by polarized M2 cells after hIL-10 treatment using ELISA. All groups had significantly higher mIL-10 secretion than the 0 group (all $p < 0.001$). Wildtype naïve RAW264.7 cells served as the negative controls (Ctrl). Note: *$p < 0.05$, **$p < 0.01$, ***$p < 0.001$, and ****$p < 0.0001$; ns: not statistically significant.

10: 0, 25, 100, 250, 500, and 1,000 ng/mL and a standard polarizing agent (mIFNγ for M1 and mIL-4 for M2). For M1 polarization, flow cytometry analysis showed that all groups treated with ≥100 ng/mL IL-10 have significantly decreased M1 polarization, but not the 25 ng/mL, when compared with the 0 ng/mL (Figures 2A, B). The ELISA assay indicated that all IL-10 treated groups have notably less mTNF-α secretion when compared with the 0 group (Figure 2C). It appeared that higher doses of IL-10 may have stronger effects in reducing M1 polarization. For M2 polarization, the 100 group exhibited the highest CD206 expression when compared with the 0, 250, and 1,000 groups (Figures 2D, E). The ELISA assay revealed that all IL-10 treated groups secrete substantially more native mIL-10 when compared with the 0 group, with the 500 group having the highest secretion (Figure 2F). These data suggested that when co-administered with a polarizing agent, IL-10 has notable dose-dependent effects over Mφ polarization, with the potential to achieve a distinct balance of M1 or M2 phenotype with the addition of an appropriate dose of IL-10.

Intramyocardial IL-10 administration exhibits dose-dependent effects on cardiac function

To evaluate the potential of IL-10 as an immunomodulatory treatment for enhancing cardiac repair post-MI, we examined the cardiac function after single intramyocardial administration of different IL-10 doses in a mouse MI model (Figure 3A). A dose range of 25–2000 ng IL-10 was chosen for testing based on the outcomes of the *in vitro* studies. The surgical mortality rate (death during the operation or within 60 min after the surgery) was ~17% (1 in 7) in all groups. Among all animals that fully recovered from the surgery, one died before the terminal time point in each of these four groups: saline control, 25, 100, and 2000, and was excluded from this study. In total, five animals (n = 5) per group with no notable behavioral abnormality were included in the 6-week repeated echocardiographic assessment.

Cardiac contractile function was estimated by LV fraction shortening (LVFS, Figure 3B) and LV ejection fraction (LVEF, Figure 3C), whereas LV chamber size was determined by LV end-diastolic area (LVEDA, Figure 3D) and end-systolic area (LVESA, Figure 3E). At 5 days post-MI, the 2000 group had significantly lower LVFS than all groups, except the 500 and 1,000 groups (Supplemental Figure 3). Particularly, the 1,000 and 2000 groups exhibited notably lower LVEF than the 250 group (Figure 3C). At 6 weeks post-MI, the 25, 250, and 500 groups showed considerably higher LVFS than the saline control (Figure 3B); however, only the 250 group exhibited notably higher LVEF than the saline control (Figure 3C, $p = 0.0067$) while showing significantly higher LVFS than the 2000 group (Figure 3B; $p = 0.0202$). These results suggest that single intramyocardial treatment with ≥1,000 ng

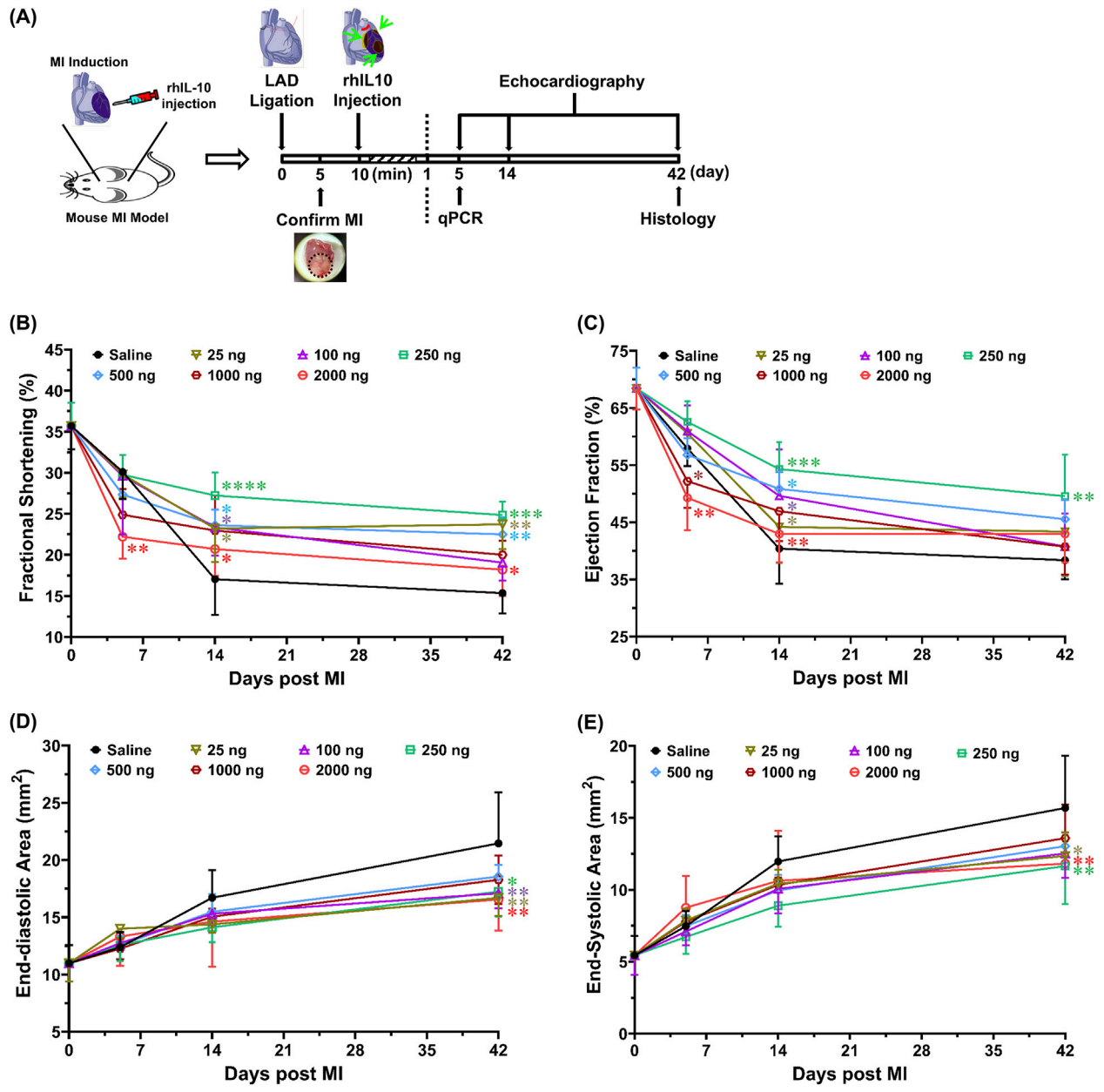

FIGURE 3
Intramyocardial injection of IL-10 improves cardiac function with dose-dependent effects. Using a mouse MI model, we investigated whether intramyocardial IL-10 administration exerts any dose-dependent efficacy or potential unwanted effect on cardiac function post-MI. **(A)** The timeline of the animal study, including surgical procedures, cardiac functional evaluations, and tissue-based analyses. Ten minutes after the induction of MI, mice received one-time intramyocardial injection of IL-10 with one of the six doses (ng): 25 (sage), 100 (purple), 250 (green), 500 (blue), 1,000 (brown), or 2000 (red) or 0.9% saline (vehicle control, black). Echocardiography was repeatedly performed by a blinded investigator to measure left ventricular **(B)** fractional shortening (5D: **$p < 0.01$, 2000 vs saline, 25, 100, and 250; 14D: *$p < 0.05$, 2000 vs 250; 42D: *$p < 0.05$, 2000 vs 250; all other comparisons vs saline), **(C)** ejection fraction (5D: **$p < 0.01$, 2000 vs 25, 100, and 250; *$p < 0.05$, 1,000 vs 250; 14D: **$p < 0.01$, 2000 vs 250; *$p < 0.05$, 25 vs 250; all other comparisons vs saline), **(D)** end-diastolic area (all comparisons vs saline), and **(E)** end-systolic area (all comparisons vs saline) at 5, 14, and 42 days post-surgery ($n = 5$ per group). Results were statistically analyzed with two-way repeated ANOVA with Tukey multiple comparison test. Notably, the 250 group exhibited the highest overall cardiac functional benefits among all treatment doses. The 1,000 and 2000 groups had decreases in cardiac contractile function at 5 days post-MI, suggesting possible transient side-effects caused by high-dose IL-10 treatment. Note: *$p < 0.05$, **$p < 0.01$, ***$p < 0.001$, and ****$p < 0.0001$.

IL-10 has an early negative impact in LV contractile function while injecting 250 ng IL-10 appears to offer more consistent LV contractile protection than other doses in the long term.

Moreover, at 6 weeks post-MI, the 25, 250, and 2000 groups exhibited significantly smaller LVEDA (Figure 3D) and LVESA (Figure 3E) when compared with the saline control. The 100 group notably reduced LVEDA ($p = 0.007$) but not LVESA (Figures 3D, E). These data suggest that single intramyocardial injection with select IL-10 doses can help ameliorate LV dilatation. Overall, our echocardiographic analyses suggest that 1)

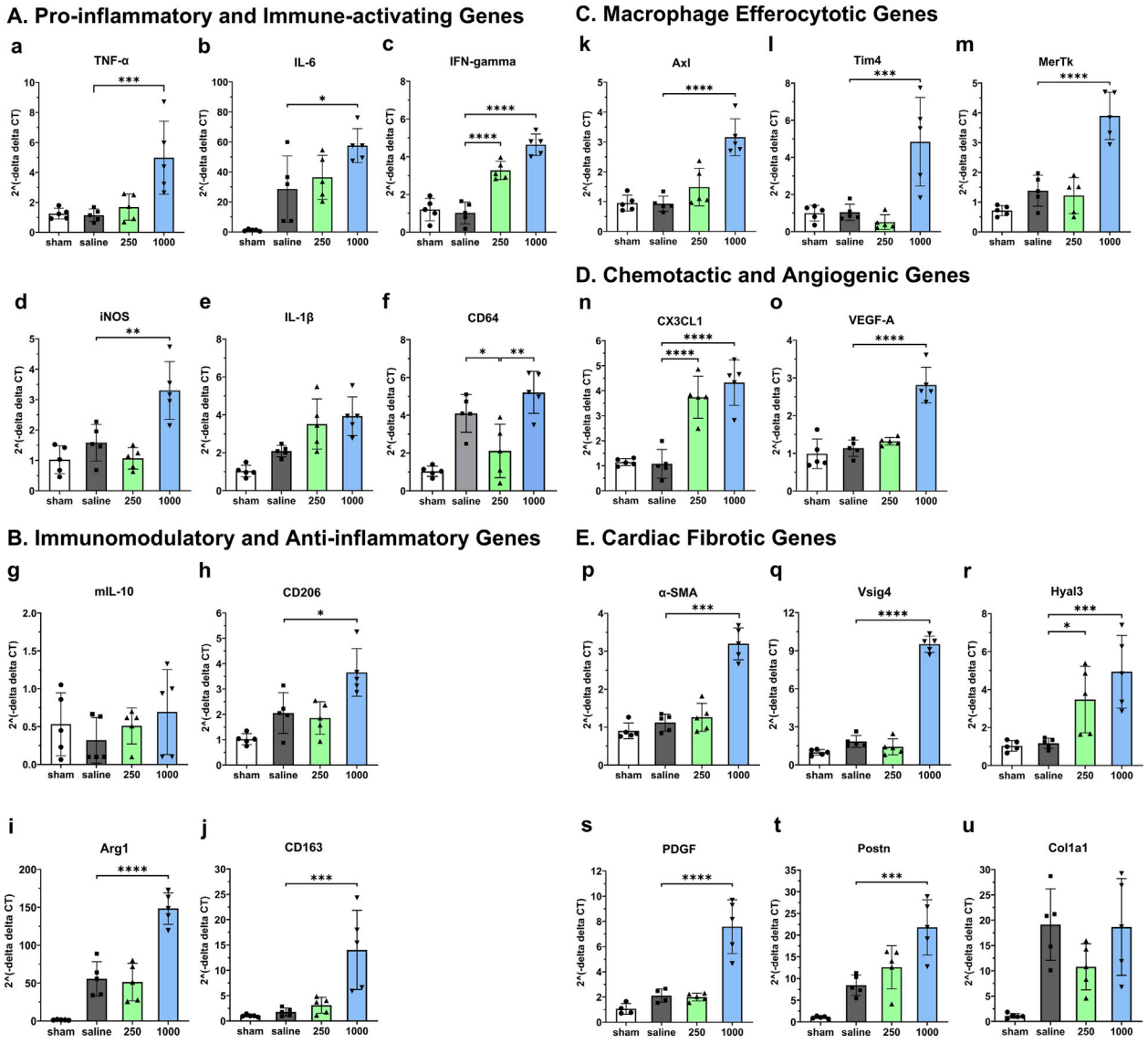

FIGURE 4
Early dose-dependent effects of intramyocardial IL-10 treatment on myocardial gene expression. We used qPCR to analyze the expression levels of five groups of genes in mouse LV treated with different doses of IL-10 (0, 250, or 1,000 ng) at 5 days of post-MI, including **(A)** pro-inflammatory and immune-activating genes (TNF-α, IL-6, IFNγ, iNOS, IL-1β, and CD64); **(B)** immunomodulatory and anti-inflammatory genes (mIL-10, CD206, Arg1, and CD163); **(C)** macrophage efferocytotic genes (Axl, Tim4, and MerTK); **(D)** chemotactic and angiogenic genes (CX3CL1 and VEGF-A); **(E)** cardiac fibrotic genes (α-SMA, Vsig4, Hyal3, PDGF, Postn, and Col1a1). Data were statistically compared using one-way ANOVA with Dunnett multiple comparisons test (n = 5 per group). The results suggest that 250 and 1,000 ng IL-10 treatment differentially activated diverse functional signaling networks, with 1,000 ng IL-10 seemingly triggering both pro-inflammatory and anti-inflammatory pathways. Note: *p < 0.05, **p < 0.01, ***p < 0.001, and ****p < 0.0001.

250 ng IL-10 treatment resulted in the most significant long-term functional benefits among all doses, and 2) IL-10 has noteworthy dose-dependent effects when administered intramyocardially, including early adverse effects in LV contractile function with excessive exogenous IL-10.

Intramyocardial IL-10 treatment modulates early myocardial recovery post-MI

To assess the early impact of intramyocardial IL-10 administration in modulating myocardial inflammation, Mφ function, and cardiac remodeling, we investigated the expression of 16 essential genes involved in relevant functional pathways in the infracted mouse hearts treated with 0 (saline control), 250, and 1,000 ng IL-10 at 5 days post-MI. Our qPCR analysis revealed that most of these genes exhibit distinct expression patterns after treating with 250 and 1,000 ng IL-10 (Figure 4).

Comparing with the saline control, despite inducing notable upregulation in multiple beneficial genes, including the anti-inflammatory CD206 (Figures 4B–H, p = 0.0166) and Arg1 (Figures 4B–I, p < 0.0001), the Mφ efferocytotic Tim4 (Figures 4C–L, p = 0.0005) and MerTK (Figures 4C–M, p < 0.0001), the chemotactic CX3CL1 (Figures 4D–N, p < 0.0001), the angiogenic

VEGF-A (Figures 4D–O, $p < 0.0001$), and the anti-fibrotic Vsig4 (Figures 4E–Q, $p < 0.0001$) genes, the 1,000 group also considerably upregulated pro-inflammatory and pro-fibrotic genes, including TNF-α (Figure 4A, $p = 0.0009$), IL-6 (Figures 4A, B, $p = 0.0159$), iNOS (Figures 4A–D, $p = 0.0015$), Axl (Figures 4C–K, $p < 0.0001$), α-SMA (Figures 4E–P, $p < 0.001$), the hyaluronan-degrading Hyal3 (Figures 4E–R, $p = 0.0009$), PDGF (Figures 4E–S, $p < 0.0001$), Postn (Figures 4E–T, $p = 0.0004$), and Col1a1 (Figures 4E–U, $p = 0.9989$).

In contrast, comparing with the saline control, the 250 group showed notable upregulation of the immune-activating IFNγ (Figures 4A–C, $p < 0.0001$), CX3CL1 (Figures 4D–N, $p < 0.0001$), and Hyal3 (Figures 4E–R, $p = 0.0348$) genes significant downregulation of macrophage M1 phenotype marker CD64 (Figures 4A–F, $p = 0.021$) as well as modest downregulation of iNOS and Col1a1 genes. These results suggest that distinct IL-10 doses differentially regulate essential genes involved in the pro- and anti-repair pathways, potentially contributing to the sustained long-term LV function in the 250 group as well as the short-term contractile dysfunction observed in high-dose IL-10 treatment at 5 days post-MI.

Single administration of IL-10 exhibits dose-dependent reduction of chronic inflammation

Based on the results of the cardiac functional studies above, we selected a dose range of 25–1,000 ng IL-10 per heart to investigate whether single intramyocardial IL-10 treatment has any dose-dependent immunomodulatory effect on chronic inflammation. At 6 weeks post-MI, phagocytic cells at the infarct site were detected with anti-CD68 immunofluorescent staining (Figure 5A). Unaffected myocardium contained few $CD68^+$ cells (Figures 5A, A). All IL-10-treated groups exhibited a trend of diminished numbers of $CD68^+$ cells within the infarct region (Figures 5A, C–F) compared with the saline-injected control (Figures 5A, B). Quantitatively, three IL-10-treated groups showed significantly less $CD68^+$ cell infiltration than the saline control group ($969.81 \pm 120.02/mm^2$): 100 ($522.20 \pm 71.62/mm^2$), 250 ($379.41 \pm 20.50/mm^2$), and 1,000 ($356.83 \pm 60.17/mm^2$) (Figure 5B, $n = 3$ per group). These results suggest that single intramyocardial administration with ≥100 ng IL-10 soon after MI has a long-lasting modulatory effect on MI-induced chronic inflammation.

Intramyocardial IL-10 treatment ameliorates left ventricular fibrosis

To investigate the effect of early intramyocardial IL-10 treatment on cardiac fibrosis, we evaluated LV scar tissue formation (stained in blue/purple) with Masson's trichrome histological staining. Healthy hearts had minimal deposition of collagen (Figures 6A, A). At 6 weeks post-infarction, hearts treated with different doses of IL-10 (Figures 6A, C–F) exhibited a trend of smaller infarct regions and less collagen deposition than the saline-injected control at the mid-infarct level (Figures 6A, B). Quantitative estimation of the LV fibrotic area fraction revealed a common trend of reduction in fibrosis in all IL-10 treated groups compared with the saline control group (Figure 6B, $n = 3$ per group). Only the 250 group exhibited a statistically significant 53% reduction in LV fibrosis (Figure 6B), suggesting that single intramyocardial IL-10 administration has a dose-dependent, long-term anti-fibrotic effect.

Intramyocardial administration of IL-10 enhances revascularization

We examined whether single administration of IL-10 enhances long-term revascularization within the ischemic myocardium. At 6 weeks post-infarction, the presence of $CD31^+$ endothelial cells (ECs) and αSMA + perivascular cells (i.e., pericytes and vascular smooth muscle cells adjacent to $CD31^+$ ECs) at the infarct region were simultaneously detected with dual immunofluorescent staining (Figure 7A). Quantitative analysis ($n = 3$ per group) showed that only the 250 group had a significantly higher density of $CD31^+$ ECs at the infarct region than the saline control (Figure 7B); all other IL-10 treatment groups had marginal benefits (Figure 7B). No IL-10 treatment groups exhibited a notable increase in $CD31^+$ EC density in the peri-infarct areas compared with the saline control group (Figure 7C).

On the other hand, only the 1,000 group had a significantly higher density of αSMA + perivascular cells at the infarct region than the saline control group (Figure 7D); all other IL-10 treatment groups contributed to the repopulation of perivascular cells post-MI marginally (Figure 7D). None of the IL-10 treatment groups showed significant increases in αSMA + cell density in the peri-infarct areas compared with the saline control group (Figure 7E). These data suggest that when intramyocardial administered, select doses of IL-10 have notable effects in enhancing long-term repopulation of myocardial microvasculature at the infarct region, but not in the peri-infarct areas.

Discussion

With its pleiotropy in the immune system, IL-10 and its family of cytokines have been widely explored as therapeutic approaches in a wide variety of human diseases involving autoimmunity or excessive inflammation, such as rheumatoid arthritis, psoriasis, and inflammatory bowel disease (Wang et al., 2019; Kwilasz et al., 2015; Tilg et al., 2002; Huynh et al., 2023). Recent reports suggest that high-dose IL-10 treatment may not lead to the expected therapeutic outcome, raising the question of whether IL-10 has dose-dependent effects for enhancing cardiac tissue repair after MI, or even unexpected side effects from overdosing. By identifying an optimal range of IL-10 doses for cardiac repair via intramyocardial administration, we believe it is possible to safely utilize IL-10 to facilitate myocardial recovery post-MI, prevent adverse effects from IL-10 overdose, and lower the total cost of the costly recombinant protein treatment. Our findings shed light on the immunomodulatory properties of IL-10 on programming Mφ phenotypes and its potential therapeutic implications for myocardial repair post-MI (Figure 8).

We examined the impact of differential doses of IL-10 on murine Mφ polarization with *in vitro* models. We demonstrated that IL-10 has notable dose-dependent effects not only on the

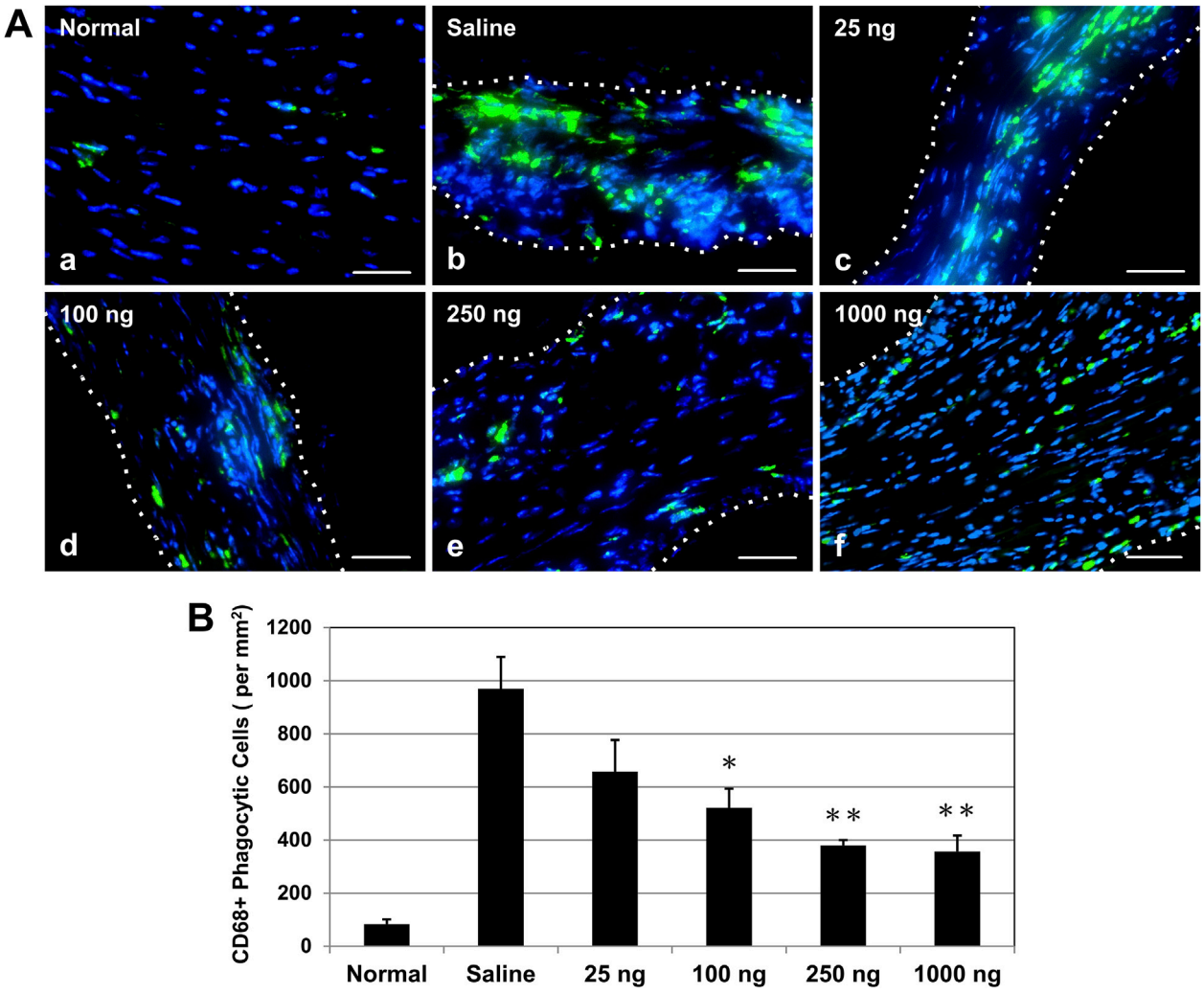

FIGURE 5
Intramyocardial IL-10 treatment decreases chronic inflammation within the infarct region. Chronic inflammation was assessed by the number of infiltrating CD68⁺ phagocytic cells (green) within the infarct region at 6 weeks post-infarction. **(A)** Representative images of anti-CD68 immunofluorescent staining revealing phagocytic cell infiltration within the infarct region at the mid-infarct level from each group (scale bars: 50 μm). Nuclei were stained in blue. Healthy (normal) hearts served as negative controls. **(B)** Three IL-10 doses (100, 250, and 1,000 ng) resulted in significant decreases of CD68⁺ cell infiltration (n = 3 per group; p = 0.046, p = 0.007, and p = 0.006, respectively, vs saline). Note: *p < 0.05, **p < 0.01.

phenotypes of differentiated M1 and M2 Mφ but also on prospective M1 and M2 polarization of naïve Mφ. Our data suggest that increasing concentrations of IL-10, up to 250 ng/mL, reduced the ratio and pro-inflammatory phenotype of M1 Mφ and increased the ratio and anti-inflammatory phenotype of M2 Mφ, with 250 ng/mL IL-10 having the highest overall potency in both populations (Figure 1). However, IL-10 concentrations ≥500 ng/mL did not efficiently reduce M1 or increase M2 ratio and phenotype, suggesting a limitation in the effective dose range of IL-10 for modulating Mφ phenotypes and possibly conflicting actions on differentiated Mφ (Figure 1). On the other hand, when co-administered with mIFNγ or mIL-4 to stimulate M1 or M2 polarization of naïve Mφ respectively, IL-10 ≥ 100 ng/mL significantly reduced M1 polarization while all tested IL-10 doses appeared to facilitate M2 polarization (Figure 2). These results suggest that given an appropriate dose, IL-10 can modulate the balance of Mφ ratio, phenotypes, and/or polarization toward an anti-inflammatory M2 state that facilitates resolution of inflammation and tissue repair (Figure 8).

Based on our *in vitro* findings, we subsequently assessed the translational potential of intramyocardial IL-10 administration and explicitly tested the impact of IL-10 dose-dependency in cardiac repair by injecting a wide range of rhIL-10 doses (up to 80-fold differences) (Figure 3). Despite the very short half-life of IL-10 *in vivo* (2.7–4.5 h), (Huhn et al., 1997), our data showed that an early intramyocardial injection of IL-10 resulted in long-term, dose-dependent effects of on cardiac function and remodeling. The 250 ng IL-10 group had the most significant cardiac contractile benefits among all tested doses, sustaining LV functions at roughly 60%–70% of their normal values. Nonetheless, treatment with ≥1,000 ng IL-10 showed short-term negative impact in cardiac function at 5 days post-MI, indicating a potential toxicity associated with injecting a high dose of IL-10 intramyocardially (Figure 3). Moreover, multiple groups exhibited improved EDA and

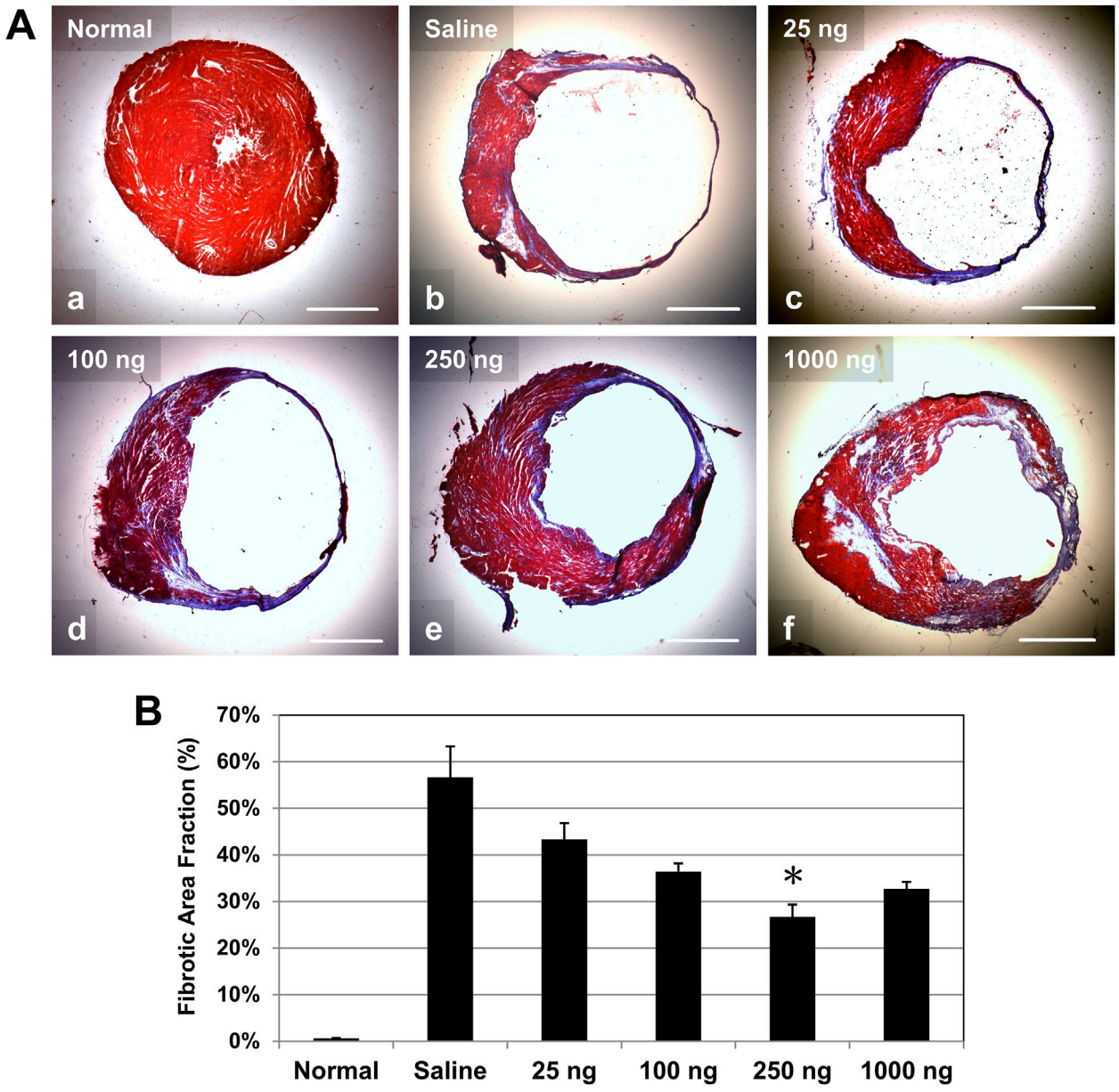

FIGURE 6
Intramyocardial IL-10 treatment reduces left ventricular myocardial fibrosis. Long-term left ventricular myocardial fibrosis was revealed by Masson's trichrome histological staining at 6 weeks post-infarction. **(A)** Representative images of Masson's trichrome-stained transverse sections of hearts at the mid-infarct level (collagen deposition stained in blue/purple, cardiac muscle stained in red; scale bars: 1 mm). Healthy (normal) hearts served as negative controls. **(B)** Quantitatively, only the 250 group exhibited significantly reduced LV fibrotic area fraction (n = 3 per group; *p = 0.05, vs saline).

ESA at 6 weeks post-MI, suggesting long-term merits on cardiac remodeling. These results further suggest that if IL-10 would be used therapeutically for MI, it may be necessary to identify an optimal IL-10 dose range for individual patients, based on their disease timeline or severity, to achieve the maximal efficacy and minimize the potential risk of IL-10 overdose.

Our qPCR analysis highlighted the early changes of gene expression associated with IL-10 administration in the infarcted myocardium. The results suggested that different doses of exogenous IL-10 differentially modulated the expression of many key genes involved in the tissue inflammation, damage and recovery processes, particularly the substantial upregulation of pro-inflammatory, efferocytotic, and fibrotic genes by 1,000 ng IL-10 treatment (Figure 4). Particularly, the 1,000 group also upregulated Axl expression, which is involved in Mφ efferocytosis and can further increase intramyocardial inflammation (Figures 4C–I) (DeBerge et al., 2021) Besides, our histological assays showed that the 250 and 1,000 groups differentially exhibited reduction of chronic inflammation at the infarct, ameliorated LV fibrosis, and, to a minor extent, enhanced revascularization, all of which potentially contributed to the improved LV contractile function and remodeling (Figures 5–7). Intriguingly, the injection of 1,000 ng IL-10 led to simultaneous upregulations of both pro- and anti-inflammatory responses post-MI. Thus, we further hypothesize that

10.3389/fphys.2024.1481460

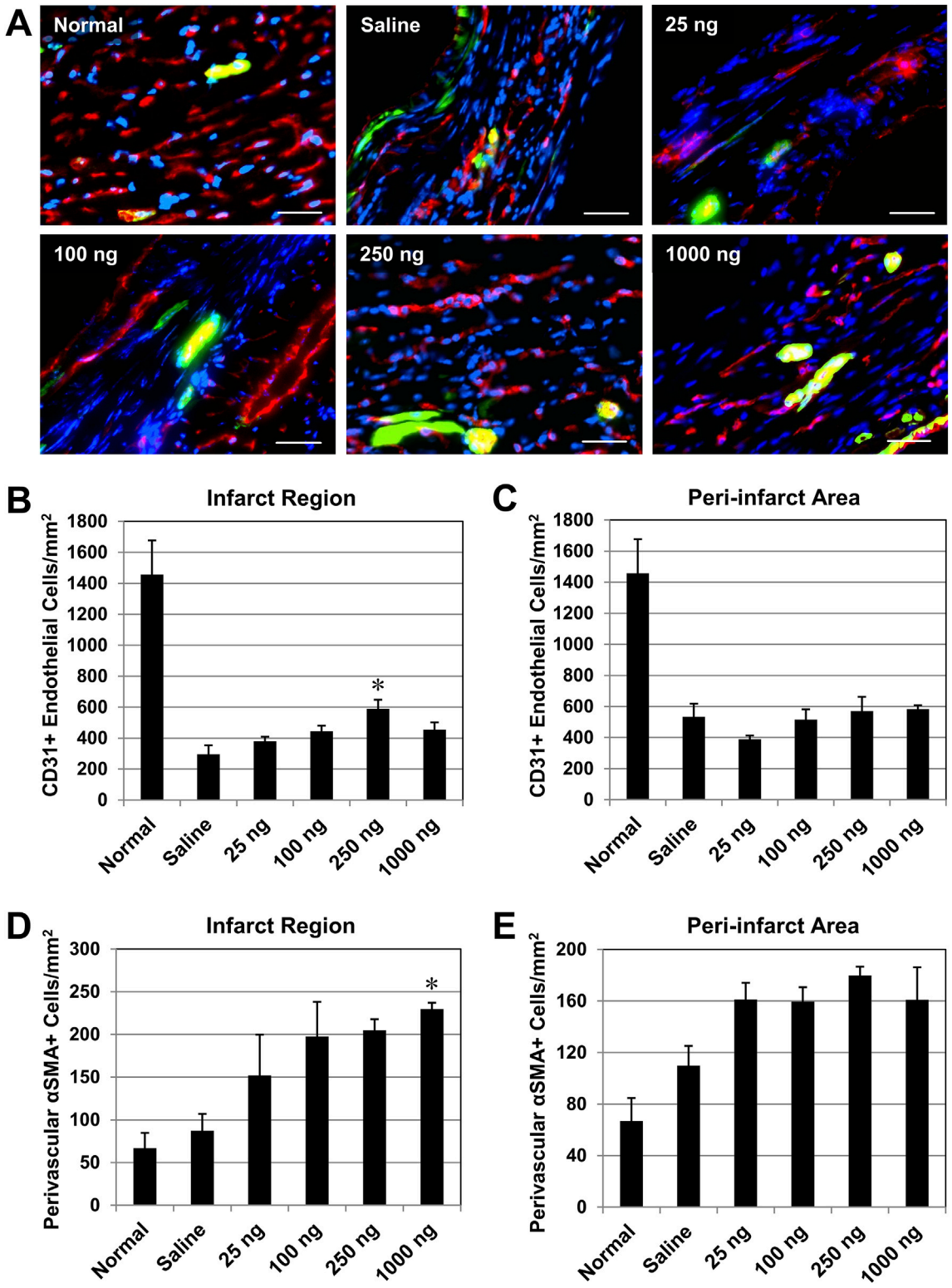

FIGURE 7
Intramyocardial injection of IL-10 enhances revascularization in the ischemic myocardium. Long-term revascularization, including angiogenesis and vasculogenesis, in the ischemic myocardium was evaluated by the presence of CD31⁺ endothelial cells (ECs) and αSMA + peri-vascular smooth muscle cells (SMCs), respectively, at 6 weeks post-infarction (n = 3 per group). Perivascular SMCs defined as αSMA + cells around CD31⁺ ECs. Healthy (normal) hearts served as baseline controls (n = 3). **(A)** Representative images of CD31⁺ ECs (red) and αSMA + SMCs (green) within the infarct region at the mid-infarct level from each group (scale bars: 50 μm). Nuclei were stained in blue. **(B)** Quantitatively, only the 250 ng group had a significantly higher density of CD31⁺ ECs at the infarct ($p = 0.013$, vs saline). **(C)** No significant difference in the CD31⁺ EC density was noted in the peri-infarct area (all $p > 0.05$, vs saline). **(D)** Only the 1,000 group had a significantly higher density of αSMA + SMCs within the infarct region ($p = 0.045$, vs saline). **(E)** No notable difference in the αSMA + SMC density in the peri-infarct area (all $p > 0.05$, vs saline). Note: *$p < 0.05$.

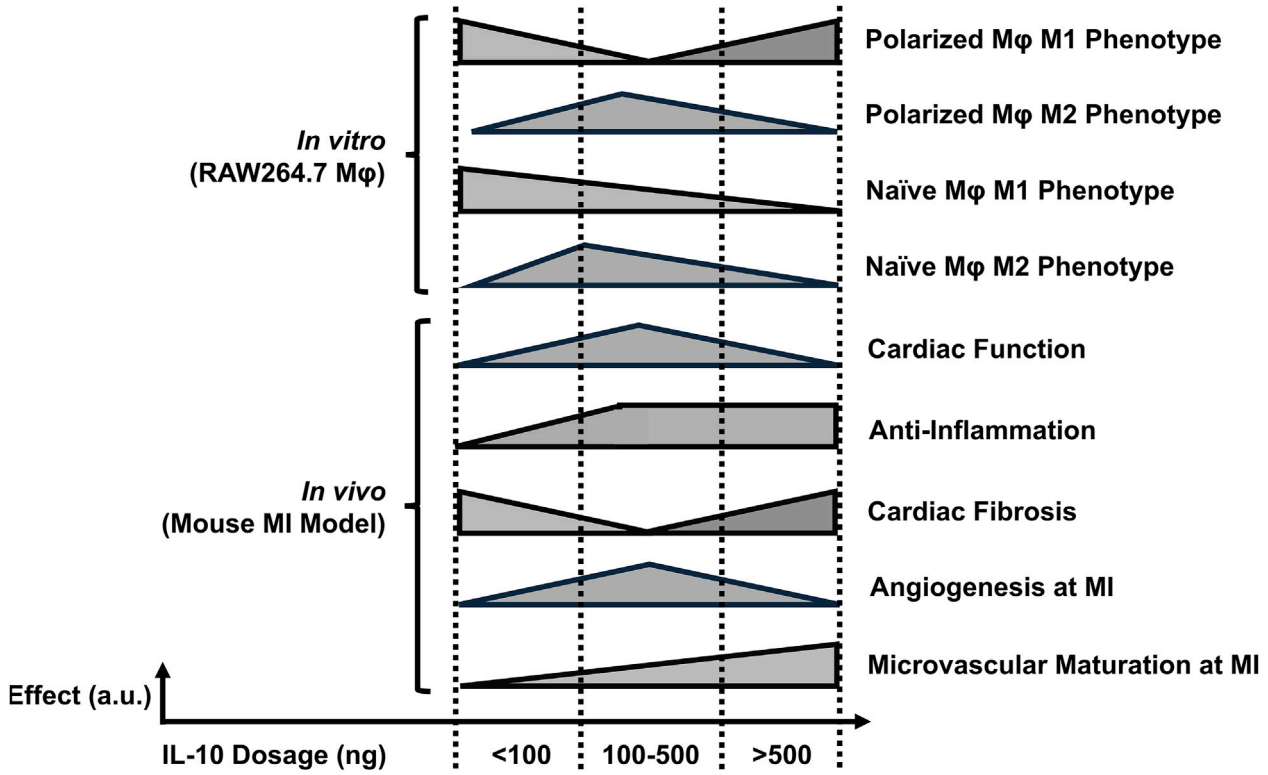

FIGURE 8
The estimated dose-dependent effects of single IL-10 administration. The illustration summarizes the overall dose-effect relationships after single IL-10 administration *in vitro* and *in vivo*. The x- and y-axis of each horizontal bar represent the IL-10 dose ranges and the estimated levels of individual annotated effects, respectively. Note: a. u.: arbitrary unit.

the dual activation of pro- and anti-resolution functional pathways by 1,000 ng IL-10 yields conflicting signals to immune cells that potentially contribute to the early transient LV contractile dysfunction observed in the echocardiographic analyses. Overall, these data align with our *in vivo* findings and suggest a complex interplay between IL-10 dosage and endogenous signaling networks that warrants future investigations with advanced approaches (Figure 8).

Previous reports demonstrated that mammalian cardiomyocytes (CMs) have active turnover during physiological conditions and may proliferate extensively after MI (Bergmann et al., 2009; Senyo et al., 2013). We further hypothesized that the reduction of chronic inflammation by intramyocardial IL-10 administration promotes CM survival and/or proliferation following MI. We then investigated whether there also exists any dose-dependent effect of IL-10 in enhancing long-term CM survival or proliferation post-MI (Supplemental Figure 4). Residual CMs at the infarct and in peri-infarct areas were identified by a mature CM marker cTn-I; proliferating CMs were detected by dual-positive signals of cTn-I and a cell proliferation marker Ki-67. To our surprise, we did not observe any notable differences in the number of either residual CMs (Supplemental Figure 4A, all $p > 0.05$) or proliferating CMs (Supplemental Figure 4B, all $p > 0.05$) within both the infarct region and peri-infarct areas among all tested IL-10 dose groups (25, 100, 250, and 1,000 ng IL-10; $n = 3$ per group). These results suggest that a single intramyocardial injection of IL-10 did not elicit notable dose-dependent efficacy in promoting long-term CM survival or proliferation, similar to a saline injection in our previous report (Chen et al., 2016).

One reason that large doses of IL-10 were used in previous investigations lies in its short half-life in the body, limiting the bioavailability in the target organ, particularly when administered via systemic routes. To reduce the amount of IL-10 required for effective treatment, appropriate delivery systems, such as exosomes or nanoparticles, may be needed for efficient, targeted delivery of IL-10 (Bu et al., 2021; Duncan et al., 2019). We and others have previously demonstrated that when locally delivered in a controlled manner, IL-10 can serve as an adjuvant for angiogenic or morphogenic cytokines to synergistically preserve heart function and improve cardiac repair after MI (Chen et al., 2015; Johnson et al., 2015). Nonetheless, whether controlled delivery of IL-10 reduces the required therapeutic dose for desirable outcomes and prevents early cardiac dysfunction observed in this study remains to be further investigated.

In addition, our findings that the beneficial effects of IL-10 can be precisely regulated by differential doses of exogenous IL-10 underscore the need for integrative systems approaches that are more efficient to interrogate experimental therapeutics, based on IL-10 or other cytokines, than conventional analytics. Due to the inherent limitations in our experimental approach, we were unable to further dissect the IL-10 dose-response relationship. Modern high-throughput computational approaches, such as machine learning (ML), may help us analyze the complex dynamics of cytokine-based therapies beyond the capacities of

conventional experimental approaches. With the ability to handle big, complex datasets and precisely discern nuanced patterns in dose-response relationships, ML algorithms may further identify potential dosing ranges for optimal therapeutic efficacy while minimizing potential adverse effects, paving the way for safer and more effective therapeutic strategies as we move towards precision therapy for MI.

Conclusion

The findings from this study suggest that given appropriate doses, IL-10 has the potential to modulate Mφ phenotypes *in vitro* and to ameliorate cardiac functional deterioration, reduce myocardial inflammation and fibrosis, and promote revascularization in the context of MI *in vivo* (Figure 8). Our study highlights the dose-dependent effects of IL-10 and underscores the potential clinical significance of appropriate IL-10 administration in managing MI. Overall, these results provide valuable insights into the development of new therapeutic strategies or adjunct therapies targeting specific myocardial pathologies to regulate Mφ phenotypes and augment cardiac repair post-MI.

Data availability statement

The original contributions presented in the study are included in the article/Supplementary Material, further inquiries can be directed to the corresponding author.

Ethics statement

The animal study was approved by the Institutional Animal Care and Use Committee (IACUC) at the University of Pittsburgh (UPitt) and the University of South Dakota (USD). The study was conducted in accordance with the local legislation and institutional requirements.

Author contributions

JZ: Data curation, Formal Analysis, Investigation, Methodology, Software, Validation, Visualization, Writing–original draft, Writing–review and editing. RR: Formal Analysis, Investigation, Methodology, Resources, Software, Writing–original draft, Writing–review and editing. XL: Data curation, Formal Analysis, Investigation, Methodology, Writing–original draft, Writing–review and editing. BL: Data curation, Formal Analysis, Investigation, Methodology, Writing–original draft, Writing–review and editing. MM: Data curation, Formal Analysis, Investigation, Methodology, Writing–original draft, Writing–review and editing. KB: Data curation, Formal Analysis, Investigation, Methodology, Writing–original draft, Writing–review and editing. KK: Formal Analysis, Funding acquisition, Investigation, Methodology, Resources, Supervision, Writing–original draft, Writing–review and editing. JH: Funding acquisition, Investigation, Project administration, Resources, Supervision, Writing–original draft, Writing–review and editing. YW: Project administration, Resources, Supervision, Writing–original draft, Writing–review and editing, Funding acquisition, Investigation. WC: Conceptualization, Data curation, Formal Analysis, Funding acquisition, Investigation, Methodology, Project administration, Resources, Software, Supervision, Validation, Visualization, Writing–original draft, Writing–review and editing.

Funding

The author(s) declare that financial support was received for the research, authorship, and/or publication of this article. This project was supported in part by the Department of Defense (W81XWH2110089 to WC; FA9550-23-1-0495 to the University of South Dakota), the American Heart Association Career Development Award (855260 to WC) and Established Investigator Award (12EIA9020016 to YW), the South Dakota Board of Regents (Governor's Research Fund to WC), the University of Pittsburgh Henry J. Mankin Endowed Chair (JH), the National Institute of Health (1R21EB016774 to JH), and the University of South Dakota Sanford School of Medicine (startup fund to WC). Echocardiography was performed using an ultrasound scanner supported by an NIH shared instrument grant (NIH1S10RR027383-01 to KK).

Acknowledgments

The authors wish to thank Dr. Jessica Freeling for her expert assistance in animal surgeries and echocardiographic analyses.

Conflict of interest

The authors declare that the research was conducted in the absence of any commercial or financial relationships that could be construed as a potential conflict of interest.

Publisher's note

Supplementary material

The Supplementary Material for this article can be found online at: https://www.frontiersin.org/articles/10.3389/fphys.2024.1481460/full#supplementary-material

References

Anderson, D. R., Poterucha, J. T., Mikuls, T. R., Duryee, M. J., Garvin, R. P., Klassen, L. W., et al. (2013). IL-6 and its receptors in coronary artery disease and acute myocardial infarction. *Cytokine* 62 (3), 395–400. doi:10.1016/j.cyto.2013.03.020

Asadullah, K., Sterry, W., and Volk, H. D. (2003). Interleukin-10 therapy—review of a new approach. *Pharmacol. Rev.* 55 (2), 241–269. doi:10.1124/pr.55.2.4

Bergmann, O., Bhardwaj, R. D., Bernard, S., Zdunek, S., Barnabé-Heider, F., Walsh, S., et al. (2009). Evidence for cardiomyocyte renewal in humans. *Science* 324 (5923), 98–102. doi:10.1126/science.1164680

Bruton, F. A., Kaveh, A., Ross-Stewart, K. M., Matrone, G., Oremek, M. E. M., Solomonidis, E. G., et al. (2022). Macrophages trigger cardiomyocyte proliferation by increasing epicardial vegfaa expression during larval zebrafish heart regeneration. *Dev. Cell* 57 (12), 1512–1528.e5. doi:10.1016/j.devcel.2022.05.014

Bu, T., Li, Z., Hou, Y., Sun, W., Zhang, R., Zhao, L., et al. (2021). Exosome-mediated delivery of inflammation-responsive IL-10 mRNA for controlled atherosclerosis treatment. *Theranostics* 11 (20), 9988–10000. doi:10.7150/thno.64229

Carlini, V., Noonan, D. M., Abdalalem, E., Goletti, D., Sansone, C., Calabrone, L., et al. (2023). The multifaceted nature of IL-10: regulation, role in immunological homeostasis and its relevance to cancer, COVID-19 and post-COVID conditions. *Front. Immunol.* 14, 1161067. doi:10.3389/fimmu.2023.1161067

Chen, C.-W., Okada, M., Proto, J. D., Gao, X., Sekiya, N., Beckman, S. A., et al. (2013). Human pericytes for ischemic heart repair. *STEM CELLS* 31 (2), 305–316. doi:10.1002/stem.1285

Chen, W. C. W., Lee, B. G., Park, D. W., Kim, K., Chu, H., Kim, K., et al. (2015). Controlled dual delivery of fibroblast growth factor-2 and Interleukin-10 by heparin-based coacervate synergistically enhances ischemic heart repair. *Biomaterials* 72, 138–151. doi:10.1016/j.biomaterials.2015.08.050

Chen, W. C. W., Wang, Z., Missinato, M. A., Park, D. W., Long, D. W., Liu, H.-J., et al. (2016). Decellularized zebrafish cardiac extracellular matrix induces mammalian heart regeneration. *Sci. Adv.* 2 (11), e1600844. doi:10.1126/sciadv.1600844

Cheng, Y., and Rong, J. (2018). Macrophage polarization as a therapeutic target in myocardial infarction. *Curr. Drug Targets* 19 (6), 651–662. doi:10.2174/1389450118666171031115025

Chu, H., Chen, C.-W., Huard, J., and Wang, Y. (2013). The effect of a heparin-based coacervate of fibroblast growth factor-2 on scarring in the infarcted myocardium. *Biomaterials* 34 (6), 1747–1756. doi:10.1016/j.biomaterials.2012.11.019

DeBerge, M., Glinton, K., Subramanian, M., Wilsbacher, L. D., Rothlin, C. V., Tabas, I., et al. (2021). Macrophage AXL receptor tyrosine kinase inflames the heart after reperfused myocardial infarction. *J. Clin. Invest* 131 (6), e139576. doi:10.1172/JCI139576

Duncan, S. A., Dixit, S., Sahu, R., Martin, D., Baganizi, D. R., Nyairo, E., et al. (2019). Prolonged release and functionality of interleukin-10 encapsulated within PLA-PEG nanoparticles. *Nanomater. (Basel)* 9 (8), 1074. doi:10.3390/nano9081074

Epelman, S., Liu, P. P., and Mann, D. L. (2015). Role of innate and adaptive immune mechanisms in cardiac injury and repair. *Nat. Rev. Immunol.* 15 (2), 117–129. doi:10.1038/nri3800

Frangogiannis, N. G. (2014). The inflammatory response in myocardial injury, repair, and remodelling. *Nat. Rev. Cardiol.* 11 (5), 255–265. doi:10.1038/nrcardio.2014.28

Frangogiannis, N. G. (2015). Inflammation in cardiac injury, repair and regeneration. *Curr. Opin. Cardiol.* 30 (3), 240–245. doi:10.1097/HCO.0000000000000158

Ganesh, G. V., and Ramkumar, K. M. (2020). Macrophage mediation in normal and diabetic wound healing responses. *Inflamm. Res. official J. Eur. Histamine Res. Soc.* 69 (4), 347–363. doi:10.1007/s00011-020-01328-y

Gao, Y., Qian, N., Xu, J., and Wang, Y. (2021). The roles of macrophages in heart regeneration and repair after injury. *Front. Cardiovasc Med.* 8, 744615. doi:10.3389/fcvm.2021.744615

Gullestad, L., Aass, H., Fjeld, J. G., Wikeby, L., Andreassen, A. K., Ihlen, H., et al. (2001). Immunomodulating therapy with intravenous immunoglobulin in patients with chronic heart failure. *Circulation* 103 (2), 220–225. doi:10.1161/01.cir.103.2.220

Haghikia, A., Ricke-Hoch, M., Stapel, B., Gorst, I., and Hilfiker-Kleiner, D. (2014). STAT3, a key regulator of cell-to-cell communication in the heart. *Cardiovasc Res.* 102 (2), 281–289. doi:10.1093/cvr/cvu034

Halade, G. V., and Lee, D. H. (2022). Inflammation and resolution signaling in cardiac repair and heart failure. *EBioMedicine* 79, 103992. doi:10.1016/j.ebiom.2022.103992

Han, H., Ma, Q., Li, C., Liu, R., Zhao, L., Wang, W., et al. (2020). Profiling serum cytokines in COVID-19 patients reveals IL-6 and IL-10 are disease severity predictors. *Emerg. microbes and Infect.* 9 (1), 1123–1130. doi:10.1080/22221751.2020.1770129

Huhn, R. D., Radwanski, E., Gallo, J., Affrime, M. B., Sabo, R., Gonyo, G., et al. (1997). Pharmacodynamics of subcutaneous recombinant human interleukin-10 in healthy volunteers. *Clin. Pharmacol. Ther.* 62 (2), 171–180. doi:10.1016/S0009-9236(97)90065-5

Huynh, T., Reed, C., Blackwell, Z., Phelps, P., Herrera, L. C. P., Almodovar, J., et al. (2023). Local IL-10 delivery modulates the immune response and enhances repair of volumetric muscle loss muscle injury. *Sci. Rep.* 13 (1), 1983. doi:10.1038/s41598-023-27981-x

Ip, W. K. E., Hoshi, N., Shouval, D. S., Snapper, S., and Medzhitov, R. (2017). Anti-inflammatory effect of IL-10 mediated by metabolic reprogramming of macrophages. *Science* 356 (6337), 513–519. doi:10.1126/science.aal3535

Iyer, S. S., and Cheng, G. (2012). Role of interleukin 10 transcriptional regulation in inflammation and autoimmune disease. *Crit. Rev. Immunol.* 32 (1), 23–63. doi:10.1615/critrevimmunol.v32.i1.30

Jian, Y., Zhou, X., Shan, W., Chen, C., Ge, W., Cui, J., et al. (2023). Crosstalk between macrophages and cardiac cells after myocardial infarction. *Cell Commun. Signal.* 21 (1), 109. doi:10.1186/s12964-023-01105-4

Johnson, N. R., Kruger, M., Goetsch, K. P., Zilla, P., Bezuidenhout, D., Wang, Y., et al. (2015). Coacervate delivery of growth factors combined with a degradable hydrogel preserves heart function after myocardial infarction. *ACS Biomater. Sci. Eng.* 1 (9), 753–759. doi:10.1021/acsbiomaterials.5b00077

Jung, M., Ma, Y., Iyer, R. P., DeLeon-Pennell, K. Y., Yabluchanskiy, A., Garrett, M. R., et al. (2017). IL-10 improves cardiac remodeling after myocardial infarction by stimulating M2 macrophage polarization and fibroblast activation. *Basic Res. Cardiol.* 112 (3), 33. doi:10.1007/s00395-017-0622-5

Kaur, K., Sharma, A. K., and Singal, P. K. (2006). Significance of changes in TNF-alpha and IL-10 levels in the progression of heart failure subsequent to myocardial infarction. *Am. J. Physiol. Heart Circ. Physiol.* 291 (1), H106–H113. doi:10.1152/ajpheart.01327.2005

Kim, Y., Nurakhayev, S., Nurkesh, A., Zharkinbekov, Z., and Saparov, A. (2021). Macrophage polarization in cardiac tissue repair following myocardial infarction. *Int. J. Mol. Sci.* 22 (5), 2715. doi:10.3390/ijms22052715

Krishnamurthy, P., Rajasingh, J., Lambers, E., Qin, G., Losordo, D. W., and Kishore, R. (2009). IL-10 inhibits inflammation and attenuates left ventricular remodeling after myocardial infarction via activation of STAT3 and suppression of HuR. *Circulation Res.* 104 (2), e9–e18. doi:10.1161/CIRCRESAHA.108.188243

Krzyszczyk, P., Schloss, R., Palmer, A., and Berthiaume, F. (2018). The role of macrophages in acute and chronic wound healing and interventions to promote pro-wound healing phenotypes. *Front. Physiol.* 9, 419. doi:10.3389/fphys.2018.00419

Kwilasz, A. J., Grace, P. M., Serbedzija, P., Maier, S. F., and Watkins, L. R. (2015). The therapeutic potential of interleukin-10 in neuroimmune diseases. *Neuropharmacology* 96, 55–69. doi:10.1016/j.neuropharm.2014.10.020

Lu, L., Zhang, H., Dauphars, D. J., and He, Y. W. (2021). A potential role of interleukin 10 in COVID-19 pathogenesis. *Trends Immunol.* 42 (1), 3–5. doi:10.1016/j.it.2020.10.012

Manning, W. J., Wei, J. Y., Katz, S. E., Litwin, S. E., and Douglas, P. S. (1994). *In vivo* assessment of LV mass in mice using high-frequency cardiac ultrasound: necropsy validation. *Am. J. Physiology - Heart Circulatory Physiology* 266 (4), H1672–H1675. doi:10.1152/ajpheart.1994.266.4.H1672

Ni, M., Zhang, J., Sosa, R., Zhang, H., Wang, H., Jin, D., et al. (2021). T-cell immunoglobulin and mucin domain-containing protein-4 is critical for kupffer cell homeostatic function in the activation and resolution of liver ischemia reperfusion injury. *Hepatology* 74 (4), 2118–2132. doi:10.1002/hep.31906

Nishio, R., Matsumori, A., Shioi, T., Ishida, H., and Sasayama, S. (1999). Treatment of experimental viral myocarditis with interleukin-10. *Circulation* 100 (10), 1102–1108. doi:10.1161/01.cir.100.10.1102

Okada, M., Payne, T. R., Drowley, L., Jankowski, R. J., Momoi, N., Beckman, S., et al. (2012). Human skeletal muscle cells with a slow adhesion rate after isolation and an enhanced stress resistance improve function of ischemic hearts. *Mol. Ther.* 20 (1), 138–145. doi:10.1038/mt.2011.229

Pluijmert, N. J., Atsma, D. E., and Quax, P. H. A. (2021). Post-ischemic myocardial inflammatory response: a complex and dynamic process susceptible to immunomodulatory therapies. *Front. Cardiovasc Med.* 8, 647785. doi:10.3389/fcvm.2021.647785

Pollick, C., Hale, S. L., and Kloner, R. A. (1995). Echocardiographic and cardiac Doppler assessment of mice. *J. Am. Soc. Echocardiogr.* 8 (5), 602–610. doi:10.1016/s0894-7317(05)80373-6

Salina, A. C. G., Dos-Santos, D., Rodrigues, T. S., Fortes-Rocha, M., Freitas-Filho, E. G., Alzamora-Terrel, D. L., et al. (2022). Efferocytosis of SARS-CoV-2-infected dying cells impairs macrophage anti-inflammatory functions and clearance of apoptotic cells. *Elife* 11, e74443. doi:10.7554/eLife.74443

Santos-Zas, I., Lemarié, J., Tedgui, A., and Ait-Oufella, H. (2018). Adaptive immune responses contribute to post-ischemic cardiac remodeling. *Front. Cardiovasc Med.* 5, 198. doi:10.3389/fcvm.2018.00198

Saraiva, M., and O'Garra, A. (2010). The regulation of IL-10 production by immune cells. *Nat. Rev. Immunol.* 10 (3), 170–181. doi:10.1038/nri2711

Saraiva, M., Vieira, P., and O'Garra, A. (2020). Biology and therapeutic potential of interleukin-10. *J. Exp. Med.* 217 (1), e20190418. doi:10.1084/jem.20190418

Schumacher, S. M., and Naga Prasad, S. V. (2018). Tumor necrosis factor-α in heart failure: an updated review. *Curr. Cardiol. Rep.* 20 (11), 117. doi:10.1007/s11886-018-1067-7

Senyo, S. E., Steinhauser, M. L., Pizzimenti, C. L., Yang, V. K., Cai, L., Wang, M., et al. (2013). Mammalian heart renewal by pre-existing cardiomyocytes. *Nature* 493 (7432), 433–436. doi:10.1038/nature11682

Stumpf, C., Seybold, K., Petzi, S., Wasmeier, G., Raaz, D., Yilmaz, A., et al. (2008). Interleukin-10 improves left ventricular function in rats with heart failure subsequent to myocardial infarction. *Eur. J. Heart Fail.* 10 (8), 733–739. doi:10.1016/j.ejheart.2008.06.007

Tesoro, L., Hernández, I., Ramírez-Carracedo, R., Díez-Mata, J., Alcharani, N., Jiménez-Guirado, B., et al. (2022). NIL10: a new IL10-receptor binding nanoparticle that induces cardiac protection in mice and pigs subjected to acute myocardial infarction through STAT3/NF-κB activation. *Pharmaceutics* 14 (10), 2044. doi:10.3390/pharmaceutics14102044

Tilg, H., van Montfrans, C., van den Ende, A., Kaser, A., van Deventer, S. J., Schreiber, S., et al. (2002). Treatment of Crohn's disease with recombinant human interleukin 10 induces the proinflammatory cytokine interferon gamma. *Gut* 50 (2), 191–195. doi:10.1136/gut.50.2.191

Tsao, C. W., Aday, A. W., Almarzooq, Z. I., Anderson, C. A. M., Arora, P., Avery, C. L., et al. (2023). Heart disease and stroke statistics—2023 update: a report from the American heart association. *Circulation* 147 (8), e93–e621. doi:10.1161/CIR.0000000000001123

Wandt, B., Bojö, L., Tolagen, K., and Wranne, B. (1999). Echocardiographic assessment of ejection fraction in left ventricular hypertrophy. *Heart* 82 (2), 192–198. doi:10.1136/hrt.82.2.192

Wang, X., Wong, K., Ouyang, W., and Rutz, S. (2019). Targeting IL-10 family cytokines for the treatment of human diseases. *Cold Spring Harb. Perspect. Biol.* 11 (2), a028548. doi:10.1101/cshperspect.a028548

Wu, M. Y., and Lu, J. H. (2019). Autophagy and macrophage functions: inflammatory response and phagocytosis. *Cells* 9 (1), 70. doi:10.3390/cells9010070

Xiang, G., Yang, Q., Wang, B., Sekiya, N., Mu, X., Tang, Y., et al. (2011). Lentivirus-mediated Wnt11 gene transfer enhances cardiomyogenic differentiation of skeletal muscle-derived stem cells. *Mol. Ther.* 19, 790–796. doi:10.1038/mt.2011.5

York, A. G., Skadow, M. H., Oh, J., Qu, R., Zhou, Q. D., Hsieh, W.-Y., et al. (2024). IL-10 constrains sphingolipid metabolism to limit inflammation. *Nature* 627 (8004), 628–635. doi:10.1038/s41586-024-07098-5

Yunna, C., Mengru, H., Lei, W., and Weidong, C. (2020). Macrophage M1/M2 polarization. *Eur. J. Pharmacol.* 877, 173090. doi:10.1016/j.ejphar.2020.173090

Zhang, Z., Tang, J., Cui, X., Qin, B., Zhang, J., Zhang, L., et al. (2021). New insights and novel therapeutic potentials for macrophages in myocardial infarction. *Inflammation* 44 (5), 1696–1712. doi:10.1007/s10753-021-01467-2

Zhao, Y., Qin, L., Zhang, P., Li, K., Liang, L., Sun, J., et al. (2020). Longitudinal COVID-19 profiling associates IL-1RA and IL-10 with disease severity and RANTES with mild disease. *JCI Insight* 5 (13), e139834. doi:10.1172/jci.insight.139834

Zuo, W., Sun, R., Ji, Z., and Ma, G. (2023). Macrophage-driven cardiac inflammation and healing: insights from homeostasis and myocardial infarction. *Cell Mol. Biol. Lett.* 28 (1), 81. doi:10.1186/s11658-023-00491-4

frontiers | Frontiers in Physiology

TYPE Original Research
PUBLISHED 26 February 2025
DOI 10.3389/fphys.2025.1547901

OPEN ACCESS

EDITED BY
Hong Zheng,
University of South Dakota, United States

REVIEWED BY
Kenichi Katsurada,
Jichi Medical University, Japan
De-Pei Li,
University of Missouri, United States

*CORRESPONDENCE
Yu-long Li,
yulongli@unmc.edu

RECEIVED 18 December 2024
ACCEPTED 04 February 2025
PUBLISHED 26 February 2025

CITATION
Evans AJ, Tu H, Li Y, Shabaltiy B, Whitney L, Carpenter K and Li Y-l (2025) Altered leptin signaling and attenuated cardiac vagal activity in rats with type 2 diabetes.
Front. Physiol. 16:1547901.
doi: 10.3389/fphys.2025.1547901

Altered leptin signaling and attenuated cardiac vagal activity in rats with type 2 diabetes

Anthony J. Evans[1], Huiyin Tu[1], Yu Li[1], Boris Shabaltiy[1], Lauren Whitney[1], Kassidy Carpenter[1] and Yu-long Li[1,2]*

[1]Department of Emergency Medicine, University of Nebraska Medical Center, Omaha, NE, United States, [2]Department of Cellular & Integrative Physiology, University of Nebraska Medical Center, Omaha, NE, United States

Introduction: The leading cause of death in type 2 diabetes mellitus (T2DM) patients is cardiovascular-related events, including myocardial infraction-induced ventricular arrhythmia. Previous studies have shown that T2DM-induced functional remodeling of cardiac vagal postganglionic (CVP) neurons contributes to ventricular arrhythmogenesis. As leptin resistance is common in T2DM patients, and CVP neurons are located in epicardial adipose pads, a tissue that secretes leptin, in this study we aimed to elucidate a correlation between leptin resistance and CVP neuronal dysfunction in T2DM.

Methods: A high fat-diet/low dose streptozotocin-induced T2DM rat model was used in this study to characterize T2DM-induced alterations in cardiac parasympathetic tone, determined by changes in baroreflex sensitivity and CVP neuronal excitability. The impact of leptin resistance on CVP neurons was also studied by examining the expression of leptin in epicardial adipose pads, and leptin receptors and uncoupling protein 2 (UCP2) in CVP neurons.

Results: T2DM rats exhibited diminished baroreflex sensitivity, and decreased CVP neuronal excitability, demonstrated by a reduced frequency of action potentials, diminished nAChR currents, and an attenuated response to nicotine stimulation. Additionally, compared to sham animals, the expression of leptin receptors and UCP2 in CVP neurons was reduced as early as 4 weeks post-T2DM although the leptin levels in epicardial adipose pads was increased during the progression of T2DM, which demonstrated the occurrence of leptin resistance in T2DM CVP neurons.

Conclusion: Cardiac parasympathetic dysfunction in T2DM rats is due, in part, to functional remodeling of CVP neurons. As leptin resistance develops as early as 4 weeks post-T2DM induction, diminished leptin receptors-UCP2 signaling may contribute to CVP neuronal dysregulation.

KEYWORDS

cardiac parasympathetic activity, intracardiac ganglia, leptin resistance, type 2 diabetes, uncoupling protein 2

Introduction

Type 2 diabetes mellitus (T2DM) is a common metabolic disease that impacts more than 500 million individuals worldwide, with an estimated healthcare cost anticipated to exceed $1054 billion by the year 2045 (International Diabetes Federation, 2021; Hossain et al., 2024). The leading cause of mortality in the T2DM population is cardiovascular-related events including stroke, myocardial infarction (MI), and sudden cardiac death (SCD) (Walker and Cubbon, 2015; Rawshani et al., 2017; Gyldenkerne et al., 2023; Wong and Sattar, 2023). The development of ventricular tachycardia/ventricular fibrillation (VT/VF) post-MI has been linked with sudden cardiac death in T2DM patients, with ventricular arrhythmias accounting for one-third of abnormal heart rhythms observed at the time of cardiac arrest (Agarwal and Singh, 2017; Mhaimeed et al., 2023; Chakraborty et al., 2024). While tight glycemic control is the typical treatment for many diabetes-related pathologies, multiple studies have reported that the risk of cardiovascular event-related deaths in T2DM patients is not reduced by glycemic control alone (Reaven et al., 2019; Scheen, 2022).

A significant contributor to ventricular arrhythmogenesis in T2DM is the remodeling of the parasympathetic division of the intrinsic cardiac nervous system which exerts autonomic control of the heart (Zhang et al., 2018; Hu et al., 2021). The efferent component of the cardiac parasympathetic nervous system begins with preganglionic parasympathetic neurons that extend from the dorsal vagal motor nucleus (DVMN) and nucleus ambiguus through the left and right cardiac trunks of the vagus nerve (Armour, 2007; Durães Campos et al., 2018). The latter ultimately innervates cardiac vagal postganglionic (CVP) neurons located in the intracardiac ganglia (ICG) embedded in the epicardial adipose pad on the heart (Armour, 2007; Durães Campos et al., 2018). Our previous work has shown that CVP neurons in T2DM exhibit reduced nicotinic acetylcholine receptor (nAChR) currents and N-type voltage-gated calcium currents, which result in compromised neuronal function and increased susceptibility to arrhythmogenesis (Liu et al., 2012; Liu et al., 2015; Zhang et al., 2022). The molecular mechanisms driving changes in CVP neuronal function as T2DM develops have not yet been elucidated.

Leptin resistance, as defined by reduced sensitivity to the hormone leptin, is a common complication of T2DM (Schmidt et al., 2006; Gruzdeva et al., 2019). Leptin, predominantly secreted by adipose tissue, binds leptin receptors on the cell membrane, which canonically activates the Janus kinase/signal transducer and activator of transcription (JAK-STAT) pathway (Procaccini et al., 2009). Previous studies have reported on leptin signaling's role in modulating neuronal excitability in Pro-opiomelanocortin (POMC) neurons (Perissinotti et al., 2021), striatal cholinergic interneurons (Mancini et al., 2022), and neuropeptide Y (NPY)/Agouti-related protein (AgRP) neurons of the hypothalamic arcuate nucleus (Takahashi and Cone, 2005). Currently, the impact of leptin resistance on CVP neuronal function has not yet been explored. As the ICG are located in epicardial adipose, the proximity of CVP neurons to epicardial adipocytes speaks to a potential role for leptin signaling in CVP neuronal function. We hypothesized that CVP neurons would develop leptin resistance as T2DM progresses, which further contributes to T2DM-induced CVP neuronal dysregulation. Therefore, this study aimed to further characterize the impact of T2DM on cardiac parasympathetic function and explore the potential role of leptin resistance in CVP functional remodeling.

Materials and methods

Animal studies

This study conforms to guidelines for the Care and Use of Laboratory Animals and was approved by the Institutional Animal Care and Use Committee (IACUC) at the University of Nebraska Medical Center (IACUC number: 23-043-09-FC and 18-023-04-FC). After *in vivo* experiments were completed, rats were euthanized via i.p. injection of 0.39 mL/kg of Fatal-Plus euthanasia (about 150 mg/kg pentobarbital, DBA Med-Vet International, Mettawa, IL, United States).

T2DM rat model

Male and female Sprague-Dawley rats (200–220 g) were housed in a controlled temperature and humidity environment and were exposed to a 12-h light to 12-h dark cycle. Water and chow were provided *ad libitum*. Sham rats were administered a standard chow diet (34% protein, 53% carbohydrate, 13% fat). T2DM was induced via introduction of a high-fat diet (HFD) (15.2% protein, 42.7% carbohydrate, 42% fat; Inotiv Pharmaceutical Company, Indianapolis, IN, United States). After 4 weeks of HFD introduction, rats were injected with a low dose of streptozotocin (STZ) (30 mg/kg, i.p.) and continued HFD feeding until sacrifice at different time-points. Fasting blood glucose was measured every 4 weeks. All experiments were performed after 4, 8, or 12 weeks on standard chow or HFD. Metabolic characteristics of rats used in this study are summarized in Supplementary Table 1. Sham rats are defined in this study as rats that did not receive HFD or STZ treatment. Sham rats used were a mix of rats age-matched to the 4, 8, and 12-week experimental groups. We chose a mixed control group as we have not observed any difference in the parameters measured in this study among sham rats of different ages.

Measurement of baroreflex sensitivity

A combination of chloralose (40 mg/kg, i.p.) and urethane (800 mg/kg, i.p.) was used to anesthetize rats, with an additional supplementation of chloralose (10 mg/kg, i.v.) every 2 h. A ventral midline neck incision was made, the trachea was cannulated, and artificial ventilation was performed via mechanical respirator (Harvard Apparatus, Holliston, MA, United States; 60 breaths/min; 2.5 mL tidal volume). A Millar pressure transducer (SPR 524, ADInstruments, Colorado Springs, CO, United States) was inserted into the right carotid artery for testing arterial blood pressure (ABP) and heart rate (HR). A polyethylene catheter was implanted into the right femoral vein for drug administration.

Baroreflex sensitivity was determined by measuring reflex changes in HR responding to changes in ABP. Sodium nitroprusside (30 μg, i.v.) was administered to decrease ABP to

approximately 50 mmHg. ABP was subsequently raised through administration of phenylephrine (10 μg, i.v.). The logistic regression curve was then fit using the equation: $HR = A/1 + e^{B(blood\ pressure-C)} + D$ (A = HR range, B = Slope coefficient, C = ABP at midpoint of range, D = minimum HR) (Zhang et al., 2014). The maximum gain, an index of baroreflex sensitivity, was determined by calculating A*B/4 of the logistic regression curve.

Isolation of CVP neurons and whole cell patch-clamp recording for nAChR currents and action potentials

CVP neurons were isolated by a two-step enzymatic digestion protocol (Liu et al., 2012). Briefly, collected ICG was minced into small pieces and incubated successively with digestion solution one containing 0.1% collagenase and trypsin, and digestion solution two containing 0.2% collagenase and 0.5% bovine serum albumin for 30 min at 37°C. The isolated neurons were cultured in the incubator for patch clamp recording or immunofluorescence staining.

Action potentials and nAChR currents were recorded by the whole cell patch-clamp technique using an Axopatch 200B patch-clamp amplifier (Axon Instruments, Foster City, CA, United States). The P-clamp 10.2 program (Axon Instruments) was used for data acquisition and analysis. Recorded traces were sampled at 10 kHz and filtered at 5 kHz. All experiments were done at room temperature (22°C–24°C).

The nAChR currents were recorded by a gap-free voltage-clamp technique. The resistance of the patch pipette was 3–5 MΩ when pipette was filled with the following solution (in mM): 140 CsCl, 2 MgATP, 10 HEPES, and 1 EGTA (pH 7.2, 300 mOsm/L). The extracellular solution consisted of (in mM): 140 NaCl, 3 KCl, 2.5 $CaCl_2$, 1.2 $MgCl_2$, 10 HEPES, and 7.7 glucose (pH 7.2; 310 mOsm/L). Series resistance of 6–13 MΩ was electronically compensated to 80%–90%. Junction potential was calculated to be +5.1 mV. CVP neurons were clamped at −90 mV and continuously perfused with extracellular solution (2 mL/min). Nicotine, a nAChR specific agonist dissolved in the extracellular solution, was applied to ICG neurons by bolus ejection (6 psi.; 100 m) through a micropipette connected to a Picopump (PV 820 Pneumatic PicoPump, World Precision Instruments, Sarasota, FL). The micropipette (5–7 μm diameter) for drug application was positioned 20–30 μm from the cell soma. After nicotine concentration (3 mM) was applied (Liu et al., 2015), peak currents were measured, and current density was calculated by dividing peak current by cell membrane capacitance (C_m).

In the current-clamp model, frequency of action potentials was measured in a 1-s current clamp (100 pA). The patch pipette solution consisted of (in mM): 105 K-Aspartate, 20 KCl, 1 $CaCl_2$, 5 MgATP, 10 HEPES, 10 EGTA, and 25 glucose (pH 7.2; 320 mOsm/L). The bath solution was composed of (in mM): 140 NaCl, 5.4 KCl, 0.5 $MgCl_2$, 2.5 $CaCl_2$, 5.5 HEPES, 11 glucose, and 10 sucrose (pH 7.4; 330 mOsm/L). Junction potential was calculated to be +12.3 mV and membrane potential was corrected using this value. Based on our preliminary data and one previous study (Alkondon et al., 2000), 30 μM nicotine was perfused to measure resting membrane potential and frequency of action potentials.

Reverse-transcriptase quantitative polymerase chain reaction (RT-qPCR)

RNA was isolated from rat ICG using Trizol reagent (Thermofisher, Walham, MA, United States) following the manufacturers protocol. Five-hundred ng of total RNA was subsequently reverse-transcribed (RT) using the iScript Reverse Transcription Supermix (Bio-rad laboratories, Hercules, CA, United States). RT was performed at 42°C for 30 min. Quantitative PCR was performed using iQ Sybr-green supermix (Bio-rad laboratories, Hercules, CA, United States) using 1 μL of cDNA as template. PCR reactions were cycled in the Step-one plus real time PCR system (Applied Biosystems, Foster City, CA, United States). PCR was performed using the following cycling parameters: 1 cycle of 95°C for 10 min, 40 cycles of 95°C for 15 s, followed by 60° for 1 min. Following the end of cycling, a melting curve analysis was performed. For quantification, each gene of interest was normalized to the housekeeping gene specified in the corresponding figure legend. The data were analyzed using the $2^{-\Delta\Delta Ct}$ method. All primers used for amplification are listed in Supplementary Table 3.

Reverse Phase protein Microarray (RPPA)

Due to the limitation of small ICG samples (1–2 mg wet weight), we could not detect the protein expression using regular Western blot analysis and instead employed a modified RPPA as previously described (Zhang et al., 2018). In short, ICG were rapidly removed, flash frozen, and stored at −80°C. ICG proteins were extracted in protein lysis buffer (10 mM Tris, 1 mM EDTA, 1% SDS; pH 7.4) plus protease inhibitor (Sigma, St. Louis, MO, United States) and incubated on ice for 1 h. Homogenates were centrifuged at 12,000×g for 30 min at 4°C and the supernatants were harvested. Protein concentrations were determined using bicinchoninic acid (BCA) assay (Thermofisher, Waltham, MA, United States) and proteins were standardized to equal concentrations. 50 nL of each protein homogenate was loaded onto nitrocellulose-coated glass slides using an 8-pin arrayer. Nitrocellulose slides were subsequently blocked using Intercept blocking buffer (LI-COR, Lincoln, NE, United States) for 1 h at room temperature while shaking. Slides were then incubated in primary antibody (Supplementary Table 2) overnight shaking at 4°C. Slides were washed 3X in TBS-T for 10 min at room temperature and incubated with appropriate fluorescence-conjugated secondary antibodies for 1 h at room temperature. Slides were subsequently washed 3X in TBS-T for 10 min and visualized using the LI-COR Odyssey DLX imaging system (Li-COR, Lincoln, NE, United States). Protein expression was quantified using ImageJ analysis software (NIH, Bethesda, MD, United States).

Immunofluorescence

Isolated CVP neurons were plated onto slides and were subsequently fixed with 4% paraformaldehyde in 0.1 M PBS for 10 min at 4°C, washed with PBS-T, and blocked with 10% normal goat serum for 1 h at room temperature. CVP neurons were

incubated with primary antibodies listed in Supplementary Table 2 overnight at 4°C. Slides were washed and subsequently incubated with appropriate secondary antibodies for 1 h at room temperature. CVP neurons were observed under a Leica fluorescent microscope with appropriate excitation/emission filters (Leica Microsystems, Buffalo Grove, IL, United States). Pictures were captured by a digital camera system. No staining was observed when PBS was used in place of primary antibody. Protein expression was quantified using Adobe Photoshop (Adobe Systems).

Western blot analysis

Rat epicardial adipose pads were rapidly removed and flash frozen until used. Rat epicardial adipose pads were homogenized in RIPA buffer (50 mM Tris-HCl, 150 mM NaCl, 50 mM NaF, 2 mM EDTA, 1 mM Na_3VO_4, 1%NP-40, 1%SDS, 1 mM PMSF) supplemented with a protease inhibitor cocktail (Sigma, St. Louis, MO, United States) using the bead blaster homogenization system (Benchmark Scientific, Sayreville, NJ, United States). Homogenates were incubated on ice for 1 h and then centrifuged (12,000×g at 4°C for 30 min) to remove excess tissue debris. Protein concentrations were determined using a BCA assay, and concentrations were standardized across all samples. 50 µg of total protein was loaded onto 13% SDS-PAGE gels and run at 100 V for 1 h at room temperature. Proteins were subsequently transferred to PVDF membranes via wet transfer method for 1.5 h at 100 V. PVDF membranes were incubated in ponceau-s solution (Thermofisher, Waltham, MA, United States) to visualize total protein content of each sample. Membranes were washed 3X in TBS-T for 10 min at room temperature and subsequently blocked in Intercept blocking buffer (LI-COR, Lincoln, NE, United States) for 1 h at room temperature. Blots were incubated in primary antibody (Supplementary Table 2) overnight at 4°C while rotating. Blots were subsequently washed 3X in TBS-T for 10 min at room temperature and probed with appropriate fluorescence-conjugated secondary antibodies for 1 h at room temperature. Blots were washed in TBS-T 3X for 10 min and visualized using the LI-COR Odyssey DLX imaging system (LI-COR, Lincoln, NE, United States). Protein expression was quantified using ImageJ analysis software (NIH, Bethesda, MA, United States).

Statistics

It has been previously reported that the pathogenesis of T2DM in patients exhibits sexual dimorphism (Kautzky-Willer et al., 2023). To determine if there was sex-based variation in CVP neuronal function, we examined nAChR currents and action potential frequency in CVP neurons of 12-week T2DM male and female rats. No significant difference in nAChR currents or action potential frequency in CVP neurons was observed between male and female rats in either the sham or T2DM condition (Supplementary Figures 1A, B). As we did not find sex differences in any parameters in the present study, we mixed sexes for statistical analyses.

Statistical analysis was performed using GraphPad Prism software (GraphPad software inc., La Jolla, CA, United States). All data are presented as mean ± SEM. An unpaired t-test or a one-way ANOVA with *post hoc* Dunnetts test was used to determine significance. Statistical significance was accepted when $P < 0.05$.

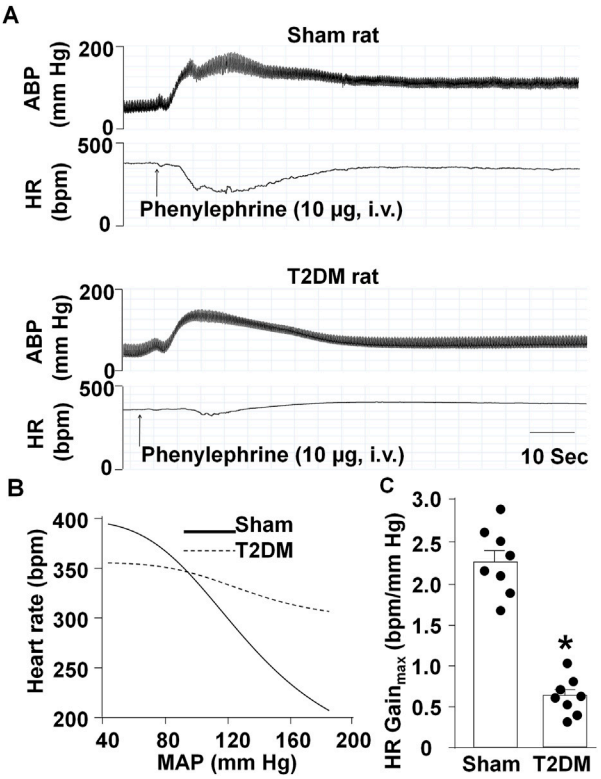

FIGURE 1
Arterial baroreflex sensitivity in sham and T2DM rats. **(A, B)** Representative recordings **(A)** and logistic regression curves **(B)** for reflex changes in heart rate (HR) in response to changes in arterial blood pressure (ABP) in anesthetized sham and T2DM rats. **(C)** Quantitative data for maximum gains of HR calculated from logistic regression curves. Arterial blood pressure was decreased to about 50 mmHg by sodium nitroprusside (30 µg, i.v.) and then increased by phenylephrine (10 µg, i.v.). Data are mean ± SEM, n = 8 rats in each group. *P < 0.05 vs. sham.

Results

Induction of T2DM

A previously described (Liu et al., 2012; Hu et al., 2021) HFD and a low-dose STZ rat model was used in this study because rats treated for 12 weeks with HFD and one-time low-dose STZ injection (deemed T2DM rats in this study) closely mimic the clinical characteristics, such as reduced insulin sensitivity, dyslipidemia, and hyperglycemia, seen in T2DM patients (Zhang et al., 2008; Liu et al., 2012; Skovsø, 2014; Cui et al., 2018). At 8 and 12 weeks post-T2DM induction, elevated levels of fasting blood glucose were observed in T2DM rats as compared to sham, indicating that HFD-STZ treatment induced a hyperglycemic state as early as 8 weeks post-T2DM induction (Supplementary Table 1). However, no significant difference was found in the body weight for T2DM and sham rats at any timepoint studied (Supplementary Table 1).

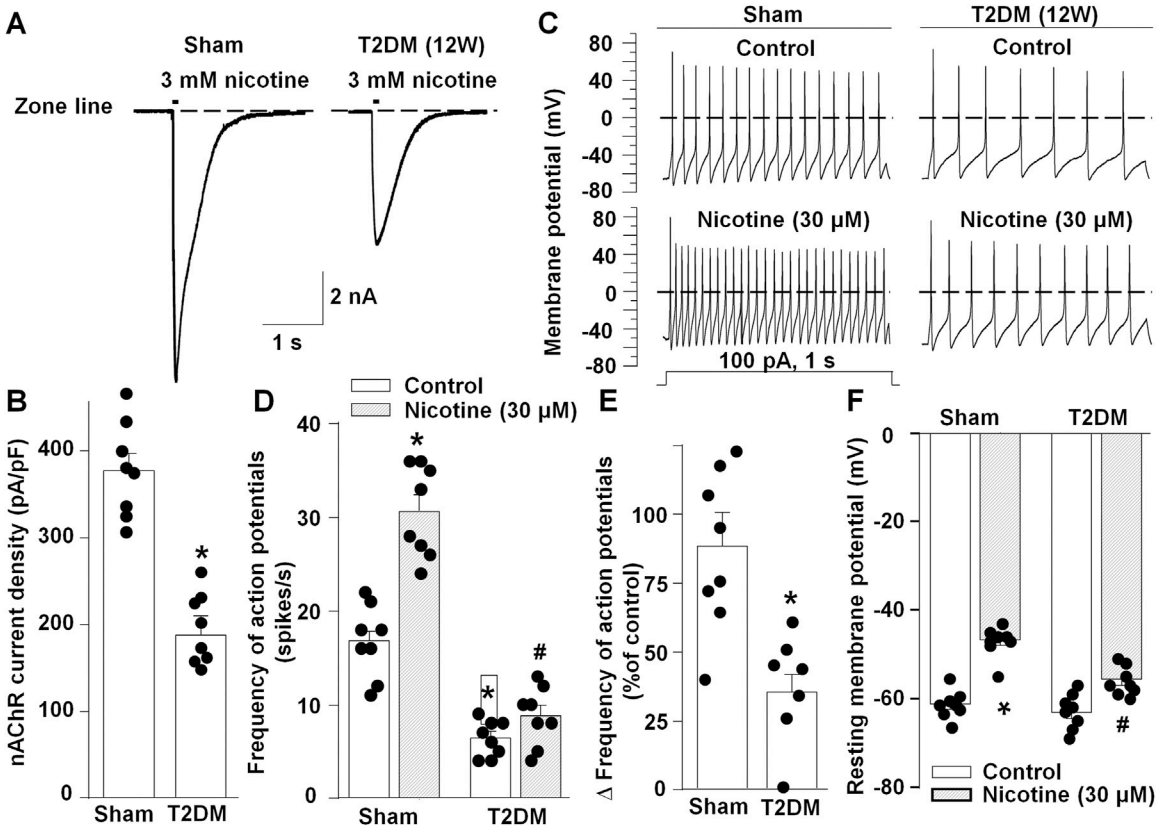

FIGURE 2
nAChR currents and cell excitability in CVP neurons from sham and T2DM rats. **(A, B)** Original recordings **(A)** and mean data **(B)** of nicotine (3 mM, 100 m)-evoked nAChR currents. **(C, D)** Original recordings of the action potential **(C)** and frequency of action potentials **(D)** before and after treatment with nicotine (30 μM) in CVP neurons. **(E)** Percent change of action potential frequency in response to nicotine in CVP neurons. **(F)** Resting membrane potentials before and after treatment with nicotine (30 μM) in CVP neurons. Data are mean ± SEM, n = 8 neurons in each group. *P < 0.05 vs. sham; #P < 0.05 vs. T2DM control.

T2DM reduced baroreflex sensitivity

To explore the impact of T2DM development on cardiac autonomic function, we examined baroreflex sensitivity. Baroreflex sensitivity was determined by measuring changes in HR in response to pharmacologically induced changes in ABP in sham and 12-week T2DM rats (Figures 1A,B). 12-week T2DM rats exhibited a significantly lower HR Gain$_{max}$ (an index of baroreflex sensitivity) as compared to sham rats (Figure 1C), indicating that T2DM development results in diminished baroreflex sensitivity.

T2DM diminished CVP neuronal excitability

Baroreflex sensitivity is regulated at multiple centers, including the efferent limb that is, in part, controlled by parasympathetic activity of the vagus nerve (Kuo et al., 2005; Dall'ago et al., 2007; Soltani et al., 2023). Furthermore, it has been reported that the vagus nerve becomes structurally and functionally compromised during T2DM progression (Guo et al., 1987; Lee et al., 2002; Dall'ago et al., 2007; Ziegler et al., 2018; Evans and Li, 2024). To explore the effect of T2DM on cardiac vagal activity, we assessed the impact of T2DM development on CVP neuronal function. In CVP neurons from sham and 12-week T2DM rats, 3 mM nicotine-induced nAChR currents were measured. A significantly lower nAChR current density was observed in CVP neurons from 12-week T2DM rats compared to sham rats, consistent with previously reported results (Liu et al., 2015) (Figures 2A,B).

To assess if reduced nAChR current densities impact CVP neuronal excitability, we recorded action potentials in isolated CVP neurons from sham and 12-week T2DM rats and measured the frequency of action potentials with or without nicotine treatment (30 μM). CVP neurons from T2DM rats exhibited fewer action potentials compared to that from sham rats (Figures 2C,D). Additionally, nicotine-increased action potential frequency was severely blunted in T2DM CVP neurons as compared to sham CVP neurons (Figures 2D,E). Furthermore, there is no difference in resting membrane potentials with or without nicotine treatment between sham and T2DM CVP neurons (Figure 2F). Taken together, these data indicate that CVP neurons exhibited attenuated neuronal functionality in T2DM rats.

Uncoupling protein 2 (UCP2) expression was reduced in T2DM

Along with diminished nAChR current density, our previous studies have reported that T2DM reduces voltage-gated calcium

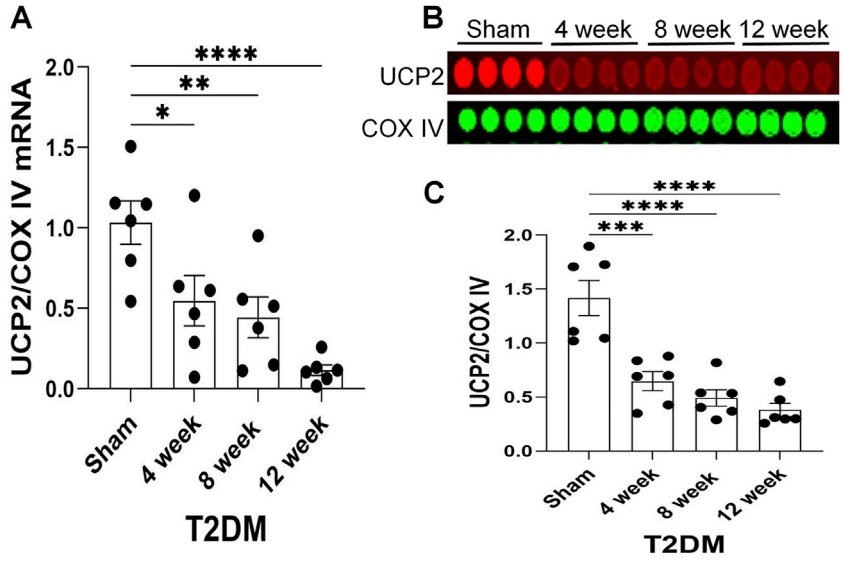

FIGURE 3
A time course of UCP2 expression as T2DM develops. **(A)** Mean RT-qPCR data of UCP2 transcript expression relative to cytochrome c oxidase subunit IV (COX IV, mitochondrial maker) transcript expression in sham, 4-week, 8-week, and 12-week post-T2DM ICG; n = 6/group. **(B, C)** Representative image **(B)** and mean data **(C)** of RPPA analysis of UCP2 and COX IV protein expression in sham, 4-week, 8-week, and 12-week post-T2DM ICG; n = 6/group. *P < 0.05, **P < 0.01, ***P < 0.001, ****P < 0.0001 vs. sham.

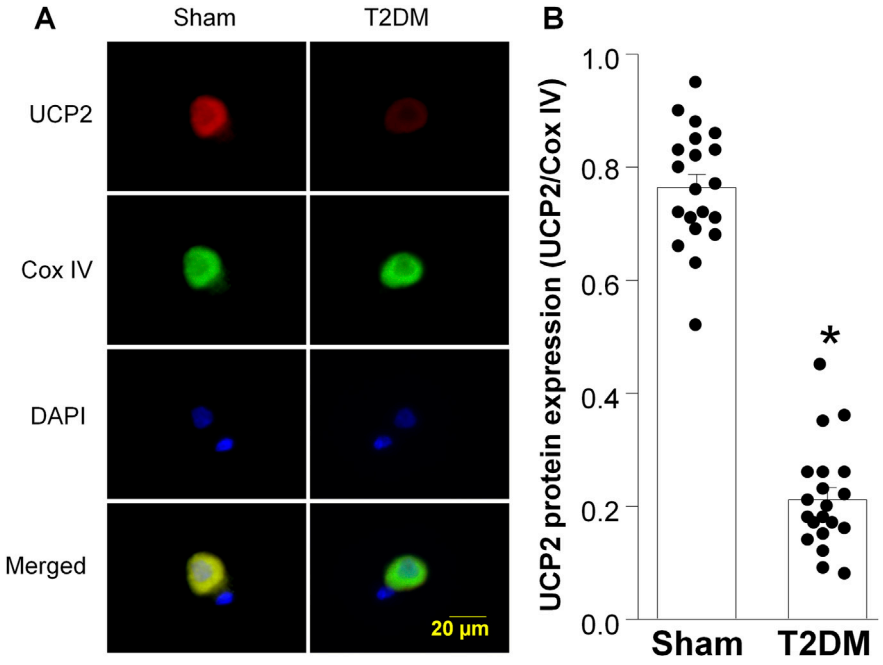

FIGURE 4
Uncoupling protein 2 (UCP2) expression in CVP neurons from sham and type 2 diabetic (T2DM) rats. **(A)** Representative images showing UCP2 (red color), cytochrome c oxidase subunit IV (Cox IV, mitochondrial marker, green color), 4,6-diamidino-2-phenylidole (DAPI, cell nucleus marker, blue color), and colocalization of UCP2 and Cox IV in mitochondria. **(B)** Quantitative data for protein expression of UCP2 in mitochondria. Data are mean ± SEM; n = 20 neurons in each group. *P < 0.05 vs. sham.

current density in CVP neurons through reducing the expression of N-type calcium channels (Liu et al., 2012). Additionally, the alteration in N-type calcium channel expression was revealed to result from elevated levels of hydrogen peroxide (H_2O_2, a type of reactive oxygen species (ROS)) (Liu et al., 2012; Zhang et al., 2022). As the mitochondria is a primary source of intracellular ROS

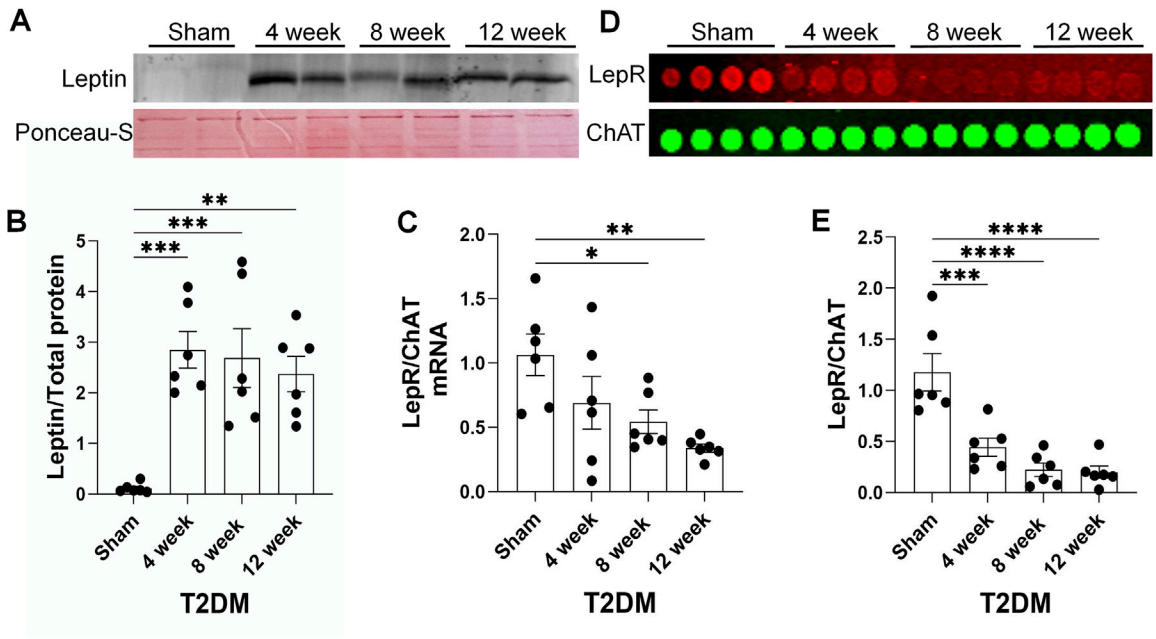

FIGURE 5
A time course of leptin resistance as T2DM develops. **(A, B)** Representative image **(A)** and mean data **(B)** of Western blot analysis of Leptin expression and ponceau-S total protein stain (housekeeping) in epicardial adipose pads from sham, 4-week, 8-week, and 12-week post-T2DM; n = 6/group. **(C)** Mean RT-qPCR data of lepR transcript expression relative to choline acetyltransferase (ChAT, cholinergic neuronal marker) transcript expression in sham, 4-week, 8-week, and 12-week post-T2DM ICG; n = 6/group. **(D, E)** Representative image **(D)** and mean data **(E)** of RPPA analysis of lepR and ChAT protein expression in sham, 4-week, 8-week, and 12-week post-T2DM ICG; n = 6/group. *P < 0.05, **P < 0.01, ***P < 0.001, ****P < 0.0001 vs. sham.

(Hernansanz-Agustín and Enríquez, 2021), we examined the impact of T2DM on the expression of Uncoupling protein 2 (UCP2), a member of the mitochondrial uncoupling protein family, which exerts antioxidant properties and downregulates oxidative stress (Jabůrek et al., 2013; Forte et al., 2021). Upon examination of UCP2 expression as T2DM progresses, RT-qPCR and RPPA analysis revealed that the expression of UCP2 mRNA and protein in T2DM ICGs was attenuated as early as 4 weeks post-T2DM induction and gradually decreased through 12-week T2DM (Figure 3). Additionally, the data from immunofluorescence staining also revealed that 12-week T2DM significantly lowered the levels of UCP2 in CVP neurons as compared to sham (Figures 4A,B).

Development of leptin resistance in T2DM ICG

Leptin resistance is a common pathology associated with T2DM development, characterized by attenuated responses to the hormone leptin, despite elevated leptin levels (Gruzdeva et al., 2019; Knight et al., 2010). As leptin has previously been shown to drive UCP2 expression (Ho et al., 2010), we examined the impact of leptin resistance in CVP neurons. In this study, leptin resistance was defined as exhibiting reduced levels of leptin receptor (lepR) expression in CVP neurons despite elevated levels of leptin protein. As our previous study reported 12-week T2DM rats exhibit hyperleptinemia (Liu et al., 2012), we examined leptin expression in epicardial adipose pads as T2DM developed. Western blot analysis revealed that levels of leptin significantly increased in the epicardial adipose pads as early as 4 weeks post-T2DM induction and remained elevated through 12-week T2DM, as compared to sham (Figures 5A,B). To determine if elevated leptin levels could be a result of a T2DM induced increase in white epicardial adipose, we visually inspected isolated rat hearts and found that 12-week T2DM rat hearts appeared to have more white epicardial adipose tissue as compared to sham (Supplementary Figure 2).

As T2DM epicardial adipose pads exhibited elevated levels of leptin, we examined lepR expression in rat ICG to determine if T2DM ICG experience leptin resistance. RT-qPCR and RPPA analyses showed that ICG lepR mRNA and protein levels were reduced 4 weeks post-T2DM induction and were continually kept at a low level through 12-week T2DM (Figures 5C–E). Additionally, immunofluorescent data also revealed a reduced level of lepR protein in the CVP neurons from 12 weeks post-T2DM rats compared to sham rats (Figures 6A,B). Taken together, these data reveal that leptin resistance develops in T2DM ICGs, which may contribute to CVP neuronal dysfunction in T2DM.

Discussion

In the present study, we found that HFD-STZ-induced T2DM reduced cardiac parasympathetic activity, which might be partially attributed to functional remodeling of CVP neurons located in the ICG. Additionally, leptin resistance possibly correlates with the functional remodeling of CVP neurons through the alteration of UCP2 in T2DM. These findings suggest that leptin resistance could

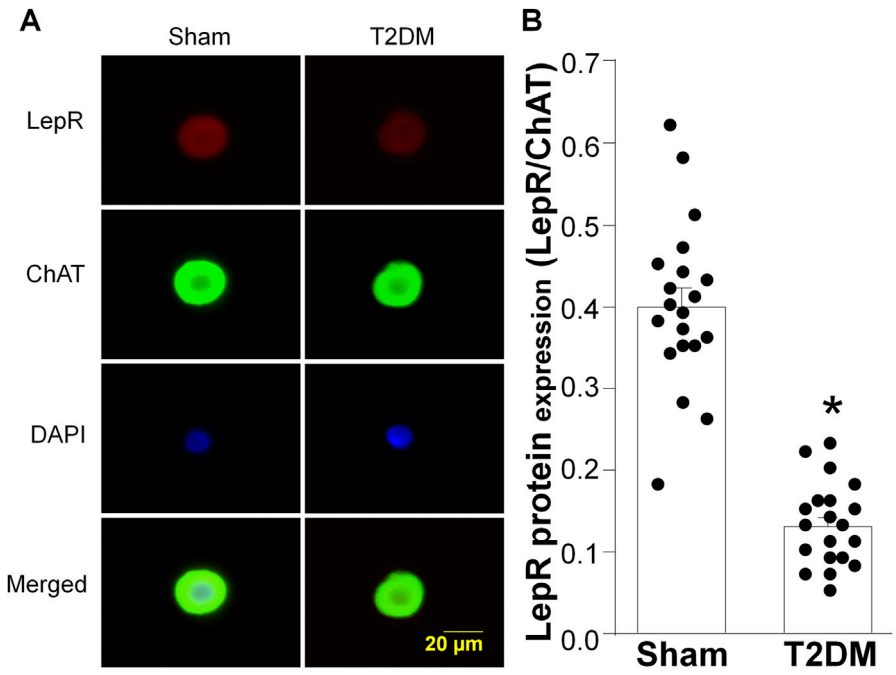

FIGURE 6
Protein expression of leptin receptors (lepR) in CVP neurons from sham and type 2 diabetic (T2DM) rats. **(A)** representative images showing lepR (red color), choline acetyltransferase (ChAT, a cholinergic neuronal marker, green color), 4,6-diamidino-2-phenylidole (DAPI, cell nucleus marker, blue color), and colocalization of lepR and ChAT in CVP neurons. **(B)** quantitative data for protein expression of lepR in CVP neurons. Data are mean ± SEM; n = 20 neurons in each group. *P < 0.05 vs. sham.

be a therapeutic target to improve CVP neuronal function and cardiac vagal activity in T2DM.

T2DM rat model

T2DM is a complex disease whose development and pathological progression is the result of synergism of many factors including nutrition, environment, and genetics (Wu et al., 2014). In the early stages of T2DM, patients develop insulin resistance. To combat this, pancreatic β-islet cells secrete greater amounts of insulin to keep homeostatic blood glucose levels (Rachdaoui, 2020; Wondmkun, 2020). As T2DM progresses, this compensatory release of insulin diminishes in effectiveness, leading to reduced glucose tolerance and a hyperglycemic state (Zheng et al., 2018). In addition to insulin resistance and hyperglycemia, individuals with T2DM often develop other pathophysiologies, such as dyslipidemia, hyperleptinemia, and increased visceral adipose accumulation (Mooradian, 2009; Hulkoti et al., 2022; Zhao and Li, 2022). The heterogeneity in the pathogenesis and complications experienced by diabetic patients makes identifying an experimental animal model that mimics the progression and clinical characteristics of human T2DM a significant challenge in studying T2DM.

Using the same rat T2DM model, in our previous study we found that T2DM rats exhibited reduced insulin sensitivity, elevated triglyceride levels, hyperleptinemia, increased visceral white adipose, and diminished brown adipose (Liu et al., 2012). Similar changes in insulin sensitivity, triglyceride levels, and blood glucose levels have also been reported in other studies using this model (Hussein et al., 2012; Khan et al., 2013; Cui et al., 2018). While the T2DM model used in this study has been reported to mimic clinical T2DM pathologies (hyperglycemia, dyslipidemia, etc.) (Srinivasan et al., 2005; Skovsø, 2014; Liu et al., 2012), we acknowledge that the possible effects that HFD-induced obesity or STZ treatment alone have on CVP neuronal function and cardiac parasympathetic activity cannot be excluded.

Baroreflex sensitivity and functional remodeling of CVP neurons in T2DM

As cardiovascular events are the leading cause of death in T2DM patients (Walker and Cubbon, 2015; Wong and Sattar, 2023), understanding the progression of cardiovascular dysfunction in T2DM is of the utmost importance in the effort to decrease T2DM mortality. A wide array of evidence in clinical studies and animal experiments has shown that diminished arterial baroreflex sensitivity is a common complication in T2DM (Kim et al., 2019; Gupta et al., 2020; Samora et al., 2023; Hamaoka et al., 2024). The baroreflex function is regulated at multiple integrative centers including the baroreceptors at the afferent limb, central components, and autonomic efferent components (Suarez-Roca et al., 2021). Dysregulation of any of these branches could contribute to T2DM-induced cardiac autonomic dysfunction. For example, studies report that baroreceptor neurons in the nodose ganglia in type 1 diabetic rats exhibit altered neuronal excitability (Tu et al., 2010; da Silva-Alves et al., 2023). It is certainly possible

that changes in sensory afferent signaling in nodose ganglia could contribute to the diminished baroreflex sensitivity we observed in this study.

Autonomic efferent control of the baroreflex includes both sympathetic components as well as parasympathetic components (Durães Campos et al., 2018; Suarez-Roca et al., 2021). Diminished baroreflex sensitivity could result from an increase in cardiac sympathetic signaling to the heart, a reduced parasympathetic signaling to the heart, or a combination of both effects (Huggett et al., 2003; Thaung et al., 2015; Young et al., 2019). This study focused on the impact of parasympathetic decline in baroreflex sensitivity because the decline in parasympathetic tone predates sympathetic overactivation in T2DM (Hadad et al., 2022; Rasmussen et al., 2022). Parasympathetic cardiac autonomic tone is regulated through the activity of preganglionic neurons in the DVMN and postganglionic CVP neurons in the ICG (Durães Campos et al., 2018). One previous study reported that isolated parasympathetic DVMN neurons depolarize in response to leptin (Li et al., 2007). As DVMN neurons activate CVP neurons, it is possible that diminished preganglionic cardiac parasympathetic neuronal activity, in response to DVMN neurons becoming resistant to leptin, could contribute to T2DM induced cardiac parasympathetic withdrawal. Similarly, our previous studies have reported that T2DM CVP neurons exhibit reduced functionality resulting in compromised cardiac parasympathetic function (Liu et al., 2012; Liu et al., 2015; Zhang et al., 2022).

In this study, we confirm that nAChR currents are reduced in T2DM CVP neurons and further found that the reduced nAChR currents could contribute to the decrease in CVP neuronal excitability, evidenced by the reduced frequency of action potentials. These data support that T2DM-induced alterations in baroreflex sensitivity is partially due to reduced cardiac parasympathetic activity at the level of the ICG. Nevertheless, the potential role of cardiac sympathetic overactivation in T2DM-induced cardiovascular autonomic dysfunction cannot be discounted. Previous studies have reported that T2DM patients exhibit sympathetic hyperactivity (Huggett et al., 2003; Young et al., 2019), which could contribute to ventricular arrhythmogenicity (Albarado-Ibañez et al., 2013; Gardner et al., 2016). Furthermore, one study identified increased sympathetic nerve activity in the stellate ganglion, which regulates sympathetic cardiac autonomic activity, of Zucker fatty acid rats (Thaung et al., 2015). As such, the symapathovagal balance must be considered when assessing changes in cardiac autonomic function in T2DM.

Potential molecular mechanisms leading to functional remodeling of CVP neurons in T2DM

As altered CVP neuronal excitability has been reported to contribute to cardiac vagal dysfunction and malignant ventricular arrhythmogenesis in T2DM (Zhang et al., 2022), understanding the molecular processes that drive CVP neuronal dysfunction is paramount in the effort to eradicate cardiac autonomic dysfunction in T2DM patients. Previous studies showed that reactive oxygen species (ROS) induce deleterious functional changes in multiple neuronal cell types in T2DM, including CVP neurons (Zherebitskaya et al., 2009; Liu et al., 2014; Zhang et al., 2022; Zhang et al., 2023). One previous study reported that T2DM elevated the levels of H_2O_2 (a type of ROS) and reduced the expression of the ROS scavenger catalase in CVP neurons, which contributed to CVP neuronal dysfunction (Zhang et al., 2022). Similarly, induction of oxidative stress in ICG neurons via H_2O_2 stimulation alters calcium and potassium currents and reduces neuronal excitability (Whyte et al., 2009). Additionally, decreasing ROS levels in CVP neurons through reestablishing antioxidant scavengers, such as catalase and superoxide dismutase, has been shown to improve CVP neuronal function (Whyte et al., 2009; Zhang et al., 2022). Although the driver of ROS accumulation in T2DM CVP neurons has not yet been elucidated, T2DM-impaired mitochondria could be a significant source of intracellular ROS (Kizhakekuttu et al., 2012; Fiorentino et al., 2021; Hernansanz-Agustín and Enríquez, 2021).

Our present study explored the impact of T2DM on UCP2, a mitochondrial ROS regulator. Normally, UCP2 functions in the maintenance of mitochondrial membrane potential and regulates mitochondrial oxidative stress through its activity to dissipate the proton gradient at the inner mitochondrial membrane (Nesci and Rubattu, 2024). Our current study demonstrated that the expression of UCP2 protein and mRNA was reduced in CVP neurons early in the development of T2DM in HFD-STZ T2DM rats (4 weeks post-T2DM induction), which is consistent with a previous study that reported reduced UCP2 expression in kidney tissue of T2DM patients (de Souza et al., 2015). Diminished UCP2 expression has been associated with increased cellular oxidative stress in a rat brain microvascular endothelial cell line, a rat renal proximal tubular endothelial cell line, and the brain tissue from a spontaneously hypertensive rat model (Rubattu et al., 2017; Forte et al., 2021). Upregulation of UCP2 expression by treatment of perindopril has been shown to rescue attenuated mitochondrial membrane potential in a rat model of diabetic retinopathy (Zheng et al., 2009). Furthermore, re-establishment of UCP2 expression in a UCP2 knockout mouse model decreased ROS accumulation and NLRP3 inflammasome activation in mouse astrocytes (Du et al., 2016). These studies, including our present and previous data (Zhang et al., 2022; Zhang et al., 2023) make a strong argument that restoring UCP2 expression may serve as a potential therapeutic strategy for improving T2DM-induced CVP neuronal dysfunction.

To further explore potential mechanisms that lead to reduction of UCP2 expression, we examined the impact of leptin resistance on T2DM CVP neurons. Canonically, leptin binds leptin receptors expressed on the cell surface and initiates the Janus kinase/signal transducer and activator of transcription (JAK-STAT) pathway to exert cellular transcriptional regulation (Procaccini et al., 2009), though activation of other signaling molecules, such as PKC and PKA, has also been reported (Barrenetxe et al., 2004). Previous studies have reported that leptin/lepR signaling induced an increase in UCP2 expression in SH-SY5Y neuronal cells and white adipose tissue of Sprague-Dawley rats (Scarpace et al., 1998; Ho et al., 2010). Furthermore, Lapp et al. reported that STAT3 could directly bind the UCP2 promoter to drive UCP2 expression (Lapp et al., 2014). These studies make a strong argument that changes in leptin/LepR signaling, such as the development of leptin resistance, during T2DM development may be a regulator of UCP2 expression.

Leptin resistance often develops as a result of T2DM (Bidulescu et al., 2020; Manglani et al., 2024; Vilariño-García et al., 2024), and we have previously reported that T2DM rats exhibit hyperleptinemia (Liu et al., 2012). However, leptin resistance may not impact all tissues, but develops selectively, which is a novel concept of selective leptin resistance (Correia et al., 2002; Mark et al., 2002). One previous study has shown that, in agouti yellow obese mice, leptin's impact on renal sympathoexcitation was preserved, despite the loss of leptin's weight reducing actions (Correia et al., 2002). Similarly, Munzberg et al. reported that neurons in the arcuate nucleus, but not the ventromedial hypothalamus, or dorsal medial hypothalamus exhibit leptin resistance in diet-induced obese mice (Münzberg et al., 2004).

To ascertain the state of leptin resistance in T2DM ICG, we first examined the state of leptin expression in epicardial adipose pads and found that T2DM epicardial adipose pads express elevated levels of leptin as early as 4 weeks post-T2DM induction. Upon visual examination of our rat hearts, we identified that T2DM rats appeared to have more white epicardial adipose as compared to sham (Supplementary Figure 2). This increase in epicardial leptin may be due to an increase in white epicardial adipose tissue, as previous studies have shown that white adipose tissue secretes more leptin than brown adipose (Moinat et al., 1995; Cinti et al., 1997). Examination of lepR expression in CVP neurons revealed T2DM induces reduced levels of lepR as early as 4 weeks post-T2DM induction, and levels stay diminished as T2DM progresses. The combination of elevated leptin levels and reduced leptin receptor expression indicates that CVP neurons in the ICG develop leptin resistance during the early stages of T2DM development. So far, we do not know whether leptin resistance in CVP neurons is a form of selective leptin resistance or if the rats experience a global leptin resistance in this T2DM rat model, which should be clarified in future studies. To our knowledge, we are the first to report that CVP neurons develop leptin resistance through reductions of lepR expression in T2DM.

As T2DM CVP neurons exhibit leptin resistance, we expect that lepR controlled intracellular signaling will become dysregulated in T2DM. As leptin/lepR signaling has previously been implicated in intracellular ROS maintenance (Bilbao et al., 2015; Frühbeck et al., 2017), and one previous study in adipose tissues of T2DM mice reported that restoration of canonical leptin/lepR signaling attenuated intracellular ROS accumulation (Frühbeck et al., 2017), it is certainly possible the leptin resistance-UCP2-ROS signaling pathway might be associated with CVP neuronal dysfunction in T2DM. It is important to acknowledge that leptin resistance is not the only possible explanation for CVP neuronal dysfunction. We have previously reported that 12-weeek T2DM rats exhibit reduced insulin sensitivity/insulin resistance (Liu et al., 2012). It may be that CVP neuron dysfunction is also driven by reduced insulin responsiveness. One previous study correlated the development of insulin resistance in human patients with diminished cardiac vagal tone (Ziegler et al., 2018). Similarly, insulin resistance in sensory dorsal root ganglion neurons has been shown to alter neuronal function through dysregulated Akt activation (Grote et al., 2013). As leptin resistance and insulin resistance occur simultaneously in T2DM, it is also certainly possible that a synergism of diminished leptin and insulin response leads to reduced CVP neuronal function. We, of course, acknowledge that our present study has not shown the direct association among leptin resistance, UCP2, and CVP neuronal function in T2DM, which need further studies to be definitively elucidated, such as *in vivo* overexpression of lepR or UCP2 in CVP neurons.

In conclusion, the data presented here identified cardiovascular parasympathetic dysfunction in HFD-STZ T2DM rats, which is partially attributed to functional remodeling of CVP neurons during T2DM development. Additionally, leptin resistance and reduced UCP2 expression initiated in the early stage of T2DM might be potential triggers to cause CVP neuronal dysfunction, and further result in attenuation of cardiovascular parasympathetic activation and cardiac arrhythmogenesis during the progression of T2DM. These triggers should be potential therapeutic targets to improve the prognosis of T2DM patients.

Data availability statement

The original contributions presented in the study are included in the article/Supplementary Material, further inquiries can be directed to the corresponding author.

Ethics statement

The animal study was approved by the Institutional Animal Care and Use Committee (IACUC) at the University of Nebraska Medical Center. The study was conducted in accordance with the local legislation and institutional requirements.

Author contributions

AE: Conceptualization, Formal Analysis, Investigation, Methodology, Validation, Visualization, Writing–original draft, Writing–review and editing. HT: Formal Analysis, Investigation, Methodology, Validation, Visualization, Writing–review and editing. YL: Investigation, Methodology, Validation, Writing–review and editing. BS: Investigation, Methodology, Validation, Writing–review and editing. LW: Investigation, Validation, Writing–review and editing. KC: Investigation, Validation, Writing–review and editing. Y-LL: Conceptualization, Formal Analysis, Funding acquisition, Investigation, Methodology, Project administration, Resources, Supervision, Validation, Visualization, Writing–original draft, Writing–review and editing.

Funding

The author(s) declare that financial support was received for the research, authorship, and/or publication of this article. This study was supported by the National Institute of Health's National Heart, Lung, and Blood Institute, Bethesda, MD, United States (R01HL144146 and R01HL168500 to Y-LL).

Conflict of interest

The authors declare that the research was conducted in the absence of any commercial or financial relationships that could be construed as a potential conflict of interest.

The author(s) declared that they were an editorial board member of Frontiers, at the time of submission. This had no impact on the peer review process and the final decision.

Generative AI statement

The author(s) declare that no Generative AI was used in the creation of this manuscript.

Publisher's note

Supplementary material

The Supplementary Material for this article can be found online at: https://www.frontiersin.org/articles/10.3389/fphys.2025.1547901/full#supplementary-material

References

Agarwal, G., and Singh, S. K. (2017). Arrhythmias in type 2 diabetes mellitus. *Indian J. Endocrinol. Metab.* 21 (5), 715–718. doi:10.4103/ijem.IJEM_448_16

Albarado-Ibañez, A., Avelino-Cruz, J. E., Velasco, M., Torres-Jácome, J., and Hiriart, M. (2013). Metabolic syndrome remodels electrical activity of the sinoatrial node and produces arrhythmias in rats. *PLoS One* 8 (11), e76534. doi:10.1371/journal.pone.0076534

Alkondon, M., Pereira, E. F. R., Almeida, L. E. F., Randall, W. R., and Albuquerque, E. X. (2000). Nicotine at concentrations found in cigarette smokers activates and desensitizes nicotinic acetylcholine receptors in CA1 interneurons of rat hippocampus. *Neuropharmacology* 39 (13), 2726–2739. doi:10.1016/S0028-3908(00)00156-8

Armour, J. A. (2007). The little brain on the heart. *Cleve Clin. J. Med.* 74, S48–S51. doi:10.3949/ccjm.74.suppl_1.s48

Barrenetxe, J., Sainz, N., Barber, A., and Lostao, M. P. (2004). Involvement of PKC and PKA in the inhibitory effect of leptin on intestinal galactose absorption. *Biochem. Biophys. Res. Commun.* 317 (3), 717–721. doi:10.1016/j.bbrc.2004.03.106

Bidulescu, A., Dinh, P. C., Jr., Sarwary, S., Forsyth, E., Luetke, M. C., King, D. B., et al. (2020). Associations of leptin and adiponectin with incident type 2 diabetes and interactions among African Americans: the Jackson heart study. *BMC Endocr. Disord.* 20 (1), 31. doi:10.1186/s12902-020-0511-z

Bilbao, M. G., Di Yorio, M. P., Galarza, R. A., Varone, C. L., and Faletti, A. G. (2015). Regulation of the ovarian oxidative status by leptin during the ovulatory process in rats. *Reproduction* 149 (4), 357–366. doi:10.1530/rep-14-0536

Chakraborty, P., Nattel, S., Nanthakumar, K., Connelly, K. A., Husain, M., Po, S. S., et al. (2024). Sudden cardiac death due to ventricular arrhythmia in diabetes mellitus: a bench to bedside review. *Heart rhythm.* 21 (10), 1827–1837. doi:10.1016/j.hrthm.2024.05.063

Cinti, S., Frederich, R. C., Zingaretti, M. C., De Matteis, R., Flier, J. S., and Lowell, B. B. (1997). Immunohistochemical localization of leptin and uncoupling protein in white and brown adipose tissue. *Endocrinology* 138 (2), 797–804. doi:10.1210/endo.138.2.4908

Correia, M. L. G., Haynes, W. G., Rahmouni, K., Morgan, D. A., Sivitz, W. I., and Mark, A. L. (2002). The concept of selective leptin resistance: evidence from agouti yellow obese mice. *Diabetes* 51 (2), 439–442. doi:10.2337/diabetes.51.2.439

Cui, X., Qian, D. W., Jiang, S., Shang, E. X., Zhu, Z. H., and Duan, J. A. (2018). Scutellariae radix and coptidis rhizoma improve glucose and lipid metabolism in T2DM rats via regulation of the metabolic profiling and MAPK/PI3K/Akt signaling pathway. *Int. J. Mol. Sci.* 19 (11), 3634. doi:10.3390/ijms19113634

Dall'ago, P., D'Agord Schaan, B., da Silva, V. O., Werner, J., da Silva Soares, P. P., de Angelis, K., et al. (2007). Parasympathetic dysfunction is associated with baroreflex and chemoreflex impairment in streptozotocin-induced diabetes in rats. *Auton. Neurosci.* 131 (1-2), 28–35. doi:10.1016/j.autneu.2006.06.005

Da Silva-Alves, K. S., Ferreira-da-Silva, F. W., Coelho-de-Souza, A. N., Weinreich, D., and Leal-Cardoso, J. H. (2023). Diabetes mellitus differently affects electrical membrane properties of vagal afferent neurons of rats. *Physiol. Rep.* 11 (4), e15605. doi:10.14814/phy2.15605

de Souza, B. M., Michels, M., Sortica, D. A., Bouças, A. P., Rheinheimer, J., Buffon, M. P., et al. (2015). Polymorphisms of the UCP2 gene are associated with glomerular filtration rate in type 2 diabetic patients and with decreased UCP2 gene expression in human kidney. *PLoS One* 10 (7), e0132938. doi:10.1371/journal.pone.0132938

Du, R. H., Wu, F. F., Lu, M., Shu, X. D., Ding, J. H., Wu, G., et al. (2016). Uncoupling protein 2 modulation of the NLRP3 inflammasome in astrocytes and its implications in depression. *Redox Biol.* 9, 178–187. doi:10.1016/j.redox.2016.08.006

Durães Campos, I., Pinto, V., Sousa, N., and Pereira, V. H. (2018). A brain within the heart: a review on the intracardiac nervous system. *J. Mol. Cell Cardiol.* 119, 1–9. doi:10.1016/j.yjmcc.2018.04.005

Evans, A. J., and Li, Y. L. (2024). Remodeling of the intracardiac ganglia during the development of cardiovascular autonomic dysfunction in type 2 diabetes: molecular mechanisms and therapeutics. *Int. J. Mol. Sci.* 25 (22), 12464. doi:10.3390/ijms252212464

Fiorentino, T. V., Monroy, A., Kamath, S., Sotero, R., Cas, M. D., Daniele, G., et al. (2021). Pioglitazone corrects dysregulation of skeletal muscle mitochondrial proteins involved in ATP synthesis in type 2 diabetes. *Metabolism* 114, 154416. doi:10.1016/j.metabol.2020.154416

Forte, M., Bianchi, F., Cotugno, M., Marchitti, S., Stanzione, R., Maglione, V., et al. (2021). An interplay between UCP2 and ROS protects cells from high-salt-induced injury through autophagy stimulation. *Cell Death Dis.* 12 (10), 919. doi:10.1038/s41419-021-04188-4

Frühbeck, G., Catalán, V., Rodríguez, A., Ramírez, B., Becerril, S., Portincasa, P., et al. (2017). Normalization of adiponectin concentrations by leptin replacement in ob/ob mice is accompanied by reductions in systemic oxidative stress and inflammation. *Sci. Rep.* 7 (1), 2752. doi:10.1038/s41598-017-02848-0

Gardner, R. T., Ripplinger, C. M., Myles, R. C., and Habecker, B. A. (2016). Molecular mechanisms of sympathetic remodeling and arrhythmias. *Circ Arrhythm Electrophysiol* 9 (2), e001359. doi:10.1161/CIRCEP.115.001359

Grote, C. W., Groover, A. L., Ryals, J. M., Geiger, P. C., Feldman, E. L., and Wright, D. E. (2013). Peripheral nervous system insulin resistance in ob/ob mice. *Acta Neuropathol. Commun.* 1 (1), 15. doi:10.1186/2051-5960-1-15

Gruzdeva, O., Borodkina, D., Uchasova, E., Dyleva, Y., and Barbarash, O. (2019). Leptin resistance: Underlying mechanisms and diagnosis. *Diabetes Metab. Syndr. Obes.* 12, 191–198. doi:10.2147/dmso.S182406

Guo, Y. P., McLeod, J. G., and Baverstock, J. (1987). Pathological changes in the vagus nerve in diabetes and chronic alcoholism. *J. Neurol. Neurosurg. Psychiatry* 50 (11), 1449–1453. doi:10.1136/jnnp.50.11.1449

Gupta, C., Bubber, P., Fahim, M., Saidullah, B., and Omanwar, S. (2020). Adiponectin in onset and progression of T2DM with cardiac dysfunction in rats. *Hum. Exp. Toxicol.* 39 (11), 1463–1474. doi:10.1177/0960327120927446

Gyldenkerne, C., Mortensen, M. B., Kahlert, J., Thrane, P. G., Warnakula Olesen, K. K., Sørensen, H. T., et al. (2023). 10-Year cardiovascular risk in patients with newly diagnosed type 2 diabetes mellitus. *J. Am. Coll. Cardiol.* 82 (16), 1583–1594. doi:10.1016/j.jacc.2023.08.015

Hadad, R., Akobe, S. F., Weber, P., Madsen, C. V., Larsen, B. S., Madsbad, S., et al. (2022). Parasympathetic tonus in type 2 diabetes and pre-diabetes and its clinical implications. *Sci. Rep.* 12 (1), 18020. doi:10.1038/s41598-022-22675-2

Hamaoka, T., Leuenberger, U. A., Drew, R. C., Murray, M., Blaha, C., Luck, J. C., et al. (2024). Glucose metabolism and autonomic function in healthy individuals and patients with type 2 diabetes mellitus at rest and during exercise. *Exp. Physiol.* 109 (2), 214–226. doi:10.1113/ep091444

Hernansanz-Agustín, P., and Enríquez, J. A. (2021). Generation of reactive oxygen species by mitochondria. *Antioxidants* 10 (3), 415. doi:10.3390/antiox10030415

Ho, P. W. L., Liu, H. F., Ho, J. W. M., Zhang, W. Y., Chu, A. C. Y., Kwok, K. H. H., et al. (2010). Mitochondrial uncoupling protein-2 (UCP2) mediates leptin protection against MPP+ toxicity in neuronal cells. *Neurotox. Res.* 17 (4), 332–343. doi:10.1007/s12640-009-9109-y

Hossain, M. J., Al-Mamun, M., and Islam, M. R. (2024). Diabetes mellitus, the fastest growing global public health concern: early detection should be focused. *Health Sci. Rep.* 7 (3), e2004. doi:10.1002/hsr2.2004

Hu, W., Zhang, D., Tu, H., and Li, Y. L. (2021). Reduced cell excitability of cardiac postganglionic parasympathetic neurons correlates with myocardial infarction-induced fatal ventricular arrhythmias in type 2 diabetes mellitus. *Front. Neurosci.* 15, 721364. doi:10.3389/fnins.2021.721364

Huggett, R. J., Scott, E. M., Gilbey, S. G., Stoker, J. B., Mackintosh, A. F., and Mary, D. A. S. G. (2003). Impact of type 2 diabetes mellitus on sympathetic neural mechanisms in hypertension. *Circulation* 108 (25), 3097–3101. doi:10.1161/01.CIR.0000103123.66264.FE

Hulkoti, V., Acharya, S., Shukla, S., Kumar, S., Kabra, R., Dubey, A., et al. (2022). Visceral adiposity index in type 2 diabetes mellitus (DM) and its correlation with microvascular complications. *Cureus* 14 (11), e31279. doi:10.7759/cureus.31279

Hussein, A. A., Abdel-Aziz, A., Gabr, M., and Hemmaid, K. Z. (2012). Myocardial and metabolic dysfunction in type 2 diabetic rats: impact of ghrelin. *Can. J. Physiol. Pharmacol.* 90 (1), 99–111. doi:10.1139/y11-103

International Diabetes Federation (2021). *IDF diabetes Atlas*. 10th ed. Brussels, Belgium: International Diabetes Federation.

Jabůrek, M., Ježek, J., Zelenka, J., and Ježek, P. (2013). Antioxidant activity by a synergy of redox-sensitive mitochondrial phospholipase A2 and uncoupling protein-2 in lung and spleen. *Int. J. Biochem. Cell Biol.* 45 (4), 816–825. doi:10.1016/j.biocel.2013.01.010

Kautzky-Willer, A., Leutner, M., and Harreiter, J. (2023). Sex differences in type 2 diabetes. *Diabetologia* 66 (6), 986–1002. doi:10.1007/s00125-023-05891-x

Khan, H. B. H., Vinayagam, K. S., Moorthy, B. T., Palanivelu, S., and Panchanatham, S. (2013). Anti-inflammatory and anti-hyperlipidemic effect of Semecarpus anacardium in a High fat diet: STZ-induced Type 2 diabetic rat model. *Inflammopharmacology* 21 (1), 37–46. doi:10.1007/s10787-011-0109-1

Kim, Y. S., Davis, S., Stok, W. J., van Ittersum, F. J., and van Lieshout, J. J. (2019). Impaired nocturnal blood pressure dipping in patients with type 2 diabetes mellitus. *Hypertens. Res.* 42 (1), 59–66. doi:10.1038/s41440-018-0130-5

Kizhakekuttu, T. J., Wang, J., Dharmashankar, K., Ying, R., Gutterman, D. D., Vita, J. A., et al. (2012). Adverse alterations in mitochondrial function contribute to type 2 diabetes mellitus–related endothelial dysfunction in humans. *Arterioscler. Thromb. Vasc. Biol.* 32 (10), 2531–2539. doi:10.1161/ATVBAHA.112.256024

Knight, Z. A., Hannan, K. S., Greenberg, M. L., and Friedman, J. M. (2010). Hyperleptinemia is required for the development of leptin resistance. *PLOS ONE* 5 (6), e11376. doi:10.1371/journal.pone.0011376

Kuo, T. B., Lai, C. J., Huang, Y. T., and Yang, C. C. (2005). Regression analysis between heart rate variability and baroreflex-related vagus nerve activity in rats. *J. Cardiovasc Electrophysiol.* 16 (8), 864–869. doi:10.1111/j.1540-8167.2005.40656.x

Lapp, D. W., Zhang, S. S., and Barnstable, C. J. (2014). Stat3 mediates LIF-induced protection of astrocytes against toxic ROS by upregulating the UPC2 mRNA pool. *Glia* 62 (2), 159–170. doi:10.1002/glia.22594

Lee, P. G., Cai, F., and Helke, C. J. (2002). Streptozotocin-induced diabetes reduces retrograde axonal transport in the afferent and efferent vagus nerve. *Brain Res.* 941 (1-2), 127–136. doi:10.1016/s0006-8993(02)02645-8

Li, T. L., Chiou, L. C., Lin, Y. S., Hsieh, J.-R., and Hwang, L.-L. (2007). Electrophysiological study on the effects of leptin in rat dorsal motor nucleus of the vagus. *Am J Physiol Regul Integr Comp Physiol* 292 (6), R2136–R2143. doi:10.1152/ajpregu.00563.2006

Liu, D., Zhang, H., Gu, W., and Zhang, M. (2014). Effects of exposure to high glucose on primary cultured hippocampal neurons: involvement of intracellular ROS accumulation. *Neurol. Sci.* 35 (6), 831–837. doi:10.1007/s10072-013-1605-4

Liu, J., Tu, H., Zheng, H., Zhang, L., Tran, T. P., Muelleman, R. L., et al. (2012). Alterations of calcium channels and cell excitability in intracardiac ganglion neurons from type 2 diabetic rats. *Am. J. Physiol. Cell Physiol.* 302 (8), C1119–C1127. doi:10.1152/ajpcell.00315.2011

Liu, J., Zhang, D., Tu, H., Muelleman, R. L., Wang, W. Z., and Li, Y. L. (2015). Nicotinic acetylcholine receptors and cardiac vagal activity in rats with type 2 diabetes. *Diabetes Metab.* S13, 012. doi:10.4172/2155-6156.s13-012

Mancini, M., Patel, J. C., Affinati, A. H., Witkovsky, P., and Rice, M. E. (2022). Leptin promotes striatal dopamine release via cholinergic interneurons and regionally distinct signaling pathways. *J. Neurosci.* 42 (35), 6668–6679. doi:10.1523/jneurosci.0238-22.2022

Manglani, K., Anika, N. N., Patel, D., Jhaveri, S., Avanthika, C., Sudan, S., et al. (2024). Correlation of leptin in patients with type 2 diabetes mellitus. *Cureus* 16 (4), e57667. doi:10.7759/cureus.57667

Mark, A. L., Correia, M. L., Rahmouni, K., and Haynes, W. G. (2002). Selective leptin resistance: a new concept in leptin physiology with cardiovascular implications. *J. Hypertens.* 20 (7), 1245–1250. doi:10.1097/00004872-200207000-00001

Mhaimeed, O., Pillai, K., Dargham, S., Al Suwaidi, J., Jneid, H., and Abi Khalil, C. (2023). Type 2 diabetes and in-hospital sudden cardiac arrest in ST-elevation myocardial infarction in the US. *Front. Cardiovasc Med.* 10, 1175731. doi:10.3389/fcvm.2023.1175731

Moinat, M., Deng, C., Muzzin, P., Assimacopoulos-Jeannet, F., Seydoux, J., Dulloo, A. G., et al. (1995). Modulation of obese gene expression in rat brown and white adipose tissues. *FEBS Lett.* 373 (2), 131–134. doi:10.1016/0014-5793(95)01030-I

Mooradian, A. D. (2009). Dyslipidemia in type 2 diabetes mellitus. *Nat. Clin. Pract. Endocrinol. Metab.* 5 (3), 150–159. doi:10.1038/ncpendmet1066

Münzberg, H., Flier, J. S., and Bjørbaek, C. (2004). Region-specific leptin resistance within the hypothalamus of diet-induced obese mice. *Endocrinol* 145 (11), 4880–4889. doi:10.1210/en.2004-0726

Nesci, S., and Rubattu, S. (2024). UCP2, a member of the mitochondrial uncoupling proteins: an overview from physiological to pathological roles. *Biomedicines* 12 (6), 1307. doi:10.3390/biomedicines12061307

Perissinotti, P. P., Martínez-Hernández, E., and Piedras-Rentería, E. S. (2021). TRPC1/5-Ca $_V$ 3 complex mediates leptin-induced excitability in hypothalamic neurons. *Front. Neurol.* 15, 679078. doi:10.3389/fnins.2021.679078

Procaccini, C., Lourenco, E. V., Matarese, G., and La Cava, A. (2009). Leptin signaling: a key pathway in immune responses. *Curr. Signal Transduct. Ther.* 4 (1), 22–30. doi:10.2174/157436209787048711

Rachdaoui, N. (2020). Insulin: the friend and the foe in the development of type 2 diabetes mellitus. *Int. J. Mol. Sci.* 21 (5), 1770. doi:10.3390/ijms21051770

Rasmussen, T. K., Finnerup, N. B., Singer, W., Jensen, T. S., Hansen, J., and Terkelsen, A. J. (2022). Preferential impairment of parasympathetic autonomic function in type 2 diabetes. *Aut. Neurosci.* 243, 103026. doi:10.1016/j.autneu.2022.103026

Rawshani, A., Rawshani, A., Franzén, S., Eliasson, B., Svensson, A. M., Miftaraj, M., et al. (2017). Mortality and cardiovascular disease in type 1 and type 2 diabetes. *N. Engl. J. Med.* 376(15), 1407–1418. doi:10.1056/NEJMoa1608664

Reaven, P. D., Emanuele, N. V., Wiitala, W. L., Bahn, G. D., Reda, D. J., McCarren, M., et al. (2019). Intensive glucose control in patients with type 2 diabetes - 15-year follow-up. *N. Engl. J. Med.* 380 (23), 2215–2224. doi:10.1056/NEJMoa1806802

Rubattu, S., Stanzione, R., Bianchi, F., Cotugno, M., Forte, M., Della Ragione, F., et al. (2017). Reduced brain UCP2 expression mediated by microRNA-503 contributes to increased stroke susceptibility in the high-salt fed stroke-prone spontaneously hypertensive rat. *Cell Death Dis.* 8 (6), e2891. doi:10.1038/cddis.2017.278

Samora, M., Huo, Y., McCuller, R. K., Chidurala, S., Stanhope, K. L., Havel, P. J., et al. (2023). Spontaneous baroreflex sensitivity is attenuated in male UCD-type 2 diabetes mellitus rats: a link between metabolic and autonomic dysfunction. *Auton. Neurosci.* 249, 103117. doi:10.1016/j.autneu.2023.103117

Scarpace, P. J., Nicolson, M., and Matheny, M. (1998). UCP2, UCP3 and leptin gene expression: modulation by food restriction and leptin. *J. Endocrinol.* 159 (2), 349–357. doi:10.1677/joe.0.1590349

Scheen, A. J. (2022). Glucose-lowering agents and risk of ventricular arrhythmias and sudden cardiac death: a comprehensive review ranging from sulphonylureas to SGLT2 inhibitors. *Diabetes Metab.* 48 (6), 101405. doi:10.1016/j.diabet.2022.101405

Schmidt, M. I., Duncan, B. B., Vigo, A., Pankow, J. S., Couper, D., Ballantyne, C. M., et al. (2006). Leptin and incident type 2 diabetes: risk or protection? *Diabetologia* 49 (9), 2086–2096. doi:10.1007/s00125-006-0351-z

Skovsø, S. (2014). Modeling type 2 diabetes in rats using high fat diet and streptozotocin. *J. Diabetes Investig.* 5 (4), 349–358. doi:10.1111/jdi.12235

Soltani, D., Azizi, B., Sima, S., Tavakoli, K., Hosseini Mohammadi, N. S., Vahabie, A. H., et al. (2023). A systematic review of the effects of transcutaneous auricular vagus nerve stimulation on baroreflex sensitivity and heart rate variability in healthy subjects. *Clin. Auton. Res.* 33 (2), 165–189. doi:10.1007/s10286-023-00938-w

Srinivasan, K., Viswanad, B., Asrat, L., Kaul, C. L., and Ramarao, P. (2005). Combination of high-fat diet-fed and low-dose streptozotocin-treated rat: a model for type 2 diabetes and pharmacological screening. *Pharmacol. Res.* 52 (4), 313–320. doi:10.1016/j.phrs.2005.05.004

Suarez-Roca, H., Mamoun, N., Sigurdson, M. I., and Maixner, W. (2021). Baroreceptor modulation of the cardiovascular system, pain, consciousness, and cognition. *Compr. Physiol.* 11 (2), 1373–1423. doi:10.1002/cphy.c190038

Takahashi, K. A., and Cone, R. D. (2005). Fasting induces a large, leptin-dependent increase in the intrinsic action potential frequency of orexigenic arcuate nucleus neuropeptide Y/Agouti-related protein neurons. *Endocrinol* 146 (3), 1043–1047. doi:10.1210/en.2004-1397

Thaung, H. P. A., Baldi, J. C., Wang, H.-Y., Hughes, G., Cook, R. F., Bussey, C. T., et al. (2015). Increased efferent cardiac sympathetic nerve activity and defective intrinsic heart rate regulation in type 2 diabetes. *Diabetes* 64 (8), 2944–2956. doi:10.2337/db14-0955

Tu, H., Zhang, L., Tran, T. P., Muelleman, R. L., and Li, Y. L. (2010). Diabetes alters protein expression of hyperpolarization-activated cyclic nucleotide-gated channel subunits in rat nodose ganglion cells. *Neuroscience* 165 (1), 39–52. doi:10.1016/j.neuroscience.2009.10.002

Vilariño-García, T., Polonio-González, M. L., Pérez-Pérez, A., Ribalta, J., Arrieta, F., Aguilar, M., et al. (2024). Role of leptin in obesity, cardiovascular disease, and type 2 diabetes. *Int. J. Mol. Sci.* 25 (4), 2338. doi:10.3390/ijms25042338

Walker, A. M., and Cubbon, R. M. (2015). Sudden cardiac death in patients with diabetes mellitus and chronic heart failure. *Diab Vasc. Dis. Res.* 12 (4), 228–233. doi:10.1177/1479164115573225

Whyte, K. A., Hogg, R. C., Dyavanapalli, J., Harper, A. A., and Adams, D. J. (2009). Reactive oxygen species modulate neuronal excitability in rat intrinsic cardiac ganglia. *Auton. Neurosci.* 150 (1-2), 45–52. doi:10.1016/j.autneu.2009.04.005

Wondmkun, Y. T. (2020). Obesity, insulin resistance, and type 2 diabetes: associations and therapeutic implications. *Diabetes Metab. Syndr. Obes.* 13, 3611–3616. doi:10.2147/dmso.S275898

Wong, N. D., and Sattar, N. (2023). Cardiovascular risk in diabetes mellitus: epidemiology, assessment and prevention. *Nat. Rev. Cardiol.* 20 (10), 685–695. doi:10.1038/s41569-023-00877-z

Wu, Y., Ding, Y., Tanaka, Y., and Zhang, W. (2014). Risk factors contributing to type 2 diabetes and recent advances in the treatment and prevention. *Int. J. Med. Sci.* 11 (11), 1185–1200. doi:10.7150/ijms.10001

Young, B. E., Holwerda, S. W., Vranish, J. R., Keller, D. M., and Fadel, P. J. (2019). Sympathetic transduction in type 2 diabetes mellitus. *Hypertension* 74 (1), 201–207. doi:10.1161/hypertensionaha.119.12928

Zhang, D., Hu, W., Tu, H., Wadman, M., and Li, Y. (2023). H2O2-REST signaling pathway is involved in cardiac vagal dysfunction and myocardial infarction-evoked ventricular arrhythmia in type 2 diabetes. *Physiology* 38 (S1), 5727640. doi:10.1152/physiol.2023.38.S1.5727640

Zhang, D., Liu, J., Tu, H., Muelleman, R. L., Cornish, K. G., and Li, Y. L. (2014). *In vivo* transfection of manganese superoxide dismutase gene or nuclear factor κB shRNA in nodose ganglia improves aortic baroreceptor function in heart failure rats. *Hypertension* 63 (1), 88–95. doi:10.1161/hypertensionaha.113.02057

Zhang, D., Tu, H., Cao, L., Zheng, H., Muelleman, R. L., Wadman, M. C., et al. (2018). Reduced N-Type Ca2+ channels in atrioventricular ganglion neurons are involved in ventricular arrhythmogenesis. *J. Am. Heart Assoc.* 7 (2), e007457. doi:10.1161/JAHA.117.007457

Zhang, D., Tu, H., Hu, W., Duan, B., Zimmerman, M. C., and Li, Y. L. (2022). Hydrogen peroxide scavenging restores N-Type calcium channels in cardiac vagal postganglionic neurons and mitigates myocardial infarction-evoked ventricular arrhythmias in type 2 diabetes mellitus. *Front. Cardiovasc Med.* 9, 871852. doi:10.3389/fcvm.2022.871852

Zhang, M., Lv, X. Y., Li, J., Xu, Z. G., and Chen, L. (2008). The characterization of high-fat diet and multiple low-dose streptozotocin induced type 2 diabetes rat model. *Exp. Diabetes Res.* 2008, 704045. doi:10.1155/2008/704045

Zhao, Y., and Li, H. (2022). Association of serum leptin and insulin levels among type 2 diabetes mellitus patients: a case-control study. *Med. Baltim.* 101 (41), e31006. doi:10.1097/md.0000000000031006

Zheng, Y., Ley, S. H., and Hu, F. B. (2018). Global aetiology and epidemiology of type 2 diabetes mellitus and its complications. *Nat. Rev. Endocrinol.* 14 (2), 88–98. doi:10.1038/nrendo.2017.151

Zheng, Z., Chen, H., Ke, G., Fan, Y., Zou, H., Sun, X., et al. (2009). Protective effect of perindopril on diabetic retinopathy is associated with decreased vascular endothelial growth factor-to-pigment epithelium-derived factor ratio: involvement of a mitochondria-reactive oxygen species pathway. *Diabetes* 58 (4), 954–964. doi:10.2337/db07-1524

Zherebitskaya, E., Akude, E., Smith, D. R., and Fernyhough, P. (2009). Development of selective axonopathy in adult sensory neurons isolated from diabetic rats: role of glucose-induced oxidative stress. *Diabetes* 58 (6), 1356–1364. doi:10.2337/db09-0034

Ziegler, D., Strom, A., Bönhof, G., Püttgen, S., Bódis, K., Burkart, V., et al. (2018). Differential associations of lower cardiac vagal tone with insulin resistance and insulin secretion in recently diagnosed type 1 and type 2 diabetes. *Metabolism* 79, 1–9. doi:10.1016/j.metabol.2017.10.013

Frontiers in Physiology

Understanding how an organism's components work together to maintain a healthy state

The second most-cited physiology journal, promoting a multidisciplinary approach to the physiology of living systems - from the subcellular and molecular domains to the intact organism and its interaction with the environment.

Discover the latest Research Topics

See more →

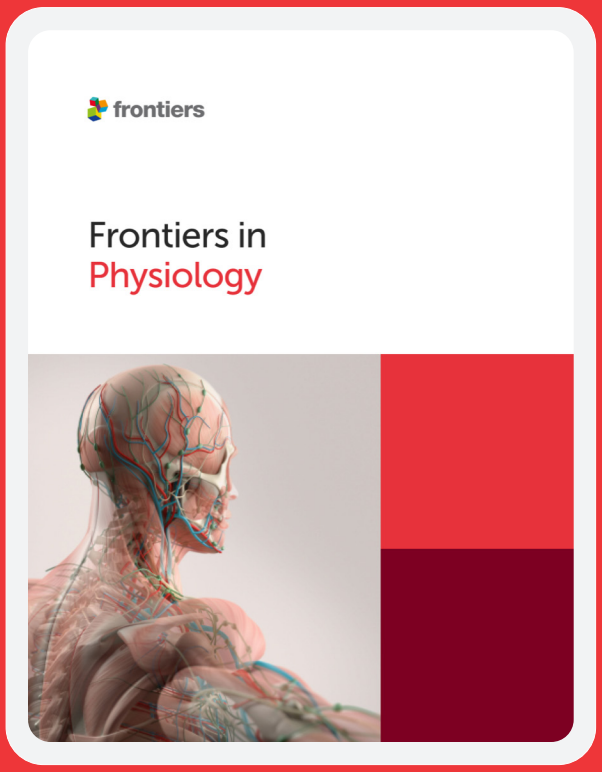

Frontiers

Avenue du Tribunal-Fédéral 34
1005 Lausanne, Switzerland
frontiersin.org

Contact us

+41 (0)21 510 17 00
frontiersin.org/about/contact